NASA CR 65561

TECHNICAL OPERATING REPORT
BOB Approval Nr. 21-R138.1

A STUDY OF ABLATION MATERIAL EFFECTS ON ANTENNA PERFORMANCE

AVCO MISSILES, SPACE AND ELECTRONICS GROUP
SPACE SYSTEMS DIVISION
201 Lowell Street
Wilmington, Massachusetts

AVSSD-0277-66-RR
NASA Contract 9-4916

12 October 1966

Prepared for

NATIONAL AERONAUTICS
AND SPACE ADMINSTRATION
MANNED SPACECRAFT CENTER
Houston, Texas

TECHNICAL OPERATING REPORT
BOB Approval Nr. 21-R138.1

This document consists of 244 pages,
76 copies, Series A

A STUDY OF ABLATION MATERIAL EFFECTS ON ANTENNA PERFORMANCE

Prepared by

R. L. Fante
J. R. McLaughlin
J. E. Trousdale

AVCO MISSILES, SPACE AND ELECTRONICS GROUP
SPACE SYSTEMS DIVISION
201 Lowell Street
Wilmington, Massachusetts

AVSSD-0277-66-RR
NASA Contract 9-4916

12 October 1966

APPROVED

T. W. Halloran
Chief, Radiating Systems Section

Prepared for

NATIONAL AERONAUTICS
AND SPACE ADMINSTRATION
MANNED SPACECRAFT CENTER
Houston, Texas

ABSTRACT

This is the final report on Contract NAS 9-4916 "A Study of Ablation Material Effects on Antenna Performance." This report summarizes the contract objectives, details the work accomplished, provides conclusions and recommends a future course of continued study.

EDITED BY:
EDITORIAL SERVICES SECTION
J. J. McCARRON

CONTENTS

CONTENTS (Concl'd)

ILLUSTRATIONS

ILLUSTRATIONS (Cont'd)

ILLUSTRATIONS (Cont'd)

ILLUSTRATIONS (Cont'd)

ILLUSTRATIONS (Cont'd)

ILLUSTRATIONS (Cont'd)

ILLUSTRATIONS (Concl'd)

TABLES

I. INTRODUCTION

This is the final report on Contract NAS 9-4916 "A Study of Ablation Material Effects on Antenna Performance". This report summarizes the contract objectives, details the work accomplished, provides conclusions and recommends a future course of continued study.

II PROGRAM OBJECTIVES

The first objective of this study program was to develop specifications for the electrical and physical properties of a series of materials as simulators of the Avcoat 5026-39 thermal protection system on the Apollo command module as it exists in the various stages of its mission. Of particular interest was the charred condition of the Avcoat during reentry. The simulators are required by NASA MSC for facile measurement of the electrical and physical conditions of the ablator on antenna performance for full-,one-third-and one-fifth-scale vehicle models using standard antenna-range equipment at ambient temperatures.

The second objective was to analyze theroretically the effects which ablative dielectric coverings have on antenna pattern, gain, efficiency, and reflection coefficient, and to express these effects in terms of the dielectric constant, loss tangent, and thickness of the dielectric covering.

The third and over-all objective of the study was to provide a high confidence level for the accuracy of measurements to be made by the NASA Manned Spacecraft Center with the simulators specified in the first objective.

BLANK PAGE

III. SUMMARY OF WORK ACCOMPLISHED

The program was divided into three major tasks as follows:

1. Determination of Avcoat 5026-39 dielectric properties from 4° K to 2000° K.

2. Development of a computer program to calculate properties of covered-slot radiation patterns and impedance.

3. Development of materials simulating the electrical conditions of Avcoat 5026-39 from 4° K to 2000° K and verification thereof with the use of slot, monopole and scimitar antennas of various scales.

In pursuit of these above tasks, the following work increments were accomplished:

1. A literature search was made that included DOD-and NASA-computerized searches for material relevant to complex permittivity measurement procedures, artificial dielectric (simulators) fabrication, performance parameter calculation of dielectric-sheathed antennas with emphasis on monopoles and slots, and literature dealing with scaling laws. The useful literature ordered and received was copied and retransmitted to NASA Houston as contractually required.

2. Avcoat 5026-39 dielectric-property screening tests and studies were made first, to determine if any differences existed between 5026-39M and 5026-39HCG; second, to determir the effect of moisture on dielectric-property stability; and third, to determine the effect of 5026-39 density and density tolerance being supplied in manufacture on dielectric properties.

Cryogenic complex permittivity test procedures were developed, appropriate equipment was fabricated, and virgin Avcoat 5026-39M dielectric properties were measured at 4° K for frequencies of 300, 450, 2200, and 5800 Mc.

Mid temperature range test procedures were developed and virgin and oven-charred 5026-39M properties were measured at 298° K and 153° K for frequencies of 300, 450, 1000, 2200, and 5800 Mc.

High-temperature range dielectric property test procedures were developed and the properties of 5026-39 were measured at 2000° K for frequencies of 250, 1000, and 3000 Mc. The measurement procedures were subsequently found to be inadequate because of the extremely high loss tangent of 5026-39 charred under intense heating. Subsequent cold-char measurements indicated that char measurements hot or cold would be limited to measurements of conductivity.

3. Formulations and a computer program were developed to calculate the radiation patterns and impedance of a lossy dielectric-covered open-ended waveguide. Impedance and pattern calculations were verified experimentally.

4. Simulators for virgin and charred Avcoat 5026-39 were successfully developed. Fidelity of the simulators was verified experimentally on open-ended waveguide, monopole and scimitar antennas of various scales by direct comparison of radiation patterns, gain and impedance alternately covered with simulator and heat shield.

IV. CONCLUSIONS AND RECOMMENDATIONS

1. It was possible to solve the problems as associated with the measurement of the complex permittivity of Avcoat 5026-39 from 4° K to 450° K and measurements were made accordingly.

2. Techniques more sophisticated than those developed for this program are required to measure 5026-39 electrical properties after the onset of pyrolysis. Heat rate, time, shear forces, local gas constituents and pressure effect the 5026-39 electrical properties and need to be controlled and related to pertinent reentry conditions. As an alternative to determining the 5026-39 complex permittivity, it is probably more advisable to measure directly the effect of hot heat shield on antenna performance during pyrolysis and then develop a simulator empirically. The simulator could then cover a large vehicle as appropriate for antenna measurements.

3. The problem of calculating the impedance and radiation pattern of a dielectric-covered waveguide was resolved. It is suggested that this study be extended to consider stratified covers as a more realistic reentry antenna condition.

4. Flexible, easy to use, reasonably low-cost simulators for full-scale and part-scale models were designed to simulate conditions of 5026-39 prior to ablation. No additional work is recommended in this area.

5. Simulators were developed for charred Avcoat 5026-39. Although the char was not related to any specific reentry condition, the simulator fabrication technique could be used or extended to any moderate or severe char condition.

6. Scaling of antennas, together with the use of heat-sheald simulators, is a valid and useful way of measuring antenna parameters. The validity of scaling is decreased, however, in lower power regions of radiation patterns unless all elements in the test set, including those that radiate spuriously, are scaled. Spurious elements are, typically, the feed structure, the antenna boom and miscellaneous cables.

Specific recommendations derived from the above are:

Pursue the high-temperature measurement of 5026-39 electrical properties or, preferably, measure effects of ablating 5026-39 directly on antennas; then, develop simulators empirically.

BLANK PAGE

V. DETAILED REPORT OF PROGRESS

A. LITERATURE SEARCH

1. Theoretical Program Literature Search

The theoretical program literature search was conducted for articles and documents pertaining to a dielectric coated monopole over a finite lossy ground plane and for a dielectric covered slot. The following abstracts and indexes were examined in search for the subject described:

STAR INDEX	1963 - Present
TAB INDEX	1963 - Present
International Aerospace Abstracts	1962 - Present
Journal of Applied Physics	1943 - Present
I.E.E.E. Proceedings	1912 - Present
PGAP	1953 - Present
Physics Abstracts	1956 - Present

A computerized literature search was performed by DDC and NASA. The DDC search listed several hundred articles of which only one reference was considered useful and there were only two useful articles from NASA's 250 citations. These articles are listed in appendix A.

2. Dielectric Measurements Literature Search

The initial literature search activity was concentrated on material pertaining to the measurement of dielectric properties and the manufacturing and control of the physical characteristics of Avcoat 5026-39 HCG. NASA and the Defense Documentation Center made literature searches on the former subject. The computer search submitted by the Department of Defense listed 26 abstracts of which 9 appeared applicable to the program. The NASA search included 49 citations of which 16 were applicable to the program. These reports were then ordered through the Avco Library.

Reprints of all the articles and some of the reports were submitted to NASA Houston. The more lengthy reports are listed in the bibliography and may be obtained readily. (See appendix A for the bibliography.)

B. AVCOAT 5026-39 DIELECTRIC MEASUREMENTS

Before any dielectric measurements were performed on the Avcoat 5026-39M and -39 HCG materials, a search was made to determine the extent of previous dielectric measurements made on these materials. In conjunction with this, a study was performed on 5026-39 physical properties such as density and moisture content to test their respective effects upon dielectric constant and loss tangent.

1. Pre-Contract 5026-39 Dielectric Measurements

The records of the Avco Advanced Electronics Department laboratories were examined in detail for measurements of dielectric constants of Avcoat 5026-22 and Avcoat 5026-39. Measurements made by this department in 1962 and 1963 giving values for the insertion loss, dielectric constant, and loss tangent are tabulated in Table 1. The majority of the measurements were made with the -22 material in various orientations and show only transmission losses. Three measurements, however, were made on the -39 material, and it is believed that the samples were of molded variety now designated -39M.

2. Study of Physical Properties

An investigation of the physical characteristics of Avcoat 5026-39 HCG was made to determine what problems, if any, would be encountered in making measurements of the dielectric constant and loss tangent with the equipment and techniques available. Machinability of the uncharred material to the tolerances required for the Rhode Schwarz dielectrometer was confirmed experimentally.

Two factors which can cause variation of the dielectric properties of a material are moisture content and density. Both were investigated for Avcoat 5026 39HCG and found to be sufficiently well controlled in the manufacturing process to limit the variation in dielectric properties to a few percent.

a. Density Measurements and Water Absorption Tests

A density check was made on the -39 HCG and -39 M bulk samples received from the Apollo manufacturing area. The density was checked by measuring a machined piece from the bulk sample and weighing it on a balance to 0.0001 gm. The water absorption test was made by measuring the weight of the sample before and after 2 hours heating at 150^{o} F. The results of these measurements are shown below

Material	Block IDN	Density gm/cm^3	Water Absorption (%)
-39HCG	A	0.517	1.249
-39M	B	0.532	1.458

TABLE I

ELECTRICAL PROPERTIES OF AVCOAT 5026

Frequency (kmc)	Description of Test Sample	Temp. (° F)	ϵ'/ϵ_0	Tan δ	Loss (db)
5026-22: Data of 9/21/62					
9.8	Post-char -- char to transmitter	Room			21
9.8	Post-char -- Smooth side to transmitter	Room			23.7
9.8	Post-char -- char to transmitter	329			28
9.8	Post-char -- smooth side to transmitter	329			23
9.8	Pre-char -- different thickness	Room	2.51 to 2.64		0.55 to 0.90 to
5.5	Post-char -- char to transmitter	350			32
5.5	Post-char -- smooth side to transmitter	350			32
5.5	Pre-char	Room	2.5		0.6
5.5	Post-char different orientations	350			28-34.5
5026-39: Data of 1/7/63					
5.7	Uncharred, *slotted line method	Room	1.86 1.96	0.024 0.021	
5.7	Uncharred, interferometer method		1.83		

*All measurements were made with interferometer, except where noted.

The densities of the -39 HCG and -39 M materials were within specification. The figures for water absorption agree with those previously given by the Apollo manufacturing personnel.

Water absorption does not present any problem in air-conditioned laboratories. If the moisture were driven completely from the sample the maximum change in dielectric constant would be 4 percent, assuming a dielectric constant of 81 for water. The composite dielectric constants for mixtures is described in the next section.

b. Density Variation and Its Effect on Dielectric Constant

The manufacturing density specification of Avcoat 5026-39 HCG allows the density to vary ± 7 percent. The major cause of this density variation is due to the gunning technique used to fill the honeycomb. To examine the effect of the density variation upon the dielectric constant, the material must be considered as a mixture of two materials--Avcoat 5026-39 and air. The total dielectric constant is a function of the relative volume of the -39 material and air and their respective dielectric constants.

The problem was analyzed in the following manner. Two generalized expressions were derived for the equivalent dielectric constant. The dielectric constant for air and -39 material were substituted into the derived expressions along with their representative volumes to determine the effect of density variation.

Expressions for the equivalent dielectric constant were derived by considering the electrostatic field across a capacitor. Consider a parallel plate capacitor composed of parallel layers of the dielectrics with permittivities ϵ_1 and ϵ_2 (see Figure 1a). The layers of the two dielectrics may be lumped together as shown in Figure 1b. Assume that there is a surface charge density of $+\sigma$ on the lower plate and $-\sigma$ on the upper plate. Then from Gauss's Law:

$$E_x = \sigma/\epsilon_2 \text{ for } 0 < X < t$$

$$E_x = \sigma/\epsilon_1 \text{ for } t < X < s$$

where E = field strength

$$E_x = \frac{\partial v}{\partial x} = -\frac{dv}{dx}$$

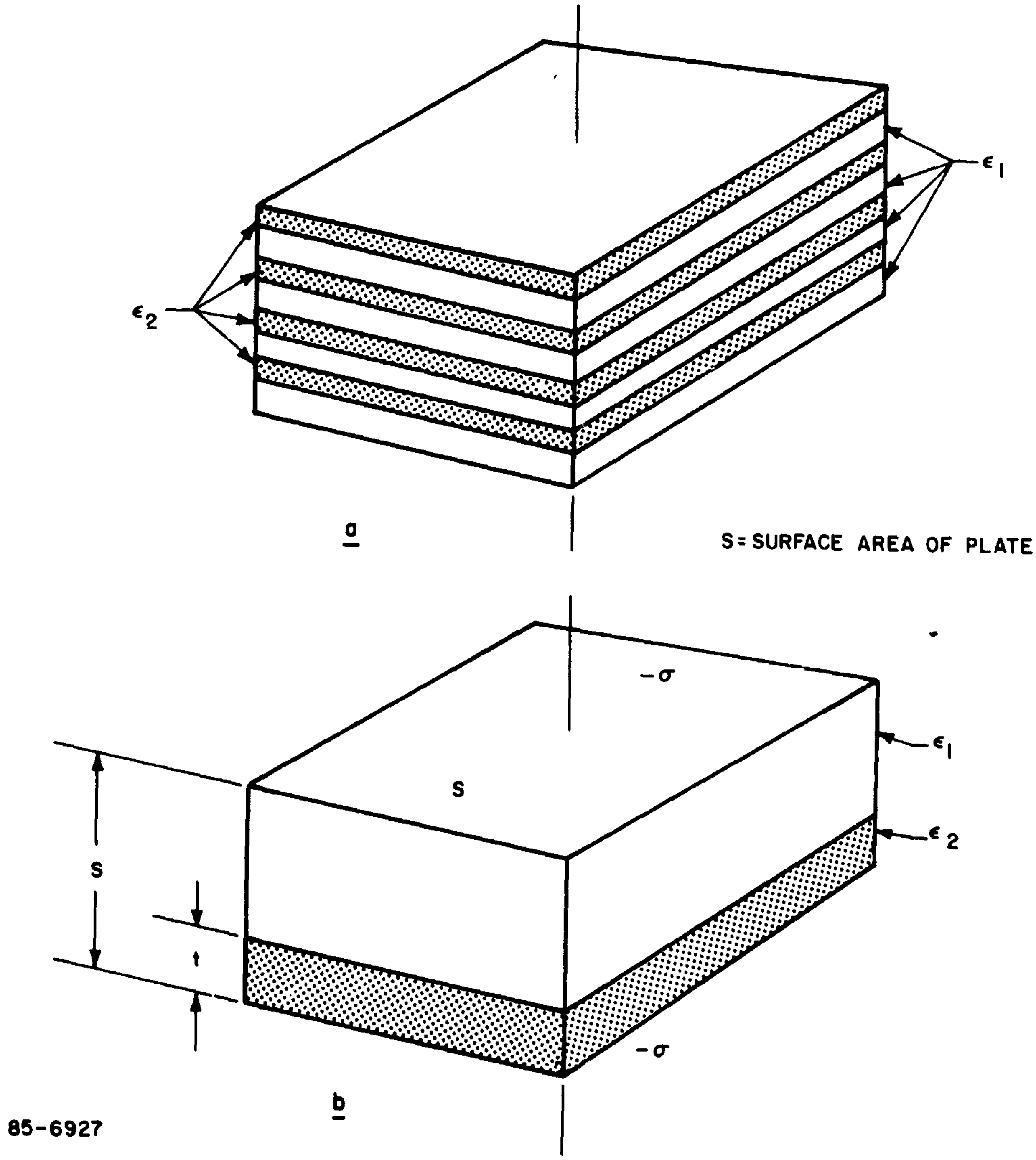

Figure 1 CAPACITOR WITH DIELECTRIC LAYERS PARALLEL TO PLATES

$$V = -\int E_x \, dx = -\int_0^t \frac{\sigma}{\epsilon_2} dx - \int_t^s \frac{\sigma}{\epsilon_1} dx = -\sigma \left(\frac{t}{\epsilon_2} - \frac{s-t}{\epsilon_1}\right)$$

$$C = \frac{Q}{V} = \frac{-\sigma S}{-\sigma \left(\frac{t}{\epsilon_2} + \frac{s-t}{\epsilon_1}\right)} \tag{1}$$

$$C = \frac{S}{(t/\epsilon_2) + (s - t/\epsilon_1)}$$

This is the equivalent capacitance for two dielectrics parallel with the plates. The capacitance for a single dielectric capacitor is:

$$C = \frac{K \epsilon_o S}{S} \tag{2}$$

Rewriting Equation (1):

$$C = \frac{\epsilon_o S}{\frac{1}{S}\left(\frac{t}{K_2} + \frac{s-t}{K_1}\right) S} \tag{3}$$

Comparing Equation (3) with Equation (2) it can be seen that the equivalent dielectric constant for the combination of two dielectrics with lamellae parallel to the plates is:

$$K_{eq.} = \frac{1}{\frac{1}{S}\left(\frac{t}{K_2} + \frac{s-t}{K_1}\right)} \tag{4}$$

Let $t = d$, $s - t = dz$, and rearranging Equation (4)

$$K_{eq.} = \frac{(d_1 + d_2) K_1 K_2}{d_1 K_2 + d_2 K_1} \tag{5}$$

Another possible alignment for the lamellae is shown in Figures 2a and 2b.

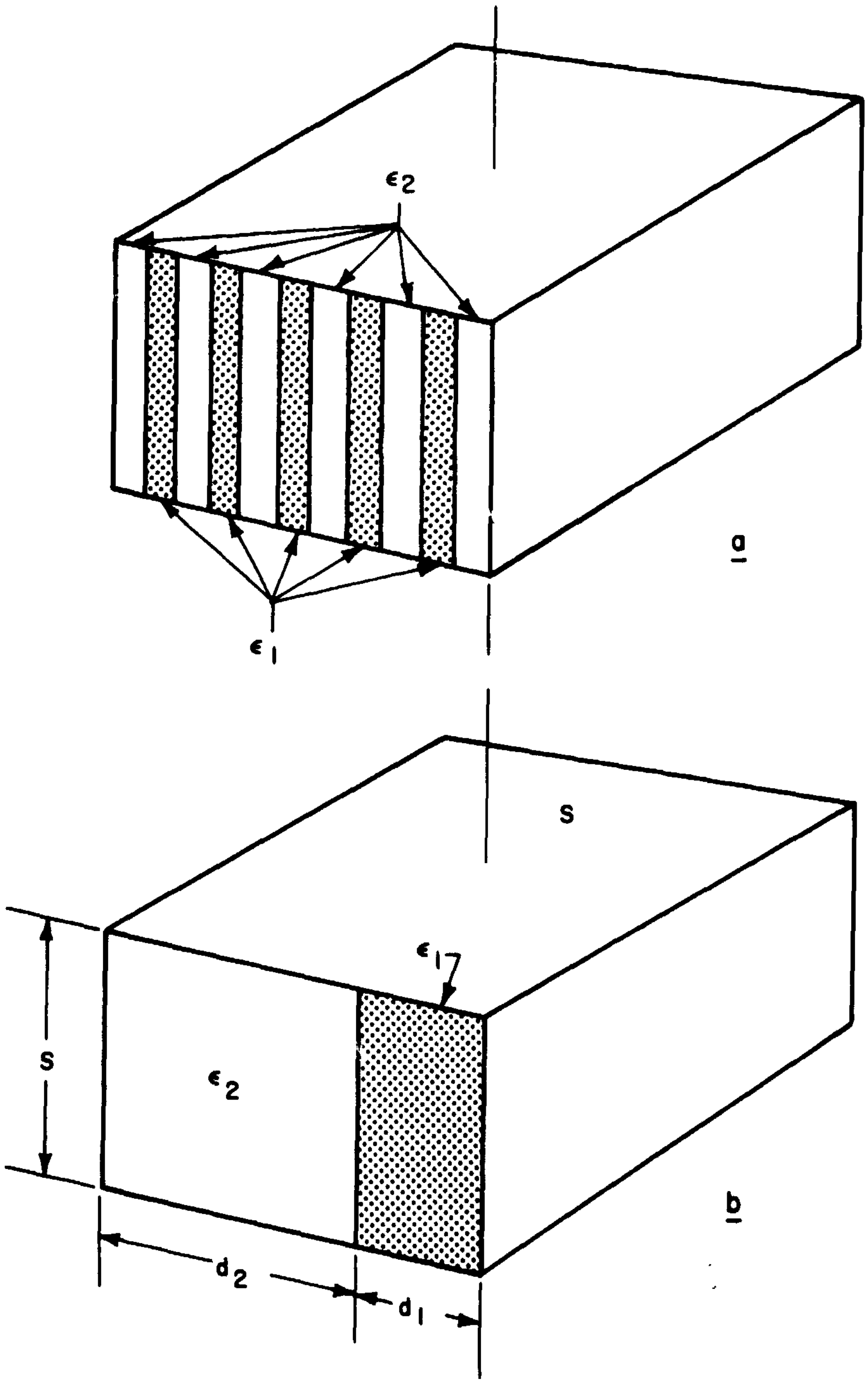

85-6926

Figure 2 CAPACITOR WITH DIELECTRIC LAYERS PERPENDICULAR TO PLATES

The equivalent capacitance for this case is:

$$C = \frac{K_1 \epsilon_o \dfrac{d_1}{d_1 + d_2} S}{S} + \frac{K_2 \epsilon_o \dfrac{d_2}{d_1 + d_2} S}{S}$$

$$C = \left(\frac{K_1 d_1 + K_2 d_2}{d_1 + d_2}\right) \frac{\epsilon_o S}{S} \tag{6}$$

The equivalent dielectric constant for this case is:

$$K_{eq.} = \frac{K_1 d_1 + K_2 d_2}{d_1 + d_2} \tag{7}$$

Equations (4) and (6) allow for the calculation of the effective dielectric constant for two different lamellae orientations. These two equations are in agreement with those given by Reynolds and Hough,[1] and the Encyclopedia of Physics.[2] There are many other orientations and particle shapes that may be assumed; however, the two lamellae formulas previously derived are the extreme cases. All other formulas for the mixture of dielectrics lie within these two limits.

A general empirical formula derived by Lichtenecker and Rothen[3] that lies within the two extremes is:

$$K^k{}_{eq.} = V_1 K_1^k + V_2 K_2^k \tag{8}$$

where $V_1 + V_2$ = total volume which becomes (7) when $k = 1$ and (5) when $k = -1$. When k is small compared with unity, the approximation $k = 1 + k \log k$ can be used for this case and we have:

$$\log K_{eq.} = V_1 \log K_1 + V_2 \log K_2 \ . \tag{9}$$

[1] Reynolds, J. A., and J. M. Hough, Formulas for Dielectric Constants and Mixtures, Proceedings of the Physical Society, London (July-December 1957) pp. 769-775.

[2] Encyclopedia of Physics Edited by S. Flugge, XVI Electric Fields and Waves; Berlin (1958) pp. 706-710.

[3] Licktenecker, K., and K. Rothen, Phys. Z, 32, p. 255 (1931).

This formula has been used extensively with very satisfactory results.

The average dielectric constant for the Avcoat 5026-39 HCG ($\frac{\epsilon'}{\epsilon_0}$ = 1.82) obtained from measured data given in this report was substituted into equations (4) and (6) and (9) along with the extreme changes in density. In equations (4), (6), and (9) the values of d_1, d_2, V_1, and V_2 are proportional to the density. For the ± 7 percent density change of the Avcoat 5026-39 HCG, the equivalent dielectric constant varied± 5.5, ±3.3, and±4.1 percent for equations (4), (6), and (9), respectively.

The ± 5.5 percent dielectric constant variation was calculated from the equation representing the greatest variation using the worst density variation. A more realistic approach to the problem is to use Lichtenecker's equation [4] because it is representative of a random orientation. Since 95 percent of the material manufactured is within ± 5 percent density change, the average dielectric constant variation will be 2.7 per cent using Lichtenecker's formula. From this analysis, it can be seen that the 5026-39 HCG density variations on the actual Apollo vehicle will cause a 2.7 percent variation in the dielectric constant over 95 percent of the vehicle.

Since it is highly unlikely that we will receive a sample with +7 percent or -7 percent density deviation, we will not be able to measure the dielectric constant at these extreme ends of the density spectrum; however, it will be possible to calculate the dielectric constant at the extreme ends by using Lichtenecker's formula.

3. Mid Temperature Range Measurements

a. Introduction

The intent of the mid-temperature range measurement was to determine dielectric constant and loss tangent of Avcoat 5026-39M and Avcoat 5026-39 HCG Apollo heat shield materials at 20 and 180° C over a frequency range 300 - 5800 mc. In addition to the above, measurements of charred samples were to be made at 20° C. Since the honeycomb is asymmetrical, the first step in measuring the dielectric constant and loss tangent was to determine if any resonance or orientation effect existed. Once this problem was resolved, the dielectric measurements were made using a Rhode and Schwarz dielectrometer.

[4] Shaw, T. M., and J. J. Windle, Microwave Techniques for the Measurement of the Dielectric Constant of Fibers and Films of High Polymer, J. Appl. Phys., 21, pp. 956-961 (October 1950).

b. Investigation of Resonance Effects

Because of the periodic honeycomb structure of the -39 HCG material, an investigation into possible resonance effects was conducted. Since the hexagonal honeycomb has a 3/8-inch dimension across the flats and the waveguide quarter wavelength, assuming a dielectric constant of 2.0, is approximately 27/64-inch at 5800 Mc, a quarter wave resonance effect might result in an apparent change in the value of complex permittivity at particular frequencies. To avoid laborious and tedious measurements inherent in point by point methods, a swept frequency test setup was devised. The sweep setup shown in Figure 3 was used over the frequency range from 5600 to 5850 Mc to determine any resonant effects. No resonance effects were noted.

c. Investigation of Orientation Effects

Dielectric constant and loss tangent measurements were made at C-band (f = 5.7 gc) in a waveguide setup at room temperature. Samples were machined so that six different orientations of the honeycomb could be measured in the waveguide. These orientations and their designation numbers are shown in figures 4 and 5. The results of the measurements are as follows:

Sample I. D. No.	Material	ϵ'/ϵ_0	Loss Tangent	Orientation
A - 1a	-39 HCG	1.82	0.020	1
A - 1b	-39 HCG	1.80	0.021	1
A - 2	-39 HCG	1.87	0.020	2
A - 3	-39 HCG	1.89	0.020	3
A - 4	-39 HCG	1.78	0.021	4
A - 5	-39 HCG	1.77	0.020	5
A - 6	-39 HCG	1.82	0.020	6
A - 7	-39 M	1.83	0.020	Homogeneous

The effect that the sample orientation had on the dielectric constant and loss tangent was insignificant. Since the dielectric properties were not sensitive to sample orientation at C-band, the S-band orientation sensitivity measurements were not pursued. The

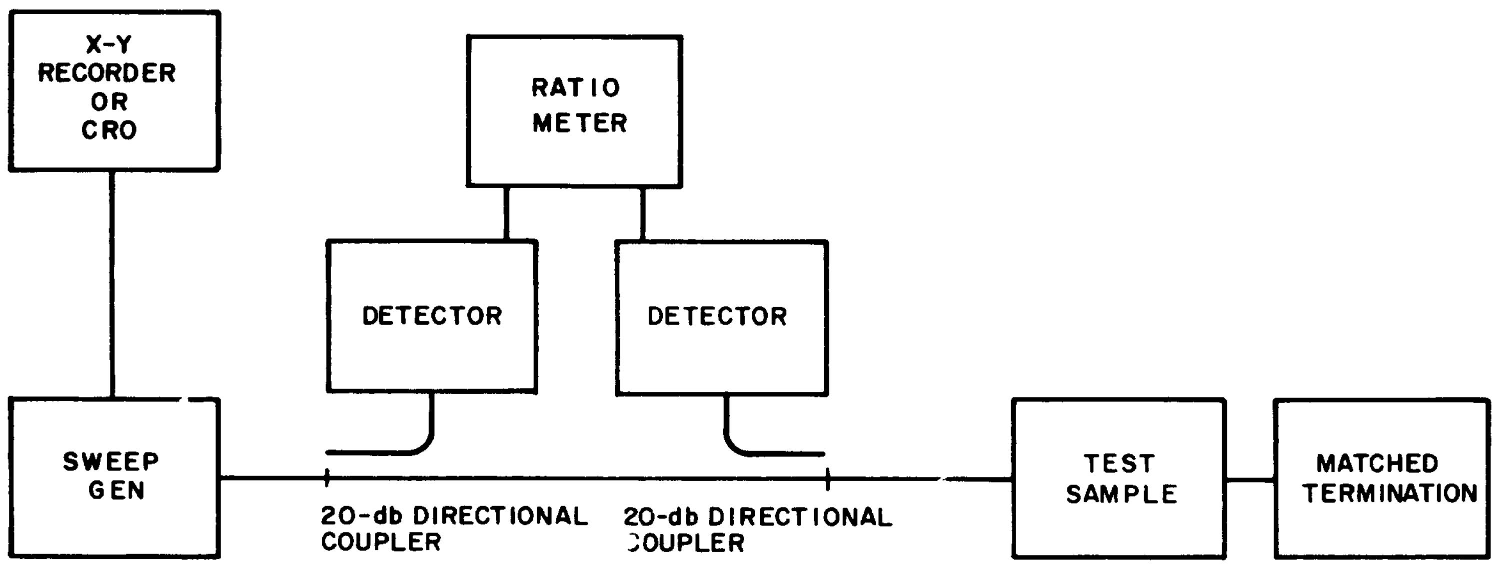

85-6927

Figure 3 SWEPT FREQUENCY EQUIPMENT SETUP

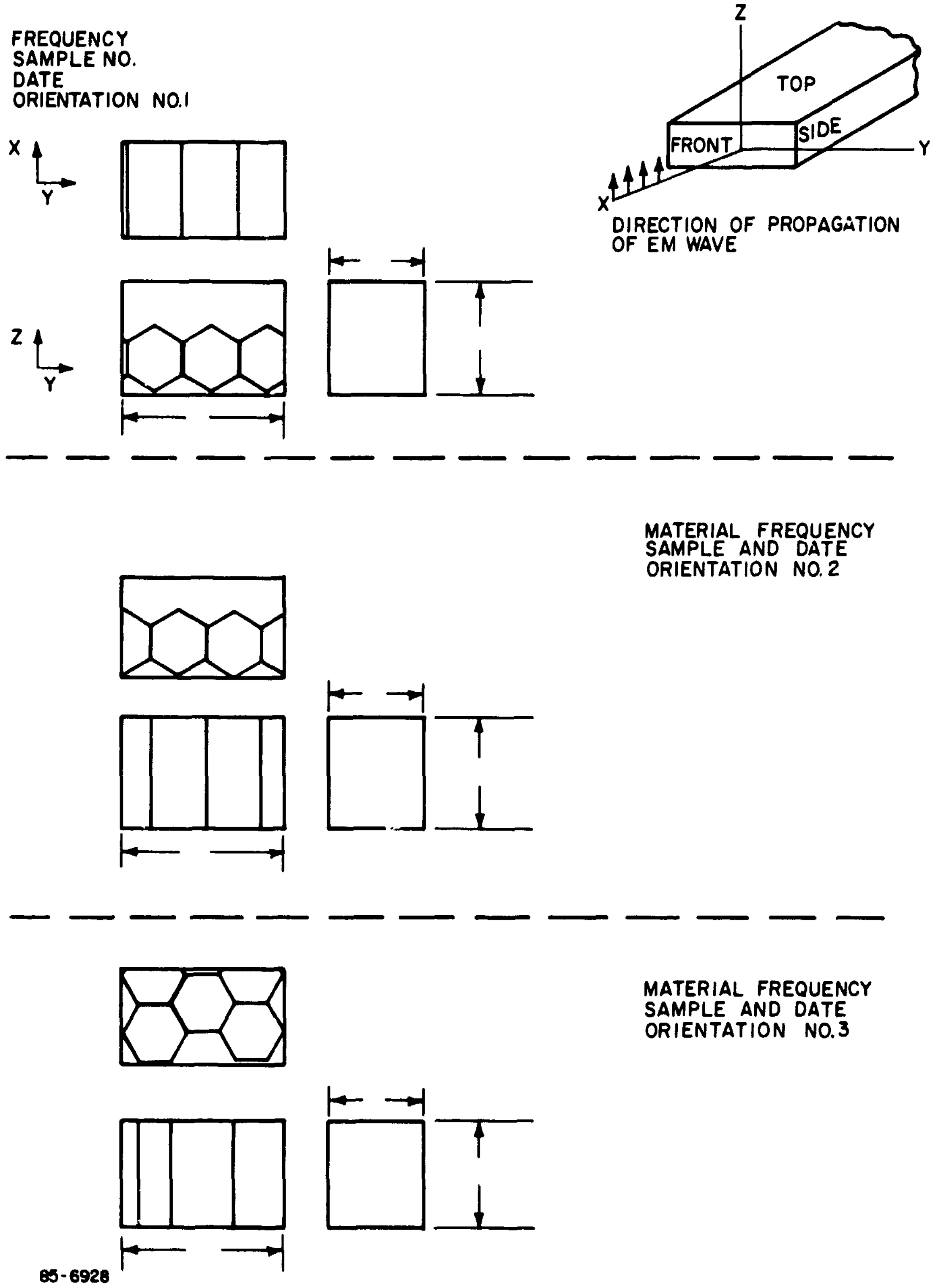

Figure 4 HONEYCOMB ORIENTATIONS

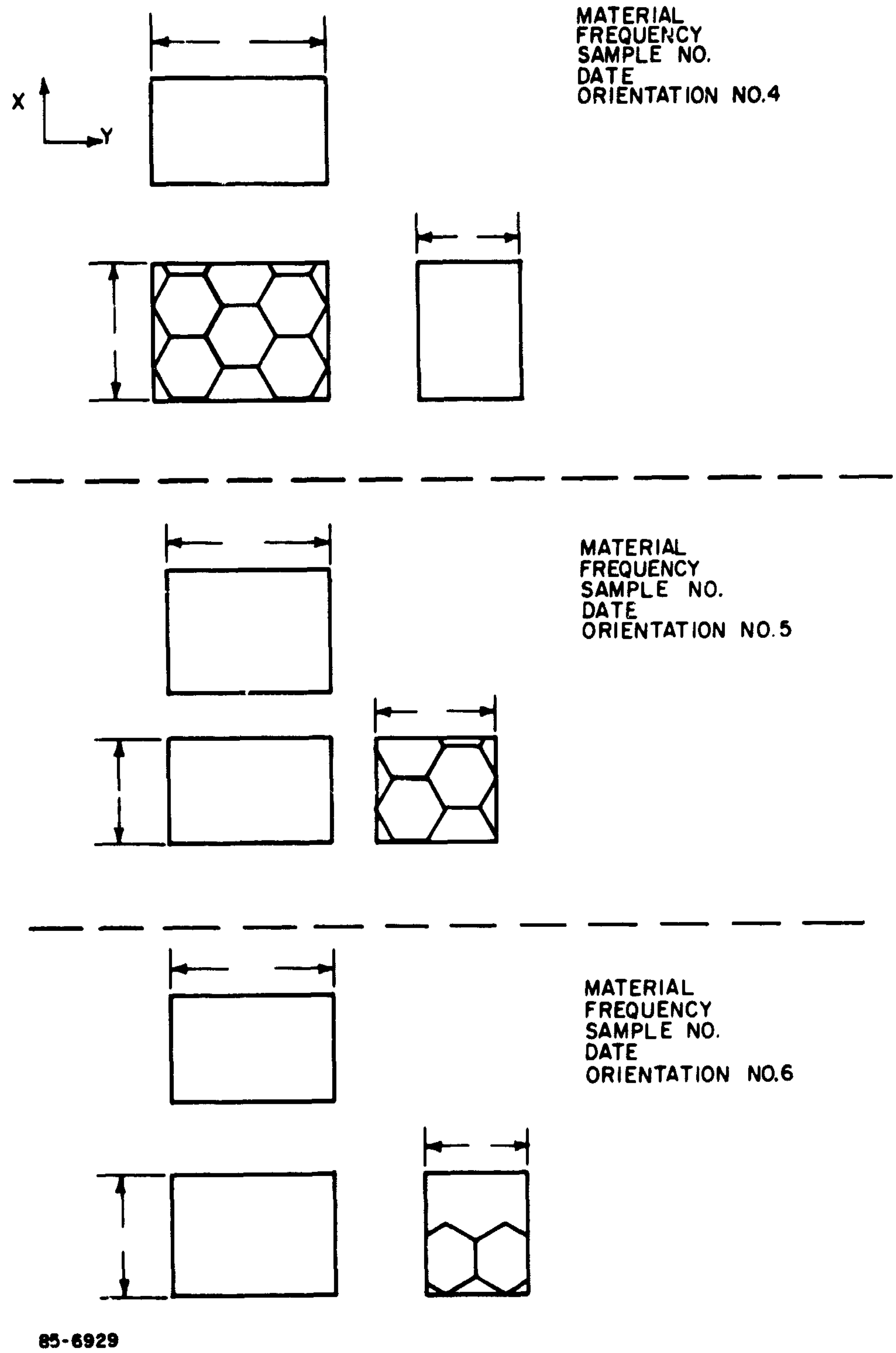

Figure 5 HONEYCOMB ORIENTATIONS

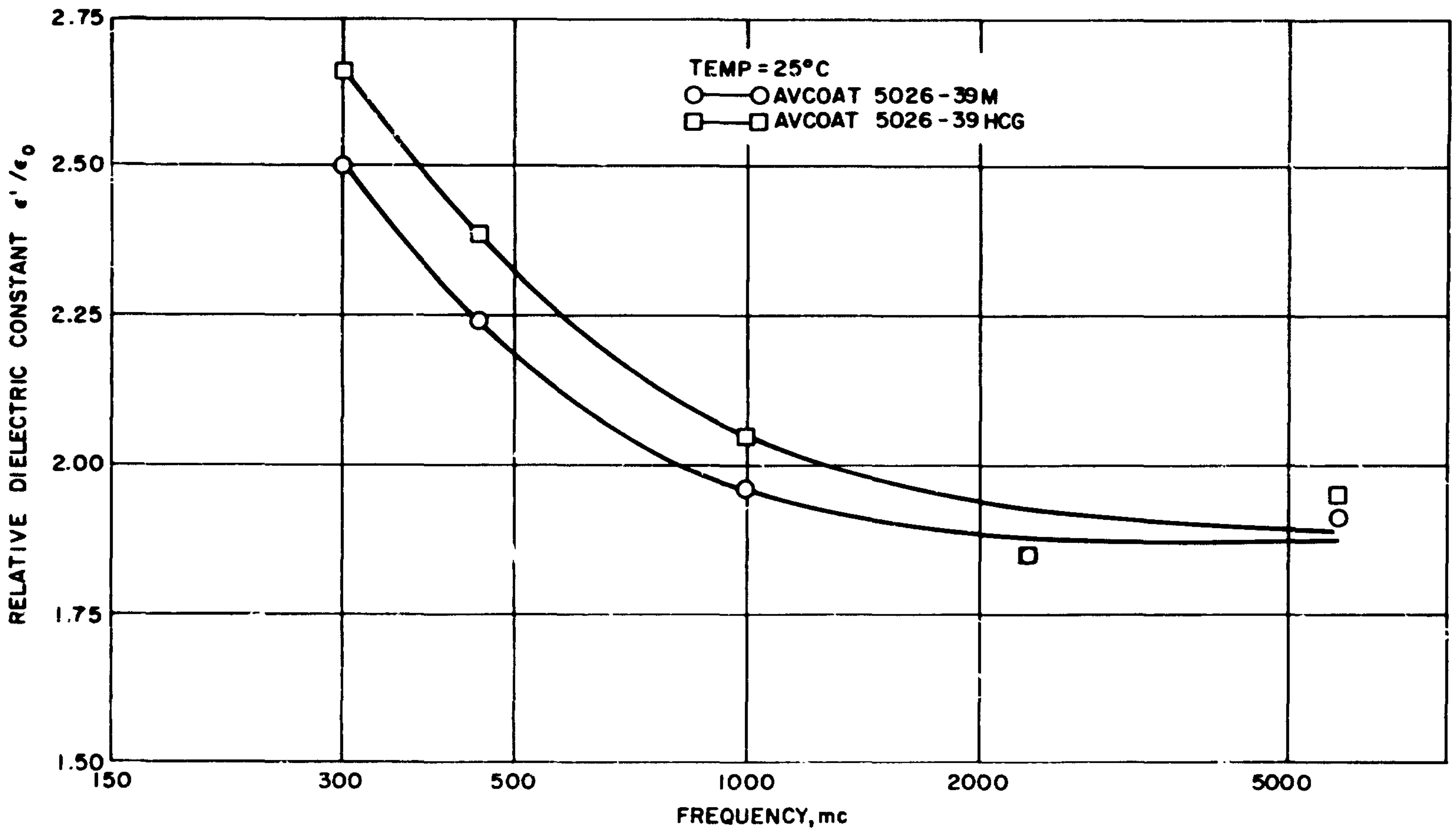

85-6930

Figure 6 DIELECTRIC CONSTANT, 5026-39M AND HCG AT 25°C aluminum oxide coating on the honeycomb walls did not have a significant effect upon the dielectric constant and loss tangent. This was observed by comparing the -39 M with the -39 HCG measurements.

d. Measurements and Results

The mid-temperature range complex dielectric constant test procedures are given in Appendix B. All the mid-temperature measurements were made using the Rohde and Schwarz dielectrometer as described in the test procedures. The samples used in the dielectrometer were machined to a tolerance of ± 0.001 inch. The results of the 25° C measurements (plotted in Figures 6 and 7a) are as follows:

Frequency (Mc)	Material	ϵ'/ϵ_0	Loss Tangent
300	-39 HCG	2.66	0.073
300	-39 M	2.50	0.082
450	-39 HCG	2.39	0.091
450	-39 M	2.24	0.096
1000	-39 HCG	2.05	0.050
1000	-39 M	1.96	0.047
1200	-39 HCG	1.85	0.020
2200	-39 M	1.85	0.022
5800	-39 HCG	1.95	0.027
5800	-39 M	1.91	0.024

The charred samples for the 25° C measurements could not be machined prior to charring because of a 20 percent dimensional shrinkage during charring. Oversized virgin samples of Avcoat 5026-39 HCG were charred for 15 hours at 1000° F in an inert atmosphere. The resulting charred samples were soft and porous and presented some difficulty in machining. However, the material was satisfactorily machined and the samples were measured. The results of the meaurements are given below

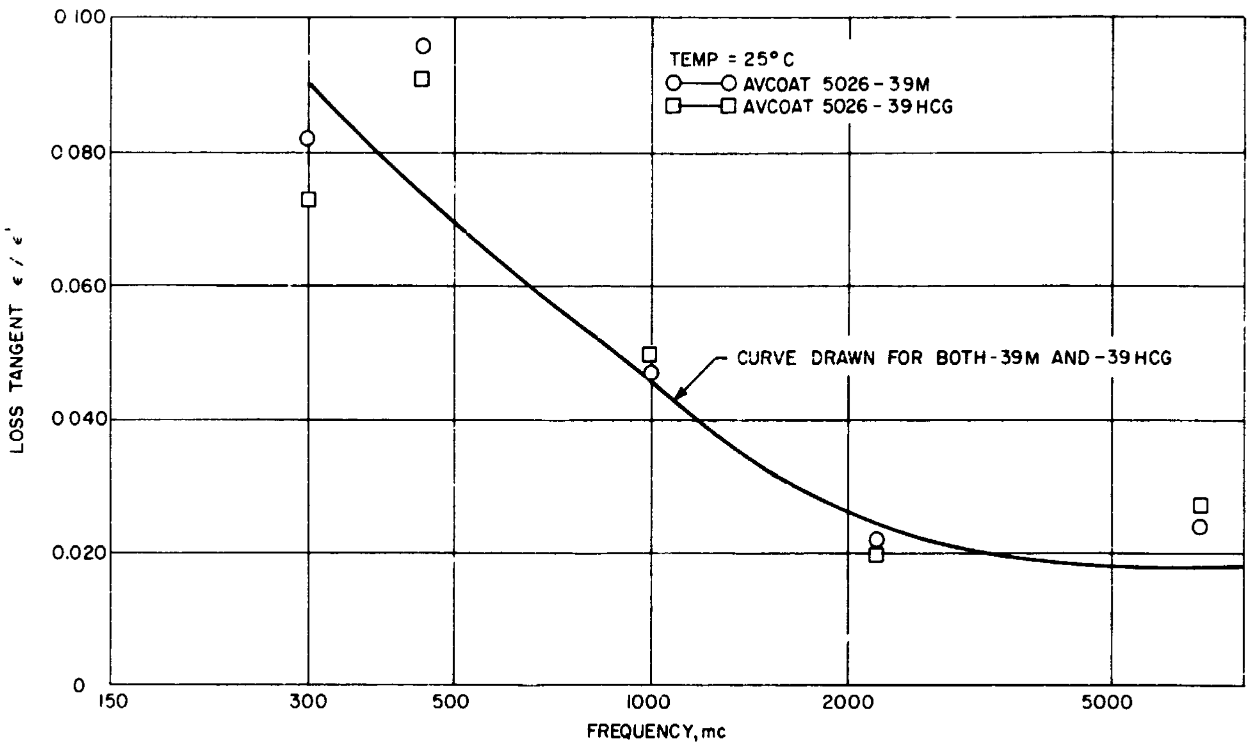

85 - 6931

Figure 7a LOSS TANGENT, 5026-39M AND HCG AT 25°C

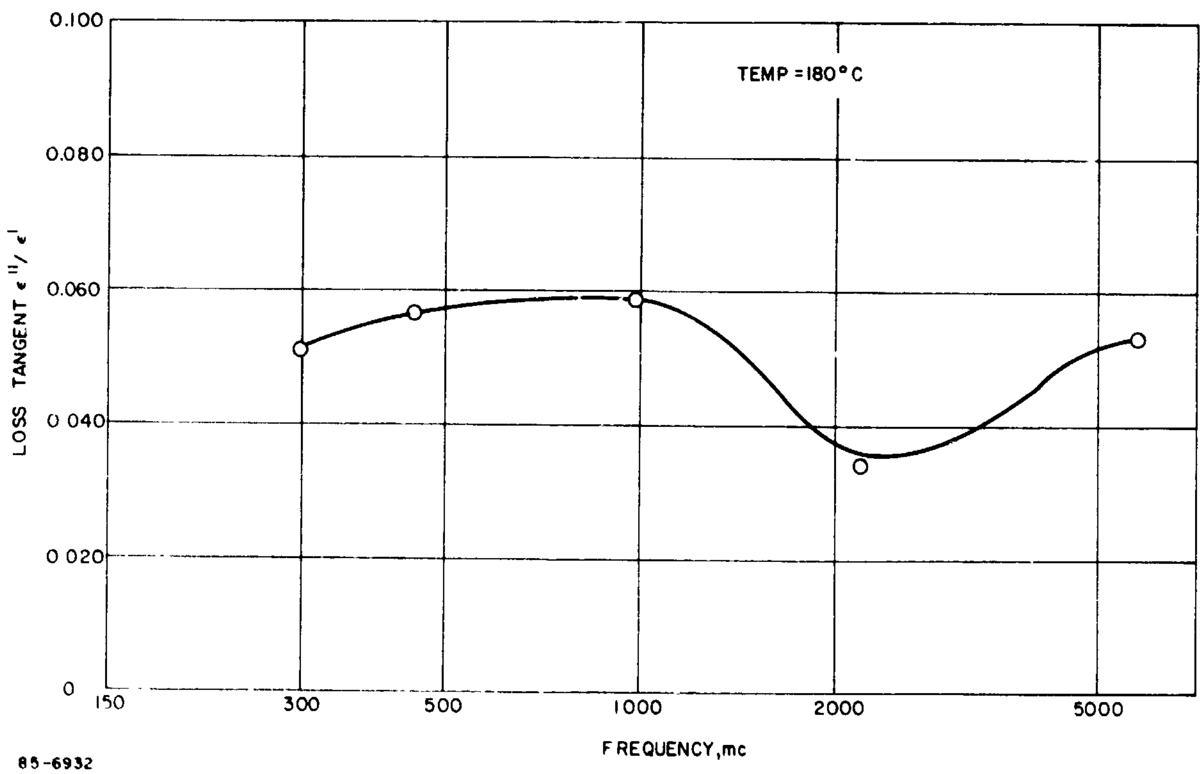

85 -6932

Figure 7b LOSS TANGENT, 5026-39 HCG AT 180°C

Charred Avcoat 5026-39 HCG Heated for 15 hours at 1000° F

Frequency (kMc)	ϵ'/ϵ_0	Loss Tangent
5.8	1.69	0.031
2.2	1.71	0.040
1.0	1.78	0.065
0.45	1.98	0.146
0.30	1.66	0.0847
0.30	1.72	0.0734

It was somewhat astounding to find that the dielectric values had not changed substantially from the uncharred case. The appearance of the charred samples was that of a fiberglass matrix with the glass fibers covered with carbon.

Further measurements will show that the char layer becomes very lossy when heated to higher temperatures. This will be discussed in the high temperature measurements section of this report.

Samples of the virgin Avcoat 5026-39 HCG were measured at 180° C in the Rohde and Schwarz dielectrometer using a temperature-controlled sample holder. One of the major problems encountered in measuring the samples at 180° C was that the heat caused further curing of the sample and the dielectric properties changed during the measurement. This problem was resolved by fully curing the sample at 180° C. Once the sample was cured, final measurements were made (see figures 7b and 8 and the tabulation below)

Frequency (kMc)	ϵ'/ϵ_0	Loss Tangent
5.8	1.836	0.0532
2.2	1.797	0.0344
1.0	1.880	0.0589
0.45	2.044	0.0566
0.30	2.048	0.0517

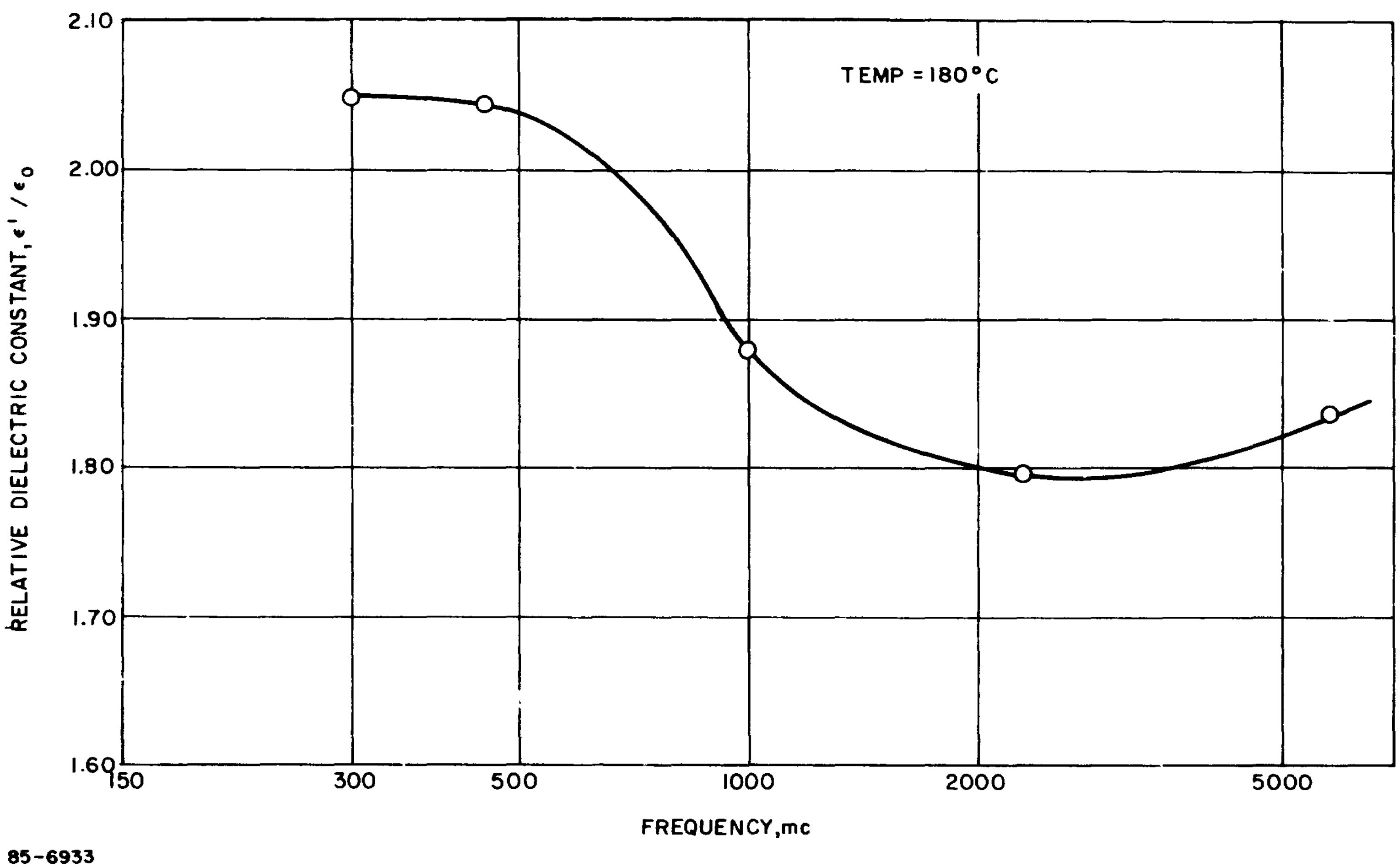

Figure 8 DIELECTRIC CONSTANT 5026-39 HCG AT 180°C

4. Cryogenic Temperature Range Measurements

a. Introduction

The intent of cryogenic temperature range measurement was to determine the dielectric constant and loss tangent of Avcoat 5026-39 HCG heat shield material at 4° K over a frequency range from 300 to 5800 Mc. This required the design and development of a sample holder that could be immersed in liquid helium. The sample holder was designed so that it would adapt to the Rohde and Schwarz equipment.

b. Cryogenic Sample Holder

A diagram of the sample holder is shown in figure 9. The sample holder was designed so that it would adapt to a helium dewar (figure 10) and the Rohde and Schwarz dielectrometer. The walls of the inner and outer conductor of the coaxial line were made of 0.020-inch stainless steel to minimize thermal conductivity. An indium washer was used as a seal to prevent leakage of the liquid helium into the sample holder. The hollow portion of the inner conductor allowed the liquid helium to cool the sample from the inside. A small hole in the inner conductor above the level of the liquid helium allowed a flow of gaseous helium through the empty portion of the sample holder. This gaseous flow purged the air from the sample holder, flushing it out through the top of the sample holder. A device to measure the liquid helium level was inserted through the brass cover plate. The performance of the cryogenic sample holder was checked at room temperature by measuring the dielectric constant and loss tangent of a sample using, in turn, the Rohde and Schwarz holder and the cryogenic sample holder and comparing the results. The test showed that the sample holder performed satisfactorily.

c. Measurements and Results

The cryogenic measurements were made by the method described in the cryogenic temperature range complex dielectric constant test procedures for Avcoat 5026-39 (appendix C).

Losses added to the Rohde and Schwarz setup by the addition of cables and connectors to the cryogenic sample holder did not allow measurement of loss tangents less than 0.005. It was determined from the data that the loss tangents were less than 0.005 for all four frequencies. Line losses did not affect the real part of the dielectric constant measurements. The reduced results are listed below and graphed in figure 11.

Frequency (kMc)	Relative Dielectric Constant ϵ'/ϵ_0
0.30	1.810
0.45	1.817
2.20	1.812
5.80	1.844

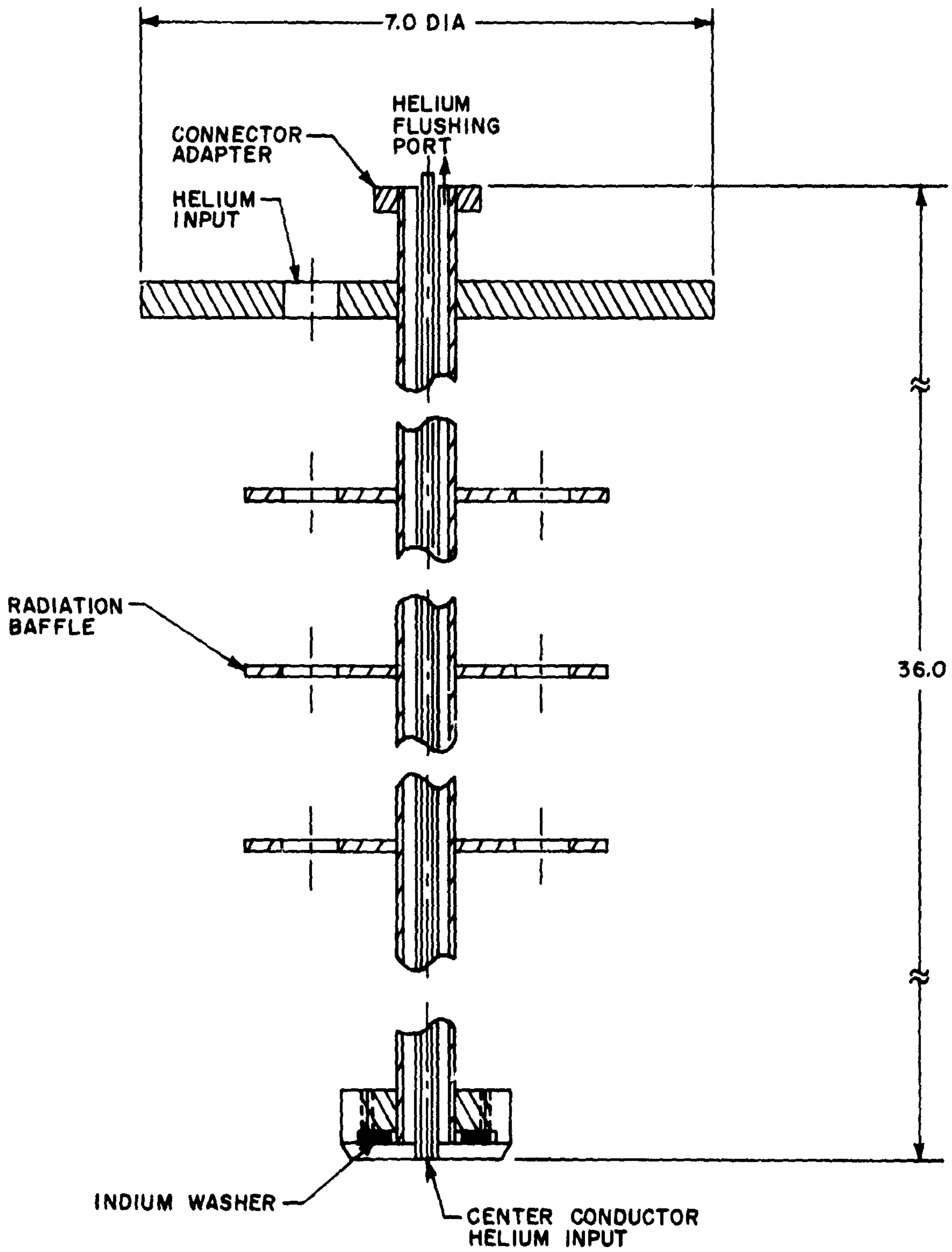

85-6934

Figure 9 CRYOGENIC SAMPLE HOLDER

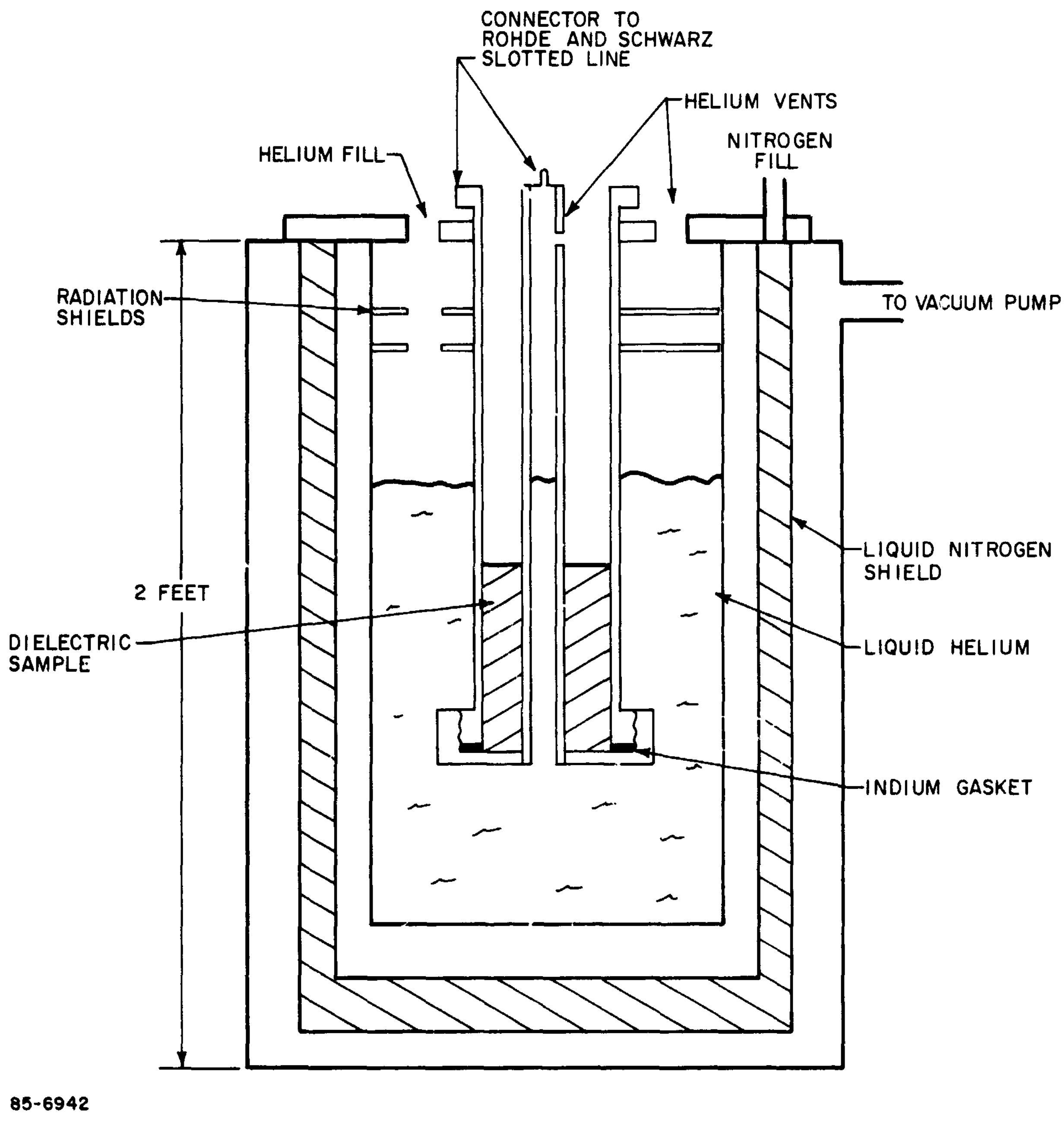

Figure 10 CRYOGENIC SAMPLE HOLDER AND DEWAR

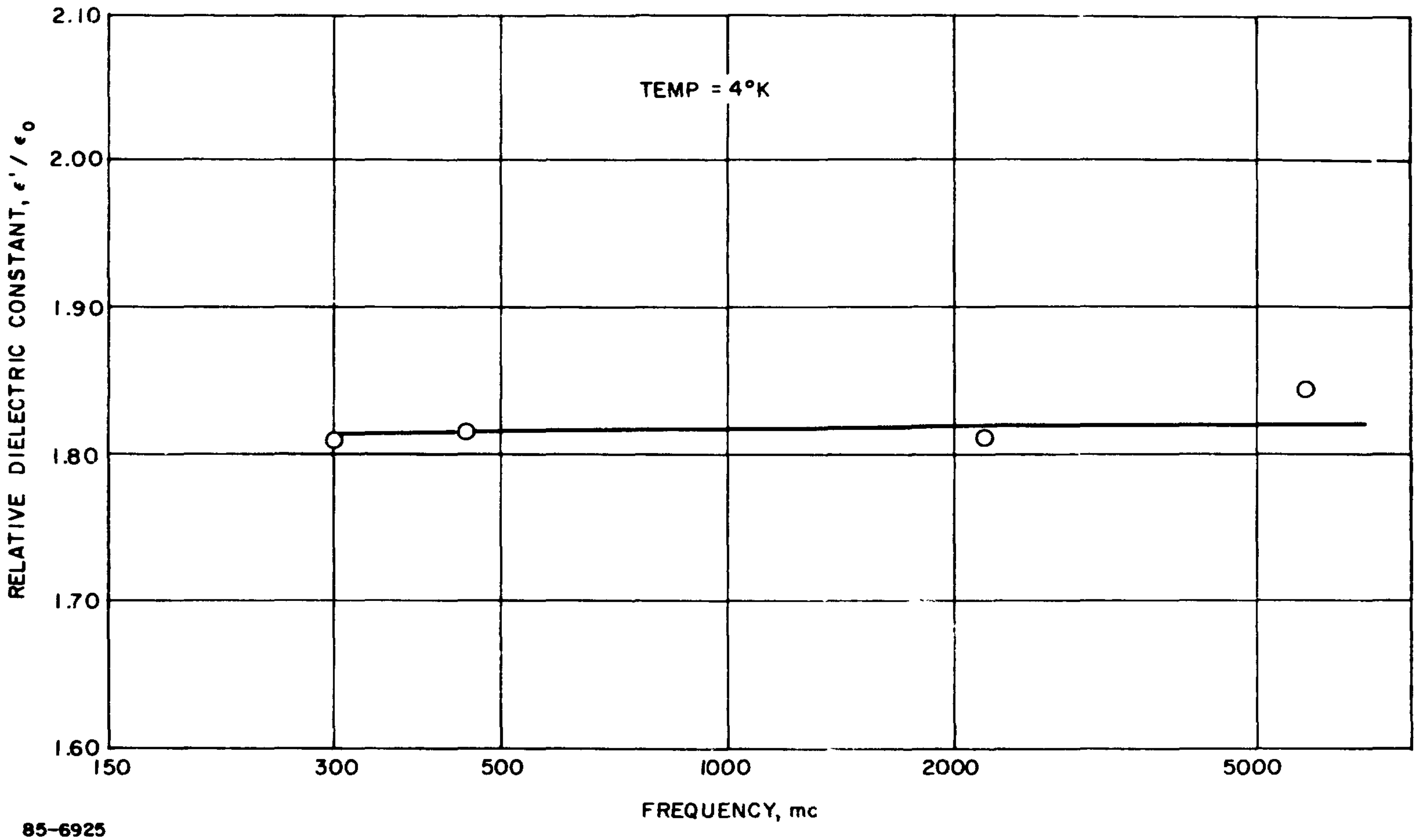

Figure 11 DIELECTRIC CONSTANT 5026-39 HCG 4°K

Note that the dielectric constants are lower than they were at room temperature and are less frequency dependent.

5. High Temperature Range Measurements

a. Introduction

The intent of the high-temperature range measurement was to determine the electrical properties of the Avcoat 5026-39M heat shield material at 2000° K in a frequency range from 250 to 5800 Mc. The measurements were to be made by the cavity perturbation method. It was discovered that the conductivity of the char layer was so high as to make measurement by this nethod impossible. Conductivity measurements had to be taken to determine the electrical properties of the samples.

b. High-Temperature Oven

The high-temperature oven had thirty-two 18-inch GE quartz heater lamps capable of producing 160 kw total output. The lamps were stationed in blocks of eight around the periphery of an octogonal wall of polished aluminum (see figure 12). Highly reflective walls directed radiation upon the sample, allowing it to reach a temperature of 2000° K. The oven was purged with nitrogen during heating to prevent oxidation of the sample.

The samples were hung from a pair of spring-loaded pincers located at the top of the oven (see figure 12 and 12a). The test set-ups shown in figure 13 with the oven mounted on top of the cavities. The sample was heated to the desired temperature and then released so it passed through the hole at the bottom of the oven and into the cavities below.

The internal temperature of the sample was not measured directly with each test due to complications that arise in removing the thermocouple from the center of the sample before it is dropped through the cavity. The sample temperature was measured indirectly by relating the sample temperature to a thermocouple located outside the sample. This was done by placing a thermocouple outside the sample along with one inside the sample and measuring the rise times of both thermocouples until they reached an equilibrium at 2000° K. Using these two curves the thermocouple outside the sample was used to monitor the sample temperature.

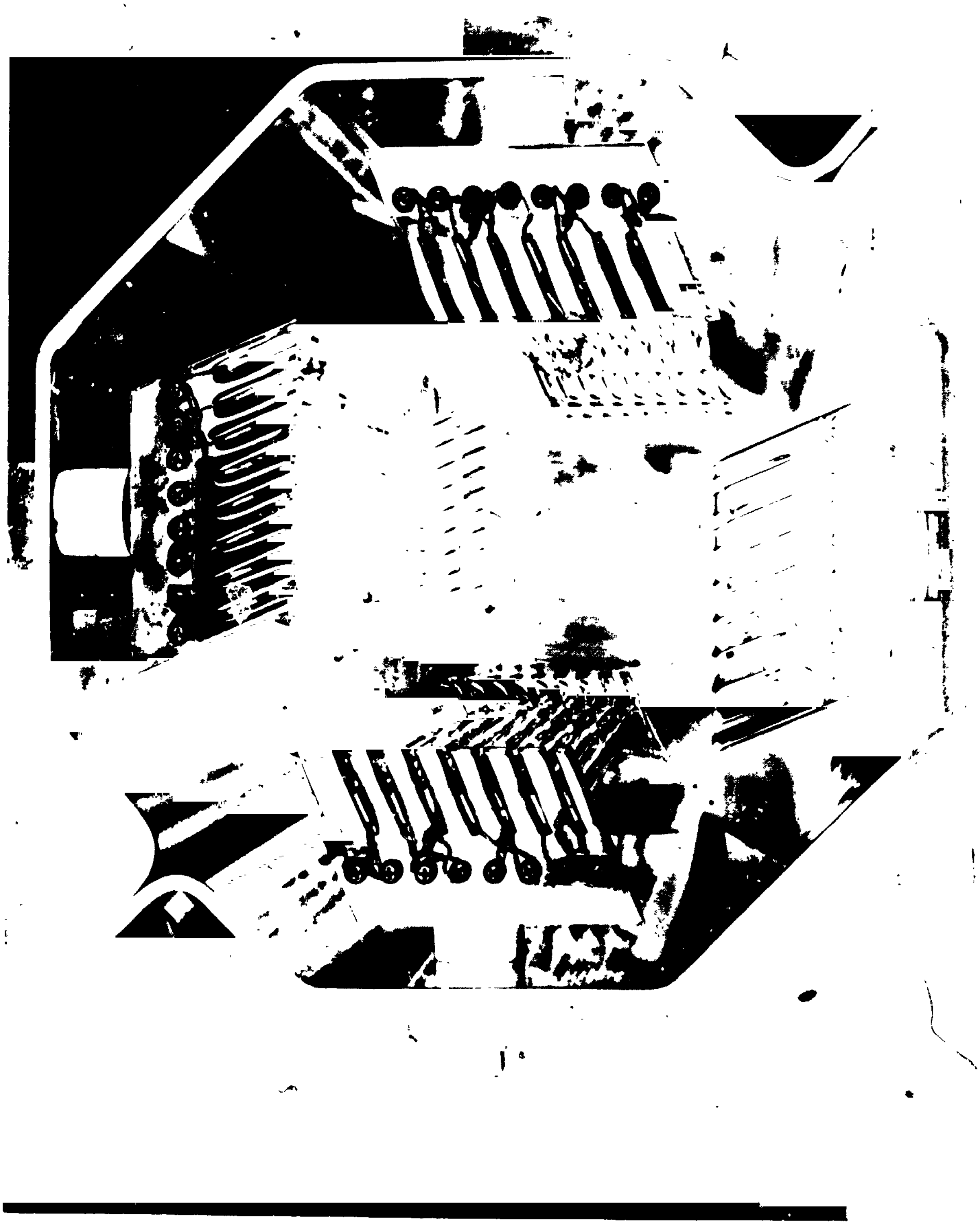

Figure 12 TOP VIEW OF HIGH-TEMPERATURE OVEN

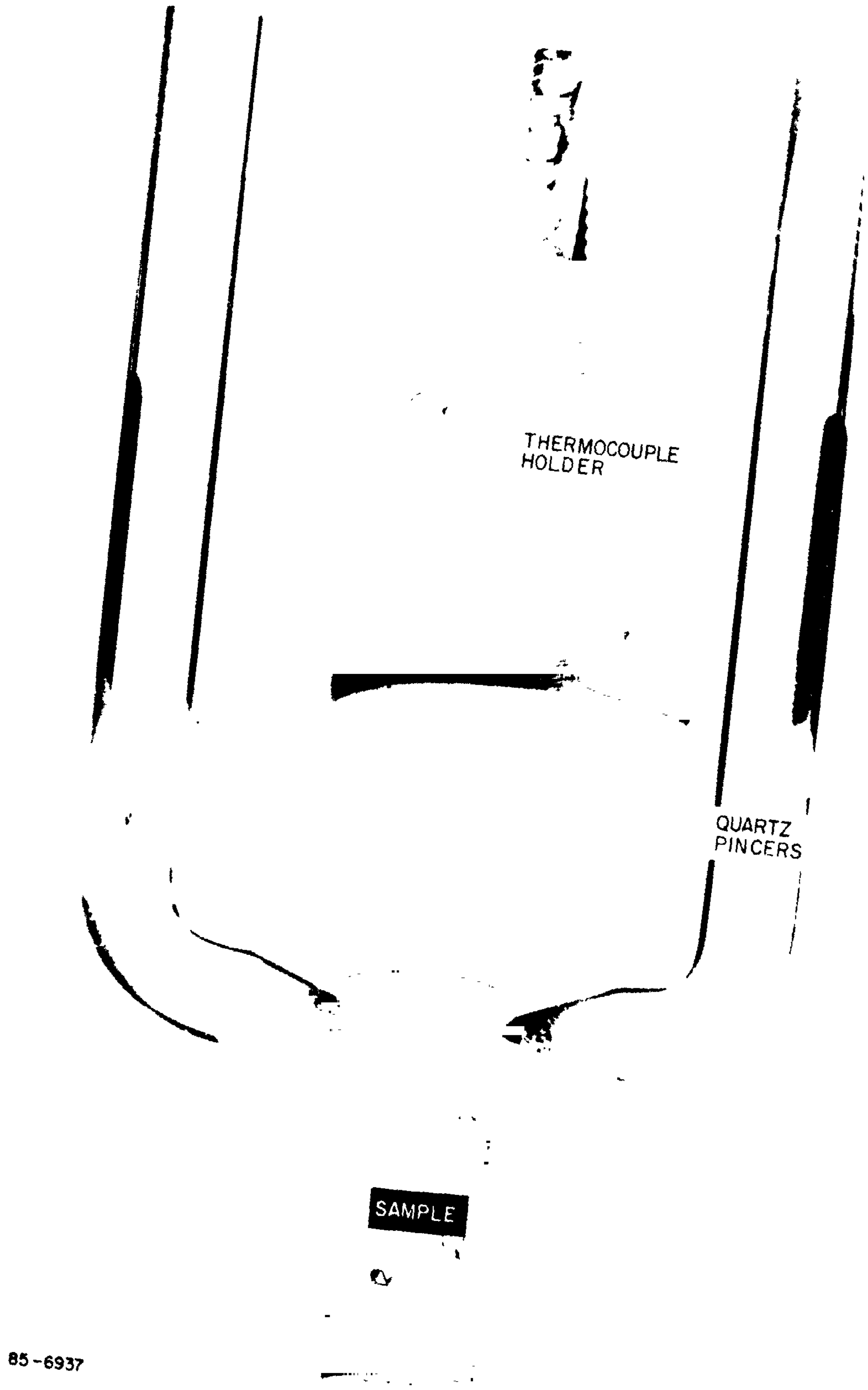

Figure 12a SAMPLE HOLDER AND SAMPLE

Figure 13 HIGH-TEMPERATURE TEST EQUIPMENT

c. Measurements and Results

The initial measurements were made according to the high-temperature range complex dielectric constant test procedures given in appendix D. When it was discovered that the samples were highly conductive, conductivity measurements were made on the material to determine the skin depth of the samples. The skin depth was so small that it was impractical to make the radius of the sample equal to the skin depth as required for cavity measurements (see Limitations of Measuring Range in test procedures). Therefore, the cavity perturbation method had to be abandoned.

Previous measurements on the samples precharred at 1000° F led us to believe that the skin depth would not present any probelm. However, the high impulse heating of the samples at 2000° K caused them to take on high values of ϵ''/ϵ' .

Conductivity measurements were subsequently taken at room temperature with an impedance bridge to determine the skin depth and ϵ''/ϵ' . The results of these measurements are given below.

Avcoat 5026-39M Precharred at 1000° F and Then Reheated for 45 Seconds at 2000° K		
Frequency (Mc)	Skin Depth (cm)	Loss Tangent
300	0.130	2.98×10^{4}
1000	0.071	8.93×10^{3}
3000	0.041	2.98×10^{3}

Virgin Avcoat 5026-39M Heated for 45 Seconds at 2000° K		
Frequency (Mc)	Skin Depth (cm)	Loss Tangent
300	0.121	3.43×10^{4}
1000	0.048	1.03×10^{3}
3000	0.038	3.43×10^{3}

The minimum dc conductivity of the samples measured was 4.96 x 10^3 mho/meter. Comparing this conductivity with the conductivities of metals (σ = 1.0 x 10^7 to 10 x 10^7 mho/meter) and dielectrics (σ = 1 x 10^{-8} to 1 x 10^{-17}) mho/meter), it can be seen that the samples will have electrical properties more like those of metals than dielectrics.

Keeping this in mind let us examine the flux density $\bar{D}$ in the dielectric:

$$\bar{D} = \epsilon_o \bar{E} + \bar{P} \tag{10}$$

where

ϵ_o = permittivity of a vacuum

$\bar{E}$ = field in dielectric

$\bar{P}$ = polarization

Rewriting equation (10):

$$\bar{D} = \left(\epsilon_o + \frac{\bar{P}}{\bar{E}}\right) \bar{E} \tag{11}$$

also

$$\bar{D} = \epsilon \bar{E}$$

and it follows that

$$\epsilon = \epsilon_o + \frac{\bar{P}}{\bar{E}} \tag{12}$$

where

ϵ = permittivity of dielectric.

In a conductor P is negligibly small enough such that we can write

P = 0(reference 5), and

substituting into equation (12), we obtain the dielectric constant of a conductor:

$$\epsilon_{conductor} = \epsilon_o$$

[5] King, R. K., Fundamental Electromagnetic Theory, Dover Publications, Inc., New York N. Y. (1963), p. 148.

The relative dielectric constant then becomes 1.

Since the conductivity of the samples is approaching that of the metals, their relative dielectric constants may be assumed to be a value of 1. With this information, the attenuation may be calculated. The equation for attenuation is as follows:[6]

$$a = 8.686a = 1.287 \times 10^{-9} f \left[K' \left(\sqrt{1 + (K''/K')^2} - 1\right)\right]^{1/2} \text{ db/cm} \qquad (13)$$

where

$$K' = \epsilon'/\epsilon_o$$

$$K'' = \epsilon''/\epsilon_o \quad .$$

Since

$$\frac{K''}{K'} >> 1$$

$$a = 1.287 \times 10^{-9} f (K'')^{1/2} \text{ db/cm} \qquad (14)$$

The attenuation for material and frequencies given previously in this section is then computed as follows:

Frequency (Mc)	Avcoat 5026-39M Precharred to 1000° F and Heated for 45 Seconds at 2000° K Attenuation (db/cm)	Virgin Avcoat 5026-39M Heated for 45 Seconds at 2000° K Attenuation (db/cm)
300	67	71
1000	122	130
2200	180	193
3000	211	226

[6] Westphal, W. B., and B. B. East, Dielectric Parameters and Equivalent Circuits, Tech. Report 189, Laboratory for Insulation Research, M.I.T. AD-601-522, p. 42.

Several comments should be made about these attenuation figures. These values of attenuation are based upon plane electromagnetic wave theory for a wave traveling in a homogenous isotropic medium. Attenuation measurements made with antennas covered with charred Avcoat 5026-39M have been made and will be discussed in detail in a latter portion of this report. However, it will not be possible to relate these measurements to the calculated values. The antenna attenuation measurements are dependent not only upon propagation through the char layer but upon reflection, antenna Q, distance of char layer from the antenna aperture, and other paramet rs.

Antenna attenuation measurements were made using a 3/8-inch-thick heat shield with a thin char layer visually 0.065 inch thick over an open-ended waveguide antenna. Radiation patterns of the E plane with and without a charred heat-shield cover were integrated to obtain an average attenuation. The attenuations were 19.4 db for 300 Mc and 11.6 db at 2200 Mc for respective conductive char thicknesses of 0.039 inch and 0.028 inch.

The attenuation measured at 300 Mc was greater than that measured at 2200 MC which is contrary to the calculated plain-wave attenuations. Higher attenuations were experienced than at 2200 Mc because the conductive char is immersed in the near fields of the 300 Mc antenna and the effect on the antenna is more profound.

Although the calculated and measured attenuations cannot be compared, they both reflect the fact that the attenuation through the char layer is very high.

C. THEORETICAL STUDY

We have studied the problem of a rectangular waveguide opening into an infinite conducting plane which is covered by a dielectric layer. We have formulated the problem in a fashion similar to the integral equation technique discussed in Marcuvitz (Waveguide Handbook, 1951). The solutions are then used to obtain the aperture admittance and its radiation pattern. The variational technique for the admittance is discussed but is not used in this analysis.

1. Formulation

Consider a TE_{10} mode denoted by $B \cos \frac{\pi x}{a} e^{-i\gamma_{10}z} e^{-i\omega t}$ propagating down a rectangular wave guide. The total H_Z field including the reflected wave can then be written (neglecting a factor $e^{-i\omega t}$) as:

$$H_z = B \cos \frac{\pi x}{a} e^{+i\gamma_{10} z} + \sum_{k,l} A_{kl} \cos\left(\frac{l\pi x}{a}\right) \cos\left(\frac{k\pi y}{b}\right) e^{-i\gamma_{kl} z}$$

$$\gamma_{kl}^2 = k_o^2 - \left(\frac{l\pi}{a}\right)^2 - \left(\frac{k\pi}{b}\right)^2 \qquad (1)$$

$$k_o = \omega/C$$

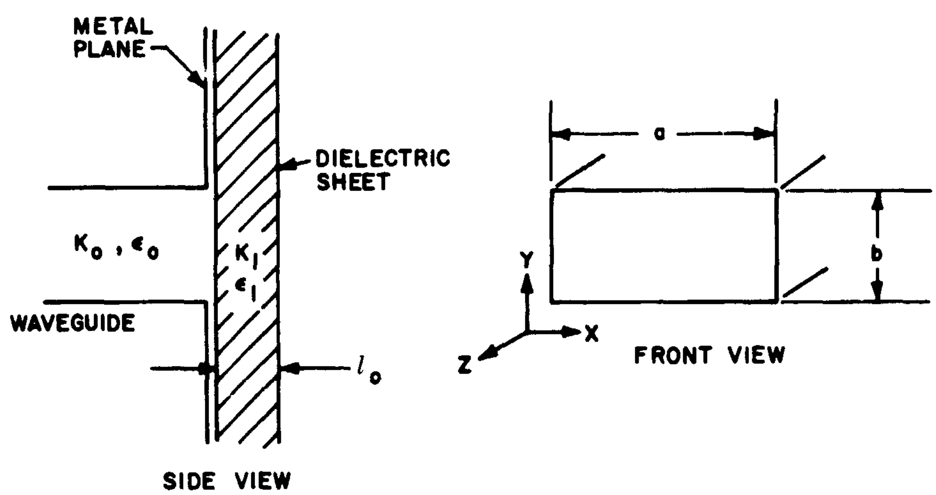

Also, it is possible that a component of E_Z will be generated in the reflected wave, even though none is present in the transmitted wave. Thus we write:

$$E_z = \sum_{k,l} B_{kl} \sin\left(\frac{l\pi x}{a}\right) \sin\left(\frac{k\pi y}{b}\right) e^{-i\gamma_{kl} z} \qquad (2)$$

The other components of the field are related to H_Z and E_Z by (for $e^{-i\gamma z}$)

$$H_x = \frac{-1}{k^2 - \gamma^2}\left[i\omega\epsilon \frac{\partial E_z}{\partial y} + i\gamma \frac{\partial H_z}{\partial x} \right]$$

$$H_y = \frac{+1}{k^2 - \gamma^2}\left[i\omega\epsilon \frac{\partial E_z}{\partial x} - i\gamma \frac{\partial H_z}{\partial y} \right] \qquad (3)$$

$$E_x = \frac{+1}{k^2 - \gamma^2}\left[-i\gamma \frac{\partial E_z}{\partial x} + i\omega\mu \frac{\partial H_z}{\partial y} \right]$$

$$E_y = \frac{-1}{k^2 - \gamma^2}\left[+i\gamma \frac{\partial E_z}{\partial y} + i\omega\mu \frac{\partial H_z}{\partial x} \right]$$

For $e^{+i\gamma z}$ we replace γ by $-\gamma$ in the above equations. Substituting equations (1) and (2) into equation (3) yields for the fields inside the waveguide:

$$H_x^{(0)} = \frac{-i\gamma_{10} B\left(\frac{\pi}{a}\right)}{k_o^2 - \gamma_{10}^2} \sin\left(\frac{\pi x}{a}\right) e^{+i\gamma_{10} z} + \sum_{k,l} \frac{\sin\left(\frac{l\pi x}{a}\right)\cos\left(\frac{k\pi y}{b}\right) e^{-i\gamma_{kl} z}}{k_o^2 - \gamma_{kl}^2}\left\{ \begin{array}{l} i\omega\epsilon_o\left(\frac{k\pi}{b}\right) B_{kl} \\ - i\gamma_{kl} A_{kl}\left(\frac{l\pi}{a}\right) \end{array} \right\} \qquad (4)$$

$$H_y^{(0)} = \sum_{k,l} \frac{\sin\left(\frac{k\pi y}{b}\right)\cos\left(\frac{l\pi x}{a}\right) e^{-i\gamma_{kl} z}}{k_o^2 - \gamma_{kl}^2}\left\{ +i\omega\epsilon_o B_{kl}\left(\frac{l\pi}{a}\right) + i\gamma_{kl}\left(\frac{k\pi}{b}\right) A_{kl} \right\} \qquad (5)$$

$$E_x^{(0)} = \sum_{k,l} \frac{\sin\left(\frac{k\pi y}{b}\right)\cos\left(\frac{l\pi x}{a}\right) e^{-i\gamma_{kl} z}}{k_o^2 - \gamma_{kl}^2}\left\{ -i\gamma_{kl}\left(\frac{l\pi}{a}\right) B_{kl} - i\omega\mu_o\left(\frac{k\pi}{b}\right) A_{kl} \right\} \qquad (6)$$

$$E_y^{(0)} = \frac{+i\omega\mu_o B}{k_o^2 - \gamma_{10}^2}\left(\frac{\pi}{a}\right)\sin\left(\frac{\pi x}{a}\right)e^{+i\gamma_{10}z}$$

$$+\sum_{k,l}\frac{\sin\left(\frac{l\pi x}{a}\right)\cos\left(\frac{k\pi y}{b}\right)e^{-i\gamma_{kl}z}}{k_o^2 - \gamma_{kl}^2}\left\{+i\omega\mu_o\left(\frac{l\pi}{a}\right)A_{kl} - i\gamma_{kl}\left(\frac{k\pi}{b}\right)B_{kl}\right\} \quad (7)$$

Now for the fields inside the slab we may write:

$$H_z^{(1)} = \int_{-\infty}^{\infty} d\xi \int_{-\infty}^{\infty} d\eta\, e^{-i(\xi x + \eta y)}\left[K(\xi,\eta)e^{+ih_1 z} + L(\xi,\eta)e^{-ih_1 z}\right] \quad (8)$$

$$E_z^{(1)} = \int_{-\infty}^{\infty} d\xi \int_{-\infty}^{\infty} d\eta\, e^{-i(\xi x + \eta y)}\left[M(\xi,\eta)e^{+ih_1 z} + R(\xi,\eta)e^{-ih_1 z}\right] \quad (9)$$

$$h_1^2 = k_1^2 - \xi^2 - \eta^2 \qquad k_1 = \frac{\omega}{c}\sqrt{\epsilon}$$

So that using equation (3) we may write:

$$H_x^{(1)} = \int_{-\infty}^{\infty}\int_{-\infty}^{\infty} d\xi d\eta\, \frac{e^{+i(\xi x + \eta y)}}{k_1^2 - h_1^2}\, e^{+ih_1 z}\{\epsilon\omega\eta M - h_1\xi K\}$$

$$+\int_{-\infty}^{\infty}\int_{-\infty}^{\infty}\frac{d\xi d\eta\, e^{+i(\xi x + \eta y)}}{k_1^2 - h_1^2}\, e^{-ih_1 z}\{\epsilon\omega\eta R + h_1\xi L\} \quad (10)$$

$$H_y^{(1)} = \int_{-\infty}^{\infty}\int_{-\infty}^{\infty}\frac{d\xi d\eta\, e^{+i(\xi x + \eta y)}}{k_1^2 - h_1^2}\, e^{+ih_1 z}[-\omega\epsilon\xi M - \eta h_1 K]$$

$$+\int_{-\infty}^{\infty}\int_{-\infty}^{\infty}\frac{d\xi d\eta\, e^{+i(\xi x + \eta y)}}{k_1^2 - h_1^2}\, e^{-ih_1 z}[-\omega\epsilon\xi R + \eta h_1 L] \quad (11)$$

$$E_x^{(1)} = \int_{-\infty}^{\infty}\int_{-\infty}^{\infty} \frac{d\xi d\eta\, e^{+i(\xi x + \eta y)}}{k_1^2 - h_1^2} e^{+ih_1 z} [-\xi h_1 M - \omega\mu_o \eta K]$$

$$+ \int_{-\infty}^{\infty}\int_{-\infty}^{\infty} \frac{d\xi d\eta\, e^{+i(\xi x + \eta y)}}{k_1^2 - h_1^2} e^{-ih_1 z} [\xi h_1 R - \omega\mu_o \eta L] \qquad (12)$$

$$E_y^{(1)} = \int_{-\infty}^{\infty}\int_{-\infty}^{\infty} \frac{d\xi d\eta\, e^{+i(\xi x+\eta y)}}{k_1^2 - h_1^2} e^{+ih_1 z} [-\eta h_1 M + \omega\mu_o \xi K]$$

$$+ \int_{-\infty}^{\infty}\int_{-\infty}^{\infty} \frac{d\xi d\eta\, e^{+i(\xi x+\eta y)}}{k_1^2 - h_1^2} e^{-ih_1 z} [\eta h_1 R + \omega\mu_o \xi L] \qquad (13)$$

Next we must write the fields outside the slab:

$$H_Z^{(2)} = \int_{-\infty}^{\infty}\int_{-\infty}^{\infty} d\xi d\eta\, e^{+i(\xi x+\eta y)}\, T(\xi,\eta)\, e^{+ih_2 z} \qquad (14)$$

$$E_Z^{(2)} = \int_{-\infty}^{\infty}\int_{-\infty}^{\infty} d\xi d\eta\, e^{+i(\xi x+\eta y)}\, S(\xi,\eta)\, e^{+ih_2 z} \qquad (15)$$

$$h_2^2 = k_o^2 - \xi^2 - \eta^2$$

so that the tangential components become:

$$H_x^{(2)} = \int_{-\infty}^{\infty}\int_{-\infty}^{\infty} \frac{d\xi d\eta}{k_o^2 - h_2^2}\, e^{+i(\xi x+\eta y)}\, e^{+ih_2 z} [\omega\epsilon_o \eta S - \xi h_2 T] \qquad (16)$$

$$H_y^{(2)} = \int_{-\infty}^{\infty} \int_{-\infty}^{\infty} \frac{d\xi d\eta}{k_o^2 - h_2^2} e^{+ih_2 z} e^{+i(\xi x+\eta y)}$$

$$\cdot[-\omega \epsilon_o \xi S(\xi,\eta) - \eta h_2 T(\xi,\eta)] \tag{17}$$

$$E_x^{(2)} = \int_{-\infty}^{\infty} \int_{-\infty}^{\infty} \frac{d\xi d\eta}{k_o^2 - h_2^2} e^{+ih_2 z} e^{+i(\xi x+\eta y)}$$

$$[-\xi h_2 S(\xi,\eta) - \eta\omega\mu_o T(\xi,\eta)] \tag{18}$$

$$E_y^{(2)} = \int_{-\infty}^{\infty} \int_{-\infty}^{\infty} \frac{d\xi d\eta}{k_o^2 - h_2^2} e^{+i(\xi x+\eta y)} e^{+ih_2 z}$$

$$\circ[-h_2 \eta S(\xi,\eta) + \omega\mu_o \xi T(\xi,\eta)] \tag{19}$$

Next we need to match boundary conditions at $z = l_o$. We obtain:

a. From the continuity of E_x:

$$e^{+ih_1 l_o}(-\xi h_1 M - \omega\mu_o\eta K) + e^{-ih_1 l_o}(\xi h_1 R - \omega\mu_o\eta L)$$

$$= e^{+ih_2 l}(-\xi h_2 S - \eta\omega\mu_o T) \tag{20}$$

b. From the continuity of E_y:

$$e^{+ih_1 l_o}(-\eta h_1 M + \omega\mu_o \xi K) + e^{-ih_1 l_o}(\eta h_1 R + \omega\mu_o \xi L)$$

$$= e^{+ih_2 l_o}(-h_2 \eta S + \omega\mu_o \xi T) \tag{21}$$

c. From the continuity of H_x:

$$e^{+ih_1 l_o}[\epsilon\omega\eta M - h_1 \xi K] + e^{-ih_1 l_o}[\epsilon\omega\eta R + \xi h_1 L]$$

$$= e^{+ih_2 l_o}[\omega\epsilon_o\eta S - \xi h_2 T] \quad \text{and} \tag{22}$$

d. From the continuity of H_y:

$$e^{+ih_1 l_o}[-\omega\epsilon\xi M - \eta h_1 K] + e^{-ih_1 l_o}[-\omega\epsilon\xi R + \eta h_1 L]$$

$$= e^{+ih_2 l_o}[-\xi\omega\epsilon_o S - \eta h_2 T] \tag{23}$$

Solving for M, K, S, and T in terms of R and L in equations (20) through (23) yields:

$$\begin{aligned}
K &= \hat{U}L & &L \text{ from } H_Z \\
M &= UR & &R \text{ from } E_Z \\
S &= WR & &S \text{ from } E_Z \\
T &= \hat{W}L & &T \text{ from } H_Z
\end{aligned} \tag{24}$$

where

$$W = \left(\frac{2h_1\epsilon_r}{h_1 - \epsilon_r h_2}\right) e^{-i(h_1+h_2)l_o} \qquad U = e^{-i2h_1 l_o}\left(\frac{h_1 + \epsilon_r h_2}{h_1 - \epsilon_r h_2}\right)$$

$$\hat{W} = e^{-i(h_1+h_2)l_o}\left(\frac{2h_1}{h_1 - h_2}\right) \qquad \hat{U} = e^{-i2h_1 l_o}\left(\frac{2h_1}{h_1 - h_2}\right)$$

We may note from equation (24) that there is no coupling between the E_Z and H_Z modes at the outer edge of the dielectric slab.

Using equation (24) to substitute for M and K in terms of R and L in equations (10) through (13) we may write for the boundary conditions at $Z = 0$.

e. From the continuity of Hx:

$$\int_{-\infty}^{\infty}\int_{-\infty}^{\infty} \frac{d\xi d\eta}{\xi^2+\eta^2} e^{+i(\xi x+\eta y)} [\epsilon\omega\eta (1+U) R + h_1 \xi (1-\hat{U}) L]$$

$$= -A_o \sin\left(\frac{\pi x}{a}\right) - \sum_{k,l} \sin\left(\frac{l\pi x}{a}\right) \cos\left(\frac{k\pi y}{b}\right)\left[i\omega\epsilon_o\left(\frac{k\pi}{b}\right) Y_{kl} \right. \quad (25)$$

$$\left. - i\gamma_{kl}\left(\frac{l\pi}{a}\right) Z_{kl}\right]$$

$0 \leq x \leq a$

$0 \leq y \leq b$

f. From the continuity of Hy:

$$\int_{-\infty}^{\infty}\int_{-\infty}^{\infty} \frac{d\xi d\eta}{\xi^2+\eta^2} e^{+i(\xi x+\eta y)} [-\omega\epsilon\xi R(1+U) + \eta n_1 L (1-\hat{U})]$$

$$= \sum_{k,} \sin\left(\frac{k\pi y}{b}\right) \cos\left(\frac{l\pi x}{a}\right) \cdot \left\{ + i\omega\epsilon_o\left(\frac{l\pi}{a}\right) Y_{kl} + i\gamma_{kl}\left(\frac{k\pi}{b}\right) Z_{kl} \right\} \quad (26)$$

$0 \leq x \leq a$

$0 \leq y \leq b$

g. From the continuity of Ex:

$$\int_{-\infty}^{\infty}\int_{-\infty}^{\infty} \cdot\frac{d\xi d\eta\, e^{+i(\xi x+\eta y)}}{\xi^2+\eta^2} [\xi h_1 R (1-U) - \omega\mu_o\eta L (1+\hat{U})]$$

$$= I(x,y) \sum_{k,l} \sin\left(\frac{k\pi y}{b}\right) \cos\left(\frac{l\pi x}{a}\right) \left[- i\gamma_{kl}\left(\frac{l\pi}{a}\right) Y_{kl} - i\omega\mu_o \left(\frac{k\pi}{b}\right) Z_{kl}\right]$$

(27)

h. From the continuity of E_y:

$$\int_{-\infty}^{\infty}\int_{-\infty}^{\infty} \frac{d\xi d\eta\, e^{+i(\xi x+\eta y)}}{\xi^2+\eta^2}\left[\eta h_1 R(1-U)+\omega\mu\xi L(1+\hat{U})\right]$$

$$= I(x,y)\left\{-B_o \sin\left(\frac{\pi x}{a}\right)+\sum_{k,l}\sin\left(\frac{l\pi x}{a}\right)\cos\left(\frac{k\pi y}{b}\right)\left[+i\omega\mu_o\left(\frac{l\pi}{a}\right)Z_{kl}\right.\right.$$

$$\left.\left. - i\gamma_{kl}\left(\frac{k\pi}{b}\right)Y_{kl}\right]\right. \qquad (28)$$

where

$$I(x,y) = \begin{cases} 1 & 0 \le x \le a \\ & 0 \le y \le b \\ 0 & \text{elsewhere} \end{cases} \qquad A_o \equiv \frac{i\gamma_{10} B\pi/a}{k_o^2-\gamma_{10}^2}$$

$$B_o \equiv \frac{-i\omega\mu_o B}{k_o^2-\gamma_{10}^2}$$

From equation (27) we may write:

$$\frac{\xi h_1 R(1-U)-\omega\mu\eta L(1+\hat{U})}{\xi^2+\eta^2} = G_o \qquad (29)$$

while from equation (28) we get:

$$\frac{\xi h_1 R(1-U)+\omega\mu\xi L(1+\hat{U})}{\xi^2+\eta^2} = F_o \qquad (30)$$

where G_o and F_o are defined as:

$$(2\pi)^2 G_o = \sum_{k,l}\int_0^a dx\int_0^b dy\, e^{-i(\xi x+\eta y)}\sin\left(\frac{k\pi y}{b}\right)\cos\left(\frac{l\pi x}{a}\right)\left[-i\gamma_k\left(\frac{l\pi}{a}\right)Y_{kl}\right.$$

$$\left.-i\omega\mu_o\left(\frac{k\pi}{b}\right)Z_{kl}\right]$$

$$(2\pi)^2 F_o = -\underline{B_o} \int_0^a dx \int_0^b dy\, e^{-i(\xi x+\eta y)} \sin\left(\frac{\pi x}{a}\right)$$

$$+ \sum_{k,l} \int_0^a dx \int_0^b dy\, e^{-i(\xi x+\eta y)} \sin\left(\frac{l\pi x}{a}\right) \cos\left(\frac{k\pi y}{b}\right) \left[+i\omega\mu_o\left(\frac{l\pi}{a}\right) Z_{kl} - i\gamma_{kl}\left(\frac{k\pi}{b}\right) Y_{kl}\right]$$

Solving equations (29) and (30) for L and R, we obtain.

$$h_1 R(1-U) = \xi G_o + \eta F_o \tag{31}$$

$$\omega\mu_o L(1+\hat{U}) = \xi F_o - \eta G_o \; . \tag{32}$$

Performing the integrations over X and Y in G_o and F_o and substituting the results into equations (31) and (32) yields:

$$(2\pi)^2 h_1 R(1-U) = + \sum_{k,l} (\xi^2+\eta^2)\, \hat{W}(l,\xi,a)\, \hat{W}(k,\eta,b) \left(\frac{k\pi}{b}\right)\left(\frac{l\pi}{a}\right) \gamma_{kl} Y_{kl}$$

$$+ \sum_{k,l} \omega\mu_o \left[\left(\frac{k\pi}{b}\right)^2 \xi^2 - \left(\frac{l\pi}{a}\right)^2 \eta^2\right] Z_{kl}\, \hat{W}(l,\xi,a)\, \hat{W}(k,\eta,b)$$

$$+ B_o\left(\frac{\pi}{a}\right) \hat{W}(1,\xi,a)\, \hat{W}(0,\eta,b)\,(-i\eta^2) \tag{33}$$

and

$$(2\pi)^2 \omega\mu_o L(1+\hat{U}) = B_o\left(\frac{\pi}{a}\right)\hat{W}(1,\xi,a)\,\hat{W}(0,\eta,b)\,(-i\eta\xi)$$

$$- \omega\mu_o \sum_{k,l} \eta\xi\, \hat{W}(l,\xi,a)\, \hat{W}(k,\eta,b)\, Z_{kl} \left[\left(\frac{l\pi}{a}\right)^2 + \left(\frac{k\pi}{b}\right)^2\right] \tag{34}$$

where

$$\hat{W}(l,\xi,a) = \left[\frac{(-1)^l e^{-i\xi a} - 1}{\xi^2 - \frac{l^2\pi^2}{a^2}}\right]$$

From equations (33) and (34) we see that there is coupling between the E_Z and H_Z modes at the waveguide-slot surface.

If equations (33) and (34) are now substituted into equations (25) and (26), we get:

$$\sum_{k,l} \Big\{ \epsilon\omega \left(\frac{l\pi}{a}\right)\left(\frac{k\pi}{b}\right) \gamma_{kl} Q_o(x,y,l,k) Y_{kl} + \omega^2 \mu_o \epsilon Q_1 (x,y,l,k) Z_{kl}$$

$$- \left(\frac{l^2\pi^2}{a^2} + \frac{k^2\pi^2}{b^2}\right) Q_2(x,y,l,k) Z_{kl} + (2\pi)^2 \sin\left(\frac{l\pi x}{a}\right) \cos\left(\frac{k\pi y}{b}\right) \left[i\omega\epsilon_o \left(\frac{k\pi}{b}\right) Y_{kl} - i\gamma_{kl} \left(\frac{l\pi}{a}\right) Z_{kl} \right] \Big\}$$

$$= -(2\pi)^2 A_o \sin\left(\frac{\pi x}{a}\right) - i\omega\epsilon B_o \left(\frac{a}{\pi}\right) Q_1 (x,y,1,0) + \frac{i B_o \pi/a}{\omega\mu_o} Q_2 (x,y,1,0) \qquad (35)$$

and

$$\sum_{k,l} \Big\{ -\omega\epsilon \left(\frac{k\pi}{b}\right)\left(\frac{l\pi}{a}\right) \gamma_{kl} \hat{Q}_o (x,y,l,k) Y_{kl} - \omega^2 \mu\epsilon Z_{kl} \hat{Q}_1 (x,y,l,k)$$

$$- \left(\frac{l^2\pi^2}{a^2} + \frac{k^2\pi^2}{b^2}\right) Z_{kl} \hat{Q}_2 (x,y,l,k) - (2\pi)^2 \sin\left(\frac{k\pi y}{b}\right) \cos\left(\frac{l\pi x}{a}\right) \left[+ i\omega\epsilon_o \left(\frac{l\pi}{a}\right) Y_{kl} + i\gamma_{kl} \left(\frac{l\pi}{b}\right) Z_{kl} \right] \Big\}$$

$$= i B_o \left(\frac{a}{\pi}\right) \omega\epsilon \hat{Q}_1 (x,y,1,0) + \frac{i B_o}{\omega\mu_o} \left(\frac{\pi}{a}\right) \hat{Q}_2 (x,y,1,0) \qquad (36)$$

where

$$Q_o(x,y,l,k) = \int_{-\infty}^{\infty}\int_{-\infty}^{\infty} \frac{d\xi d\eta\,(1+U)\,\eta\,\hat{W}(l,\xi,a)\,\hat{W}(k,\eta,b)\,e^{+i(\xi x+\eta y)}}{h_1\,(1-U)}$$

$$Q_1(x,y,l,k) = \int_{-\infty}^{\infty}\int_{-\infty}^{\infty} \frac{d\xi d\eta\,(1+U)\left[\frac{k^2\pi^2}{b^2}\,\xi^2 - \frac{l^2\pi^2}{a^2}\,\eta^2\right]\eta\,\hat{W}(l,\xi,a)\hat{W}(k,\eta,b)\,e^{+i(\xi x+\eta y)}}{h_1(1-U)\,(\xi^2+\eta^2)}$$

$$Q_2(x,y,l,k) = \int_{-\infty}^{\infty}\int_{-\infty}^{\infty} \frac{d\xi d\eta\,h_1\,\xi^2\eta\hat{W}(l,\xi,a)\hat{W}(k,\eta,b)(1-\hat{U})\,e^{+i(\xi x+\eta y)}}{(\xi^2+\eta^2)\,(1+\hat{U})}$$

$$\hat{Q}_o(x,y,l,k) = \int_{-\infty}^{\infty}\int_{-\infty}^{\infty} \frac{d\xi d\eta\,(1+U)\,\xi\hat{W}(l,\xi,a)\,\hat{W}(k,\eta,b)\,e^{+i(\xi x+\eta y)}}{h_1(1-U)}$$

$$\hat{Q}_1(x,y,l,k) = \int_{-\infty}^{\infty}\int_{-\infty}^{\infty} \frac{d\xi d\eta\,(1+U)\left[\frac{k^2\pi^2}{b^2}\,\xi^2 - \frac{l^2\pi^2}{a^2}\,\eta^2\right]\xi\hat{W}(l,\xi,a)\hat{W}(k,\eta,b)\,e^{+i(\xi x+\eta y)}}{h_1\,(1-U)\,(\xi^2+\eta^2)}$$

$$\hat{Q}_2(x,y,l,k) = \int_{-\infty}^{\infty}\int_{-\infty}^{\infty} \frac{d\xi d\eta\xi\eta^2\,\hat{W}(l,\xi,a)\,\hat{W}(k,\eta,b)(1-\hat{U})\,e^{+i(\xi x+\eta y)}h_1}{(\xi^2+\eta^2)\,(1+\hat{U})}$$

Equations (35) and (36) represent a pair of coupled equations for the coefficients Y_{kl} and Z_{kl}. If these equations could be solved for Y_{kl} and Z_{kl}, then R and L could then be obtained from equations (33) and (34), and finally the coefficients T and S (of the transmitted fields) from equation (24). The difficult part of the solution is to evaluate the Q functions.

2. Some Properties of the Q Functions

Consider the expression for Q_1

$$Q_1(x,y,l,k) = \int_{-\infty}^{\infty} d\xi \int_{-\infty}^{\infty} d\eta \frac{(1+U)\left[\frac{k^2\pi^2}{b^2} \quad \xi^2 - \frac{l^2\pi^2}{a^2}\right]\eta^2 \quad \eta\, W(l,\xi,a)W(k,\eta,b)e^{i(\xi x+\eta y)}}{h_1(1-U)(\xi^2+\eta^2)} \qquad (37)$$

Now let us make a coordinate transformation so that the new coordinates x' and y' are measured from the center of the aperture. That is, let $x = \frac{a}{2} + x'$ and $y = \frac{b}{2} + y'$ so that (37) becomes:

$$Q_1(x', y', l, k) = \int_{-\infty}^{\infty} d\xi \int_{-\infty}^{\infty} d\eta\, F(\xi^2, \eta^2) \overline{W}(l,\xi,a)\overline{W}(k,\eta,b)\eta\, e^{i(\xi x' + \eta y')} \qquad (38)$$

where

$$F(\xi^2,\eta^2) = \frac{(1+U)\left[\frac{k^2\pi^2}{b^2} \quad \xi^2 - \frac{l^2\pi^2}{a^2} \quad \eta^2\right]}{h_1(1-U)(\xi^2+\eta^2)\left(\xi^2 - \frac{l^2\pi^2}{a^2}\right)\left(\eta^2 - \frac{k^2\pi^2}{b^2}\right)} \qquad (39)$$

$$(40)$$

$$\overline{W}(l,\xi,a) = \left[(-1)^l e^{-i\frac{\xi}{2}a} - e^{i\frac{\xi}{2}a}\right]$$

$$\overline{W}(k,\eta,b) = \left[(-1)^k e^{-i\frac{\eta}{2}b} - e^{i\frac{\eta}{2}b}\right] \qquad (41)$$

From (40) and (41) we may note that

$$\overline{W}(l,-\xi,a) = \overline{W}(l,\xi,a) \qquad \text{if } l = \text{odd} \qquad (42)$$

$$\overline{W}(l,-\xi,a) = -\overline{W}(l,\xi,a) \qquad \text{if } l = \text{even} \qquad (42)$$

Now using (38) let us compute $Q_1(-x', y', l, k)$. This

$$Q_1(-x', y', l, k) = \int_{-\infty}^{\infty} d\xi \int_{-\infty}^{\infty} d\eta \, F(\xi^2, \eta^2) \, \overline{W}(l, -\xi) \, \overline{W}(k, \eta) \, e^{i(\xi x + \eta y)} \tag{43}$$

Next let $\xi = -\xi$. to get

$$Q_1(-x', y', l, k) = \int_{-\infty}^{\infty} d\xi \int_{-\infty}^{\infty} d\eta \, F(\xi^2, \eta^2) \, \overline{W}(l, -\xi) \, \overline{W}(l, \eta) \, e^{i(\xi x + \eta y)} \tag{44}$$

Using Equation (42) we may conclude from (44) that

$$\begin{aligned} Q_1(-x', y', l, k) &= Q_1(x', y', l, k) \qquad \text{if } l = \text{odd} \\ Q_1(-x', y', l, k) &= -Q_1(x', y', l, k) \qquad \text{if } l = \text{even} \end{aligned} \tag{45}$$

or more compactly

$$Q_1(-x', y', l, k) = -(-1)^l \, Q_1(x', y', l, k) \tag{46}$$

By similiar argument we also find

$$Q_1(x', -y', l, k) = (-1)^k \, Q_1(x', y', l, k) \tag{47}$$

The functions Q_o and Q_1 can be shown to have the same symmetry properties in X and Y as Q_1 while for $\hat{Q}_o$, $\hat{Q}_1$, $\hat{Q}_2$ we find

$$\hat{Q}_{o|2}(-x', y', l, k) = (-1)^l \, \hat{Q}_{o|2}(x', y', l, k) \tag{48}$$

$$\hat{Q}_{o|2}(x', -y', l, k) = (-1)^k \, \hat{Q}_{o|2}(x', y', l, k) \tag{49}$$

From Equation (46) we also have setting $x' = 0$ that

$$Q_1(o, y', l, k) = -(-1)^l \, Q_1(o', y', l, k) \tag{50}$$

Therefore

$$Q_1(o, y', l, k) = 0 \qquad \text{if } l = \text{even} \tag{51}$$

Also setting $y' = 0$ in Equation (47) gives:

$$Q_1(x', o, l, k) = (-1)^k \, Q_1(x', o, l, k)$$

Therefore

$$Q_1(x', o, l, k) = 0 \qquad \text{if } k = \text{odd} \tag{52}$$

The functions Q_o and Q_2 have the same properties as Q_1 when x' or y' are zero. By similar argument we also find

$$\hat{Q}_{\substack{o\\2}}(o, y', l, k) = 0 \qquad \text{if } l = \text{odd} \tag{53}$$

$$\hat{Q}_{\substack{o\\2}}(x', c, l, k) = 0 \qquad \text{if } k = \text{even} \tag{54}$$

These properties have proven a valuable aid to the numerical evaluation of the Q's, and to their use in obtaining the Z_{lk} and Y_{lk}.

3. Discussion of the Method of Solution of Equations (35) and (36)

In the section Cl, we derived a pair of equations for the quantities coefficients Z_{lk} and Y_{lk}. The problem now is to solve these equations for some set of Z's and Y's. Obviously, it would be too costly (because of the cost of computation of the Q functions) to try to compute Z_{lk} and Y_{lk} for $l = 0$ to ∞ and $k = 0$ to ∞. Fortunately, it generally turns out that only the Z_{lk} and Y_{lk} for the lowest few l's and k's are significant. To discuss equations (35) and (36) further let us rewrite them as:

$$\sum_{k, l = 0}^{\infty} \left\{ F(l, k, x, y)\, Y_{lk} + G(l, k, x, y)\, Z_{lk} \right\} = \Phi(x, y) \tag{55}$$

and

$$\sum_{k, l = 0}^{\infty} \left\{ H(l, k, x, y)\, Y_{lk} + J(l, k, x, y)\, Z_{lk} \right\} = \psi(x, y) \tag{56}$$

where

$$F(l, k, x, y) = +\epsilon\,\omega \left(\frac{l\pi}{a}\right)\left(\frac{k\pi}{b}\right) \gamma_{lk}\, Q_o(x, y, l, k)$$

$$+ \, i\,\omega\,\epsilon_o \left(\frac{k\pi}{b}\right) \sin\left(\frac{l\pi x}{a}\right) \cos\left(\frac{k\pi y}{b}\right)$$

$$G(l,k,x,y) = \omega^2 \mu_o \epsilon \; Q_1(x,y,l,k) - \left(\frac{l^2 \pi^2}{a^2} + \frac{k^2 \pi^2}{b^2}\right) Q_2(x,y,l,k)$$

$$- i \gamma_{lk} \left(\frac{l\pi}{a}\right) \sin\left(\frac{l\pi x}{a}\right) \cos\left(\frac{k\pi y}{b}\right)$$

$$\Phi(x,y) = - A_o \sin\left(\frac{\pi x}{a}\right) - i\omega\epsilon \; B_o\left(\frac{a}{\pi}\right) Q_1(x,y,1,o) + \frac{i B_o\left(\frac{\pi}{a}\right)}{\omega \mu_o} Q_2(x,y,1,o)$$

$$H(l,k,x,y) = -\omega\epsilon \left(\frac{k\pi}{b}\right)\left(\frac{l\pi}{a}\right) \gamma_{lk} \; \hat{Q}_o(x,y,l,k) - i\omega\epsilon_o \left(\frac{l\pi}{a}\right) \sin\left(\frac{k\pi y}{b}\right) \cos\left(\frac{l\pi x}{a}\right)$$

$$J(l,k,x,y) = -\omega^2 \mu_o \epsilon \; \hat{Q}_1(x,y,l,k) - \left[\left(\frac{l^2 \pi^2}{a^2}\right) + \left(\frac{k^2 \pi^2}{b^2}\right)\right] \hat{Q}_2(x,y,l,k)$$

$$- i \gamma_{lk} \left(\frac{k\pi}{b}\right) \sin\left(\frac{k\pi y}{b}\right) \cos\left(\frac{l\pi x}{a}\right)$$

$$\Psi(x,y) = i B_o\left(\frac{a}{\pi}\right) \omega\epsilon \; \hat{Q}_1(x,y,1,o) + \frac{i B_o}{\omega \mu_o} \left(\frac{\pi}{a}\right) \hat{Q}_2(x,y,1,o)$$

One can also note from the definitions above that

$$F(l,o,x,y) = F(o,k,x,y) = H(l,o,x,y) = H(o,k,x,y) = 0$$

Now suppose that we have a waveguide for which the x dimension "a" is 2/3 of a wavelength, and the y dimension b is 1/3 of a wavelength. For such a case, we know from our previous work on the infinite slot antenna that only the lowest mode will have any significant amplitude in the y direction while in the x direction only the lowest two or three modes will be significantly excited. Thus we need keep only the terms with $k = 0$ (or possibly 1) and those with $l = 1$ and 2 (and possibly 3). Therefore, a fair approximation would involve retaining only Z_{10}, Z_{20}, Y_{10}, and Y_{20}. For this example, equations (55) and (56) become (note that the coefficients of the Y_{10} and Y_{20} terms are zero):

$$G(1,0,x,y) Z_{10} + G(2,0,x,y) Z_{20} = \Phi(x,y) \tag{57}$$

$$J(1,0,x,y) Z_{10} + J(2,0,x,y) Z_{20} = \Psi(x,y) \tag{58}$$

Then by specifying some point (x, y) over the antenna surface for the evaluation of the G, J, Φ, and ψ functions, we will be able to solve equations (57) and (58) for Z_{10} and Z_{20}. Actually because of the way we have truncated the infinite series in equations (55) and (56), it turns out that our selection of the point of evaluation (x, y) should not be completely arbitrary.

Previous experience with the infinite slot antenna has taught us that when only one point is to be specified, it should be at the center of the slot. Thus we pick X = a/2 and Y = b/2 to get:

$$G(1,0, a/2, b/2) Z_{10} + G(2,0, a/2, b/2) Z_{20} = \Phi(a/2, b/2) \qquad (59)$$

$$J(1,0,a/2, b/2) Z_{10} + J(2,0, a/2, b/2) Z_{20} = \psi(a/2, b/2) \qquad (60)$$

and the solution for Z_{10} and Z_{20} is:

$$Z_{10} = \frac{\Phi(a/2, b/2) J(2,0, a/2, b/2) - \psi(a/2, b/2) G(2,0, a/2, b/2)}{J(2,0,a/2,b/2) G(1,0, a/2, b/2) - J(1,0, a/2, b/2) G(2,0, a/2, b/2)}$$

$$Z_{20} = \frac{\psi(a/2, b/2) G(1,0, a/2, b/2) - \Phi(a/2, b/2) J(1,0, a/2, b/2)}{J(2,0, a/2, b/2) G(1,0, a/2, b/2) - J(1,0, a/2, b/2) G(2,0, a/2, b/2)}$$

Note that this solution only involves the computation of $Q_1(1,0,a/2, b/2)$, $Q_1(2,0,a/2,b/2)$, $Q_2(1,0,a/2,b/2)$, $Q_2(2,0,a/2,b/2)$, $\hat{Q}_1(1,0, a/2,b/2)$, $\hat{Q}_1(2,0,a/2,b/2)$, $\hat{Q}_2(1,0,a/2,b/2)$, $\hat{Q}_2(2,0,a/2,b/2)$, or 8 Q calculations.

For the case when we desire to solve for an arbitrary number of Z's and Y's we simply choose enough points (x, y) so that we have a number of unknowns.

4. The Computer Programs for the Solution of Equations (35) and (36)

A computer program (No. 2128) has been developed which evaluates the Q functions. The output of this program is then used in Equations (35) and (36) to solve for Z_{lk} and Y_{lk}. This is achieved for an arbitrary (l, k) by use of computer program No. 2187. As a test case, we considered the slot antenna with frequency 2200 Mc and dimensions 0.1092 x 0.0546 meter. The waveguide used was covered by a slab of relative dielectric constant ϵ_r = 1.85 + i.041, and thickness, 0.025 meter. We assumed that the important mode coefficients were Z_{10}, Z_{20},

Z_{21}, Z_{11}, Z_{01}, and the corresponding Y's. This required that we pick four (only 4 sets were needed since Y_{10}, Y_{01}, and Y_{20} do not enter the equations) sets of (x, y) across the waveguide aperture, obtain the Q functions from program 2128, and then use program 2187 to get the Z's and Y's. Using these values we computed the impedance Z_L to the TE_{10} mode from

$$\frac{Z_L}{Z_o} = \frac{1 - \frac{\pi}{a}\,\frac{i Z_{10}\,\omega\,\mu_o}{B_o}}{1 + \frac{\pi}{a}\,\frac{i\,\omega\,\mu_o Z_{10}}{B_o}} \tag{61}$$

Z_o is the characteristic impedance of the guide for the TE_{10} mode The result we obtained for Z_L was $Z_L = 176 + i\,95$ (or if $e^{j\omega t}$ were used instead of $e^{-i\omega t}$, $Z_L = 176 - j\,95$).

Since it was relatively costly to compute all the Q functions necessary to determine Z_{10}, Z_{20}, Z_{21}, Z_{11}, and Z_{01}, we then attempt to develop a simpler solution. This involved neglecting all the coefficients Z_{lk} and Y_{lk} except Z_{10} and Y_{10}. This led to a simplified program (No. 2206). The results for Z_L, for the same waveguide as above, was $Z_L = 181 - j\,99$. We thus found that there was relatively good agreement between the simple model and the more complex method of solution. (It is felt however that the closeness of this approximate result to the more exact result in this case was largely a matter of luck since in some of the cases tried Z_{01} and Z_{11} were a significant fraction of Z_{10}, and keeping merely Z_{10} in the equations should be less accurate than the present case.) In a later section, more detailed discussion of the computer results will be given as well as a discussion of the experiments.

5. A Variational Expression for the Admittance of the Plasma-Covered Rectangular Waveguide

In the preceding sections, we derived expressions for the fields, etc. produced by a dielectric covered waveguide. We previously used an approximate method (Program 2206) to compute the impedance and obtained antenna impedances which were accurate to within about 10%. We would now like to present a variational formulation for the antenna admittance which we feel will be accurate to within 5%. (Of course, the solution of 35 and 36, retaining a large number of items, is more accurate than either of these).

The fields within the waveguide can be written as:

$$\underline{E}^{(1)} = \sum_n V_n \underline{e}_n + V_{n'} \underline{e}_{n'}$$

$$\underline{H}^{(1)} = \sum_n I_n \underline{e}_n + I_{n'} \underline{h}_{n'} \tag{62}$$

For the definition of $\underline{e}_n$, h_n etc., see Marcuvitz (1951). Similarly in Section C1. we showed that the E fields at the plasma-antenna interface could be written as

$$E_x = \iint_{-\infty}^{\infty} \frac{d\xi d\eta}{\xi^2 + \eta^2} e^{i(\xi x + \eta y)} [\xi h_1 R(1-U) - \omega \mu_o \eta (1 + \hat{U})]$$

$$E_y = \iint_{\infty}^{\infty} \frac{d\xi d\eta}{\xi^2 + \eta^2} e^{i(\xi x + \eta y)} [\eta h_1 R(1-U) + \omega \mu \xi (1 + \hat{U})] \tag{63}$$

Matching boundary conditions across the interface gives:

$$\frac{\xi h_1 R(1-U) - \omega \mu_o \eta (i + \hat{U}) L}{\xi^2 + \eta^2} = \hat{E}_x$$

$$\frac{\eta h_1 R(1-U) + \omega \mu_o \xi (1 + \hat{U}) L}{\xi^2 + \eta^2} = \hat{E}_y$$

where

$$\hat{E}_x = \frac{1}{(2\pi)^2} \iint_{\text{Aperture}} dx\, dy\; E_x(x, y)\; e^{-i(\xi x + \eta y)} \tag{64}$$

Solving (64) for R and L yields:

$$R = \frac{\xi \hat{E}_x + \eta \hat{E}_y}{h_1 (1-U)} \tag{65}$$

$$L = \frac{\xi \hat{E}_y - \eta \hat{E}_x}{\omega \mu_o (1 + \hat{U})} \qquad (66)$$

where $\hat{U}$, U, etc., are all defined in Section C1

Now the H field in the plasma can be written:

$$H_x = \iint_{-\infty}^{\infty} \frac{d\xi d\eta}{\xi^2 + \eta^2} e^{i(\xi x + \eta y)} [\epsilon \omega \eta (1 + U) R + h_1 \xi (1 - \hat{U}) L]$$

$$H_y = \iint_{-\infty}^{\infty} \frac{d\xi d\eta}{\xi^2 + \eta^2} e^{i(\xi x + \eta y)} [-\omega \epsilon \xi R (1 + U) + \eta h_1 L (1 - \hat{U})] \qquad (67)$$

The components of (67) can be written in vector form as:

$$\underline{H} = \iint_{-\infty}^{\infty} \frac{d\xi d\eta}{\xi^2 + \eta^2} e^{i(\xi x + \eta y)} [\epsilon \omega R (1 + U)(\underline{\Omega} \times Z_o) + h_1 L (1 - \hat{U}) \underline{\Omega}] \qquad (68)$$

where

$$\Omega = \underline{i}_x \xi + \underline{i}_y \eta$$

$\underline{Z_o}$ = unit vector in Z direction

Matching the tangential H across the aperture gives:

$$\sum_n (I_n \underline{h}_n + I_n' \underline{h}_n') = \iint_{-\infty}^{\infty} \frac{d\xi d\eta}{\xi^2 + \eta^2} e^{i(\xi x + \eta y)} [\epsilon \omega R (1 + U)(\Omega \times Z_o) + h_1 L (1 - \hat{U}) \Omega] \qquad (69)$$

Assuming only the dominant H mode is transmitted down the guide, we can rewrite (69) as (upon substituting from (65) and (66) for R & L):

$$+ I_o' \underline{h}_o' = -\left(\sum_n I_n \underline{h}_n + \sum_{n \neq 0} I_n' \underline{h}_n' \right)$$

$$+ \iint_{-\infty}^{\infty} \frac{d\xi \, d\eta}{\xi^2 + \eta^2} e^{i(\xi x + \eta y)} \left\{ \frac{\epsilon \, \omega (1 + U) (\underline{\Omega} \times \underline{Z}_o) [\xi \hat{E}_x + \eta \hat{E}_y]}{h_1 (1 - U)} + \frac{h_1 \underline{\Omega} (1 - \hat{U}) [\xi \hat{E}_y - \eta \hat{E}_x]}{\omega \mu_o (1 + \hat{U})} \right\} \quad (70)$$

Taking the cross product of Z_o with (70) yields:

$$- I_o' \underline{e}_o' = \left(\sum_n I_n \underline{e}_n + \sum_{n \neq 0} I_n' \underline{e}_n' \right)$$

$$+ \iint \frac{d\xi \, d\eta}{\xi^2 + \eta^2} e^{i(\xi x + \eta y)} \left\{ \frac{\omega \epsilon (1 + U)}{h_1 (1 - U)} \, \underline{\Omega} \, (\xi \hat{E}_x + \eta \hat{E}_y) \right.$$

$$\left. + \frac{h_1 (\underline{Z}_o \times \underline{\Omega}) (1 - \hat{U})}{\omega \mu_o (1 + \hat{U})} (\xi \hat{E}_y - \eta \hat{E}_x) \right\} \quad (71)$$

Now taking the dot product of the aperture field E with (71), and using the fact that for the reflected modes we have $I_n = - Y_n V_n$, we have:

$$I_o \int \underline{e}_o' \cdot \underline{E} \, dS = \sum_n Y_n V_n \int \underline{e}_n \cdot \underline{E} \, dS + \sum_{n \neq 0} Y_n' V_n' \int \underline{e}_n' \cdot \underline{E} \, dS$$

$$- \iint_{-\infty}^{\infty} \frac{d\xi \, d\eta}{\xi^2 + \eta^2} (2\pi)^2 \left\{ \frac{\epsilon \omega (1 + U)}{h_1 (1 - U)} (\underline{\Omega} \cdot \hat{\underline{E}}) (\underline{\Omega} \cdot \hat{\underline{E}}^*) \right.$$

$$\left. + \frac{h_1 (1 - \hat{U})}{\omega \mu_o (1 + \hat{U})} [\underline{Z}_o \times \underline{\Omega} \cdot \hat{\underline{E}}^*] [\underline{Z}_o \times \underline{\Omega} \cdot \hat{\underline{E}}] \right\} \quad (72)$$

where

$$\hat{\underline{E}}(\xi,\eta) = \underline{i}_x \hat{E}_x(\xi,\eta) + \underline{i}_y \hat{E}_y(\xi,\eta)$$

$$\hat{\underline{E}}^*(\xi,\eta) = \hat{\underline{E}}(-\xi,-\eta)$$

and

$$dS \equiv dx\,dy$$

Finally dividing through both sides of (72) by $V_o' \int \underline{e}_o' \cdot \underline{E}\, dS$ we get a variational expression for the admittance:

$$Y_o' = \frac{I_o'}{V_o'} = \frac{\sum_n V_n Y_n \int_{Ap} \underline{e}_n \cdot \underline{E}\, dS + \sum_{n \neq 0} Y_n' V_n' \int_{Ap} \underline{e}_n' \cdot \underline{E}\, dS}{\left(\int_{Ap} \underline{e}_o' \cdot \underline{E}\, dS\right)^2}$$

$$\frac{-\int_{-\infty}^{\infty} \frac{d\xi\, d\eta}{\xi^2+\eta^2} (2\pi)^2 \left\{ \frac{\epsilon\omega(1+U)}{h_1(1-U)} |\underline{\Omega}\cdot\hat{\underline{E}}|^2 + \frac{h_1(1-\hat{U})}{\omega\mu_o(1+\hat{U})} |\underline{Z}_o \times \underline{\Omega}\cdot\hat{E}|^2 \right\}}{\left(\int_{Ap} \underline{e}_o' \cdot \underline{E}\, dS\right)^2} \tag{73}$$

It can be shown that Equation (73) is stationary. If one were to assume that the aperture field is approximately the field of the dominant mode ($\underline{E}$ $V_o \underline{e}_o'$) we would have from (73)

$$Y_o' = -\iint_{-\infty}^{\infty} \frac{d\xi\, d\eta}{\xi^2+\eta^2} (2\pi)^2 \left\{ \frac{\epsilon\omega(1+U)}{h_1(1-U)} |\underline{\Omega}\cdot\hat{\underline{e}}_o'|^2 + \frac{h_1(1-\hat{U})}{\omega\mu_o(1+\hat{U})} |\underline{Z}_o \times \underline{\Omega}\cdot\hat{\underline{e}}_o'|^2 \right\} \tag{74}$$

where

$$\hat{\underline{e}}_o' \equiv \frac{1}{(2\pi)^2} \iint dx\, dy\, \underline{e}_o'(x,y)\, e^{-i(\xi x + \eta y)}$$

The integrals which need to be evaluated in (74) are very similar to the Q functions already evaluated by Avco computer program No. 2128. At a future time we will endeavor to have the integrals in Equation (14) programmed.

6. Steepest-Descent Calculation of Far Fields

In this section we will use the results of the previous section to derive formal solutions for the far fields radiated by a dielectric covered rectangular slot. In order for our results to be ultimately useful for experimental verification, we shall first convert all our results from rectangular to spherical coordinates as shown in the figure below.

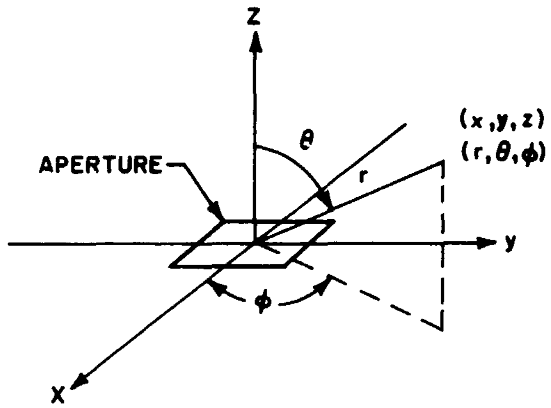

In spherical coordinates the transverse components of the fields are:

$$H_\theta = H_x \cos\phi \cos\theta + H_y \sin\phi \cos\theta - H_z \sin\theta$$

$$H_\phi = -H_x \sin\phi + H_y \cos\phi$$

and the same for the fields. Also $z = r\cos\theta$, $x = r\sin\theta\cos\phi$ and $y = r\sin\theta\sin\phi$.

Applying these equations to equation (14) through (19) gives:

$$H_\theta = \int_{-\infty}^{\infty} d\eta \int_{-\infty}^{\infty} d\xi \; e^{ir(\xi\sin\theta\cos\phi + \eta\sin\theta\sin\phi + h_2\cos\theta)} \; \Lambda(\xi,\eta) \qquad (75)$$

$$H_\phi = \int_{-\infty}^{\infty} d\eta \int_{-\infty}^{\infty} d\xi \; e^{ir(\xi\sin\theta\cos\phi + \eta\sin\theta\sin\phi + h_2\cos\theta)} \; \Gamma(\xi,\eta) \qquad (76)$$

where

where

$$\Lambda(\xi,\eta) \equiv \left\{ \left[\frac{\omega \epsilon_0 \eta S - \xi h_2 T}{\xi^2 + \eta^2} \right] \cos\phi \cos\theta + \left[\frac{-\omega \epsilon_0 \xi S - \eta h_2 T}{\xi^2 + \eta^2} \right] \sin\phi \cos\theta - T \sin\theta \right\}$$

$$\Gamma(\xi,\eta) \equiv \left\{ - \left[\frac{\omega \epsilon_0 \eta S - \xi h_2 T}{\xi^2 + \eta^2} \right] \sin\phi + \left[\frac{-\omega \epsilon_0 \xi S - \eta h_2 T}{\xi^2 + \eta^2} \right] \cos\phi \right\}$$

Similarly for the electric fields we get:

$$E_\theta = \int_{-\infty}^{\infty} d\eta \int_{-\infty}^{\infty} d\xi \; e^{ir(\xi \sin\theta \cos\phi + \eta \sin\theta \sin\phi + h_2 \cos\theta)} \; C(\xi,\eta) \quad (77)$$

$$E_\phi = \int_{-\infty}^{\infty} d\xi \int_{-\infty}^{\infty} d\eta \; e^{ir(\xi \sin\theta \cos\phi + \eta \sin\theta \sin\phi + h_2 \cos\theta)} \; D(\xi,\eta) \quad (78)$$

where

$$C(\xi,\eta) \equiv \left\{ \left[\frac{-\xi h_2 S - \eta \omega \mu_0 T}{\xi^2 + \eta^2} \right] \cos\phi \cos\theta + \left[\frac{-h_2 \eta S + \omega \mu_0 \xi T}{\xi^2 + \eta^2} \right] \sin\phi \cos\theta - S \sin\theta \right\}$$

$$D(\xi,\eta) \equiv \left\{ - \left[\frac{-\xi h_2 S - \eta \omega \mu_0 T}{\xi^2 + \eta^2} \right] \sin\phi + \left[\frac{-h_2 \eta S + \omega \mu_0 \xi T}{\xi^2 + \eta^2} \right] \cos\phi \right\}$$

Now that we have these fields in spherical coordinates we need to evaluate the integrals for the far field (i. e., $r \to \infty$). Let us consider equation (70). This can be rewritten as:

$$H_\theta = \int_{-\infty}^{\infty} d\eta \; e^{ir\eta \sin\theta \sin\phi} \int_{-\infty}^{\infty} d\xi \; e^{ir(\xi \sin\theta \cos\phi + h_2 \cos\theta)} \; \Lambda(\xi,\eta) \quad (79)$$

If $\Lambda(\xi,\eta)$ is well behaved, it can be shown that for $r \to \infty$ most of the contribution to equation (79) comes in the vicinity of the saddle point in the exponential function. Consider the inner integral in equation (79) and rewrite it as

$$I = \int_{-\infty}^{\infty} d\xi \; e^{irf(\xi,\eta)} \; \Lambda(\xi,\eta) \tag{80}$$

where

$$f(\xi,\eta) = \xi \sin\theta \cos\phi + \sqrt{k_o^2 - \xi^2 - \eta^2} \; \cos\theta \tag{81}$$

The saddle point occurs when $f'(\xi) = 0$ or at

$$f'(\xi_o) = 0 = \sin\theta\cos\phi - \frac{\xi_o \cos\theta}{\sqrt{k_o^2 - \xi_o^2 - \eta^2}} \tag{82}$$

The solution of equation (77) is:

$$\xi_o = \frac{\sqrt{k_o^2 - \eta^2} \quad \sin\theta\cos\phi}{(\cos^2\theta + \sin^2\theta\cos^2\phi)^{1/2}} .$$

Now in order to see how we must deform the contour to pass through the saddle point, it is necessary to examine the behavior of $\exp[irf(\xi,\eta)]$ in the vicinity of ξ_o. To do this we expand

$$f(\xi) = f(\xi_o) + \frac{(\xi-\xi_o)^2}{2} \quad f''(\xi_o) + \cdots \tag{83}$$

Note that $f'(\xi_o) = 0$ since this is the saddle point. Using equation (82) in equation (81) gives:

$$f(\xi_o) = \sqrt{k_o^2 - \eta^2} \; (\cos^2\theta + \sin^2\theta\cos^2\phi)^{1/2} \tag{84}$$

and differentiating equation (82) gives:

$$f''(\xi_o) = - \frac{(\cos^2\theta + \sin^2\theta\cos^2\phi)^{1/2}}{\cos^2\theta \; \sqrt{k_o^2 - \eta^2}} \tag{85}$$

Thus in the vicinity of the saddle point, the exponential in equation (85) behaves as:

$$e^{ir\Omega\sqrt{k_o^2 - \eta^2}} \qquad e^{- i \frac{(\xi-\xi_o)^2 r\rho^2}{\sqrt{k_o^2 - \eta^2}}} \tag{86}$$

where

$$\Omega \equiv (\cos^2\theta + \sin^2\theta \cos^2\phi)^{1/2}$$

$$\rho^2 = \frac{1}{2} \frac{\Omega}{\cos^2\theta}$$

Next, we may write $(\xi - \xi_o) = Se^{i\gamma}$ so that equation (86) becomes

$$e^{ir\Omega\sqrt{k_o^2-\eta^2}} \quad e^{-i\frac{\rho^2 S^2 r(\cos^2\gamma + 2i\cos\gamma\sin\gamma - \sin^2\gamma)}{\sqrt{k_o^2-\eta^2}}} \tag{87}$$

<u>Case I</u> - Suppose $k_o > \eta$; then as $r \to \infty$, the dominant behavior of equation (87) is determined by

$$e^{\frac{2\rho^2 S^2 r\cos\gamma\sin\gamma}{\sqrt{k_o^2-\eta^2}}}$$

This function in the complex plane grows as we move away from the saddle point for $0 \leq \gamma \leq \pi/2$, $\pi \leq \gamma \leq 3\pi/2$, but decays rapidly as $r \to \infty$ for $\pi/2 < \gamma < \pi$ and $3\pi/2 < \gamma < 2\pi$. Thus for $k_o > \eta$ we deform the contour C through the saddle point as:

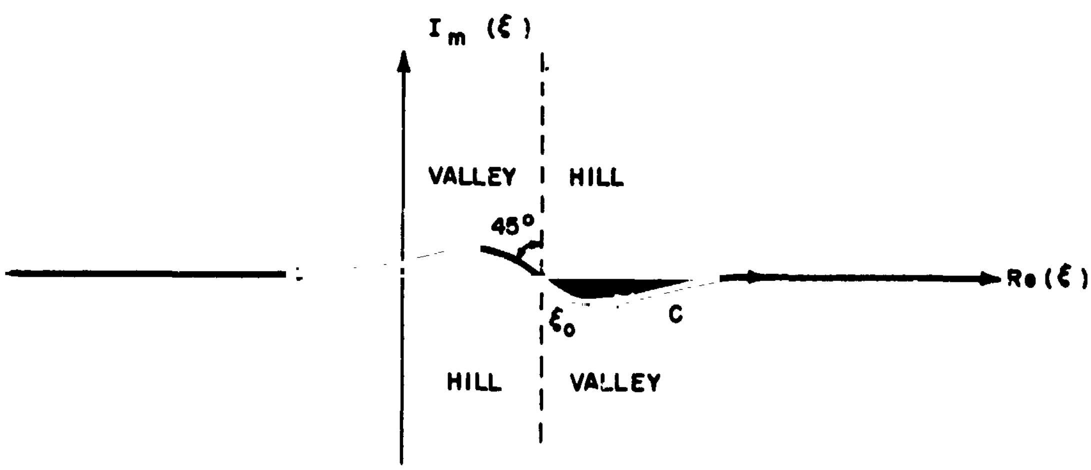

<u>Case II</u> - Suppose $\eta > k_o$; then as $r \to \infty$, the dominant behavior of equation (87) is governed by:

$$e^{-\frac{\rho^2 S^2 r\cos 2\gamma}{\sqrt{\eta^2-k_o^2}}}$$

Here the function grows and decays as we move away from the saddle point as shown below:

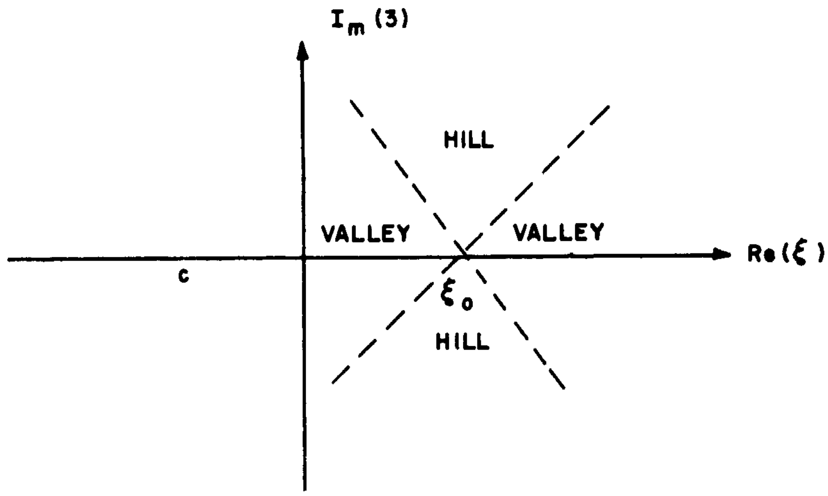

Thus we may pass the contour directly through ξ_0 parallel to the real (ξ) axis.

Now that we have discussed the contour, we can apply the method of steepest descents to equation (80). From equation (4.6.13) in Morse and Feshbach[7] we get:

$$I = \Lambda\left(\xi = \lambda\sqrt{k_o^2 - \eta^2}\,,\ \eta\right) e^{ir\Omega\sqrt{k_o^2-\eta^2}}\ e^{-i\frac{\pi}{4}} \sqrt{\frac{2\pi\,(k_o^2-\eta^2)^{1/2}\cos^2\theta}{r\,\Omega^3}}$$

$$\Omega \equiv (\cos^2\theta + \sin^2\theta\cos^2\phi)^{1/2} = (1 - \sin^2\theta\sin^2\phi)^{1/2}$$

$$\lambda = (\sin\theta\cos\phi)/\Omega \qquad (88)$$

Now substituting equation (88) into equation (79), we have:

$$H_\theta = \int_{-\infty}^{\infty} d\eta\ \frac{e^{ir\left(\eta\sin\theta\sin\phi + \Omega\sqrt{k_o^2-\eta^2}\right)}}{\sqrt{r}}\ \Lambda_o(\eta) \qquad (89)$$

where

$$\Lambda_o(\eta) = \Lambda\left(\xi = \lambda\sqrt{k_o^2-\eta^2}\,,\ \eta\right) e^{-i\frac{\pi}{4}} \sqrt{\frac{2\pi\,(k_o^2-\eta^2)^{1/2}\cos^2\theta}{\Omega^3}}$$

---

[7] Morse, P.M., and H. Fethbach, Methods of Theoretical Physics, McGraw-Hill, New York (1953), p. 441.

Next, we may rewrite equation (84) as:

$$H_\theta = \frac{1}{\sqrt{r}} \int_{-\infty}^{\infty} d\eta \; e^{irg(\eta)} \; \Lambda_o(\eta) \tag{90}$$

where

$$g(\eta) \equiv \eta \sin\theta \sin\phi + \Omega \sqrt{k_o^2 - \eta^2}$$

Again, we wish to apply the method of steepest descents (saddle point integration) to evaluate equation (90). Setting $g'(\eta_o) = 0$ gives:

$$g' = 0 = \sin\theta \sin\phi - \frac{\Omega\,\eta_o}{\sqrt{k_o^2 - \eta_o^2}} \tag{91}$$

and the solution to equation (85) is:

$$\eta_o = k_o \sin\theta \sin\phi$$

Again it is necessary to compute $g(\eta_o)$, $g''(\eta_o)$. These are

$$g(\eta_o) = k_o \tag{92}$$

$$g''(\eta_o) = \frac{-1}{k_o\,[1 - \sin^2\theta \sin^2\phi]} \tag{93}$$

Thus in the vicinity of the saddle point the exponential

$$e^{irg(\eta)} = e^{ik_o r}\; e^{-ir(\eta-\eta_o)^2 q} \tag{94}$$

where

$$q \equiv \frac{1}{2k_o\,[1 - \sin^2\theta \sin^2\phi]}$$

Writing $\eta - \eta_o = S e^{i\gamma}$ we may rewrite equation (94) as

$$e^{irg(\eta_o)} = e^{ik_o r}\; e^{-irqS^2(\cos^2\gamma + 2i\cos\gamma\sin\gamma - \sin^2\gamma)} \tag{95}$$

The dominant behavior of equation (95) is determined by

$$e^{2rqS^2 \cos\gamma \sin\gamma}$$

and for large r we find that this function decays rapidly for $3\pi/2 \leq \gamma \leq 2\pi$ and $\pi/2 \leq \gamma \leq \pi$, while for $0 \leq \gamma \leq \pi/2$, and $\pi \leq \gamma \leq 3\pi/2$ this grows without bound as $r \to \infty$. Thus the contour in the η plane we must choose is:

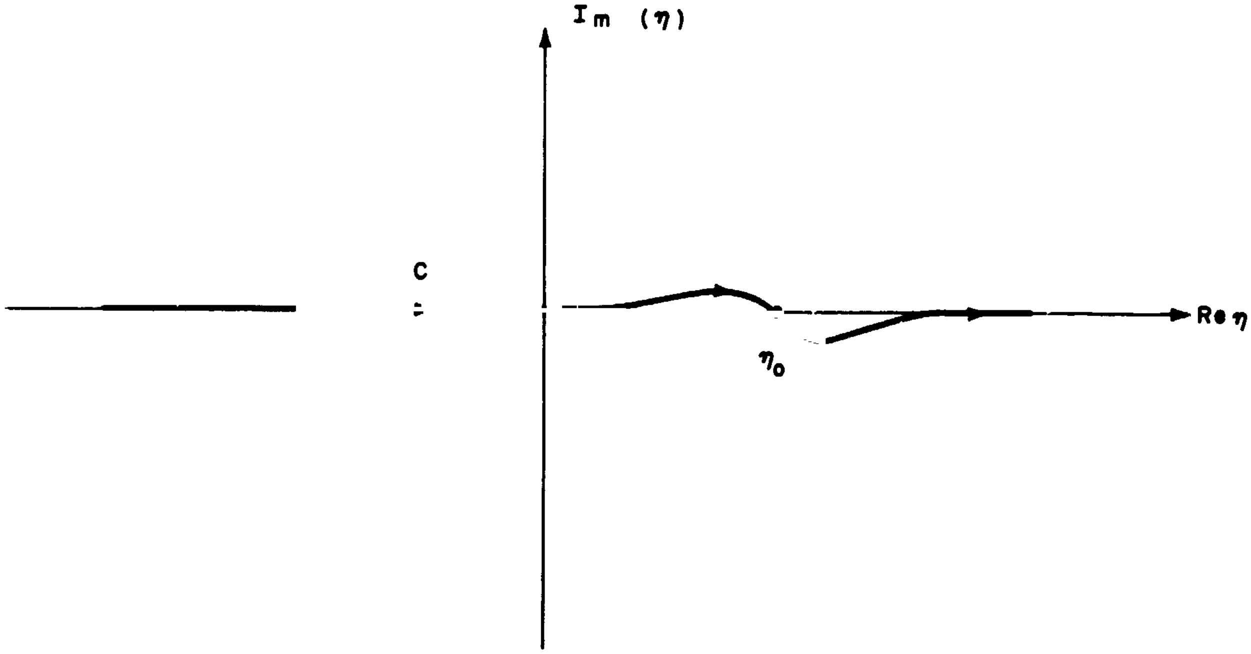

Applying equation (4.6.13) in Morse and Feshbach[7] to equation (90) then yields:

$$H_\theta = \frac{\sqrt{2\pi k_o}}{\sqrt{r}} \Lambda(\xi = k_o \sin\theta\cos\phi, \eta = k_o \sin\theta\sin\phi) \frac{e^{-i\frac{\pi}{4}}\cos\theta}{\Omega}$$

$$e^{ik_o r}\sqrt{\frac{2\pi k_o [1 - \sin^2\theta\sin^2\phi]}{ir e^{i\pi} e^{i\pi}}}$$

or

$$H_\theta = \frac{2\pi k_o}{r} e^{i\left(k_o r - \frac{\pi}{2}\right)} \cos\theta\,\Lambda(\xi = k_o \sin\theta\cos\phi,\ \eta = k_o\sin\theta\sin\phi) \tag{96}$$

for $r \to \infty$

---

[7] Morse and Ferhbach, op. cit.

By analogy with equation (96) we also have for $r \to \infty$

$$H_\phi = \frac{2\pi k_o}{r} e^{i\left(k_o r - \frac{\pi}{2}\right)} \cos\theta\, \Gamma \;(\xi = k_o \sin\theta\cos\phi,\ \eta = k_o \sin\theta\sin\phi) \tag{97}$$

$$E_\theta = \frac{2\pi k_o}{r} e^{i\left(k_o r - \frac{\pi}{2}\right)} \cos\theta\, C\,(\xi = k_o \sin\theta\cos\phi,\ \eta = k_o \sin\theta\sin\phi) \tag{98}$$

and

$$E_\phi = \frac{2\pi k_o}{r} e^{i\left(k_o r - \frac{\pi}{2}\right)} \cos\theta\, D\,(\xi = k_o \sin\theta\cos\phi,\ \eta = k_o \sin\theta\sin\phi) \tag{99}$$

7. Radiation Pattern of a Slot Antenna

The next step is to derive an expression for the radiated power. The Poynting vector N is

$$\underline{N} = \frac{1}{2}\, \underline{E} \times \underline{H}^* \tag{100}$$

and using equations (96) through (99), we may write for the radial component of $\underline{N}$:

$$(N)_r = \frac{1}{2}\left(E_\theta H_\phi^* - E_\phi H_\theta^*\right) = \frac{1}{2}\left(\frac{2\pi k_o}{e}\right)^2 \cos^2\theta\,(C\Gamma^* - D\Lambda^*)\Bigg|_{\substack{\xi = k_o \sin\theta\cos\phi \\ \eta = k_o \sin\theta\sin\phi}}$$

Substituting for C, D, Γ, Λ from section G, we get after a great deal of manipulation:

$$N_r = \frac{\omega\, 2\pi^2 k_o}{r^2 (2\pi)^4}\, \frac{\cos^2\theta}{\sin^2\theta} \left\{\epsilon_o |S|^2 + \mu_o |T|^2\right\} \quad \begin{matrix}\xi = k_o \sin\theta\cos\phi \\ \eta = k_o \sin\theta\sin\phi\end{matrix} \tag{101}$$

The quantities S and T in equation (101) were defined in equation (24). Substituting $\xi = k_o \sin\theta\cos\phi$ and $\eta = k_o \sin\theta\sin\phi$ in the expressions given there yields:

$$\begin{aligned} S &= W R \\ T &= \hat{W} L \end{aligned} \tag{102}$$

where

$$W = \frac{2 h_1 \epsilon_r}{h_1 - \epsilon_r h_2} \quad e^{-i(h_1 + h_2) l_o}$$

$$\hat{W} = \frac{2 h_1}{h_1 - h_2} \quad e^{-i(h_1 + h_2) l_o}$$

$$h_1 = \sqrt{k_1^2 - k_o^2 \sin^2 \theta}$$

$$h_2 = k_o \cos \theta$$

Also $\epsilon_r \equiv \epsilon/\epsilon_o$ from Section C1, we get:

$$R = \frac{k_o^2 \sin^2 \theta}{h_1 (1 - U)} \Bigg\{ \omega \mu_o \sum_{kl} \left[\left(\frac{k\pi}{b}\right)^2 \cos^2 \phi - \left(\frac{l\pi}{a}\right)^2 \sin^2 \phi \right] W_1^l W_2^k Z_{kl}$$

$$- i B_o \left(\frac{\pi}{a}\right) \sin^2 \phi \, W_1 \, W_2^o + \sum_{l,k} W_1^l W_2^k \left(\frac{k\pi}{b}\right)\left(\frac{l\pi}{a}\right) y_{lk} Y_{lk} \Bigg\} \qquad (104)$$

$$L = \frac{k_o^2 \sin^2 \theta \sin \phi \cos \phi}{\omega \mu_o (1 + U)} \Bigg\{ - i B_o \left(\frac{\pi}{a}\right) W_1^1 \, W_2^o$$

$$- \omega \mu_o \sum_{k,l} \left[\left(\frac{l\pi}{a}\right)^2 + \left(\frac{k\pi}{b}\right)^2 \right] Z_{kl} \, W_1^l \, W_2^k \Bigg\} \qquad (105)$$

where

$$\hat{U} = e^{-i 2 h_1 l_o} \left(\frac{h_1 + h_2}{h_1 - h_2}\right)$$

$$U = e^{-i 2 h_1 l_o} \left(\frac{h_1 + \epsilon_r h_2}{h_1 - \epsilon_r h_2}\right)$$

$$W_1^l = \left[\frac{(-1)^l \; e^{-iak_o \sin\theta \cos\phi} - 1}{k_o^2 \cos^2\phi \sin^2\theta - \left(\frac{l\pi}{a}\right)^2} \right]$$

$$W_2^k = \left[\frac{(-1)^k \; e^{-ibk_o \sin\theta \sin\phi} - 1}{k_o^2 \sin^2\phi \sin^2\theta - \left(\frac{k\pi}{b}\right)^2} \right]$$

$$\gamma_{lk} = \sqrt{k_o^2 - \left(\frac{l\pi}{a}\right)^2 - \left(\frac{k\pi}{b}\right)^2}$$

Thus once the coefficients Z_{lk} and Y_{lk} are determined by the solution of equations (35) and (36), the radiation pattern may be readily computed from equation (101). Equation (101) has been programmed, and is evaluated as a function of θ and ϕ in program No. 2141.

Theoretical patterns for the open-ended waveguide were computed for the following cases: 300 Mc with one-inch heat-shield cover, 2200 Mc with one-inch heat-shield cover, and 6600 Mc with 0.33-inch heat-shield cover. The E- and H-plane patterns for these cases are presented in Figure 14 through 17. The 6600-Mc case is an exact scale of the 2200-Mc case with all its computer-input parameters scaled by a factor of a third. The scaled 6600-Mc patterns show good correlation with 2200-Mc patterns as can be seen by the superimposed patterns in Figure 16 and 17.

The theoretical program determines pattern shape but is not designed to provide absolute power. However, for each waveguide size, the relative attenuation due to the heat-shield cover was determined by referencing the computed power levels with heat shield to those without heat shield. The power levels without heat shield were obtained by replacing the complex permittivity of the heat shield with a permittivity similar to that of free space (ϵ'/ϵ_o = 1.0 - j 0.001).* In Figures 14 through 17, the decibel values are referenced to the peak gain without heat shield at $\phi = 0°, \theta = 0°$ for each case. Calculated peak gain reduction due to the heat-shield cover at $\phi = 0.$, $\theta = 0°$ is given below:

Frequency (Mc)	Heat-Shield Thickness (inches)	Guide	Relative Permittivity of Dielectric Cover (ϵ/ϵ_o)	Peak Gain Reduction (db)
300	1.0	WR - 2300	2.5 - j0.200	2.07
2200	1.0	WR - 430	1.85 - j0.014	2.30
6600	0.33	WR - 137	1.85 - j0.014	2.15

* For computational purposes, the imaginary part of the complex permittivity cannot be zero.

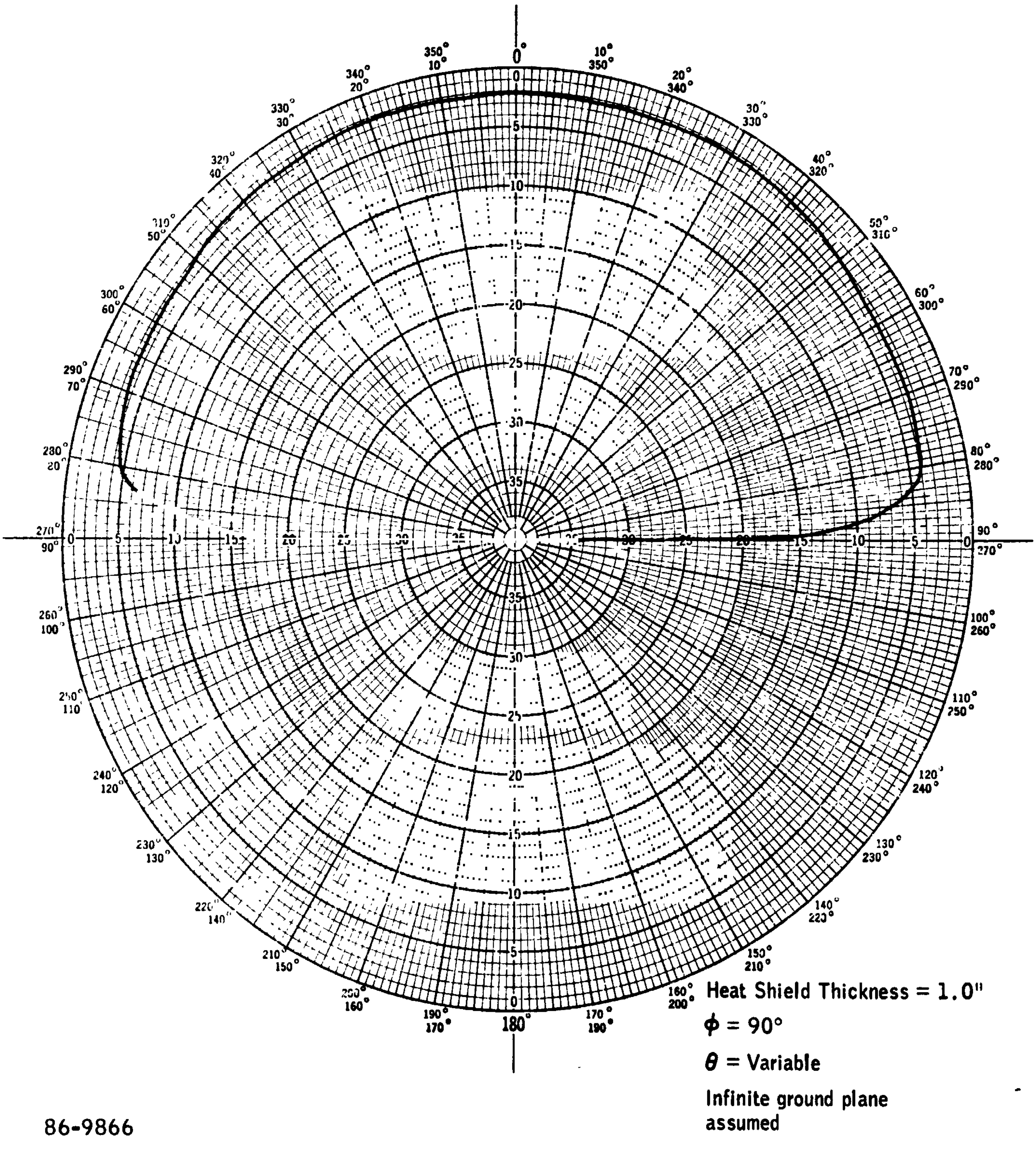

Heat Shield Thickness = 1.0"

$\phi = 90°$

θ = Variable

Infinite ground plane assumed

86-9866

Figure 14 THEORETICAL PATTERN OF 300 MC OPEN-ENDED WAVEGUIDE COVERED WITH AVCOAT 5026-39M. PRINCIPAL E PLANE

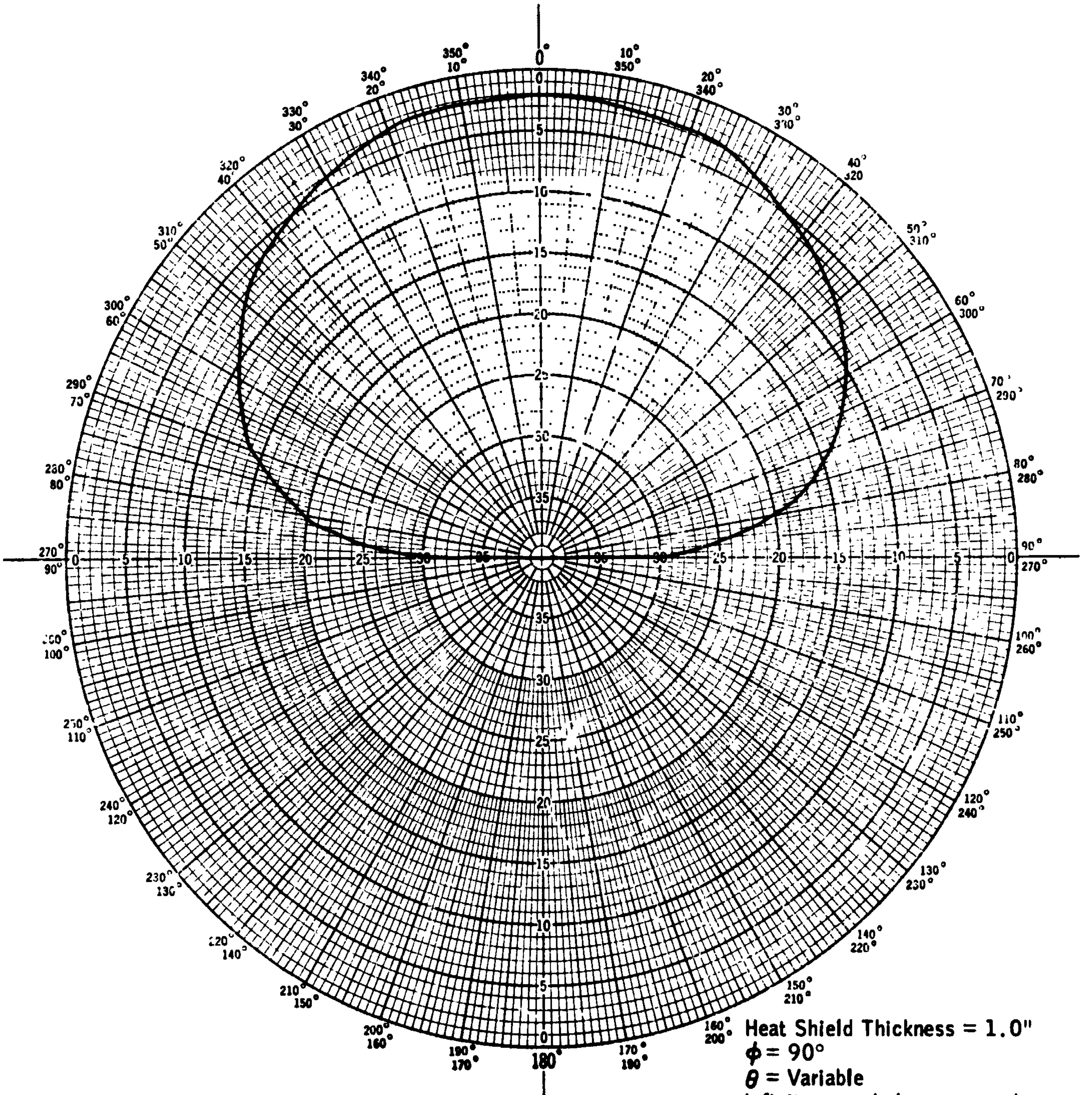

86-9867

Figure 15 THEORETICAL PATTERN OF 300 MC OPEN-ENDED WAVEGUIDE COVERED WITH AVCOAT 5026-39M. PRINCIPAL H PLANE

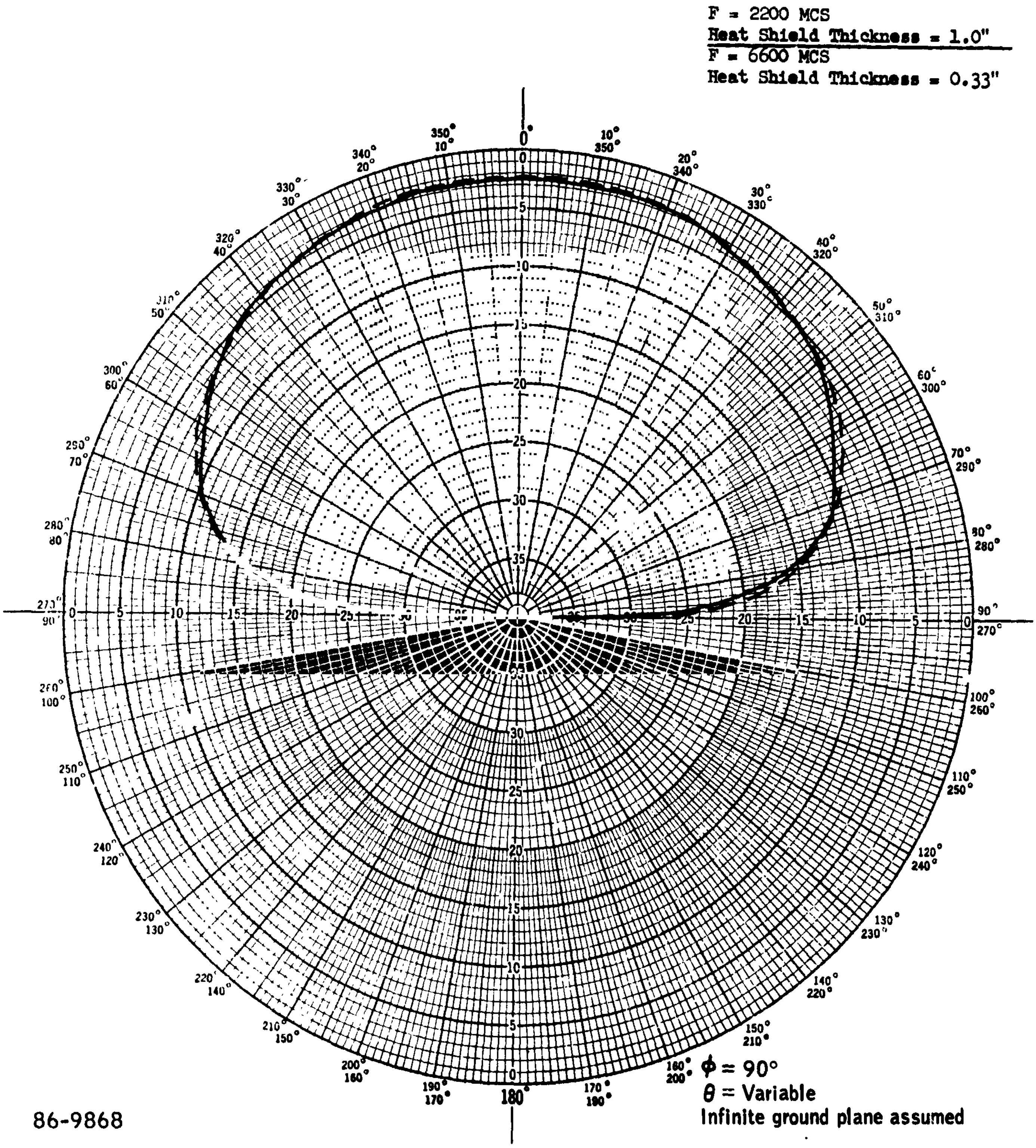

Figure 16 THEORETICAL PATTERNS OF 2200 MC AND 6600 MC OPEN-ENDED WAVEGUIDE COVERED WITH AVCOAT 5026-39M. PRINCIPAL E PLANE

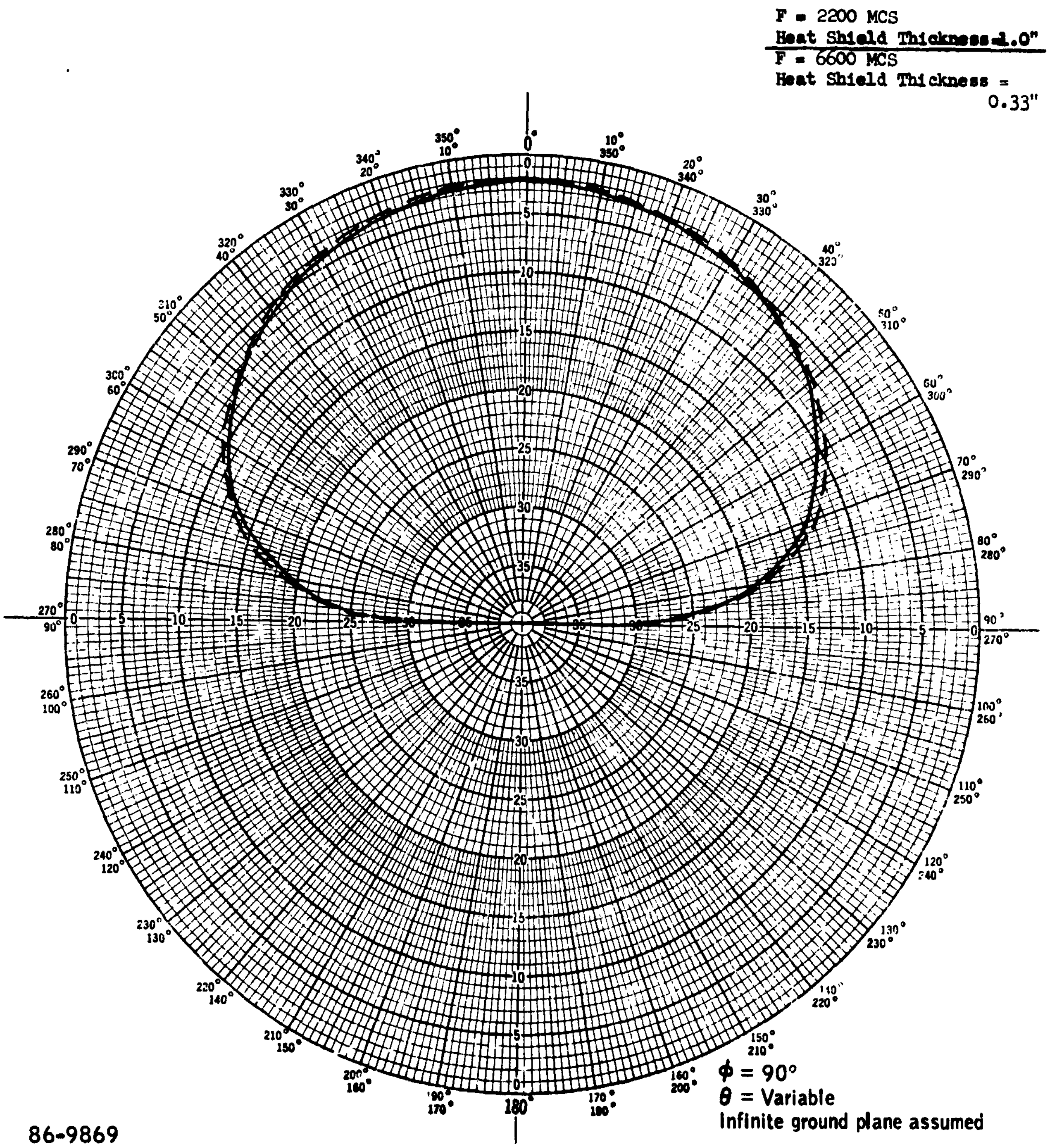

86-9869

Figure 17 THEORETICAL PATTERNS OF 2200 MC AND 6600 MC OPEN-ENDED WAVEGUIDE COVERED WITH AVCOAT 5026-39M. PRINCIPAL H PLANE

In addition to the antenna patterns, the aperture impedances of the open-ended waveguide were calculated for the cases given in the following table.

Frequency (Mc)	Guide	Relative Permittivity of Dielectric Cover (ϵ/ϵ_0)	Antenna Aperture Impedance (ohms)
300	WR-2300	2.5 - j 0.200	549 - j 69
300	WR-2300	1.00 - j 0.000	885 - j 219
2200	WR-430	1.85 - j 0.014	181 - j 99
2200	WR-430	1.00 - j 0.000	411 - j 245
6600	WR-137	1.85 - j 0.014	186 - j 125
6600	WR-137	1.00 - j 0.000	478 - j 278
11000	WR-90	1.85 - j 0.041	210 - j 106
11000	WR-90	1.00 - j 0.000	427 - j 240

8. Computer Program in Fortran

The computer programs to calculate the impedance and radiation patterns of the dielectric-covered open-ended waveguide appear on the subsequent pages.

The programs are used in the order of the block diagram below.

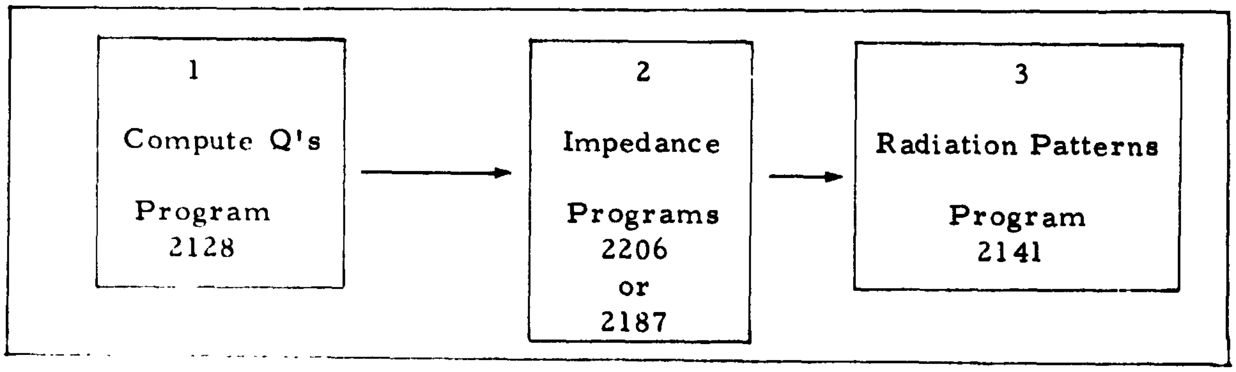

PROGRAM 2128

```
$IBFTC MICRØ    LIST
      DIMENSIØN RAD(520),H1(520),H2(520),U(520),W(520),YY(520),V(520),
     1XX(520),UP(520),VP(520),XXP(520),VO(520),VOP(520)
      CØMPLEX Z0,K1,Q1,Q2,H1SQ,H1,H2SQ,H2,Z1,U,W,YY,FANS,FINT,GANS,V,
     1XINT,XX,QT1,QT2,Z2,Z3,Z4,F2,F3,F4,SUMEV,SUMØD,TF1,SUMT,ANS,SUM,
     2EPS1,EPSN,UP,VP,XXP,Q1P,Q2P,QT1P,QT2P,FANS2,VO,VOP,Q0,QT0,Q0P,QT0P
     3,FANS3,FANS4
      REAL K0,L0
      CØMMØN H1,H2,U,W,YY,V,XX,UP,Z0,JMAX,RAD,A,R,B,X,Y,PI,FL,FK,CA,CB,
     1DELTA,CL,CK,CØNV,IQ0,IQ0P,IQ1,IQ1P,IQ2,IQ2P
      NAMELIST/NAMIN/A,B,K,L,L0,FRF,EPSN,X,Y,EPS,DELTA,RSTEP,CØNV,NSTEP
       NAMELIST/NAMØUT/ØMEGA,K0,K1,EPS1
      NAMELIST/NAMIQ/IQ0,IQ0P,IQ1,IQ1P,IQ2,IQ2P
 3333 READ(5,NAMIN)
      IF(A.EQ.9999.)CALL EXIT
      WRITE(6,1003)
 1003 FØRMAT(1H1)
      WRITE(6,NAMIN)
      CL=1.
      CK=1.
      L2=L-2*(L/2)
      IF(L2.EQ.1)CL=-1
      K2=K-2*(K/2)
      IF(K2.EQ.1)CK=-1
      FL=L
      FK=K
      PI=3.14159265
      CC1=1.0E-8
      EPS0=8.85E-12
      ØMEGA=2.*PI*FRF
      EPS1=EPS0*EPSN
      K0=ØMEGA*CC1/3.
      K1=K0*CSQRT(EPSN)
      WRITE(6,NAMØUT)
      CA=FL*PI/A
      CB=FK*PI/B
      Z0=CMPLX(0.,1.)
      PK1=REAL(K1)
      PPK1=AIMAG(K1)
      RMIN=0.
      RMAX=RSTEP
      IQ0=0
      IQ0P=0
      IQ1=0
      IQ2=0
      IQ1P=0
      IQ2P=0
      READ(5,NAMIQ)
      RTEST=PK1-EPS
      IRTEST=0
      WRITE(6,1002)RTEST
 1002 FØRMAT(1H0 10X,6HRTEST=,E15.6)
      IF(RMAX.GT.RTEST)RMAX=RTEST
      Q0=CMPLX(0.,0.)
      Q0P=CMPLX(0.,0.)
      Q1=CMPLX(0.,0.)
      Q2=CMPLX(0.,0.)
      Q1P=CMPLX(0.,0.)
      Q2P=CMPLX(0.,0.)
      QT0=CMPLX(0.,0.)
```

```
      QT1=CMPLX(0.,0.)
      QT2=CMPLX(0.,0.)
      QT0P=CMPLX(0.,0.)
      QT1P=CMPLX(0.,0.)
      QT2P=CMPLX(0.,0.)
  100 N=NSTEP
      J0=1
      JSTEP=1
    1 JMAX=N+1
      ILL=0
      SMAX=N
      RDEL=(RMAX-RMIN)/SMAX
      DØ 2 J=J0,JMAX,JSTEP
      STEP=J
      R=RMIN+RDEL*(STEP-1.)
      RAD(J)=R
      H1SQ=K1*K1-R*R
      H1(J)=CSQRT(H1SQ)
      H2SQ=K0*K0-R*R
      H2(J)=CSQRT(H2SQ)
      Z1=-2.*Z0*H1(J)*L0
      U(J)=(H1(J)+EPSN*H2(J))*CEXP(Z1)/(H1(J)-EPSN*H2(J))
      UP(J)=(H1(J)+H2(J))*CEXP(Z1)/(H1(J)-H2(J))
      W(J)=     (1.+U(J))/(1.-U(J))
      YY(J)=(1.-UP(J))*H1(J)/(1.+UP(J))
C     THIS CØMPLETES PRELIMINARY SET UP. NØW DØ INTEGRATIØN
      CALL SIMV(FANS,FANS2,FANS3,FANS4)
      V(J)=FANS-CØNJG(FANS)
      VP(J)=FANS2-CØNJG(FANS2)
      V0(J)=FANS3-CØNJG(FANS3)
      V0P(J)=FANS4-CØNJG(FANS4)
      CALL SIMX(FANS,FANS2)
      XX(J)=FANS-CØNJG(FANS)
      XXP(J)=FANS2-CØNJG(FANS2)
    2 CØNTINUE
C     NØW DØ Q1 AND Q2
      IF(IQ0.EQ.0)CALL SIMQ1(ILL,QT0,V0)
      WRITE(6,1005)RMIN,RMAX,Q0,QT0,Q0P,QT0P
      IF(ILL.EQ.1)GØ TØ 3
      IF(IQ0P.EQ.0)CALL SIMQ1(ILL,QT0P,V0P)
      WRITE(6,1005)RMIN,RMAX,Q0,QT0,Q0P,QT0P
      IF(ILL.EQ.1)GØ TØ 3
      IF(IQ1.EQ.0)CALL SIMQ1(ILL,QT1,V)
      WRITE(6,1001)RMIN,RMAX,Q1,QT1,Q1P,QT1P
      IF(ILL.EQ.1)GØ TØ 3
      IF(IQ1P.EQ.0)CALL SIMQ1(ILL,QT1P,VP)
      WRITE(6,1001)RMIN,RMAX,Q1,QT1,Q1P,QT1P
      IF(ILL.EQ.1)GØ TØ 3
      IF(IQ2.EQ.0)CALL SIMQ2(ILL,QT2,XX)
      WRITE(6,1004)RMIN,RMAX,Q2,QT2,Q2P,QT2P
      IF(ILL.EQ.1)GØ TØ 3
      IF(IQ2P.EQ.0)CALL SIMQ2(ILL,QT2P,XXP)
      WRITE(6,1004)RMIN,RMAX,Q2,QT2,Q2P,QT2P
      IF(ILL.EQ.1)GØ TØ 3
      IF(RMAX.EQ.RTEST)GØ TØ 6
      T1=CABS(QT0)
      T2=CABS(Q0)
      IF(T2.GT.1.)GØ TØ 17
      IF(T1.LT.CØNV)IQ0=1
      GØ TØ 15
```

```
   17 IF(T1.LT.(CØNV*T2))IQ0=1
   15 T1=CABS(QTOP)
      T2=CABS(Q0P)
      IF(T2.GT.1.)GØ TØ 18
      IF(T1.LT.CØNV)IQ0P=1
      GØ TØ 16
   18 IF(T1.LT.(CØNV*T2))IQ0P=1
   16 T1=CABS(QT1)
      T2=CABS(Q1)
      IF(T2.GT.1.)GØ TØ 116
      IF(T1.LT.CØNV)IQ1=1
      GØ TØ 11
  116 IF(T1.LT.(CØNV*T2))IQ1=1
   11 T1=CABS(QT2)
      T2=CABS(Q2)
      IF(T2.GT.1.)GØ TØ 111
      IF(T1.LT.CØNV)IQ2=1
      GØ TØ 12
  111 IF(T1.LT.(CØNV*T2))IQ2=1
   12 T1=CABS(QT1P)
      T2=CABS(Q1P)
      IF(T2.GT.1.)GØ TØ 112
      IF(T1.LT.CØNV)IQ1P=1
      GØ TØ 13
  112 IF(T1.LT.(CØNV*T2))IQ1P=1
   13 T1=CABS(QT2P)
      T2=CABS(Q2P)
      IF(T2.GT.1.)GØ TØ 113
      IF(T1.LT.CØNV)IQ2P=1
      GØ TØ 14
  113 IF(T1.LT.(CØNV*T2))IQ2P=1
   14 IF((IQ1*IQ2*IQ1P*IQ2P*IQ0*IQ0P).EQ.0)GØ TØ 4
      Q0=QT0+Q0
      Q0P=QT0P+Q0P
      Q1=Q1+QT1
      Q2=Q2+QT2
      Q1P=Q1P+QT1P
      Q2P=Q2P+QT2P
      GØ TØ 200
    4 RT1=RMIN
      RT2=RMAX
      RMIN=RMAX
      RMAX=RMAX+RSTEP
      IF(IRTEST.EQ.1)GØ TØ 30
      IF(RMAX.GT.RTEST)RMAX=RTEST
   30 IF(IQ1.EQ.0)Q1=Q1+QT1
      IF(IQ2.EQ.0)Q2=Q2+QT2
      IF(IQ1P.EQ.0)Q1P=Q1P+QT1P
      IF(IQ2P.EQ.0)Q2P=Q2P+QT2P
      IF(IQ0.EQ.0)Q0=Q0+QT0
      IF(IQ0P.EQ.0)Q0P=Q0+QT0P
      WRITE(6,1005)RT1,RT2,Q0,QT0,Q0P,QT0P
      WRITE(6,1001)RT1,RT2,Q1,QT1,Q1P,QT1P
      WRITE(6,1004)RT1,RT2,Q2,QT2,Q2P,QT2P
 1001 FØRMAT(1H0 10X,5HRMIN=,F6.1,5HRMAX=,F6.1/10X,3HQ1=,2F9.3,4HQT1=,
     12F9.3/10X,4HQ1P=,2F9.3,5HQT1P=,2F9.3)
 1004 FØRMAT(1H0 10X,5HRMIN=,F6.1,5HRMAX=,F6.1/10X,3HQ2=,2F9.3,4HQT2=,
     12F9.3/10X,4HQ2P=,2F9.3,5HQT2P=,2F9.3)
 1005 FØRMAT(1H0 10X,5HRMIN=,F6.1,5HRMAX=,F6.1/10X,3HQ0=,2F9.3,4HQT0
     12F9.3/10X,4HQ0P=,2F9.3,5HQT0P=,2F9.3)
```

```
      GØ TØ 100
    6 RMIN=RTEST+2.*EPS
      RMAX=RMIN+RSTEP
      IRTEST=1
      IF(IQ2.EQ.0)Q2=Q2+QT2
      IF(IQ2P.EQ.0)Q2P=Q2P+QT2P
      Q1=QT1+(W(JMAX)*V(JMAX)*2.*(CSQRT(Z0*PPK1+EPS)-CSQRT(Z0*PPK1-EPS))
     1)/CSQRT(2.*PK1+Z0*PPK1)+Q1
      Q0=QT0+(W(JMAX)*V(JMAX)*2.*(CSQRT(Z0*PPK1+EPS)-CSQRT(Z0*PPK1-EPS))
     1)/CSQRT(2.*PK1+Z0*PPK1)+Q0
      Q1P=QT1P+(W(JMAX)*VP(JMAX)*2.*(CSQRT(Z0*PPK1+EPS)-CSQRT(Z0*PPK1-EP
     1S)))/CSQRT(2.*PK1+Z0*PPK1)+Q1P
      Q0P=QT0P+(W(JMAX)*VP(JMAX)*2.*(CSQRT(Z0*PPK1+EPS)-CSQRT(Z0*PPK1-EP
     1S)))/CSQRT(2.*PK1+Z0*PPK1)+Q0P
      GØ TØ 100
    3 IF((2*JMAX).GT.600)GØ TØ 10
      DØ 5 J=1,JMAX
      L=JMAX+1-J
      LL=2*L-1
      RAD(LL)=RAD(L)
      H1(LL)=H1(L)
      H2(LL)=H2(L)
      U(LL)=U(L)
      UP(LL)=UP(L)
      W(LL)=W(L)
      YY(LL)=YY(L)
      V(LL)=V(L)
      VP(LL)=VP(L)
      XXP(LL)=XXP(L)
      V0(LL)=V0(L)
      V0P(LL)=V0(L)
    5 XX(LL)=XX(L)
      J0=2
      JSTEP=2
      N=2*N
      GØ TØ 1
   10 WRITE(6,1000)RMAX,N
 1000 FØRMAT(1H1 10X,14HPØØR ITERATIØN,5X,5HRMAX=,F7.1,5X,2HN=,I5)
   20 GØ TØ 3333
  200 CØNTINUE
      WRITE(6,2000)Q1,Q1P,Q2,Q2P,Q0,Q0P
 2000 FØRMAT(1H0 10X,9HSØLUTIØN,5X,3HQ1=,2F9.3,5X,4HQ1P=,2F9.3/24X,3HQ2=
     1,2F9.3,5X,4HQ2P=,2F9.3/24X,3HQ0=,2F9.3,5X,4HQ0P=,2F9.3)
      GØ TØ 3333
      END
$IBFTC SIMV1    LIST
      SUBRØUTINE SIMV(ANS,ANS2,ANS3,ANS4)
      DIMENSIØN RAD(520),H1(520),H2(520),U(520),W(520),YY(520),V(520),
     1XX(520),UP(520)
      CØMPLEX Z0,K1,Q1,Q2,H1SQ,H1,H2SQ,H2,Z1,U,W,YY,FANS,FINT,GANS,V,
     1XINT,XX,QT1,QT2,Z2,Z3,Z4,F2,F3,F4,SUMEV,SUMØD,TF1,SUMT,ANS,SUM,
     2EPS1,EPSN,UP,DUM,TFT,TF2,SUMT2,ANS2,ANS3,ANS4,SUMT3,SUMT4,TF3,TF4,
     3FØNT
      REAL K0,L0
      CØMMØN H1,H2,U,W,YY,V,XX,UP,Z0,JMAX,RAD,A,R,B,X,Y,PI,FL,FK,CA,CB,
     1DELTA,CL,CK,CØNV,IQ0,IQ0P,IQ1,IQ1P,IQ2,IQ2P
      N=8
      TEST=0.0001
      TESTT=0.0001
      TESTT3=0.0001
```

```
      TESTT4=0.0001
      IF(IQ1.EQ.1)TEST=0.
      IF(IQ1P.EQ.1)TESTT=0.
      IF(IQ0.EQ.1)TESTT3=0.
      IF(IQ0P.EQ.1)TESTT4=0.
      DEL=3.*PI/2.
    1 V2=N
      TDEL=PI/(2.*V2)
      C1=4.
      C2=-2.
      SUMT=CMPLX(0.,0.)
      SUMT2=CMPLX(0.,0.)
      SUMT3=CMPLX(0.,0.)
      SUMT4=CMPLX(0.,0.)
      NN=N/2
      DØ 2 K=1,NN
      V1=K
      Z=TDEL*(2.*V1-1.)
      SU=SIN(Z)
      CU=CØS(Z)
      TFT=FINT(SU,CU,Z)
      IF(IQ1.EQ.0)TF1=CU*TFT
      IF(IQ1P.EQ.0)TF2=SU*TFT
      TFT=FØNT(SU,CU,Z)
      IF(IQ0.EQ.0)TF3=CU*TFT
      IF(IQ0P.EQ.0)TF4=SU*TFT
      Z=Z+3.*PI/2.
      TEM=CU
      CU=SU
      SU=-TEM
      TFT=FINT(SU,CU,Z)
      IF(IQ1.EQ.0)TF1=TF1+CU*TFT
      IF(IQ1P.EQ.0)TF2=TF2+SU*TFT
      TFT=FØNT(SU,CU,Z)
      IF(IQ0.EQ.0)TF3=TF3+CU*TFT
      IF(IQ0P.EQ.0)TF4=TF4+SU*TFT
      IF(IQ1.EQ.0)SUMT=SUMT+C1*TF1
      IF(IQ1P.EQ.0)SUMT2=SUMT2+C1*TF2
      IF(IQ0.EQ.0)SUMT3=SUMT3+C1*TF3
      IF(IQ0P.EQ.0)SUMT4=SUMT4+C1*TF4
      C1=C1+C2
      C2=-C2
      Z=TDEL*(2.*V1)
      SU=SIN(Z)
      CU=CØS(Z)
      TFT=FINT(SU,CU,Z)
      IF(IQ1.EQ.0)TF1=CU*TFT
      IF(IQ1P.EQ.0)TF2=SU*TFT
      TFT=FØNT(SU,CU,Z)
      IF(IQ0.EQ.0)TF3=CU*TFT
      IF(IQ0P.EQ.0)TF4=SU*TFT
      Z=Z+3.*PI/2.
      TEM=CU
      CU=SU
      SU=-TEM
      TFT=FINT(SU,CU,Z)
      IF(IQ1.EQ.0)TF1=TF1+CU*TFT
      IF(IQ1P.EQ.0)TF2=TF2+SU*TFT
      TFT=FØNT(SU,CU,Z)
      IF(IQ0.EQ.0)TF3=TF3+CU*TFT
```

```
      IF(IQ0P.EQ.0)TF4=TF4+SU*TFT
      IF(IQ1.EQ.0)SUMT=SUMT+C1*TF1
      IF(IQ1P.EQ.0)SUMT2=SUMT2+C1*TF2
      IF(IQ0.EQ.0)SUMT3=SUMT3+C1*TF3
      IF(IQ0P.EQ.0)SUMT4=SUMT4+C1*TF4
      C1=C1+C2
      C2=-C2
    2 CØNTINUE
      IF(IQ1P.EQ.0)SUMT2=SUMT2-FINT(-1.,0.,3.*PI/2.)-FINT(1.,0.,PI/2.)
      IF(IQ0P.EQ.0)SUMT4=SUMT4-FØNT(-1.,0.,3.*PI/2.)-FØNT(1.,0.,PI/2.)
      SUMT=TDEL*SUMT/3.
      SUMT2=TDEL*SUMT2/3.
      SUMT3=TDEL*SUMT3/3.
      SUMT4=TDEL*SUMT4/3.
      TEST1=CABS(SUMT)
      TEST2=CABS(SUMT2)
      TEST3=CABS(SUMT3)
      TEST4=CABS(SUMT4)
      IF(TEST.GT.1.)GØ TØ 6
      IF(ABS(TEST-TEST1).LT. CØNV)GØ TØ 5
      GØ TØ 100
    6 IF(ABS(1.-TEST1/TEST).LT. CØNV)GØ TØ 5
  100 CØNTINUE
      N=2*N
      TEST=TEST1
      TESTT=TEST2
      TESTT3=TEST3
      TESTT4=TEST4
      GØ TØ 1
    5 IF(TESTT.GT.1.)GØ TØ 26
      IF(ABS(TESTT-TEST2).LT.CØNV)GØ TØ 25
      GØ TØ 100
   26 IF(ABS(1.-TEST2/TESTT).LT.CØNV)GØ TØ 25
      GØ TØ 100
   25  IF(TESTT3.GT.1.)GØ TØ 27
      IF(ABS(TESTT3-TEST3).LT.CØNV)GØ TØ 28
      GØ TØ 100
   27 IF(ABS(1.-TEST3/TESTT3).LT.CØNV)GØ TØ 28
      GØ TØ 100
   28 IF(TESTT4.GT.1.)GØ TØ 29
      IF(ABS(TESTT4-TEST4).LT.CØNV)GØ TØ 30
      GØ TØ 100
   29 IF(ABS(1.-TEST4/TESTT4).LT.CØNV)GØ TØ 30
      GØ TØ 100
   30 ANS=SUMT
      ANS3=SUMT3
      ANS4=SUMT4
      ANS2=SUMT2
      RETURN
      END
$IBFTC SIMX1    LIST
      SUBRØUTINE SIMX(ANS,ANS2)
      DIMENSIØN RAD(520),H1(520),H2(520),U(520),W(520),YY(520),V(520),
     1XX(520),UP(520)
      CØMPLEX Z0,K1,Q1,Q2,H1SQ,H1,H2SQ,H2,Z1,U,W,YY,FANS,FINT,GANS,V,
     1XINT,XX,QT1,QT2,Z2,Z3,Z4,F2,F3,F4,SUMEV,SUMØD,TF1,SUMT,ANS,SUM,
     2EPS1,EPSN,UP,DUM,TFT,TF2,SUMT2,ANS2,XINTP
      REAL K0,L0
      CØMMØN H1,H2,U,W,YY,V,XX,UP,Z0,JMAX,RAD,A,R,B,X,Y,PI,FL,FK,CA,CB,
     1DELTA,CL,CK,CØNV,IQ0,IQ0P,IQ1,IQ1P,IQ2,IQ2P
```

```
      N=8
      TEST=0.0001
      TESTT=0.0001
      IF(IQ2.EQ.1)TEST=0.
      IF(IQ2P.EQ.1)TESTT=0.
      DEL=3.*PI/2.
    1 V2=N
      TDEL=PI/(2.*V2)
      C1=4.
      C2=-2.
      SUMT=CMPLX(0.,0.)
      SUMT2=CMPLX(0.,0.)
      TFT=CMPLX(0.,0.)
      TF2=CMPLX(0.,0.)
      TF1=CMPLX(0.,0.)
      NN=N/2
      DØ 2 K=1,NN
      V1=K
      Z=TDEL*(2.*V1-1.)
      IF(IQ2.EQ.0)TF1=XINT(Z)
      IF(IQ2P.EQ.0)TF2=XINTP(Z)
      Z=Z+DEL
      IF(IQ2.EQ.0)TF1=TF1+XINT(Z)
      IF(IQ2P.EQ.0)TF2=TF2+XINTP(Z)
      IF(IQ2.EQ.0)SUMT=SUMT+C1*TF1
      IF(IQ2P.EQ.0)SUMT2=SUMT2+C1*TF2
      C1=C1+C2
      C2=-C2
      Z=TDEL*(2.*V1)
      IF(IQ2.EQ.0)TF1=XINT(Z)
      IF(IQ2P.EQ.0)TF2=XINTP(Z)
      Z=Z+DEL
      IF(IQ2.EQ.0)TF1=TF1+XINT(Z)
      IF(IQ2P.EQ.0)TF2=TF2+XINTP(Z)
      IF(IQ2.EQ.0)SUMT=SUMT+C1*TF1
      IF(IQ2P.EQ.0)SUMT2=SUMT2+C1*TF2
      C1=C1+C2
      C2=-C2
    2 CØNTINUE
      IF(IQ2.EQ.0)SUMT=SUMT+XINT(DEL)-XINT(PI/2.)
      IF(IQ2P.EQ.0)SUMT2=SUMT2+XINTP(DEL)-XINTP(PI/2.)
      SUMT=TDEL*SUMT/3.
      SUMT2=TDEL*SUMT2/3.
      TEST1=CABS(SUMT)
      TEST2=CABS(SUMT2)
      IF(TEST.GT.1.)GØ TØ 6
      IF(ABS(TEST-TEST1).LT. CØNV)GØ TØ 5
      GØ TØ 100
    6 IF(ABS(1.-TEST1/TEST).LT. CØNV)GØ TØ 5
  100 CØNTINUE
      N=2*N
      TEST=TEST1
      TESTT=TEST2
      GØ TØ 1
    5 IF(TESTT.GT.1.)GØ TØ 26
      IF(ABS(TESTT-TEST2).LT.CØNV)GØ TØ 25
      GØ TØ 100
   26 IF(ABS(1.-TEST2/TESTT).LT.CØNV)GØ TØ 25
      GØ TØ 100
   25 ANS=SUMT
```

```
      ANS2=SUMT2
  200 CØNTINUE
      RETURN
      END
$IBFTC FINT1   LIST
      CØMPLEX FUNCTIØN FINT(SU,CU,Z)
      DIMENSIØN RAD(520),H1(520),H2(520),U(520),W(520),YY(520),V(520),
     1XX(520),UP(520)
      CØMPLEX Z0,K1,Q1,Q2,H1SQ,H1,H2SQ,H2,Z1,U,W,YY,FANS,FINT,GANS,V,
     1XINT,XX,QT1,QT2,Z2,Z3,Z4,F2,F3,F4,SUMEV,SUMØD,TF1,SUMT,ANS,SUM,
     2EPS1,EPSN,UP,DUM
      REAL K0,L0
      CØMMØN H1,H2,U,W,YY,V,XX,UP,Z0,JMAX,RAD,A,R,B,X,Y,PI,FL,FK,CA,CB,
     1DELTA,CL,CK,CØNV,IQ0,IQ0P,IQ1,IQ1P,IQ2,IQ2P
      Z1=-Z0*A*R*SU
      Z2=-Z0*B*R*CU
      Z3=Z0*R*(X*SU+Y*CU)
      F1=((CB*SU)**2-(CA*CU)**2)*R*R
      IF(CA.EQ.0.)F1=CB*CB
      IF(CB.EQ.0.)F1=-CA*CA
      IF(FL.NE.0.)F2=-0.5*Z0*A*A/(FL*PI)
      IF(Z.GT.(PI/2.))F2=-F2
      IF(FK.NE.0.)F3=-0.5*Z0*B*B/(FK*PI)
      TEM1=(R*SU)**2-CA*CA
      TEM2=(R*CU)**2-CB*CB
      IF(CA.EQ.0.)TEM1=1.
      IF(CB.EQ.0.)TEM2=1.
      IF(ABS(TEM1).LT.DELTA)GØ TØ 1
      F2=(CL*CEXP(Z1)-1.)/TEM1
    1 IF(ABS(TEM2).LT.DELTA)GØ TØ 2
      F3=(CK*CEXP(Z2)-1.)/TEM2
    2 F4=CEXP(Z3)
      SUMT=F1*F2*F3*F4
  100 CØNTINUE
      FINT=SUMT
      RETURN
      END
$IBFTC FØNT1   LIST
      CØMPLEX FUNCTIØN FØNT(SU,CU,Z)
      DIMENSIØN RAD(520),H1(520),H2(520),U(520),W(520),YY(520),V(520),
     1XX(520),UP(520)
      CØMPLEX Z0,K1,Q1,Q2,H1SQ,H1,H2SQ,H2,Z1,U,W,YY,FANS,FINT,GANS,V,
     1XINT,XX,QT1,QT2,Z2,Z3,Z4,F2,F3,F4,SUMEV,SUMØD,TF1,SUMT,ANS,SUM,
     2EPS1,EPSN,UP,FØNT
      REAL K0,L0
      CØMMØN H1,H2,U,W,YY,V,XX,UP,Z0,JMAX,RAD,A,R,B,X,Y,PI,FL,FK,CA,CB,
     1DELTA,CL,CK,CØNV,IQ0,IQ0P,IQ1,IQ1P,IQ2,IQ2P
      IF(FL.EQ.0.)GØ TØ 20
      IF(FK.EQ.0.)GØ TØ 20
      Z1=-Z0*A*R*SU
      Z2=-Z0*B*R*CU
      Z3=Z0*R*(X*SU+Y*CU)
      F2=-0.5*Z0*A*A/(FL*PI)
      IF(Z.GT.(PI/2.))F2=-F2
      F3=-0.5*Z0*B*B/(FK*PI)
      TEM1=(R*SU)**2-CA*CA
      TEM2=(R*CU)**2-CB*CB
      IF(ABS(TEM1).LT.DELTA)GØ TØ 1
      F2=(CL*CEXP(Z1)-1.)/TEM1
    1 IF(ABS(TEM2).LT.DELTA)GØ TØ 2
```

```
      F3=(CK*CEXP(Z2)-1.)/TEM2
    2 F4=CEXP(Z3)
      FØNT=F2*F3*F4
   21 RETURN
   20 FØNT=CMPLX(0.,0.)
      GØ TØ 21
      END
$IBFTC XINT1    LIST
      CØMPLEX FUNCTIØN XINT(Z)
      DIMENSIØN RAD(520),H1(520),H2(520),U(520),W(520),YY(520),V(520),
     1XX(520),UP(520)
      CØMPLEX Z0,K1,Q1,Q2,H1SQ,H1,H2SQ,H2,Z1,U,W,YY,FANS,FINT,GANS,V,
     1XINT,XX,QT1,QT2,Z2,Z3,Z4,F2,F3,F4,SUMEV,SUMØD,TF1,SUMT,ANS,SUM,
     2EPS1,EPSN,UP,DUM
      REAL K0,L0
      CØMMØN H1,H2,U,W,YY,V,XX,UP,Z0,JMAX,RAD,A,R,B,X,Y,PI,FL,FK,CA,CB,
     1DELTA,CL,CK,CØNV,IQ0,IQ0P,IQ1,IQ1P,IQ2,IQ2P
      CU=CØS(Z)
      SU=SIN(Z)
      Z1=-Z0*A*R*SU
      Z2=-Z0*B*R*CU
      Z3=Z0*R*(X*SU+Y*CU)
      F1=R*R*SU*SU*CU
      IF(CA.EQ.0.)F1=CU
      IF(CB.EQ.0.)F1=SU*SU
      IF(FL.NE.0.)F2=-0.5*Z0*A*A/(FL*PI)
      IF(Z.GT.(PI/2.))F2=-F2
      IF(FK.NE.0.)F3=-0.5*Z0*B*B/(FK*PI)
      IF(CB.EQ.0.)F3=-Z0*B*R
      TEM1=(R*SU)**2-CA*CA
      TEM2=(R*CU)**2-CB*CB
      IF(CA.EQ.0.)TEM1=1.
      IF(CB.EQ.0.)TEM2=CU
      IF(ABS(TEM1).LT.DELTA)GØ TØ 1
      F2=(CL*CEXP(Z1)-1.)/TEM1
    1 IF(ABS(TEM2).LT.DELTA)GØ TØ 2
      F3=(CK*CEXP(Z2)-1.)/TEM2
    2 F4=CEXP(Z3)
      SUMT=F1*F2*F3*F4
      XINT=SUMT
      RETURN
      END
$IBFTC XIP1     LIST
      CØMPLEX FUNCTIØN XINTP(Z)
      DIMENSIØN RAD(520),H1(520),H2(520),U(520),W(520),YY(520),V(520),
     1XX(520),UP(520)
      CØMPLEX Z0,K1,Q1,Q2,H1SQ,H1,H2SQ,H2,Z1,U,W,YY,FANS,FINT,GANS,V,
     1XINT,XX,QT1,QT2,Z2,Z3,Z4,F2,F3,F4,SUMEV,SUMØD,TF1,SUMT,ANS,SUM,
     2EPS1,EPSN,UP,DUM,XINTP
      REAL K0,L0
      CØMMØN H1,H2,U,W,YY,V,XX,UP,Z0,JMAX,RAD,A,R,B,X,Y,PI,FL,FK,CA,CB,
     1DELTA,CL,CK,CØNV,IQ0,IQ0P,IQ1,IQ1P,IQ2,IQ2P
      SU=SIN(Z)
      CU=CØS(Z)
      Z1=-Z0*A*R*SU
      Z2=-Z0*B*R*CU
      Z3=Z0*R*(X*SU+Y*CU)
      F1=R*R*CU*CU*SU
      IF(CA.EQ.0.)F1=CU*CU
      IF(CB.EQ.0.)F1=SU
```

```
      IF(FL.NE.0.)F2=-0.5*Z0*A*A/(FL*PI)
      IF(Z.GT.(PI/2.))F2=-F2
      IF(FK.NE.0.)F3=-0.5*Z0*B*B/(FK*PI)
      IF(CA.EQ.0.)F2=-Z0*A*R
      TEM1=(R*SU)**2-CA*CA
      TEM2=(R*CU)**2-CB*CB
      IF(CA.EQ.0.)TEM1=SU
      IF(CB.EQ.0.)TEM2=1.
      IF(ABS(TEM1).LT.DELTA)GØ TØ 1
      F2=(CL*CEXP(Z1)-1.)/TEM1
    1 IF(ABS(TEM2).LT.DELTA)GØ TØ 2
      F3=(CK*CEXP(Z2)-1.)/TEM2
    2 F4=CEXP(Z3)
      SUMT=F1*F2*F3*F4
      XINTP=SUMT
      RETURN
      END
$IBFTC SIQ1    LIST
       SUBRØUTINE SIMQ1(ILL,ANS,VXT)
      DIMENSIØN RAD(520),H1(520),H2(520),U(520),W(520),YY(520),V(520),
     1XX(520),UP(520),VXT(520)
      CØMPLEX Z0,K1,Q1,Q2,H1SQ,H1,H2SQ,H2,Z1,U,W,YY,FANS,FINT,GANS,V,
     1XINT,XX,QT1,QT2,Z2,Z3,Z4,F2,F3,F4,SUMEV,SUMØD,TF1,SUMT,ANS,SUM,
     2EPS1,EPSN,UP,VXT
      CØMMØN H1,H2,U,W,YY,V,XX,UP,Z0,JMAX,RAD,A,R,B,X,Y,PI,FL,FK,CA,CB,
     1DELTA,CL,CK,CØNV,IQ0,IQ0P,IQ1,IQ1P,IQ2,IQ2P
      KDEL=(JMAX-1)/2
      TEST=0.0001
    2 SUM=CMPLX(0.,0.)
      C1=2.
      C2=+2.
      DØ 1 K=1,JMAX,KDEL
      SUM=SUM+C1*W(K)*VXT(K)/H1(K)
      C1=C1+C2
      C2=-C2
    1 CØNTINUE
      SUM=SUM-W(1)*VXT(1)/H1(1)-W(JMAX)*VXT(JMAX)/H1(JMAX)
      SUM=SUM* (RAD(KDEL+1)-RAD(1))/3.
      TEST1=CABS(SUM)
      IF(TEST.GT.1.)GØ TØ 4
      IF(ABS(TEST-TEST1).LT. CØNV)GØ TØ 3
      GØ TØ 100
    4 IF(ABS(1.-TEST1/TEST).LT. CØNV)GØ TØ 3
  100 CØNTINUE
      TEST=TEST1
      KDEL=KDEL/2
      IF(KDEL.GE.1)GØ TØ 2
      ILL=1
    3 ANS=SUM
      RETURN
      END
$IBFTC SIQ2    LIST
      SUBRØUTINE SIMQ2(ILL,ANS,VXT)
      DIMENSIØN RAD(520),H1(520),H2(520),U(520),W(520),YY(520),V(520),
     1XX(520),UP(520),VXT(520)
      CØMPLEX Z0,K1,Q1,Q2,H1SQ,H1,H2SQ,H2,Z1,U,W,YY,FANS,FINT,GANS,V,
     1XINT,XX,QT1,QT2,Z2,Z3,Z4,F2,F3,F4,SUMEV,SUMØD,TF1,SUMT,ANS,SUM,
     2EPS1,EPSN,UP,VXT
      REAL K0,L0
      CØMMØN H1,H2,U,W,YY,V,XX,UP,Z0,JMAX,RAD,A,R,B,X,Y,PI,FL,FK,CA,CB,
```

```
     1DELTA,CL,CK,CØNV,IQ0,IQ0P,IQ1,IQ1P,IQ2,IQ2P
      KDEL=(JMAX-1)/2
      TEST=0.0001
    2 SUM=CMPLX(0.,0.)
      C1=2.
      C2=+2.
      DØ 1 K=1,JMAX,KDEL
      SUM=SUM+C1*VXT(K)*YY(K)
      C1=C1+C2
      C2=-C2
    1 CØNTINUE
      SUM=SUM-VXT(1)*YY(1)-VXT(JMAX)*YY(JMAX)
      SUM=SUM* (RAD(KDEL+1)-RAD(1))/3.
      TEST1=CABS(SUM)
      IF(TEST.GT.1.)GØ TØ 4
      IF(ABS(TEST-TEST1).LT. CØNV)GØ TØ 3
      GØ TØ 100
    4 IF(ABS(1.-TEST1/TEST).LT. CØNV)GØ TØ 3
  100 CØNTINUE
      TEST=TEST1
      KDEL=KDEL/2
      IF(KDEL.GE.1)GØ TØ 2
      ILL=1
    3 ANS=SUM
      RETURN
      END
```

PROGRAM 2206

```
*ØLIVER BIN 54
$JØB             * 2206  RCC  R540W121A200010 ØLIVER   54 MAYHAN        30
$EXECUTE         IBJØB
$IBJØB           GØ,MAP
$IBFTC IMPED     LIST
      CØMPLEX Q1,Q2,R,S,Z10,Z,EPSR,ZO,TEM
      REAL KG
      NAMELIST/NAMIN/A0,B0,F,A,X,EPSR,Q1,Q2,KG
      PI=3.1415926
      UM=4.*PI*1.0E-7
      EPS0=8.85E-12
      C=3.0E8
      Z0=CMPLX(0.,1.)
    2 READ(5,NAMIN)
      IF(A0.EQ.999.)CALL EXIT
      WRITE(6,NAMIN)
      ØMEGA=2.0*PI*F
      GAM10=SQRT(KG*(ØMEGA/C)**2-(PI/A)**2)
      A0=-GAM10*B0/(UM*ØMEGA)
      R=-A0*SIN(PI*X/A)-Z0*ØMEGA*EPSR*EPS0*B0*A*Q1/(4.*PI**3)+Z0*B0*Q2
     1/(4.0*PI*A*ØMEGA*UM)
      S=EPSR*EPS0*UM*ØMEGA*ØMEGA*Q1/(4.0*PI*PI)-Q2/(4.0*A*A)-Z0*GAM10*
     1PI*SIN(PI*X/A)/A
      Z10=R/S
      TEM=Z0*PI*Z10*ØMEGA*UM/(A*B0)
      RCC=CABS(TEM)
      Z=(1.-TEM)/(1.+TEM)
      Z=120.0*PI*Z*ØMEGA/(GAM10*C)
      WRITE(6,1)Z,Z10,RCC
    1 FØRMAT(1H1 10X,2HZ=,2E13.4,5X,4HZ10=,2E13.4,5X,4HRCC=E13.4)
      GØ TØ 2
      END
$DATA
 $NAMIN A0=-.002,B0=1.0,F=2.2E9,A=.492E-1,X=.368E-1,EPSR=(.716,.248),
 Q1=(-17.547,-4.321),Q2=(-6.867,1.264),KG=3.75$
 $NAMIN A0=-.002,B0=1.0,F=2.2E9,A=.492E-1,X=.164E-1,EPSR=(.716,.248),
 Q1=(-20.826,-3.998),Q2=(-20.270,1.393),KG=3.75$

$IBSYS
$PAUSE
```

PROGRAM 2187

```
$IBFTC SØLVR    LIST,DD
      DIMENSIØN GAM(3,2),X(4),Y(4),DUM(100),U(7,7),G(7),W(7),Q0(4,3,2),
     1Q0P(4,3,2),Q1(4,3,2),Q1P(4,3,2),Q2(4,3,2),Q2P(4,3,2)
      CØMPLEX GAM,U,G,W,Q0,Q0P,Q1,Q1P,Q2,Q2P,Z0,EP1,EPN,F1,F2,H1,H2,GP,
     1 GPP,A0,PED,PED1,PED2
      CØMMØN GAM,U,G,W,Q0,Q0P,Q1,Q1P,Q2,Q2P,EP1,Z0,A0,X,Y,DUM,ØMEGA,PIA,
     1PIB,EP0,UM0,B0,XJ,YJ,PI
      REAL K0
      NAMELIST/NAMIN/EPN,FRF,A,B,A0,B0
      NAMELIST/NAMXY/X,Y
      NAMELIST/NAMQ/Q0,Q0P,Q1,Q1P,Q2,Q2P
      DØ 4 J=1,4
      DØ 4 K=1,3
      DØ 4 L=1,2
       Q0(J,K,L)=CMPLX(0.,0.)
      Q0P(J,K,L)=CMPLX(0.,0.)
      Q1P(J,K,L)=CMPLX(0.,0.)
       Q1(J,K,L)=CMPLX(0.,0.)
       Q2(J,K,L)=CMPLX(0.,0.)
      Q2P(J,K,L)=CMPLX(0.,0.)
    4 CØNTINUE
      READ(5,NAMIN)
      READ(5,NAMXY)
      READ(5,NAMQ)
      EP0=8.85E-12
      UM0=12.5663706E-7
      Z0=CMPLX(0.,1.)
      PI=3.1415927
      C1=3.0E+08
      ØMEGA=2.*PI*FRF
      K0=ØMEGA/C1
      EP1=EPN*EP0
      TK=K0*K0
      PIA=PI/A
      PIB=PI/B
      TA=PIA*PIA
      TB=PIB*PIB
      TEMP=SQRT(ABS(TK-TB))
      GAM(1,2)=CMPLX(TEMP,0.)
      IF((TK-TB).LT.0.)GAM(1,2)=CMPLX(0.,TEMP)
      TEMP=SQRT(ABS(TK-TA))
      GAM(2,1)=CMPLX(TEMP,0.)
      IF((TK-TA).LT.0.)GAM(2,1)=CMPLX(0.,TEMP)
      TEMP=SQRT(ABS(TK-TA-TB))
      GAM(2,2)=CMPLX(TEMP,0.)
      IF((TK-TA-TB).LT.0.)GAM(2,2)=CMPLX(0.,TEMP)
      TEMP=SQRT(ABS(TK-4.*TA))
      GAM(3,1)=CMPLX(TEMP,0.)
      IF((TK-4.*TA).LT.0.)GAM(3,1)=CMPLX(0.,TEMP)
      TEMP=SQRT(ABS(TK-4.*TA-TB))
      GAM(3,2)=CMPLX(TEMP,0.)
      IF((TK-4.*TA-TB).LT.0.)GAM(3,2)=CMPLX(0.,TEMP)
      DØ 2 J=1,4
      XJ=X(J)
      YJ=Y(J)
      U(2*J-1,1)=F1(1.,1.,J,1,1)
      U(2*J-1,2)=F1(2.,1.,J,2,1)
      U(2*J-1,3)=H1(0.,1.,J,0,1)
      U(2*J-1,4)=H1(1.,0.,J,1,0)
      U(2*J-1,5)=H1(1.,1.,J,1,1)
```

```
      U(2*J-1,6)=H1(2.,0.,J,2,0)
      U(2*J-1,7)=H1(2.,1.,J,2,1)
      G(2*J-1)=GP(J)
      IF(J.EQ.4)GØ TØ 2
      U(2*J,1)=F2(1.,1.,J,1,1)
      U(2*J,2)=F2(2.,1.,J,2,1)
      U(2*J,3)=H2(0.,1.,J,0,1)
      U(2*J,4)=H2(1.,0.,J,1,0)
      U(2*J,5)=H2(1.,1.,J,1,1)
      U(2*J,6)=H2(2.,0.,J,2,0)
      U(2*J,7)  =H2(2.,1.,J,2,1)
      G(2*J)=GPP(J)
    2 CØNTINUE
      U(7,2)=CMPLX(0.,0.)
      U(1,6)=U(7,2)
      U(7,6)=U(7,2)
      U(7,7)=U(7,2)
    5 CØNTINUE
    6 CØNTINUE
      CALL CØMINV(U,7,7,DUM)
      DØ 3 J=1,7
      W(J)=CMPLX(0.,0.)
      DØ 3 KJ=1,7
      W(J)=W(J)+U(J,KJ)*G(KJ)
    3 CØNTINUE
      WRITE(6,1001)W(1)
      WRITE(6,1002)W(2)
      WRITE(6,1003)W(3)
      WRITE(6,1004)W(4)
      WRITE(6,1005)W(5)
      WRITE(6,1006)W(6)
      WRITE(6,1007)W(7)
 1001 FØRMAT(1H1 10X,6HY(1,1),5X,2E14.5)
 1002 FØRMAT(1H0 10X,6HY(2,1),5X,2E14.5)
 1003 FØRMAT(1H0 10X,6HZ(0,1),5X,2E14.5)
 1004 FØRMAT(1H0 10X,6HZ(1,0),5X,2E14.5)
 1005 FØRMAT(1H0 10X,6HZ(1,1),5X,2E14.5)
 1006 FØRMAT(1H0 10X,6HZ(2,0),5X,2E14.5)
 1007 FØRMAT(1H0 10X,6HZ(2,1),5X,2E14.5)
      PED1=Z0*PIA*W(4)*ØMEGA*UMO/BO
      PED=(1.+PED1)/(1.-PED1)
      WRITE(6,1008)PED
 1008 FØRMAT(1H0 10X,6HYL/Y0=,2E14.5)
      PED2=376.7/PED
      WRITE(6,1009)PED2
 1009 FØRMAT(1H0 10X,10HIMPEDANCE=,2E14.5)
      CALL EXIT
      END
$IBFTC CØMINV  FULIST,REF,DECK,M94,DD,XR7
      SUBRØUTINE CØMIN(A,NN,MAXDIM,LABEL )
CØMPLEX MATRIX INVERSIØN
      DIMENSIØN A(MAXDIM,MAXDIM)
      DIMENSIØN LABEL(1)
      CØMPLEX  FRE ,  A ,X , Y
      N=NN
      DØ 38 I=1,N
   38 LABEL(I)=I
    1 DØ 24 I=1,N
    2 FRE=(0. ,0. )
    3 DØ 7 M=1,N
```

```
      X= CABS ( A(M,I))
      Y=FRE
    4 IF(X-Y)  7,7, 5
    5  FRE = X
    6 IBIG=M
    7 CØNTINUE
    9 IF(IBIG-I)10,14,10
   10 DØ 13 M=1,N
   11 FRE=A(I,M)
   12 A(I,M)=A(IBIG,M)
   13 A(IBIG,M)=FRE
      M=LABEL(I)
      LABEL(I)=LABEL(IBIG)
      LABEL(IBIG)=M
   14 FRE=A(I,I)
   15 A(I,I)=( 1.0, 0.0 )
   16 DØ 17 M=1,N
   17 A(I,M)=A(I,M)/FRE
   18 DØ 24 J=1,N
   19 IF(J-I)20,24,20
   20 FRE=A(J,I)
   21 A(J,I)=(0. ,0.)
   22 DØ 23 K=1,N
   23 A(J,K)=A(J,K)-FRE*A(I,K)
   24 CØNTINUE
   25 M=N-1
   26 DØ 36 I=1,M
   27 DØ 30 J=I,N
   28 IF(LABEL(J)-I)30,29,30
   29 IF(I-J)31,36,31
   30 CØNTINUE
   31 DØ 34 K=1,N
   32 FRE=A(K,I)
   33 A(K,I)=A(K,J)
   34 A(K,J)=FRE
   35 LABEL(J)=LABEL(I)
   36 CØNTINUE
   37 RETURN
      END
$IBFTC TF1      LIST,DD
      CØMPLEX FUNCTIØN F1(FL,FK,J,L,K)
      DIMENSIØN GAM(3,2),X(4),Y(4),DUM(100),U(7,7),G(7),W(7),Q0(4,3,2),
     1Q0P(4,3,2),Q1(4,3,2),Q1P(4,3,2),Q2(4,3,2),Q2P(4,3,2)
      CØMPLEX GAM,U,G,W,Q0,Q0P,Q1,Q1P,Q2,Q2P,Z0,EP1,EPN,F1,F2,H1,H2,GP,
     1 GPP,A0,FF1
      REAL K0
      CØMMØN GAM,U,G,W,Q0,Q0P,Q1,Q1P,Q2,Q2P,EP1,Z0,A0,X,Y,DUM,ØMEGA,PIA,
     1PIB,EP0,UM0,B0,XJ,YJ,PI
                         FF1=+EP1*ØMEGA*FL*FK*PIA*PIB*GAM(L+1,K+1)*
     1Q0(J,L+1,K+1)+Z0*ØMEGA*EP0*FK*PIB*SIN(FL*PIA*XJ)*CØS(FK*PIB*YJ)
     2*4.*PI*PI
      F1=FF1
    1 CØNTINUE
      RETURN
      END
$IBFTC TH1      LIST,DD
      CØMPLEX FUNCTIØN H1(FL,FK,J,L,K)
      DIMENSIØN GAM(3,2),X(4),Y(4),DUM(100),U(7,7),G(7),W(7),Q0(4,3,2),
     1Q0P(4,3,2),Q1(4,3,2),Q1P(4,3,2),Q2(4,3,2),Q2P(4,3,2)
      CØMPLEX GAM,U,G,W,Q0,Q0P,Q1,Q1P,Q2,Q2P,Z0,EP1,EPN,F1,F2,H1,H2,GP,
```

```
      1 GPP,AO,HH1
       REAL KO
       COMMON GAM,U,G,W,QO,QOP,Q1,Q1P,Q2,Q2P,EP1,ZO,AO,X,Y,DUM,OMEGA,PIA,
      1PIB,EPO,UMO,BO,XJ,YJ,PI
                   HH1=OMEGA*OMEGA*UMO*EP1*Q1(J,L+1,K+1)
      1-(FL*FL*PIA*PIA+FK*FK*PIB*PIB)*Q2(J,L+1,K+1)-ZO*GAM(L+1,K+1)*FL*
      2PIA*SIN(FL*PIA*XJ)*COS(FK*PIB*YJ)*4.*PI*PI
       H1=HH1
     1 CONTINUE
       RETURN
       END
$IBFTC TH2      LIST,DD
       COMPLEX FUNCTION H2(FL,FK,J,L,K)
       DIMENSION GAM(3,2),X(4),Y(4),DUM(100),U(7,7),G(7),W(7),QO(4,3,2),
      1QOP(4,3,2),Q1(4,3,2),Q1P(4,3,2),Q2(4,3,2),Q2P(4,3,2)
       COMPLEX GAM,U,G,W,QO,QOP,Q1,Q1P,Q2,Q2P,ZO,EP1,EPN,F1,F2,H1,H2,GP,
      1 GPP,AO,HH2
       REAL KO
       COMMON GAM,U,G,W,QO,QOP,Q1,Q1P,Q2,Q2P,EP1,ZO,AO,X,Y,DUM,OMEGA,PIA,
      1PIB,EPO,UMO,BO,XJ,YJ,PI
                   HH2=-OMEGA*OMEGA*UMO*EP1*Q1P(J,L+1,K+1)
      1-(FL*FL*PIA*PIA+FK*FK*PIB*PIB)*Q2P(J,L+1,K+1)-ZO*GAM(L+1,K+1)*FK*
      2PIB*SIN(FK*PIB*YJ)*COS(FL*PIA*XJ)*4.*PI*PI
     1 CONTINUE
       H2=HH2
       RETURN
       END
$IBFTC TF2      LIST,DD
       COMPLEX FUNCTION F2(FL,FK,J,L,K)
       DIMENSION GAM(3,2),X(4),Y(4),DUM(100),U(7,7),G(7),W(7),QO(4,3,2),
      1QOP(4,3,2),Q1(4,3,2),Q1P(4,3,2),Q2(4,3,2),Q2P(4,3,2)
       COMPLEX GAM,U,G,W,QO,QOP,Q1,Q1P,Q2,Q2P,ZO,EP1,EPN,F1,F2,H1,H2,GP,
      1 GPP,AO,FF2
       REAL KO
       COMMON GAM,U,G,W,QO,QOP,Q1,Q1P,Q2,Q2P,EP1,ZO,AO,X,Y,DUM,OMEGA,PIA,
      1PIB,EPO,UMO,BO,XJ,YJ,PI
                   FF2=-EP1*OMEGA*FL*FK*PIA*PIB*GAM(L+1,K+1)*
      1QOP(J,L+1,K+1)-ZO*OMEGA*EPO*FL*PIA*SIN(FK*PIB*YJ)*COS(FL*PIA*XJ)
      2*4.*PI*PI
        F2=FF2
     1 CONTINUE
       RETURN
       END
$IBFTC TG2
       COMPLEX FUNCTION GPP(J)
       DIMENSION GAM(3,2),X(4),Y(4),DUM(100),U(7,7),G(7),W(7),QO(4,3,2),
      1QOP(4,3,2),Q1(4,3,2),Q1P(4,3,2),Q2(4,3,2),Q2P(4,3,2)
       COMPLEX GAM,U,G,W,QO,QOP,Q1,Q1P,Q2,Q2P,ZO,EP1,EPN,F1,F2,H1,H2,GP,
      1 GPP,AO
       REAL KO
       COMMON GAM,U,G,W,QO,QOP,Q1,Q1P,Q2,Q2P,EP1,ZO,AO,X,Y,DUM,OMEGA,PIA,
      1PIB,EPO,UMO,BO,XJ,YJ,PI
       GPP    =ZO*OMEGA*EP1*BO*Q1P(J,2,1)/PIA+ZO*BO*PIA*Q2P(J,2,1)/(OMEGA*
      1UMO)
       RETURN
       END
$IBFTC TGP
       COMPLEX FUNCTION GP(J)
       DIMENSION GAM(3,2),X(4),Y(4),DUM(100),U(7,7),G(7),W(7),QO(4,3,2),
      1QOP(4,3,2),Q1(4,3,2),Q1P(4,3,2),Q2(4,3,2),Q2P(4,3,2)
```

```
      CØMPLEX GAM,U,G,W,Q0,Q0P,Q1,Q1P,Q2,Q2P,Z0,EP1,EPN,F1,F2,H1,H2,GP,
     1 GPP,A0
      REAL K0
      CØMMØN GAM,U,G,W,Q0,Q0P,Q1,Q1P,Q2,Q2P,EP1,Z0,A0,X,Y,DUM,ØMEGA,PIA,
     1PIB,EP0,UMC,B0,XJ,YJ,PI
      GP=-4.*PI*PI*A0*SIN(PIA*XJ)-Z0*ØMEGA*EP1*B0*Q1(J,2,1)/PIA+Z0*B0
     1*PIA*Q2(J,2,1)/(ØMEGA*UM0)
      RETURN
      END
 $NAMIN EPN=(1.85,0.022),FRF=2.2E+09,A=.1092,B=.0546,A0=(-.002,0.),B0=1.$
 $NAMXY X=.0546,.0819,.0819,.0546,Y=.0273,.0273,.04095,.04095$
 $NAMQ
 Q0(3,2,2)=(.002,0.),Q0(3,3,2)=(-.001,0.),
 Q0P(1,3,2)=(-.008,0.),Q0P(2,2,2)=(-.011,0.),
 Q0P(2,3,2)=(.002,0.),Q0P(3,2,2)=(-.010,0.),
 Q0P(3,3,2)=(.001,0.),Q0P(4,3,2)=(-.008,0.),
 Q1(1,2,1)=(-11.440,-15.672),Q1(2,2,1)=(-7.931,-13.204),
 Q1(2,3,1)=(17.431,10.262),Q1(3,1,2)=(-3.015,-3.498),
 Q1(3,2,1)=(-4.851,-11.293),Q1(3,2,2)=(0.,-.033),
 Q1(3,3,1)=(12.359,9.047),Q1(3,3,2)=(-.001,-.001),
 Q1(4,2,1)=(-7.478,-13.466),Q1(4,2,2)=(-.002,-.045),
 Q1P(1,1,2)=(-2.020,17.505),Q1P(1,3,2)=(-9.992,-8.732),
 Q1P(2,1,2)=(5.204,11.432),Q1P(2,2,2)=(-12.741,-15.468),
 Q1P(2,3,2)=(7.689,-1.727),Q1P(3,1,2)=(3.926,10.752),
 Q1P(3,2,1)=(2.908,2.199),Q1P(3,2,2)=(-11.629,-14.929),
 Q1P(3,3,1)=(1.685,3.391),Q1P(3,3,2)=(5.221,-1.878),
 Q1P(4,1,2)=(-2.415,16.497),Q1P(4,3,1)=(11.540,5.743),
 Q1P(4,3,2)=(-14.248,-8.785),
 Q2(1,2,1)=(2.462,27.281),Q2(2,2,1)=(4.992,20.632),
 Q2(2,3,1)=(15.544,-6.441),Q2(3,1,2)=(-2.749,-.954),
 Q2(3,2,1)=(5.037,20.145),Q2(3,2,2)=(.972,-.763),
 Q2(3,3,1)=(12.175,-6.289),Q2(3,3,2)=(.001,.010),
 Q2(4,2,1)=(4.262,26.633),Q2(4,2,2)=(6.327,-1.005),
 Q2P(1,1,2)=(-15.313,14.185),Q2P(1,3,2)=(21.491,-1.135),
 Q2P(2,1,2)=(-17.176,13.627),Q2P(2,2,2)=(15.278,-1.903),
 Q2P(2,3,2)=(-2.057,-0.815),Q2P(3,1,2)=(-.975,12.609),
 Q2P(3,2,1)=(4.487,-2.170),Q2P(3,2,2)=(3.432,-1.747),
 Q2P(3,3,1)=(-1.015,-.944),Q2P(3,3,2)=(-.840,-.760),
 Q2P(4,1,2)=(1.375,13.617) $
-
$IBSYS
$PAUSE
```

PROGRAM 2141

```
$IBFTC A2141    LIST,SDD
      DIMENSION   P(100)     ,THETA(100),PHI(100),W1L( 50 ),W2K( 50 ),
     1 ZLKD(50,50),YLKD(50,50),V1L(50),V2K(50),S1L(50),S2K(50)
      COMPLEX     EPSR,ZLK,YLK,ZK12,H1,EIM,WSH,WSLV,WHAT,WSU,USLV,UHAT,
     1 WSW1,WSW2,SUM1,SUM2,SUM3,W1L,W2K,W1,W2,WS1,WS2,WS3, R,XL,S,T
     2 ,ZLKD,YLKD,W11,     GLK,V1L,V2K,S1L,S2K,SUM4,SUM5,WS4,WS5,
     3 RCON,ELCON,S.,S2,V1,V2,V20,S20
      REAL  MEMO
      CALL BCDCON(180HW,EPSR,      ELZ,A,B,                    M,N,
     1 BZ,C,EPSZ,EMUZ,THETA,PHI,NTHETA,NPHI
     2
     3
     6  ,W,EPSR,         ELZ,A,B,                      MM,NN,BZ,C,EPSZ,
     5  EMUZ,THETA,PHI,NTHETA,NPHI   )
      CALL BCDCON(36HZLK(50,50),YLK(50,50)
     1  ,ZLKD,YLKD)
      CALL BCDCON(36HDATE,CASE,MEMO
     1  ,DATE,CASE,MEMO )
      PTST = 1.0E-5
      RAD = .174532925F-1
      PI = 3.14159265
      LTAP5 = 6
      C     = 3.0E8
      EPSZ = 8.85E-12
      EMUZ = 12.566371E-7
      E.M =  (0.0,-1.0)
   99 CONTINUE
      CALL SYMBLS(IN     )
      ZKZ= W/C
      ZKZ2 = ZKZ **2
      ZK12 = EPSR * ZKZ2
      N = NN+1
      M = MM+1
      WRITE(LTAP5,100) DATE,CASE,MEMO
  100 FORMAT(1H1,49X,5HDATE F8.3,5X,5HCASE F8.3,5X,5HMEMO F8.3 )
      DO 1000 I=1,NTHETA
      THET = THETA(I)
      TH =    THET *RAD
      STH = SIN(TH)
      CTH = COS(TH)
      STH2 = STH**2
      CTH2 = CTH**2
      SCTH = STH*CTH
      H2 = ZKZ*CTH
      H1 = CSQRT ( ZK12    - ZKZ2    *STH2 )
      IF(AIMAG(H1)) 30,31,31
   30 H1 = -H1
   31 WSH =  CEXP ( EIM*(H1+H2)*ELZ )
      WSLV =(2.0*H1*EPSR)/(H1-EPSR*H2)   * WSH
      WHAT = (2.0*H1)/(H1-H2)* WSH
      WSU = CEXP ( EIM *2.0*H1*ELZ)
      USLV=  WSU *(H1+EPSR*H2)/(H1-EPSR*H2)
      UHAT=  WSU *(H1+H2)/(H1-H2)
   20 KM=1
      DO 2000 J=1,NPHI
      PH = PHI(J)*RAD
      SPH= SIN(PH)
      CPH= COS(PH)
      SPH2 = SPH**2
      CPH2 = CPH**2
```

```
      STCP = STH*CPH
      S2TC2P = STCP**2  * ZKZ2
      STSP = STH*SPH
      S2TS2P=  STSP**2  * ZKZ2
      WSW1 =  CEXP (EIM* A *ZKZ * STCP )
      WSW2 =  CEXP (EIM* B *ZKZ * STSP )
   22 KM=1
      V1L(1) = (WSW1-1.0)/(ZKZ2*STH2)
      V2K(1) = (WSW2-1.0)/(ZKZ2*STH2)
      IF(ABS(PH-1.570796325)-PTST) 60,60,50
   50 IF(ABS(PH-4.71238898)-PTST) 60,60,51
   60 S1 = (EIM*A*SPH)/(ZKZ*STH)
      GØ TØ 52
   51 LL=0
      EL = LL
      DEN = S2TC2P -(EL*PI/A)**2
      IF(ABS(DEN)-1.0E-5) 56,56,57
   56 W1 =(0.0,0.0)
      GØ TØ 58
   57 W1 = ((-1.0)**LL*WSW1-1.0)/DEN
   58 S1 = SPH*CPH*W1
   52 S1L(1) = S1
      IF(PH-PTST) 61,61,53
   53 IF(ABS(PH-3.14159265)-PTST) 61,61,54
   61 S2 = (EIM*B*CPH)/(ZKZ*STH)
      GØ TØ 55
   54 KK =0
      ZK=KK
      DEN = S2TS2P-(ZK*PI/B)**2
      IF(ABS(DEN)-1.0E-5) 63,63,64
   63 W2 = (0.0,0.0)
      GØ TØ 65
   64 W2 = ((-1.0)**KK*WSW2-1.0)/DEN
   65 S2 = SPH*CPH*W2
   55 S2K(1) = S2
      DØ 3000 L=2,N
      LL=L-1
      EL=LL
      DEN = S2TC2P - (EL*PI/A)**2
      IF(ABS(DEN)-1.0E-5)  2,2,3
    2 W1 = (0.0,0.0)
      GØ TØ 4
    3 W1 = ((-1.0)**LL *WSW1-1.0)/DEN
    4 V1 = CPH2*W1
      S1 = SPH*CPH*W1
      W1L(L) = W1
      V1L(L) = V1
      S1L(L) = S1
 3000 CØNTINUE
      DØ 4000 K=2,M
      KK= K-1
      ZK = KK
      DEN = S2TS2P -(ZK*PI/B)**2
      IF(ABS(DEN)- 1.0E-5)  5,5,6
    5 W2 = (0.0,0.0)
      GØ TØ 7
    6 W2 =  ((-1.0)**KK*WSW2 -1.0)/DEN
    7 V2 = SPH2*W2
      S2 = SPH*CPH*W2
      W2K(K) = W2
```

```
      V2K(K) = V2
      S2K(K) = S2
 4000 CØNTINUE
      SUM1 = (0.0,0.0)
      SUM2 = (0.0,0.0)
      SUM3 = (0.0,0.0)
      SUM4 = (0.0,0.0)
      SUM5 = (0.0,0.0)
      W11 =  W1L(2)
      V20 = V2K(1)
      S20 = S2K(1)
   23 KM=1
      DØ 5000 L=1,N
      W1 = W1L(L)
      EL = L -1
      WS2L= EL*PI/A
      WS3L=WS2L**2
      V1 = V1L(L)
      S1 = S1L(L)
   21 KM=1
      DØ 5000 K=1,M
      W2 = W2K(K)
      ZK = K-1
      WS2K=ZK*PI/B
      WS3K=WS2K**2
      V2 = V2K(K)
      S2 = S2K(K)
      YLK = YLKD(L,K)
      ZLK = ZLKD(L,K)
      GLK =CSQRT (ZKZ2 - WS3L - WS3K )
      IF(AIMAG(GLK)) 32,33,33
   32 GLK = -GLK
   33 WS1 = WS3K * V1*W2 *ZLK
      WS2 = WS3L * W1*V2 *ZLK
      WS3 = WS2K*WS2L*GLK*YLK*W1* W2
      WS4 = WS3L* ZLK *W1* S2
      WS5 = WS3K* ZLK *S1* W2
      IF(K-1) 41,41,42
   41 IF(L-1) 5000,5000,43
   43 SUM2 = SUM2 + WS2
      SUM4 = SUM4 + WS4
      GØ TØ 5000
   42 IF(L-1) 44,44,45
   45 SUM3 = SUM3 + WS3
      SUM2 = SUM2 + WS2
      SUM4 = SUM4 + WS4
   44 SUM1 = SUM1 + WS1
      SUM5 = SUM5 + WS5
 5000 CØNTINUE
      RCØN = ZKZ2 *STH2/(H1*(1.0-USLV))
      R = RCØN * (W*EMUZ*SUM1 - W*EMUZ*SUM2 + E1M*BZ*(PI/A)*W11*V20 +
     1  SUM3 )
      ELCØN = ZKZ2*STH2/(W*EMUZ*(1.0+UHAT))
      XL = ELCØN *(E1M*BZ*(PI/A)*W11*S20 - W*EMUZ*SUM4 - W*EMUZ*SUM5 )
      S =  WSLV*R
      T =  WHAT*XL
      SR = REAL(S)
      SI=AIMAG(S)
      TR = REAL(T)
      TI = AIMAG(T)
```

```
      PSØLV = 19.739209 *W*ZKZ *(CTH2/STH2) *(EPSZ *(SR   **2 +SI   **2)
     1  +  EMUZ *(TR   **2 + TI   **2) )
      P(J) = PSØLV
 2000 CØNTINUE
      WRITE(LTAP5,101) THET
  101 FØRMAT(1HO,8HTHETA = F8.3 /,9X,3HPHI,15X,1HP  )
      WRITE(LTAP5,102) (PHI(IP),P(IP),IP=1,NPHI )
  102 FØRMAT(F15.5,E20.8 )
 1000 CØNTINUE
      GØ TØ 99
      END
   W  18.849556E8  EPSR  3.0  0.2  ELZ  0.5  A  1.0  B  0.75
   M  1  N  2  BZ  1.0  THETA  10.0   PHI  20.0  NTHETA  1  NPHI  1
    ZLK(1)
      0.0  0.0  3.0  2.0  1.0  0.5  (101)  0.5  0.1  1.0  1.0
  0.5  0.0
   YLK(1)
      0.0  0.0  1.0  0.1  0.5  0.0  (101)  0.5  0.1  0.2  0.5
   0.1  0.1
   THETA  0.0(10.0)90.0    NTHETA  10
   PHI  0.0(20.0)360.0   NPHI  19
   THETA  1.0   NTHETA  1
1
END ØF DATA
$IBDBL
*DEBUG A2141    23
      DUMP V1L,V2K,W1L,W2K,S1L,S2K
*DEBUG A2141    20
      DUMP TH,H1,H2,WSH,WSLV,WHAT,WSU,USLV,UHAT
*DEBUG A2141    5000
      DUMP WS1,WS2,WS3,WS4,WS5,SUM1,SUM2,SUM3,SUM4,SUM5,K,L
*DEBUG A2141    2000
      DUMP RCØN,R,ELCØN,XL,S,T,PSØLV
*DEND
```

Programs 2206 or 2187 can be used to calculate impedance at the end of the open-ended waveguide. Number 2206 is the short-form program and provides less accuracy than program 2187. The results of programs 2206 and 2187 must be multiplied by Z_c/Z_o where Z_c is the characteristic impedance of the waveguide and Z_o is 377 ohms.

D. SIMULATOR VERIFICATION TESTS

1. Simulator Sources

Prior to the formulation of the simulator requirements, a survey was made of the qualified manufacturers of artificial dielectrics. The results of the survey showed that there were only four suppliers capable of producing dielectric simulators. They were as follows: Armstrong Cork Company, Avco Corporation, Custom Materials, Inc., and Emerson and Cuming, Inc.

Specifications for the simulators were formulated about the requirements stated in the original RFP. The requirements for the dielectric simulators were as follows: 1) They must be flexible; 2) Specific gravity must be less than 0.5; 3) They must be bondable to metal surfaces; 4) They should not permanently deform if inadvertently subjected to pressure; 4) They must be easy to machine; 6) Their electrical properties should not change in a temperature range from 0° F to 140° F; and 7) Moisture absorption over the above temperature range should be less than 0.5 percent.

The electrical and dimensional specifications for the simulators were carried out by the laws of scaling derived by Sinclair from Maxwell's Equations. The laws, which are applicable to all dielectrics, are as follows:

Quantity	Full Scale System	Model System
Length (Physical dimensions)	l	$l' = l/p$
Frequency	f	$f' = pf$
Complex Permittivity	$\epsilon' - j\epsilon''$	$[\epsilon' - j\epsilon''] = [\epsilon' - j\epsilon'']$
Loss Tangent	ϵ''/ϵ'	$[\epsilon''/\epsilon']' = [\epsilon''/\epsilon']$
Permeability	$u' - ju''$	$[u' - ju'']' = [u' - ju'']$
Conductivity	σ	$\sigma' = p\sigma$

where p is the scale factor.

Simulators for virgin Avcoat 5026-39M had to have identical dielectric constant and loss tangent for 1/3-, 1/5 , and full-scale tests as prescribed by the above electromagnetic laws of scaling. A simulator thickness of one inch was chosen for the full scale tests thus setting the 1/3- and 1/5-scale thickness to 0.33 inch and 0.20 inch, respectively. The low frequency simulators, 300 Mc, 900 Mc, and 1500 Mc, were assigned the following electrical properties: $\epsilon'/\epsilon_0 = 2.50 \pm 0.10$; $\epsilon''/\epsilon' = 0.082 \pm 0.005$. The electrical properties assigned to the high-frequency simulators (2200 Mc, 6600 Mc, and 11000 Mc) were as follows: $\epsilon'/\epsilon_0 = 1.85 \pm 0.10$; $\epsilon''/\epsilon' = 0.022 \pm 0.005$. These dielectric constant and loss tangent values were taken from the room-temperature dielectric measurements made at 300 Mc and 2200 Mc.

Once the physical and electrical properties of the virgin heat-shield simulators had been measured, requests for quotations were sent to the potential suppliers. Armstrong Cork Company was contracted to supply the simulators. This decision was based upon price, dielectric tolerances, and quality control standards stated by the supplier in their answer to Avco's RFQ.

In their development of the simulator material, Armstrong Cork Company had no problem in holding the tolerances on the 2.2 kMc, 6.6 kMc and 11 kMc simulators and supplying these simulators on schedule. They experienced extreme difficulty in trying to attain the same tolerances with 300 Mc, 900 Mc, and 1500 Mc simulators. The tolerance on the loss tangent was relaxed to +.005, -.027 so that the program would not be delayed any further. The specific-gravity tolerance was also relaxed to 0.6 in order to facilitate rapid development of the simulators. All other mechanical and electrical properties requirements remained unaltered. The simulator data supplied by the Armstrong Cork Company is given in the following table.

	2200 Mc to 11000 Mc	300 Mc	900 Mc	1500 Mc
Density (lb/ft^3)	22.9 - 23.5	28.8 - 31.0	28.1	28.7
Dielectric Constant	1.84 - 1.86	(x-z)2.49-2.60 (y)2.24-2.35	2.58 2.58	2.58 2.28
Loss Tangent	0.021 - 0.022	0.055 (avg.)	0.080	0.092

The properties of the char simulators were defined by volume conductivity measurements. The original intent was to char the heat shield to its full depth and simulate it with a single simulator. Serious problems arose in charring the heat shield to its full depth. For instance, the heat shield became badly cracked making it impossible to take valid attenuation measurements. The heat shield was therefore charred to an average depth of approximately 0.065 inch only. The intact, uncharred heat shield below the char layer was simulated with the virgin simulator material while the char layer was simulated by a thin conductive layer bonded onto the virgin heat-shield simulator.

Surface resistivity measurements made on the charred samples varied from 1.3 ohms per square to 46 ohms per square. It was decided that a versatile simulator material whose resistivity could be varied would be required. The appropriate char simulator would be attained by varying the resistivity until the antenna patterns matched those taken with the charred heat shield.

Eccosorb Space Cloth, a thin woven conductive fabric, was best suited for these requirements. The resistivity can be varied by laying sheets atop one another. The resultant resistivity may be obtained by considering the sheets as resistors in parallel. The material is self-extinguishing, weatherproof, and can be easily cut with scissors. Listed below is the data supplied by Emerson and Cuming Inc.

Type	Surface Resistivity (ohms/square)	Insertion Loss (db) (X-Band)	Thickness (inch)
SC-100	100	7.0	0.015
SC-200	200	4.0	0.010
SC-377	377	2.0	0.010

2. Simulator Inspection

Complex permittivity measurements were made on virgin heat-shield simulators at their respective operating frequencies. The measurements were made with the Rohde and Schwarz dielectrometer using the method described in Appendix B. All values are approximately 5 percent high because of sample compression in the sample holder. The results of the measurements are as follows:

Frequency (Mc)	ϵ'/ϵ_0	ϵ''/ϵ'
300	2.56	0.065
900	2.60	0.083
1500	2.62	0.095
2200	1.98	0.019
6600	1.97	0.020
11000	1.95	0.020

The above values of ϵ'/ϵ_0 and ϵ''/ϵ' were all within the specified tolerances except from the 1500 Mc simulator. Since these measurements were within +5 percent, the 1500 Mc simulator was allowed to pass inspection.

A density check was made on the 2200 Mc simulator with results showing that the material had a specific gravity of 0.509. This value of specific gravity was slightly above the purchase-order limit of 0.5. Density checks made on the 300 Mc simulator showed that the specific gravity was well within the 0.6 purchase order limit.

The simulator material adhered to the requirements of the original RFP. The material was flexible and did not permanently deform when subjected to pressure. The material was easy to machine with hand tools and was bondable to metal surfaces. Armstrong Cork recommended their J-1170/E-18 epoxy adhesive to be used but stated that a contact cement could be used without affecting the dielectric properties of the material if the bond line was thin. Weldwood Contact Cement was tested and provided an excellent bond. This was used as the bonding agent for both heat-shield and simulator material.

Resistivity measurements were made on the Eccosorb Space Cloth. Random samples from each of the sheets supplied were measured and the results showed that the resistivity was not uniform. An average resistivity was obtained from the sample measurements for each of the three resistivities purchased. These average values differ considerably from those supplied by the manufacturer. The results of the measurements are given below.

Type	Surface Resistivity* (ohms per square)	Surface Resistivity** (ohms per square)
SC-100	100	81
SC-200	200	480
SC-377	377	660

*Data supplied by manufacturer
**Measured Data

3. Verification Tests

The verification tests were performed for the following reasons:

a. To demonstrate the effects of the Apollo heat shield on antenna performance;

b. To demonstrate the validity of simulator use and the scaling of models;

c. To verify the theoretical computation of antenna impedance and radiation pattern.

Four different antennas were used as experimental mediums to perform these tasks. They were as follows: open ended waveguide, scimitar, scimitar-slot, and monopole antennas. Two base frequencies of 300 Mc and 2200 Mc were used along with their respective 1/3 and 1/5-scale frequencies of 900 Mc, 1500 Mc, 6600 Mc and 11000 Mc. The antennas were mounted on flat, square ground planes with lengths of 1.22λ and 8.88λ for the respective base frequencies of 300 Mc and 2200 Mc. The 300 Mc tests were limited to $1.22\ \lambda$ ground planes because of size restrictions.

For scaled tests, the ground planes were dimensionally scaled by factors of 1/3 and 1/5 so that their electrical length remained the same at the scaled frequencies. The simulators were scaled by retaining their full-scale complex permittivity at the scaled frequencies.

The 300 Mc and 900 Mc verification tests were made on one of Avco's outdoor antenna ranges while the tests from 1500 Mc to 11000 Mc inclusive were performed in Avco's 60-x 20-x 20-foot anechoic chamber.

The verification tests required the use of Avcoat 5026-39 virgin ablator. Two forms of the Avcoat 5026-39 heat shield are used on the Apollo vehicle; the molded (-39M) and the honeycomb (-39 HCG). The dielectric properties of the -39M and -39 HCG material were essentially the same at both 300 Mc and 2200 Mc. Prior to performing any verification tests, the -39M and -39 HCG materials were compared in terms of their effect on antenna impedance and radiation patterns. Antenna impedance and radiation patterns of an open-ended waveguide covered with both materials were taken at 6600 Mc. The results showed negligible difference between the molded (-39M) and the honeycomb (-39 HCG) in regard to antenna radiation patterns. The measured antenna-aperture impedances were identical. Since either material could be used for the verification tests, Avcoat 5026-39M was chosen because of its immediate availability and lower cost.

a. Open-Ended Waveguide, Full , 1/3 , and 1/5-Scale-Model Patterns and Impedance

Verification tests made with the open-ended-waveguide antenna are presented in matrix form in Table II. The matrix references a series of figures which are reprints of measured data. The figures, in turn, have related patterns superimposed to enable the reader to compare them readily.

Waveguide transitions were used as open-ended-waveguide antennas. Standard waveguide sizes available did not facilitate exact 1/3 and 1/5-scaling. However, guide sizes for scaled tests were chosen as close as possible to the required scale factors. Deviations from the scale factors for the antenna aperture were less than 7 percent.

The spherical coordinate system used for the open-ended-waveguide antenna patterns is defined in Figure 18 along with the location of the a and b guide dimensions.

The antenna efficiencies were calculated for the 300-Mc and 2200-Mc open-ended-waveguide antennas without heat shield, with virgin heat shield, with charred heat shield, and charred heat shield with antenna window. Antenna efficiency may be defined as follows:

(1) $$\alpha = \frac{G_o}{D} \quad \text{where } \alpha = \text{efficiency}$$

G_o = $\dfrac{\text{maximum radiation intensity (test antenna)}}{\text{radiation intensity from (lossless) isotropic source with same power input.}}$

D = $\dfrac{\text{maximum radiation intensity}}{\text{average radiation intensity}}$

TABLE II

VERIFICATION TESTS - OPEN ENDED WAVEGUIDE

Experiment No.	Anetnna Cover	Frequency (Mc)	Scale Factor	Efficiency (percent)	Measured 5026-39 Patterns versus Simulator Patterns Exp. No.	Figure No.	Measured 5026-39 Impedance versus Simulator Impedance
1	no cover	300	1	84.94		19, 20	Figure 36
2	virgin 5026-39	300	1	76.85	1 with 2	19, 20	Figure 36
3	virgin simulator	300	1		2 with 3	21, 22	Figure 36
4	virgin simulator	900	1/3		2 with 4	23, 24	Figure 36
5	virgin simulator	1500	1/5		2 with 5	25, 26	Figure 36
6	no cover	2200	1	71.74		27, 28	Figure 37
7	virgin 5026-39	2200	1	65.59	6 with 7	27, 28	Figure 37
8	virgin simulator	2200	1		7 with 8	29, 30	Figure 37
9	virgin simulator	6600	1/3		7 with 9	31, 32	Figure 38
10	virgin simulator	11000	1/5		7 with 10	33, 34	Figure 39

Experiment No.	Antenna Cover	Frequency (Mc)	Scale Factor	Efficiency (percent)	Measured 5026-39 Patterns versus Simulator Patterns Exp. No.	Figure No.	Measured 5026-39 Impedance versus Simulator Impedance
11	charred 5026-39	300	1	4.65	11 with 12	44, 45	Figure 60
12	char simulator	300	1		11 with 12	44, 45	Figure 60
13	char simulator	900	1/3		11 with 13	46, 47	Figure 61
14	char simulator	1500	1/5		11 with 14	48, 49	Figure 62
15	charred 5026-39	2200	1	8.25	15 with 16	50, 51	Figure 63
16	char simulator	2200	1		15 with 16	50, 51	Figure 63
17	char simulator	6600	1/3		15 with 17	52, 53	Figure 64
18	char simulator	11000	1/5		15 with 18	54, 55	Figure 65
19	charred 5026-39 with window	300	1	79.64	11 with 19	56, 57	Figure 60
20	charred 5026-39 with window	2200	1	70.45	15 with 20	58, 59	Figure 63

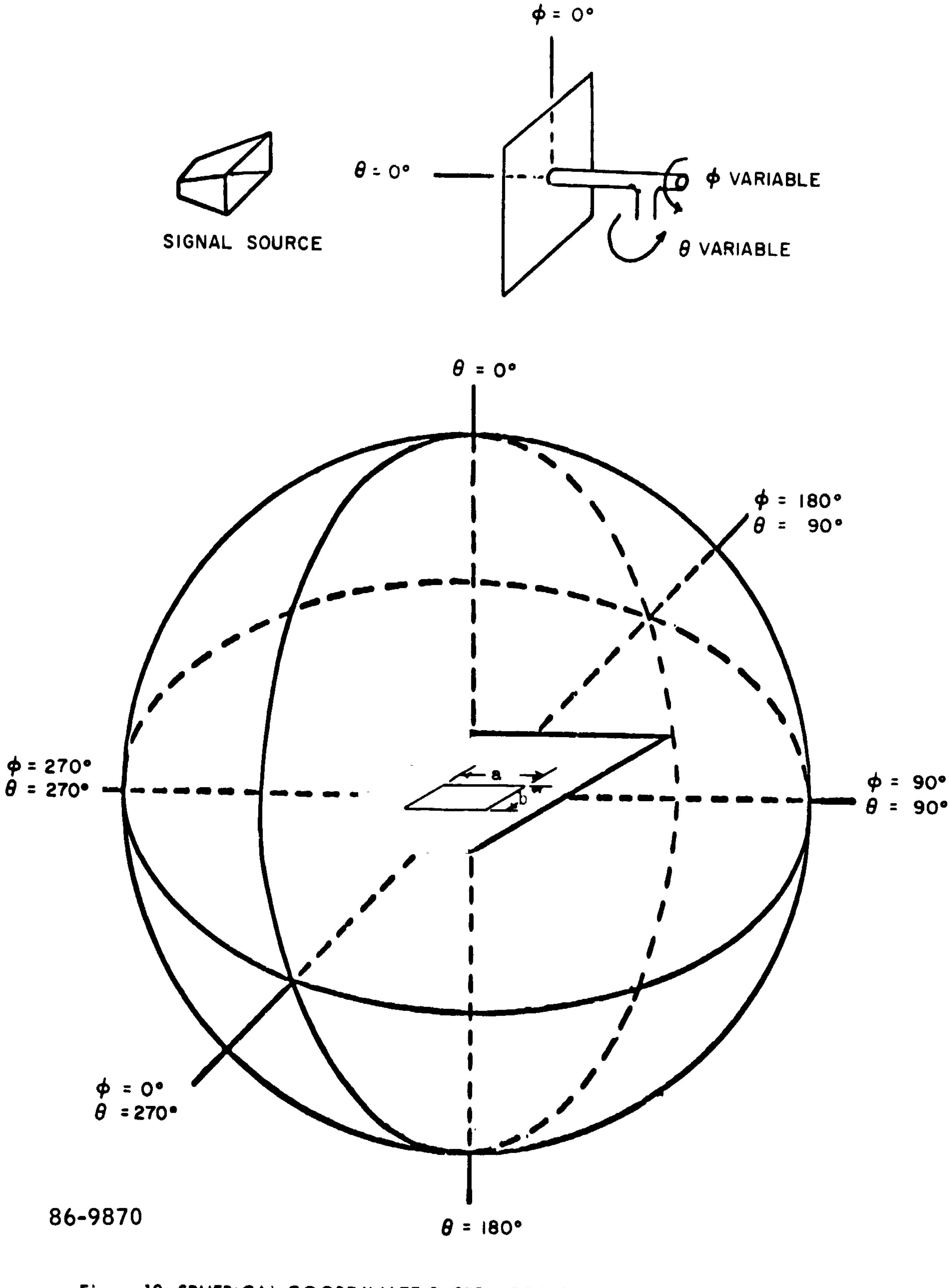

Figure 18 SPHERICAL COORDINATE SYSTEM FOR OPEN-ENDED WAVEGUIDE

therefore

$$(2) \quad \alpha = \frac{\dfrac{U_{max_T}}{U_{iso}}}{\dfrac{U_{max_T}}{U_{ave_T}}} = \frac{U_{max_T}\, U_{ave_T}}{U_{iso}\, U_{max_T}}$$

Since $U_{ave_T} = \dfrac{W_{ave_T}}{4\pi}$

$$(3) \quad \alpha = \frac{W_{ave_T}}{4\pi U_{iso}}$$

$$(4) \quad \alpha = \frac{\iint F^2 (\theta, \phi) \sin\theta d\theta\phi}{W_{iso}}$$

where F = relative field intensity

θ = polar angle

ϕ = azimuth angle

Equation (4) describes efficiency as the ratio of the power radiated by the antenna under test to the power radiated by an isotropic antenna. The integral in the numerator of Equation (4) was integrated graphically. In order to integrate accurately, antenna patterns were taken in 10-degree increments of θ from 0 degrees to 180 degrees for ϕ variable in both horizontal and vertical polarizations. These patterns were taken in voltage on polar paper. This allowed the area to be measured with a planimeter to obtain the average power of each pattern.

Average power levels for each pattern were multiplied by the sine of their associated θ angle. The average power level was then totaled for both polarizations and divided by the average value of the sine. The efficiency was obtained from the ratio of the average power of the test antenna to the isotropic power level.

Several conclusions can be made from the virgin-heat-shield and simulator tests. Patterns taken at 300 Mc with and without heat shield show that there is negligible distortion in the antenna-radiation patterns due to the heat-shield cover. The E- and H-plane patterns exhibited an average attenuation of approximately 1.5db in the main beam (θ = 270 degrees to 90 degrees). Antenna patterns taken with simulators for full-scale and scaled tests showed good correlation with the patterns taken with the Avcoat heat shield.

Considerable antenna-pattern distortion was observed with the heat-shield cover at 2200 Mc. Further test results indicated that the side radiation was caused by a surface wave coming off the ends of the ground plane and that the null and ripples were caused by the edges acting as an array element. These antenna patterns were in contrast to those taken at 300 Mc where little antenna-pattern distortion was observed with the heat-shield cover. The heat-shield thickness accounts for the differing effects. Both cases were taken with one-inch-thick heat-shield covers but their electrical thicknesses were 0.0254λ and 0.186λ for the 300 Mc and 2200 Mc cases, respectively. Antenna-radiation patterns taken with the 2200 Mc simulator deviated little from the Avcoat 5026-39M patterns. Considering the amount of antenna-pattern distortion, the simulators for the full-scale and scaled frequencies performed very well.

Impedance measurements made on the 300 Mc open-ended waveguide are referenced to the input terminal of the transition. The measurements were made in accordance with the test procedures; that is, without heat shield, with heat shield, and with simulator. At the scaled frequencies, the open-ended-waveguide impedance without heat shield were different from those of the 300 Mc transition.

Although the antenna apertures were scaled accurately, it was impossible to scale the probes and connectors of transition pieces. This omission in the scaling procedure caused the scaled impedances to differ. In order to compare the effects of the scaled simulators on antenna impedance to those of the heat shield, the antenna impedances of the scaled antennas were matched to the 300 Mc antenna without heat shield. The impedance measurements were then made with the simulator. Scaled impedance measurements did not show good correlation.

Impedance measurements made at 2200 Mc were more encouraging. At the scaled frequencies of 6600 Mc and 11000 Mc it was not required to match the antenna impedances to those of 2200 Mc. The scaled simulators were compared directly with the Avcoat 5026-39M heat shield which has the same complex permittivity as the simulators at the scaled frequencies. The heat-shield thickness was scaled to 0.33 inch and 0.20 inch for these tests. The impedance data compared very well with the Avcoat 5026-39M.

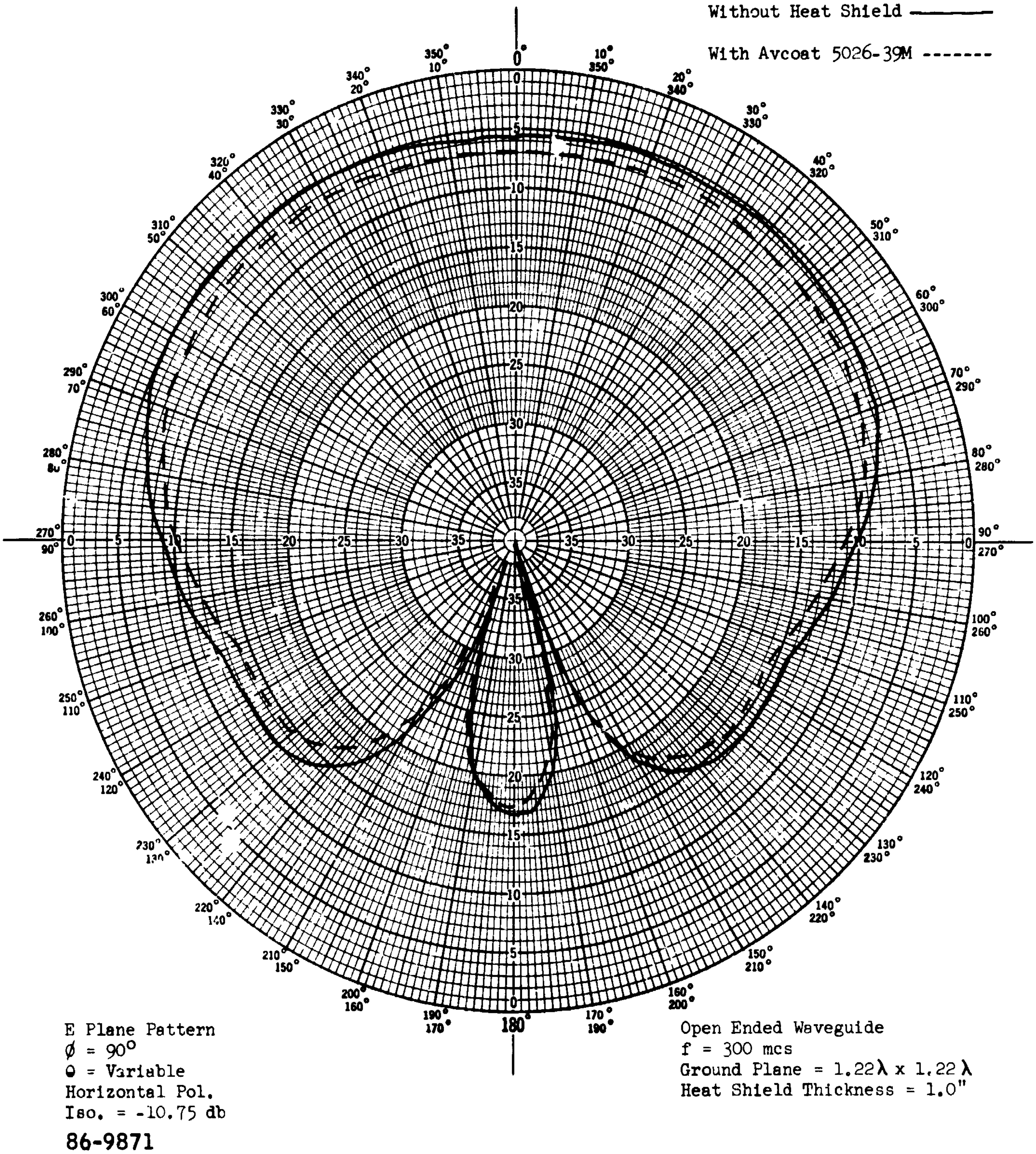

Figure 19 300 MC OPEN-ENDED WAVEGUIDE, WITH AND WITHOUT AVCOAT 5026-39M. E PLANE

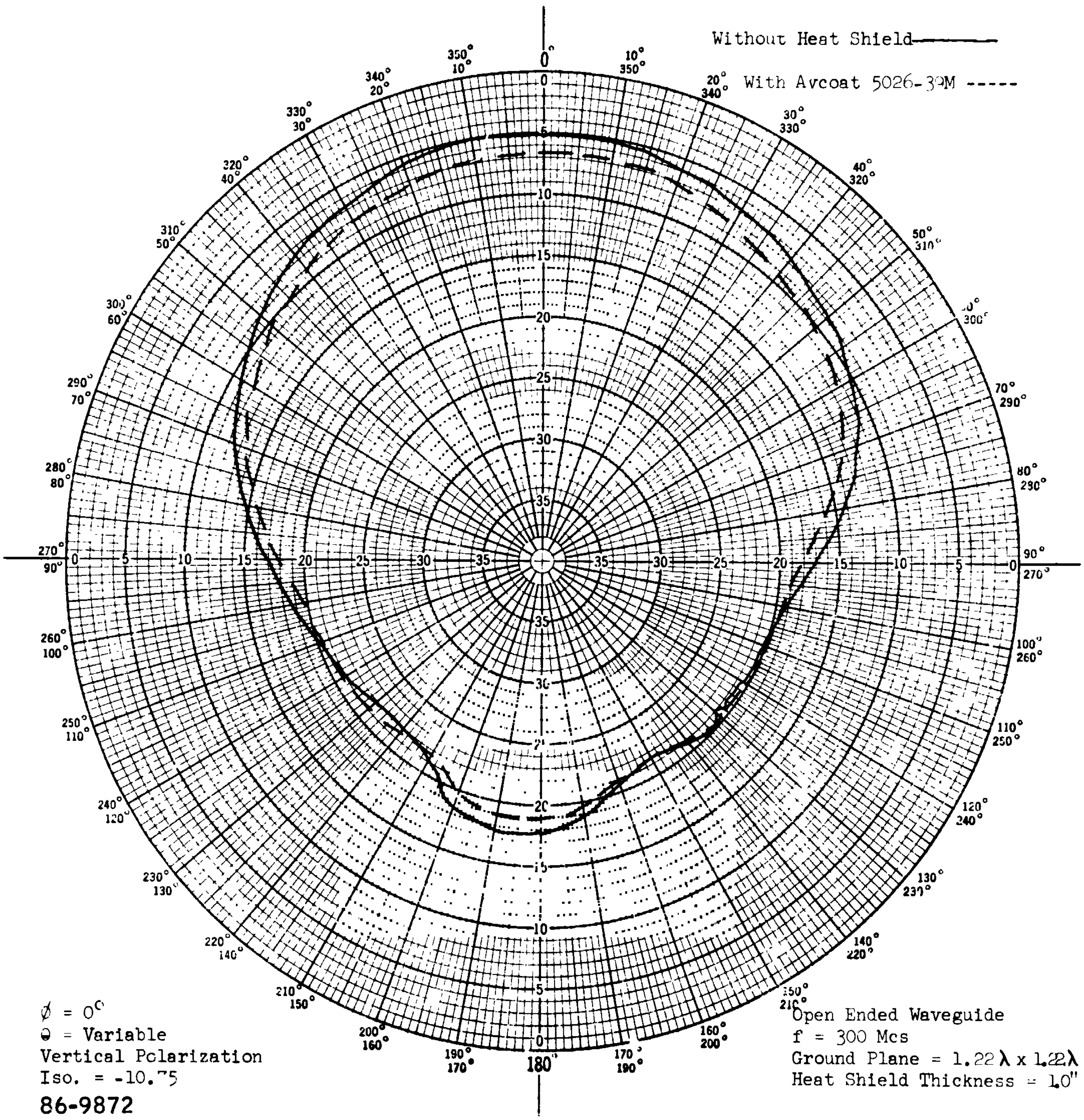

Figure 20 300 MC OPEN-ENDED WAVEGUIDE, WITH AND WITHOUT AVCOAT 5026-39M. H PLANE

With Avcoat 5026-39M ———

With Simulator --------

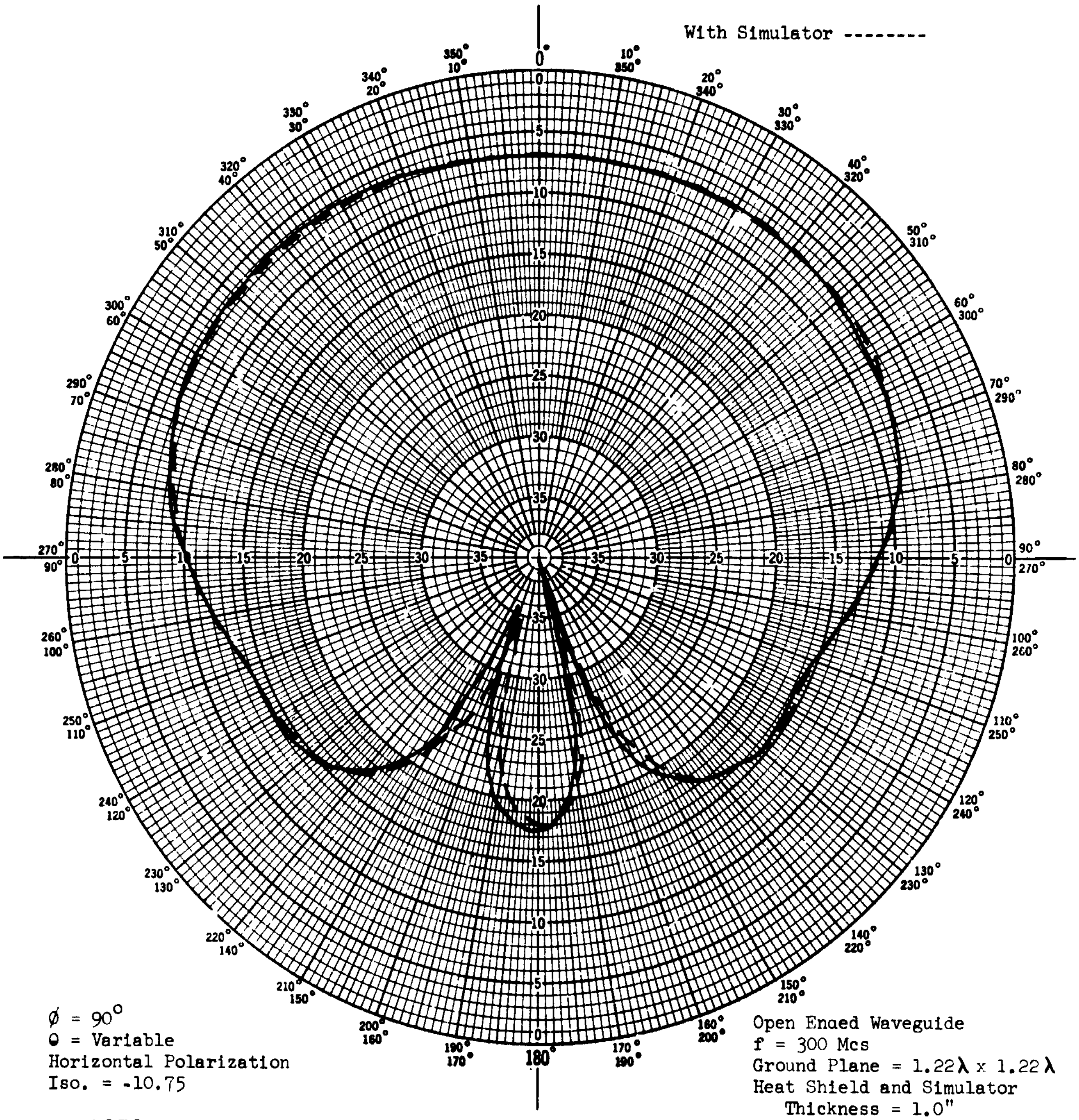

ϕ = 90°
Θ = Variable
Horizontal Polarization
Iso. = -10.75

Open Ended Waveguide
f = 300 Mcs
Ground Plane = 1.22λ x 1.22λ
Heat Shield and Simulator
Thickness = 1.0"

86-9873

Figure 21 300 MC OPEN-ENDED WAVEGUIDE, COMPARISON BETWEEN AVCOAT 5026-39M AND SIMULATOR. E PLANE

With Avcoat 5026-39M ———

With Simulator -------

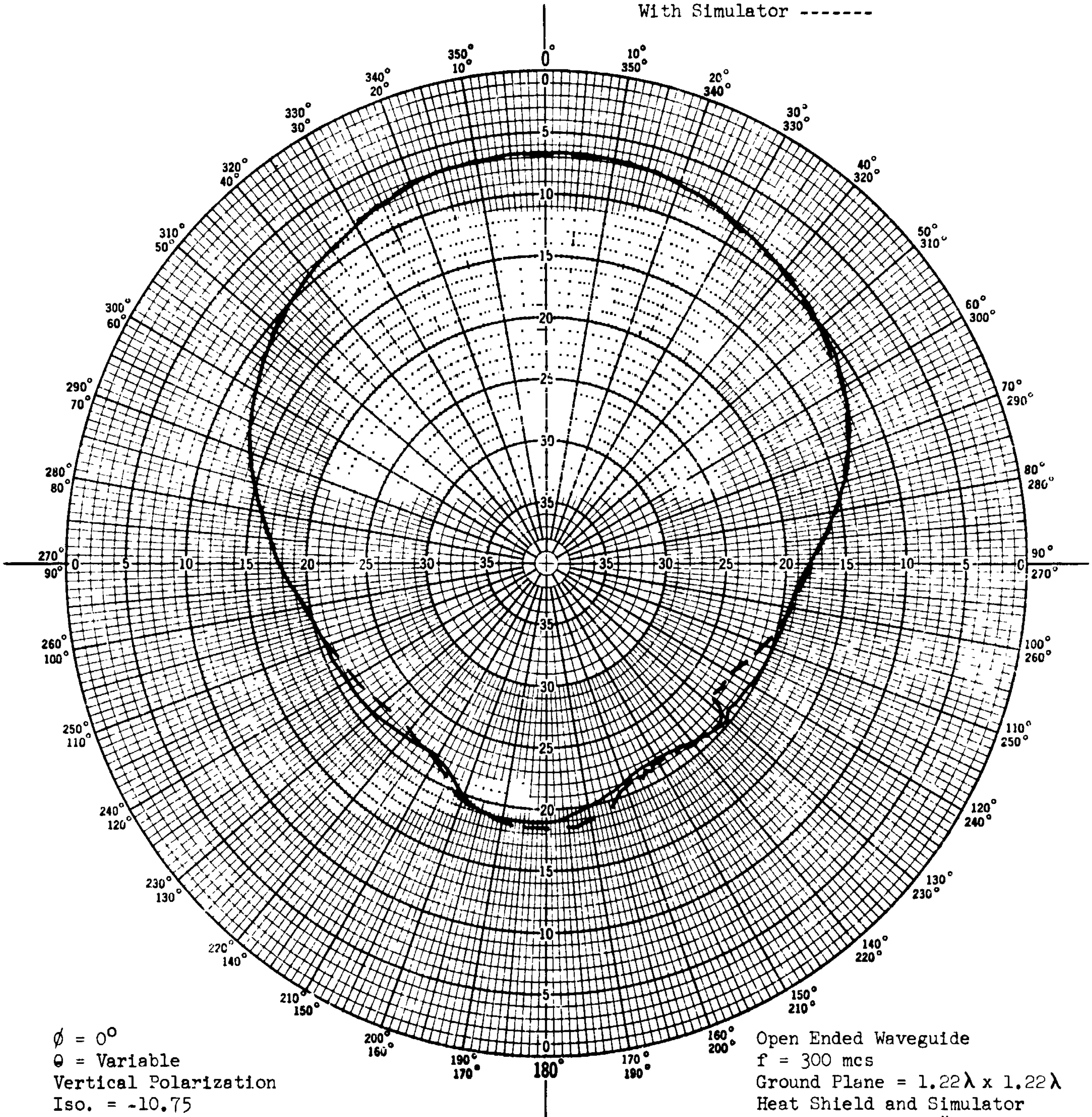

ø = 0°
Θ = Variable
Vertical Polarization
Iso. = -10.75

Open Ended Waveguide
f = 300 mcs
Ground Plane = 1.22λ x 1.22λ
Heat Shield and Simulator
Thickness = 1.0"

86-9874

Figure 22 300 MC OPEN-ENDED WAVEGUIDE, COMPARISON BETWEEN AVCOAT 5026-39M AND SIMULATOR. H PLANE

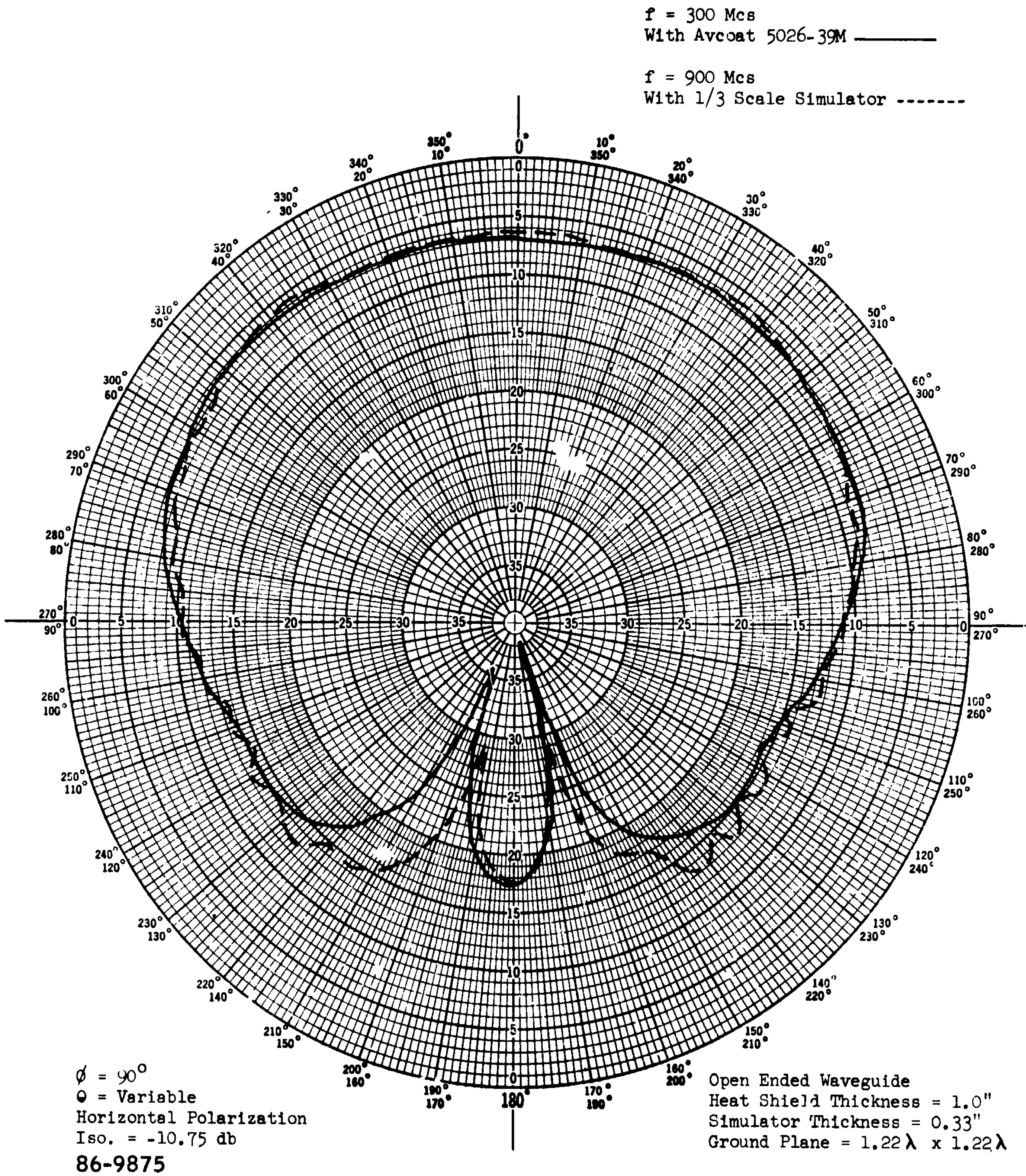

Figure 23 300 MC AND 900 MC OPEN-ENDED WAVEGUIDE, COMPARISON BETWEEN AVCOAT 5026-39M AND THIRD-SCALE SIMULATOR. E PLANE

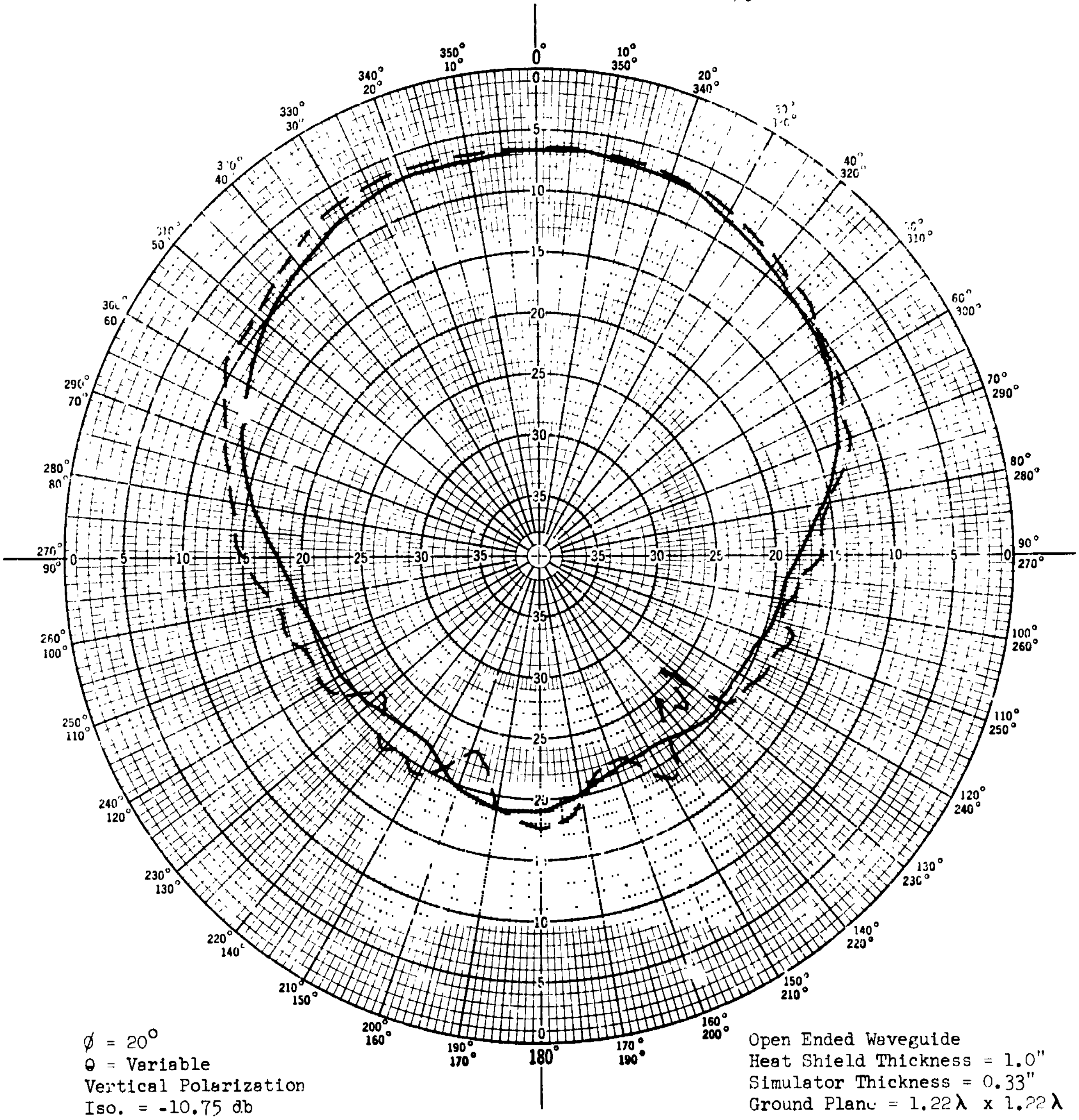

Figure 24 300 MC AND 900 MC OPEN-ENDED WAVEGUIDE, COMPARISON BETWEEN AVCOAT 5026-39M AND THIRD-SCALE SIMULATOR. H PLANE

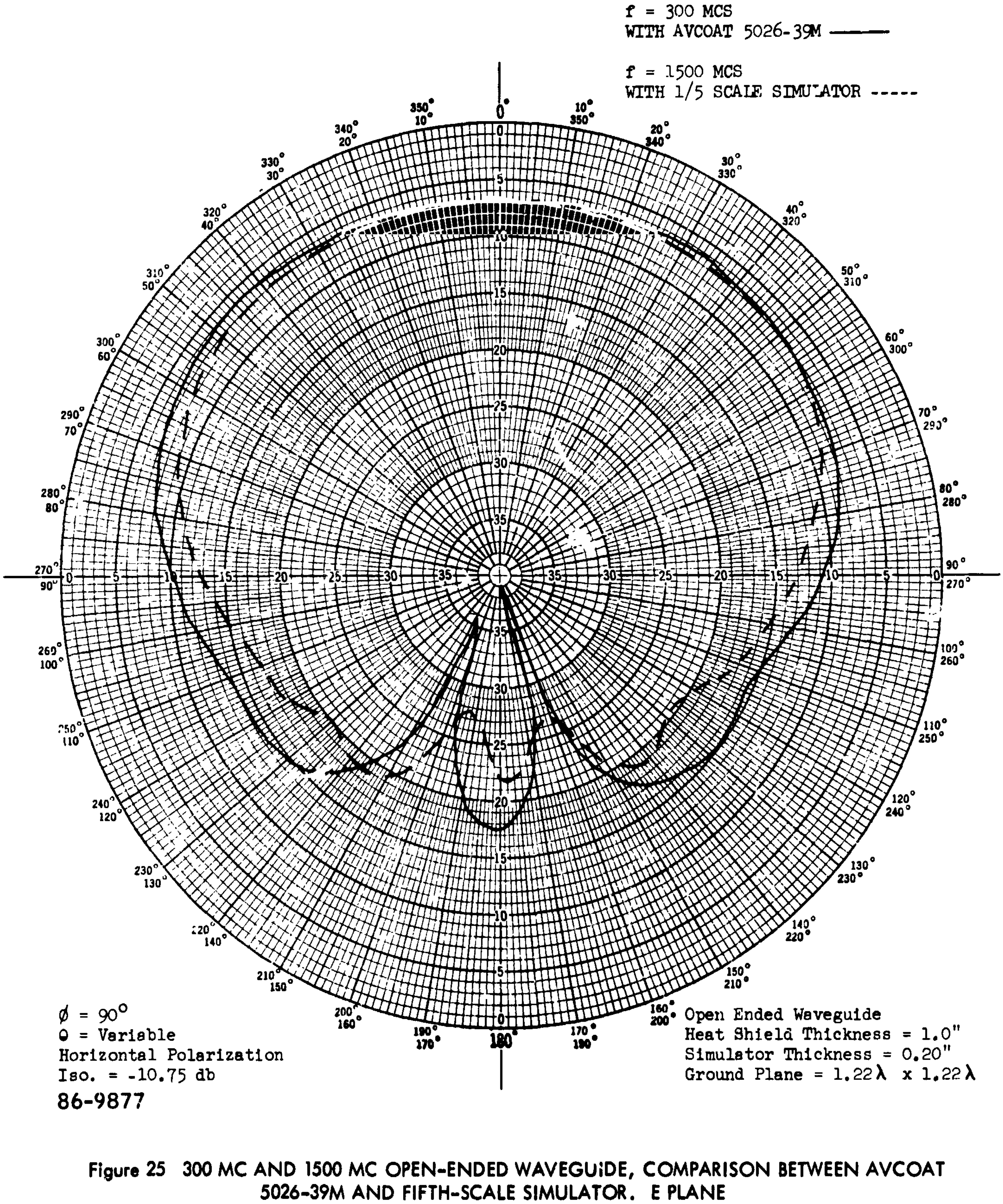

Figure 25 300 MC AND 1500 MC OPEN-ENDED WAVEGUIDE, COMPARISON BETWEEN AVCOAT 5026-39M AND FIFTH-SCALE SIMULATOR. E PLANE

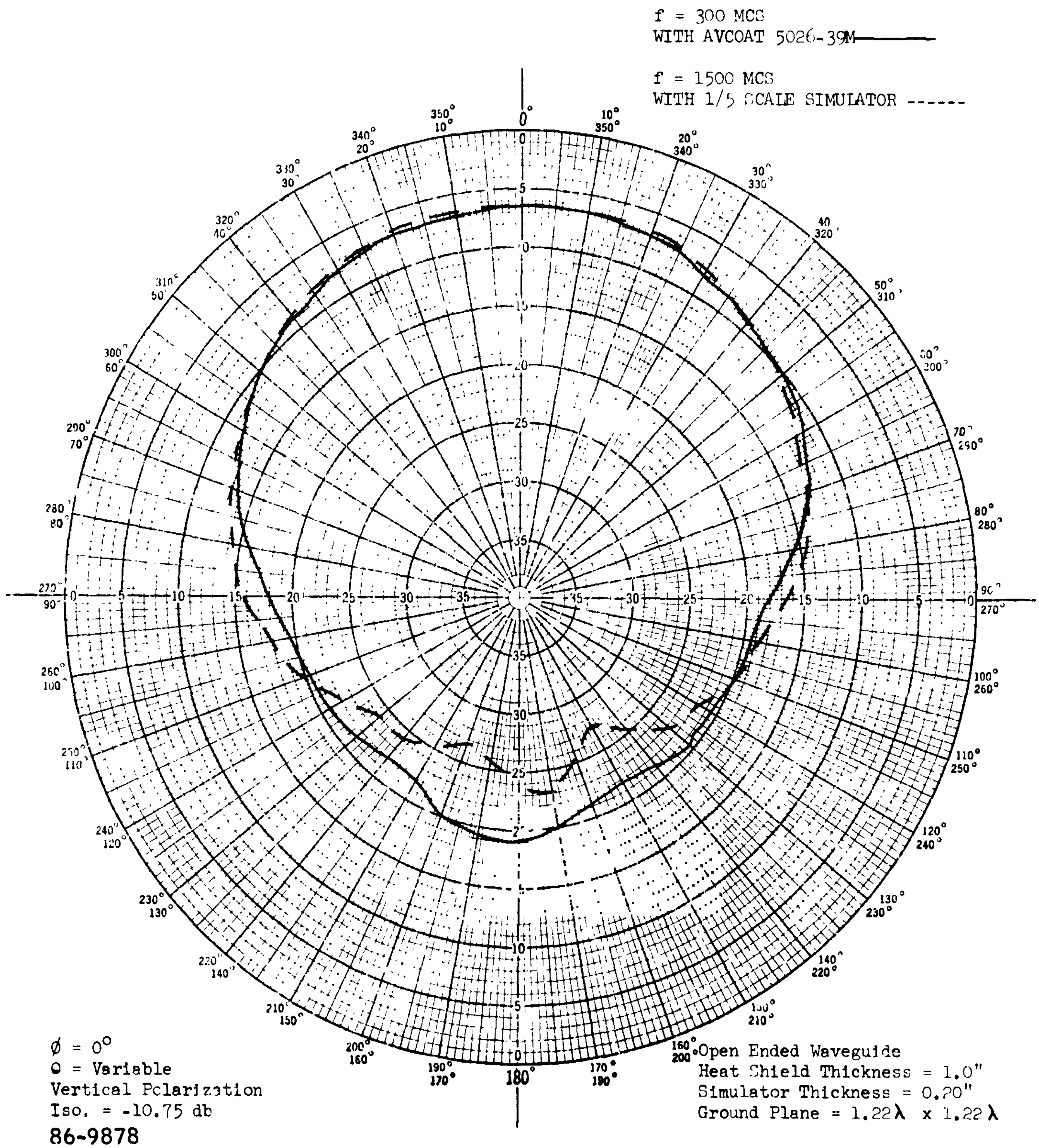

Figure 26 300 MC AND 1500 MC OPEN-ENDED WAVEGUIDE, COMPARISON BETWEEN AVCOAT 5026-39M AND FIFTH-SCALE SIMULATOR. H PLANE

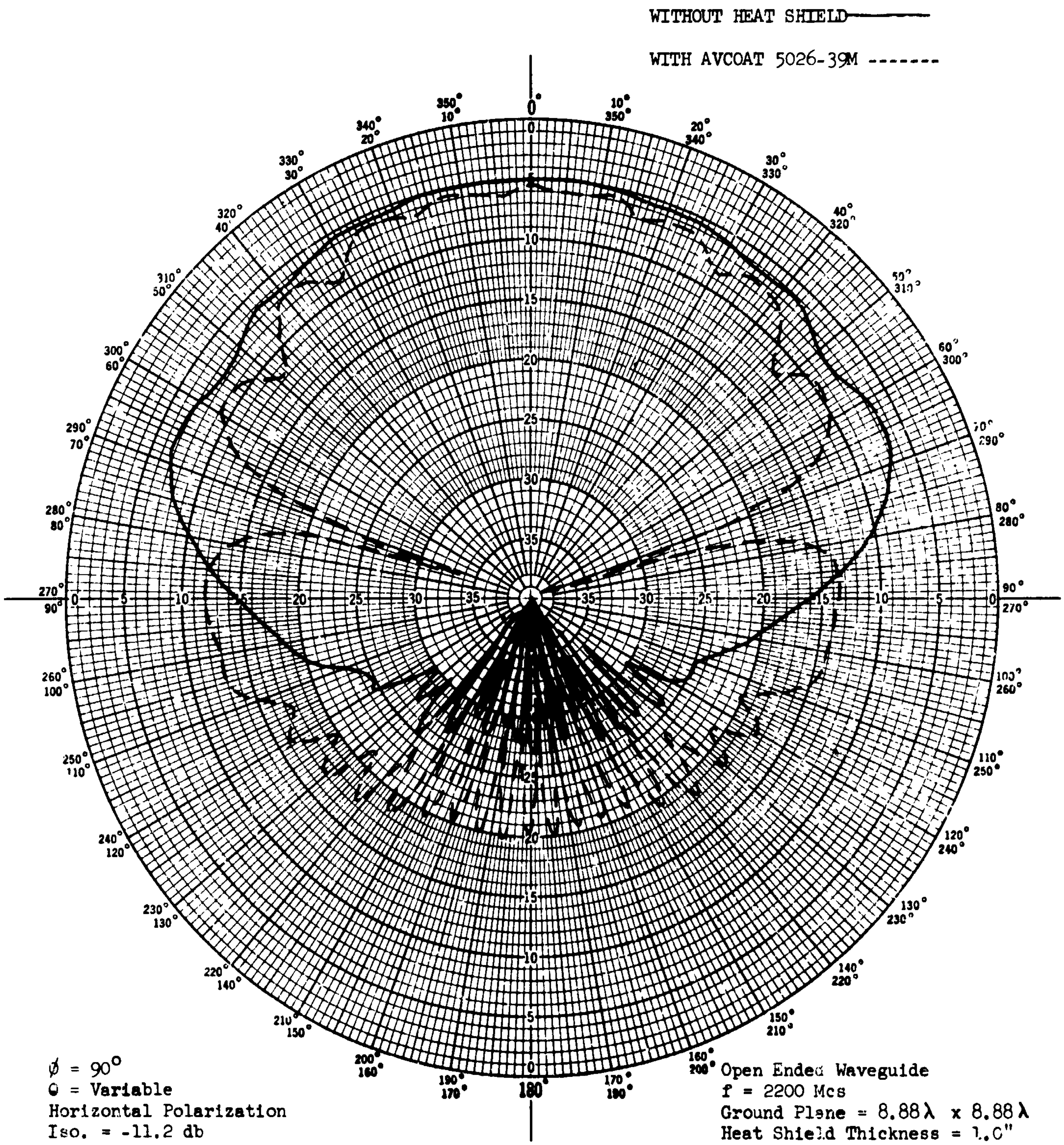

86-9879

Figure 27 2200 MC OPEN-ENDED WAVEGUIDE, WITH AND WITHOUT AVCOAT 5026-39M. E PLANE

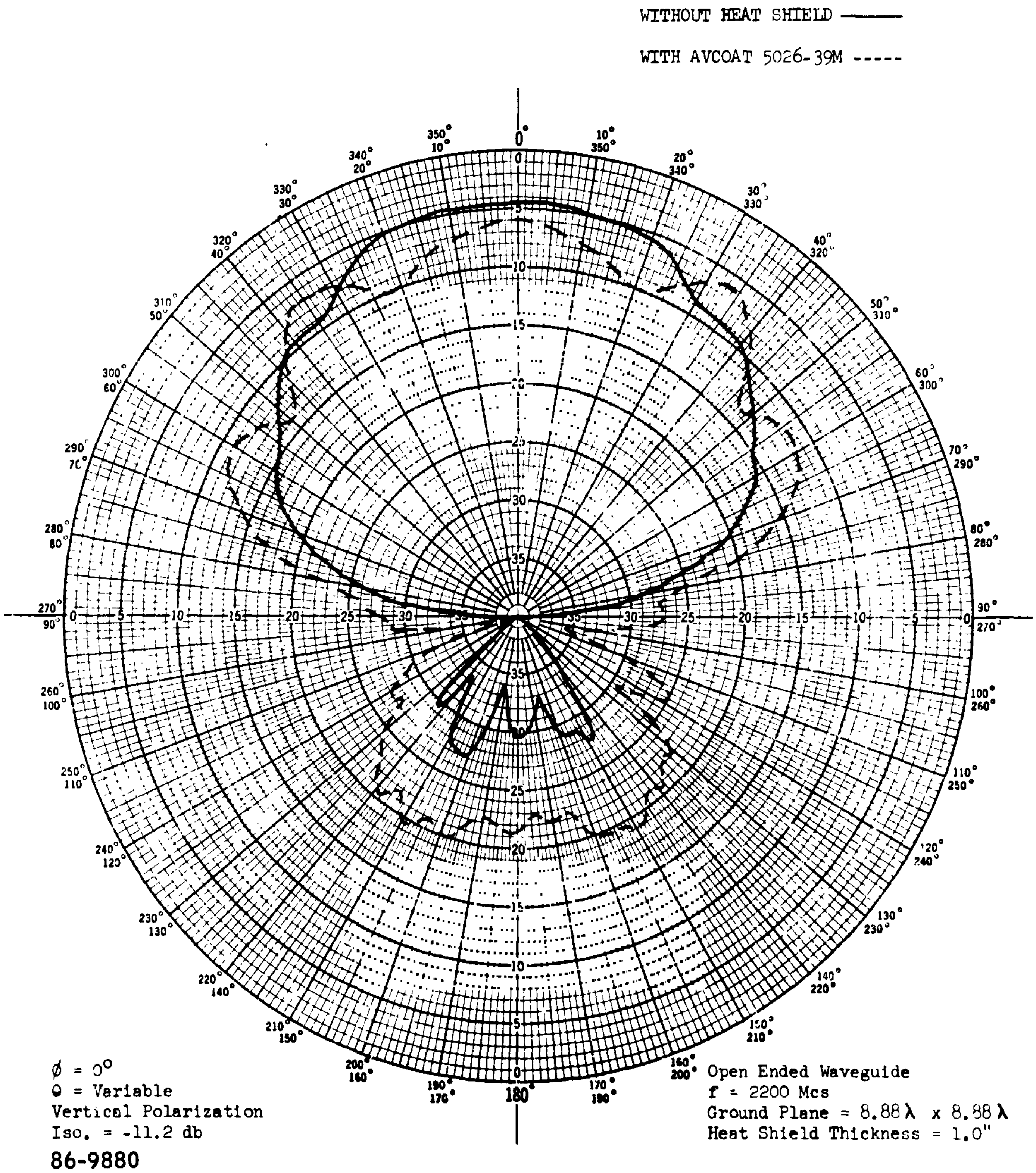

Figure 28 2200 MC OPEN-ENDED WAVEGUIDE, WITH AND WITHOUT AVCOAT 5026-39M. H PLANE

WITH AVCOAT 5026-39M ———

WITH SIMULATOR -------

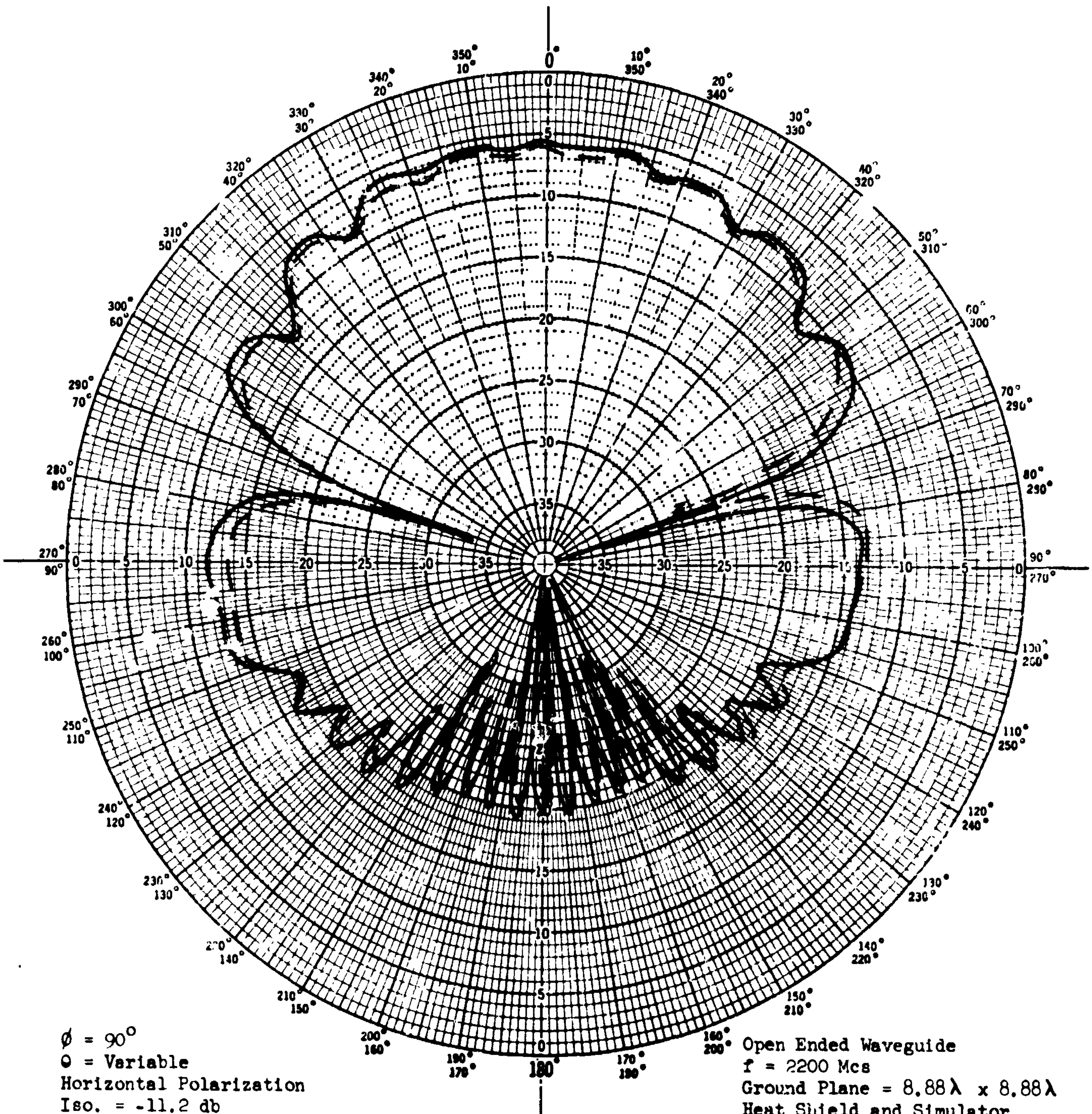

Ø = 90°
Θ = Variable
Horizontal Polarization
Iso. = -11.2 db
86-9881

Open Ended Waveguide
f = 2200 Mcs
Ground Plane = 8.88λ x 8.88λ
Heat Shield and Simulator
Thickness = 1.0"

Figure 29 2200 MC OPEN-ENDED WAVEGUIDE, COMPARISON BETWEEN AVCOAT 5026-39M AND SIMULATOR. E PLANE

WITH AVCOAT 5026-39M ———

WITH SIMULATOR ------

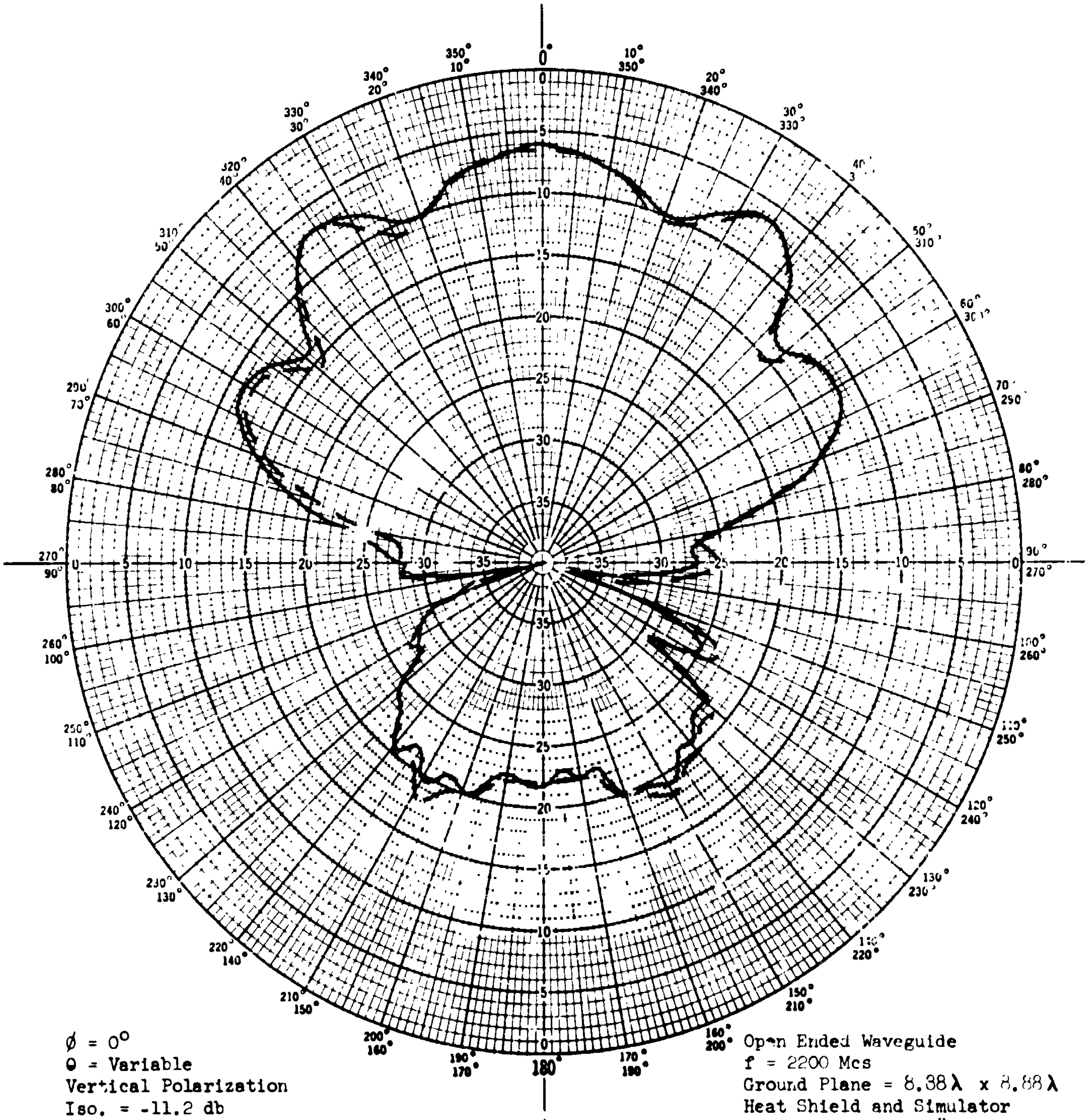

ϕ = 0°
θ = Variable
Vertical Polarization
Iso. = -11.2 db
86-9882

Open Ended Waveguide
f = 2200 Mcs
Ground Plane = 8.88λ x 8.88λ
Heat Shield and Simulator
Thickness = 1.0"

Figure 30 2200 MC OPEN-ENDED WAVEGUIDE, COMPARISON BETWEEN AVCOAT 5026-39M AND SIMULATOR. H PLANE

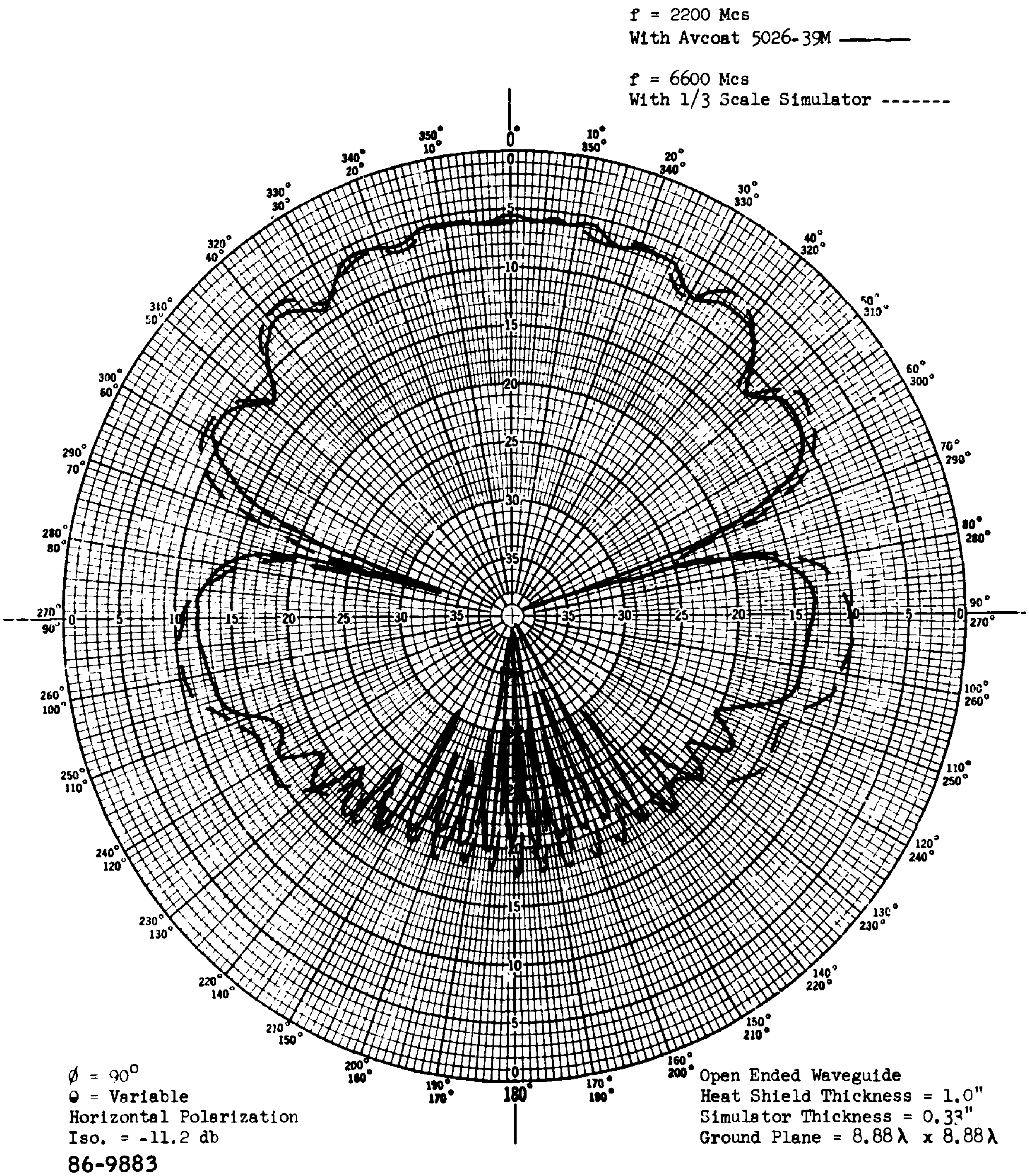

Figure 31 2200 MC AND 6600 MC OPEN-ENDED WAVEGUIDE, COMPARISON BETWEEN AVCOAT 5026-39M AND THIRD-SCALE SIMULATOR. E PLANE

f = 2200 Mcs
WITH AVCOAT 5026-39M ———

f = 6600 Mcs
WITH 1/3 SCALE SIMULATOR -----

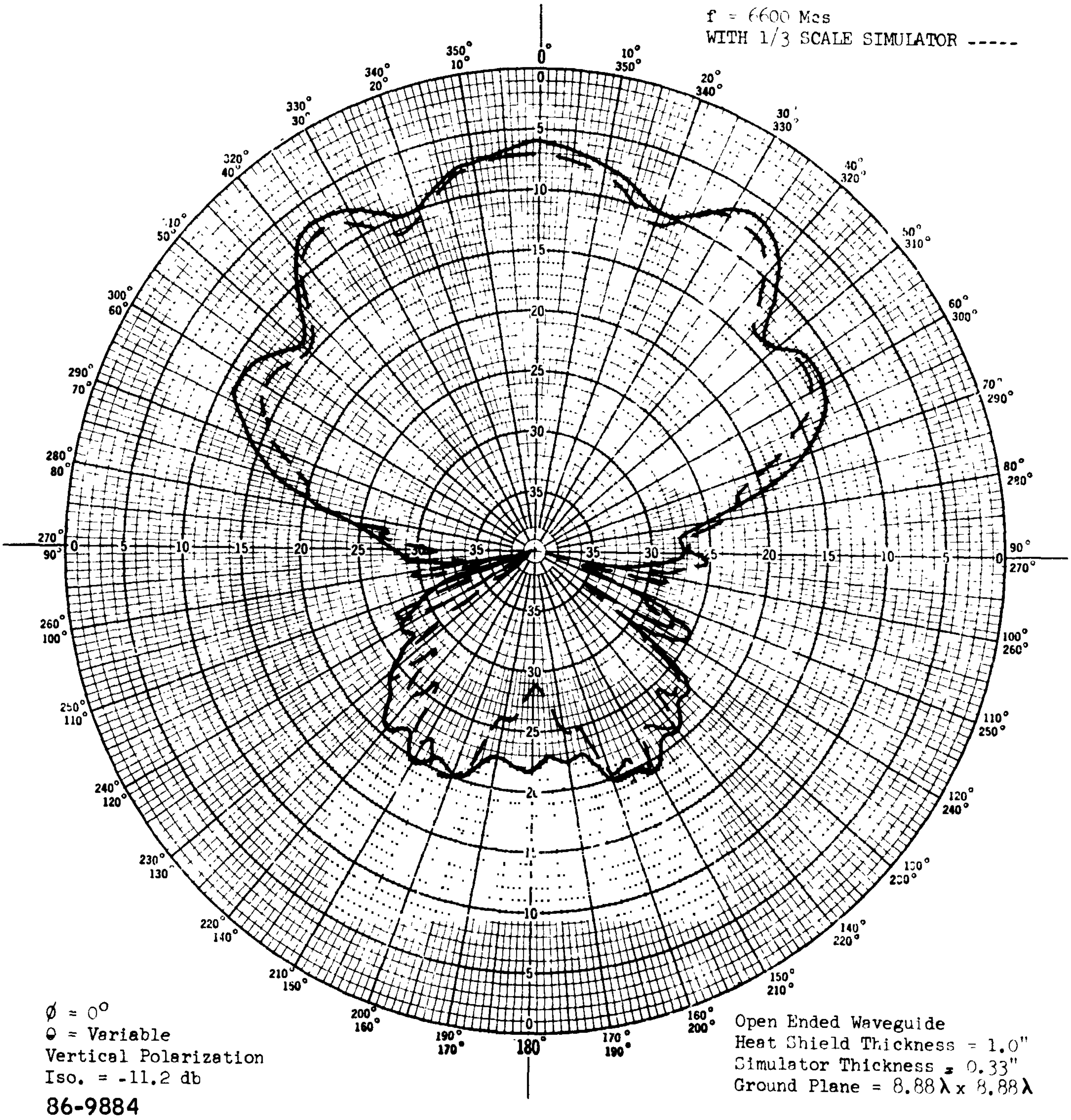

ϕ = 0°
θ = Variable
Vertical Polarization
Iso. = -11.2 db

Open Ended Waveguide
Heat Shield Thickness = 1.0"
Simulator Thickness ≈ 0.33"
Ground Plane = 8.88λ x 8.88λ

86-9884

Figure 32 2200 MC AND 6600 MC OPEN-ENDED WAVEGUIDE, COMPARISON BETWEEN AVCOAT 5026-39M AND THIRD-SCALE SIMULATOR. H PLANE

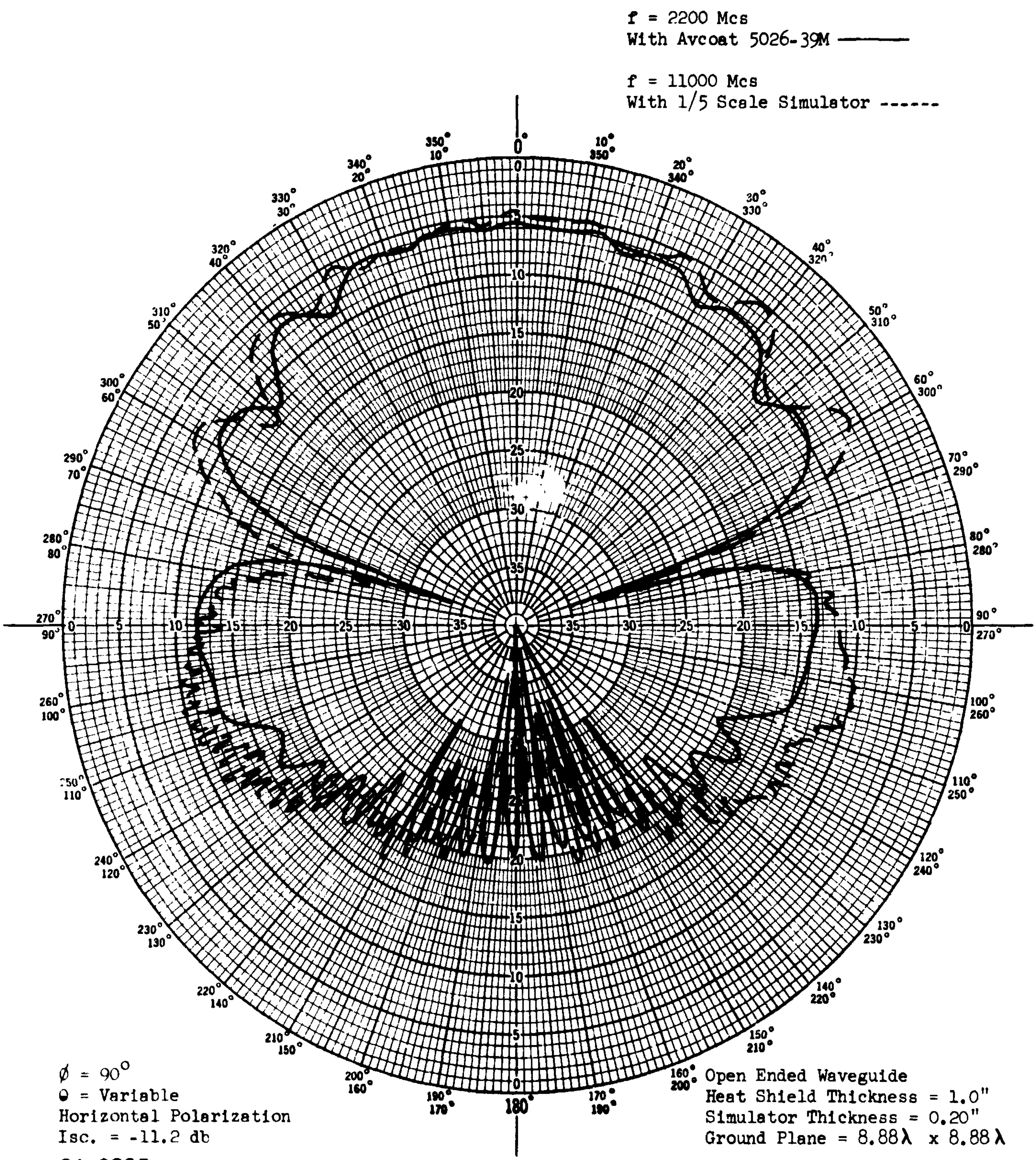

86-9885

Figure 33 2200 MC AND 11000 MC OPEN-ENDED WAVEGUIDE, COMPARISON BETWEEN AVCOAT 5026-39M AND FIFTH-SCALE SIMULATOR. E PLANE

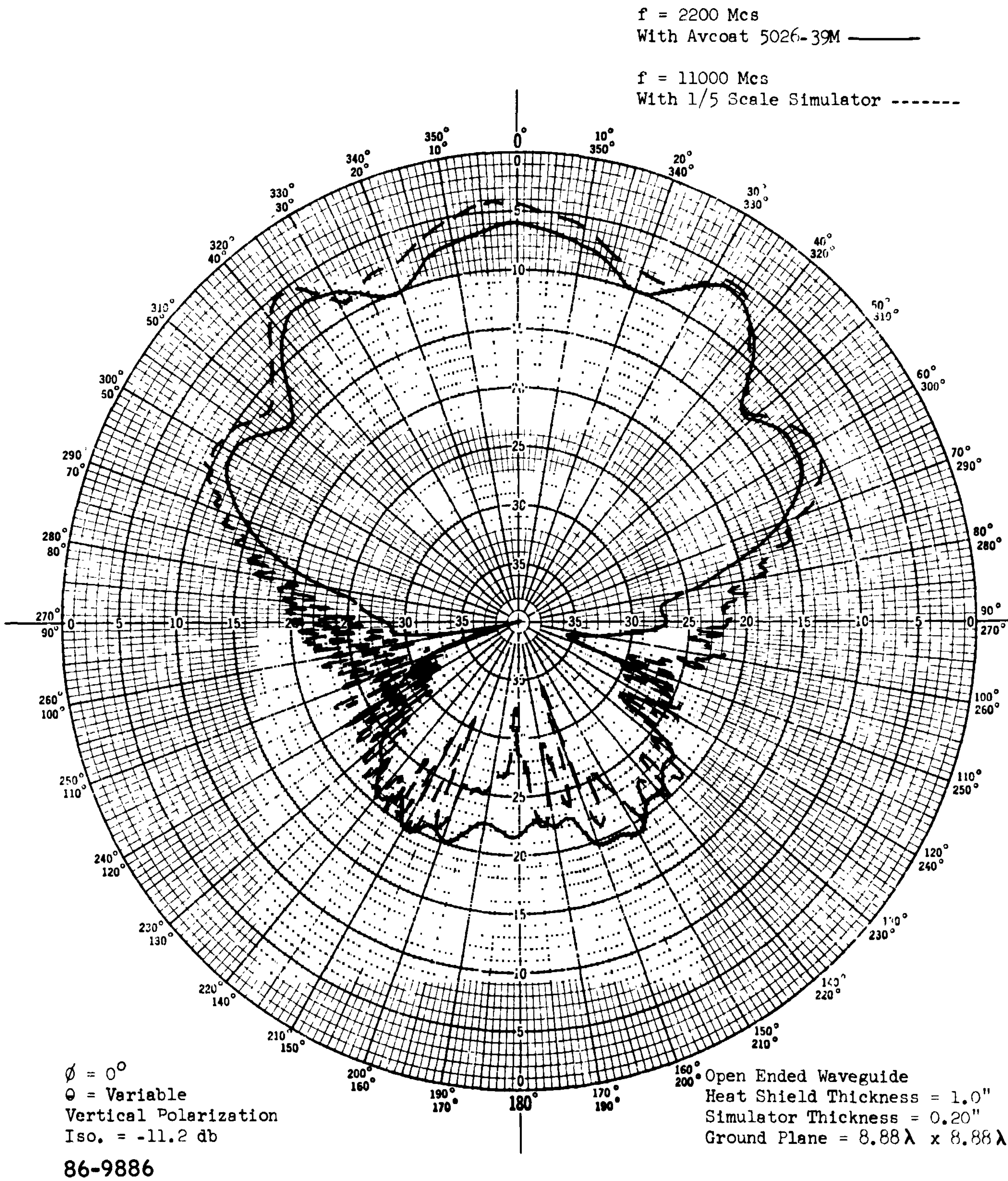

Figure 34 2200 MC AND 11000 MC OPEN-ENDED WAVEGUIDE, COMPARISON BETWEEN AVCOAT 5026-39M AND FIFTH-SCALE SIMULATOR. H PLANE

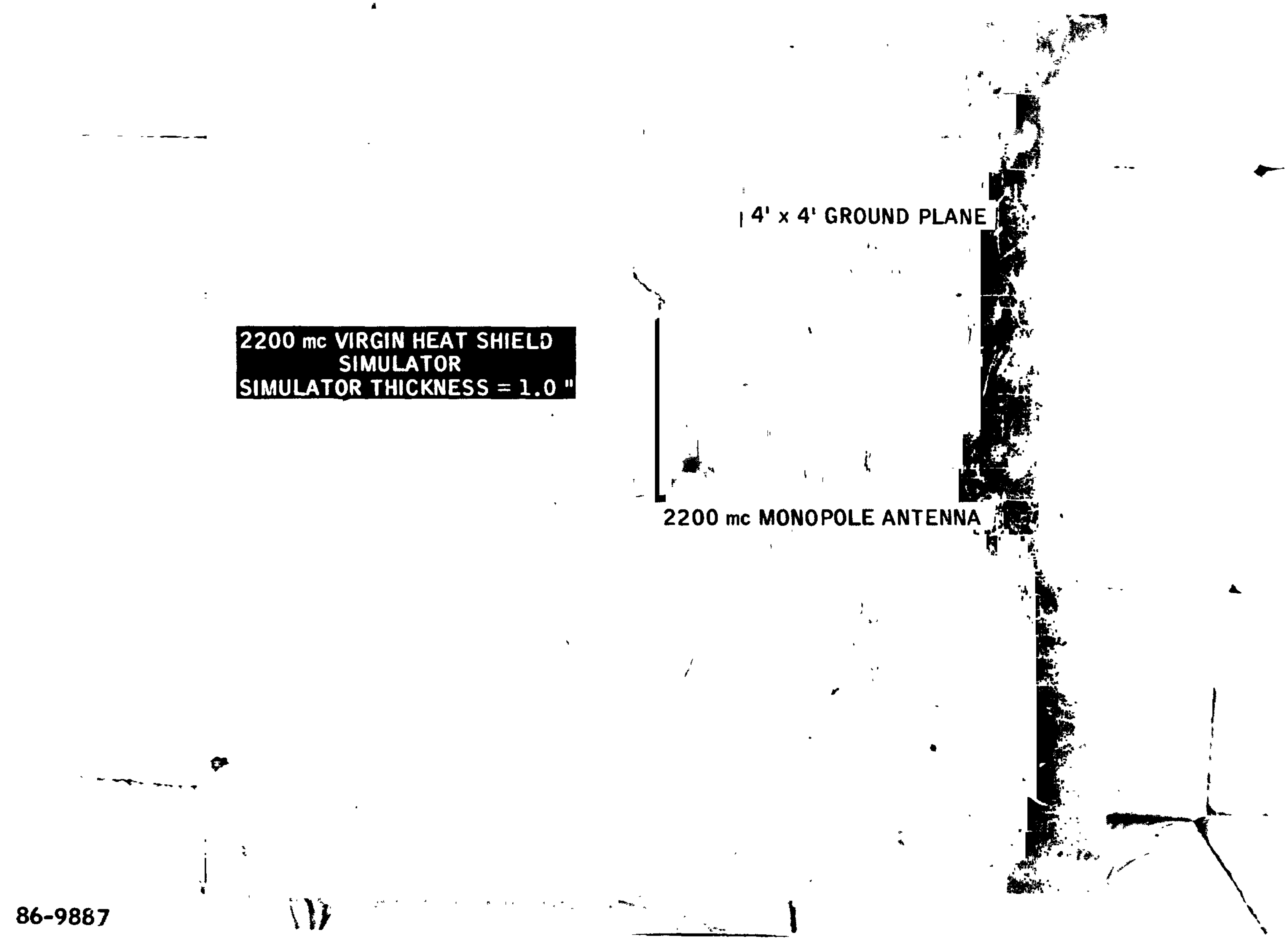

Figure 35 2200 MC OPEN ENDED WAVEGUIDE ANTENNA PARTIALLY COVERED WITH VIRGIN HEAT-SHIELD SIMULATOR

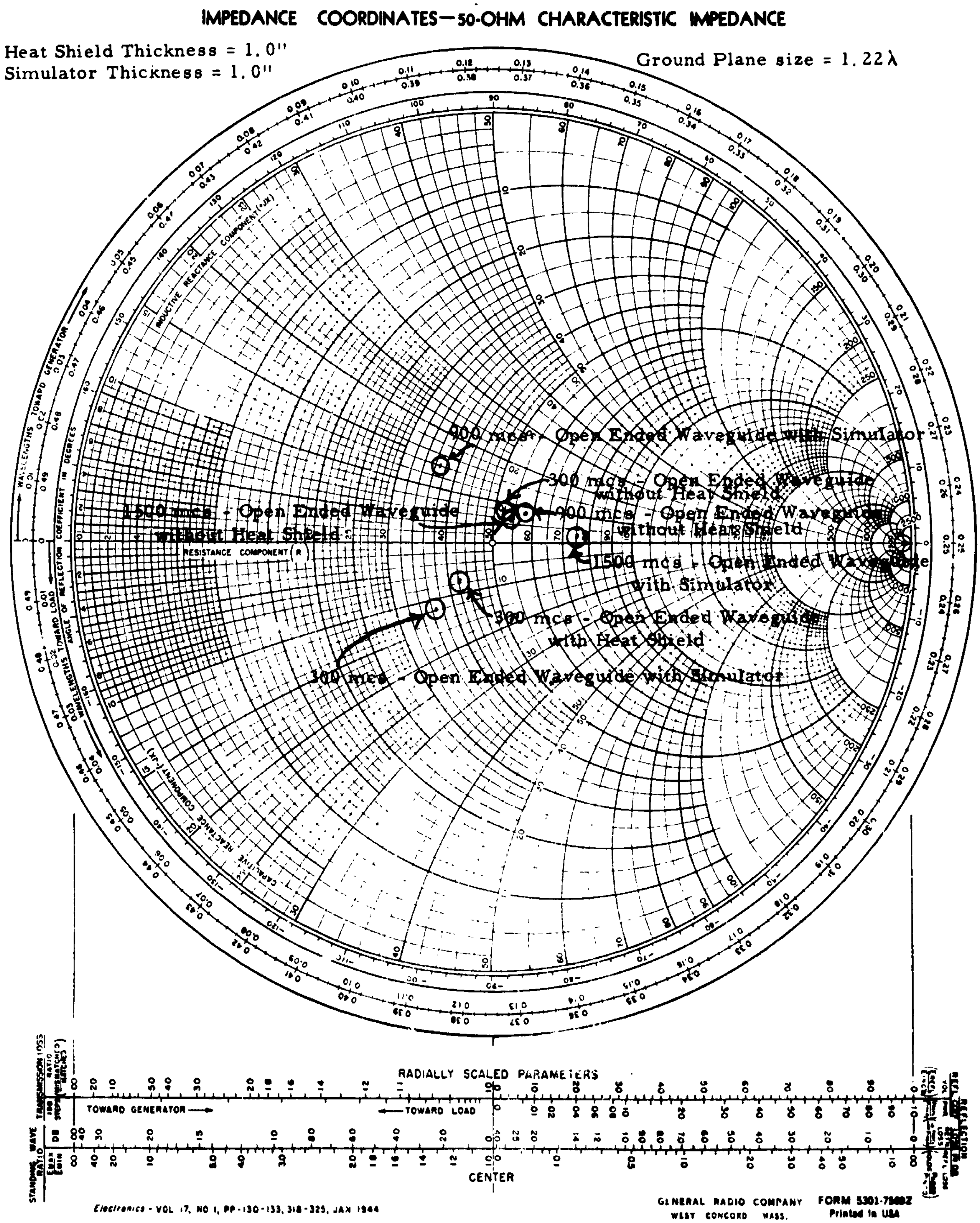

86-9888

Figure 36 IMPEDANCE OF 300 MC, 900 MC AND 1500 MC OPEN-ENDED WAVEGUIDE

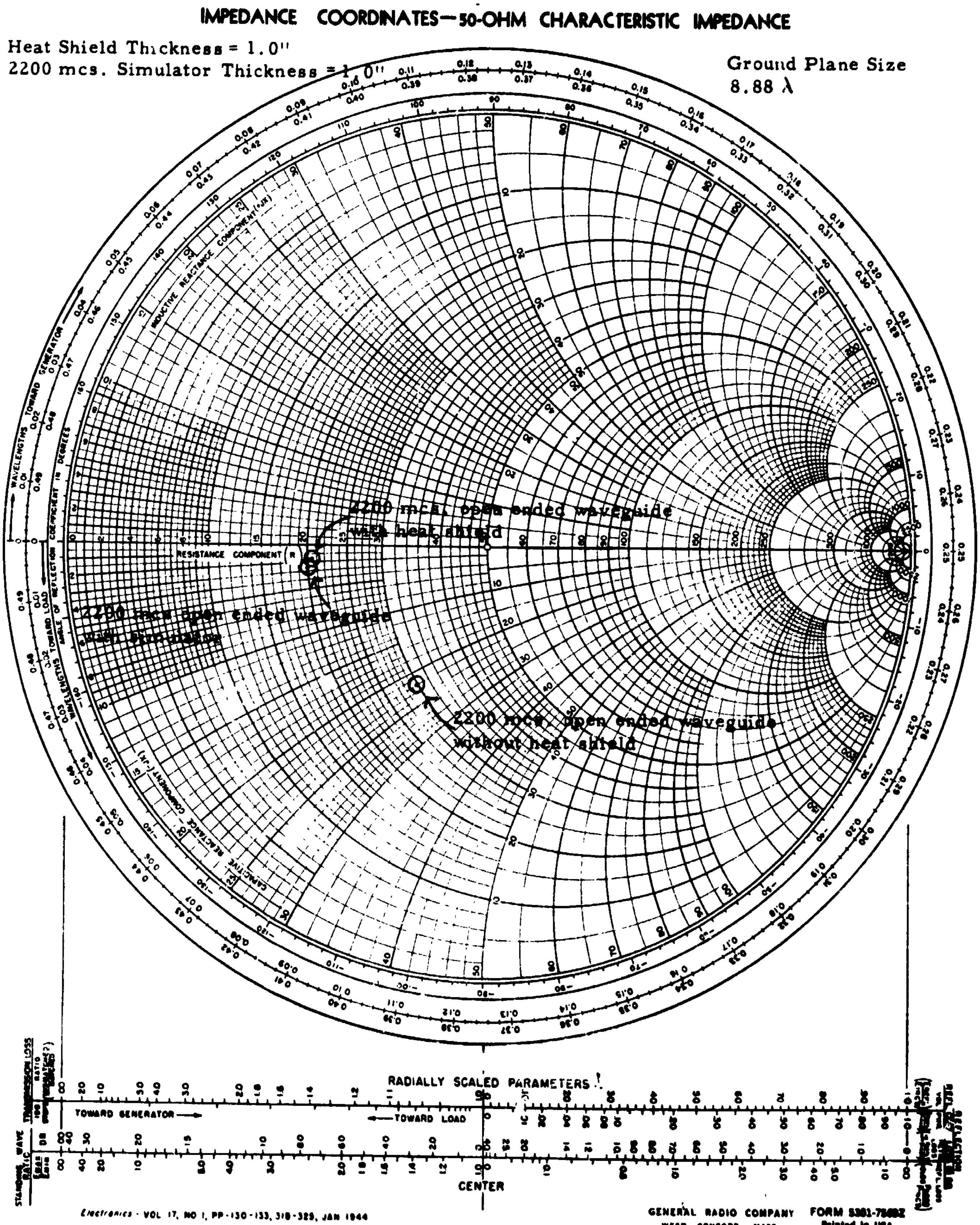

86-9889

Figure 37 IMPEDANCE OF 2200 MC OPEN-ENDED WAVEGUIDE

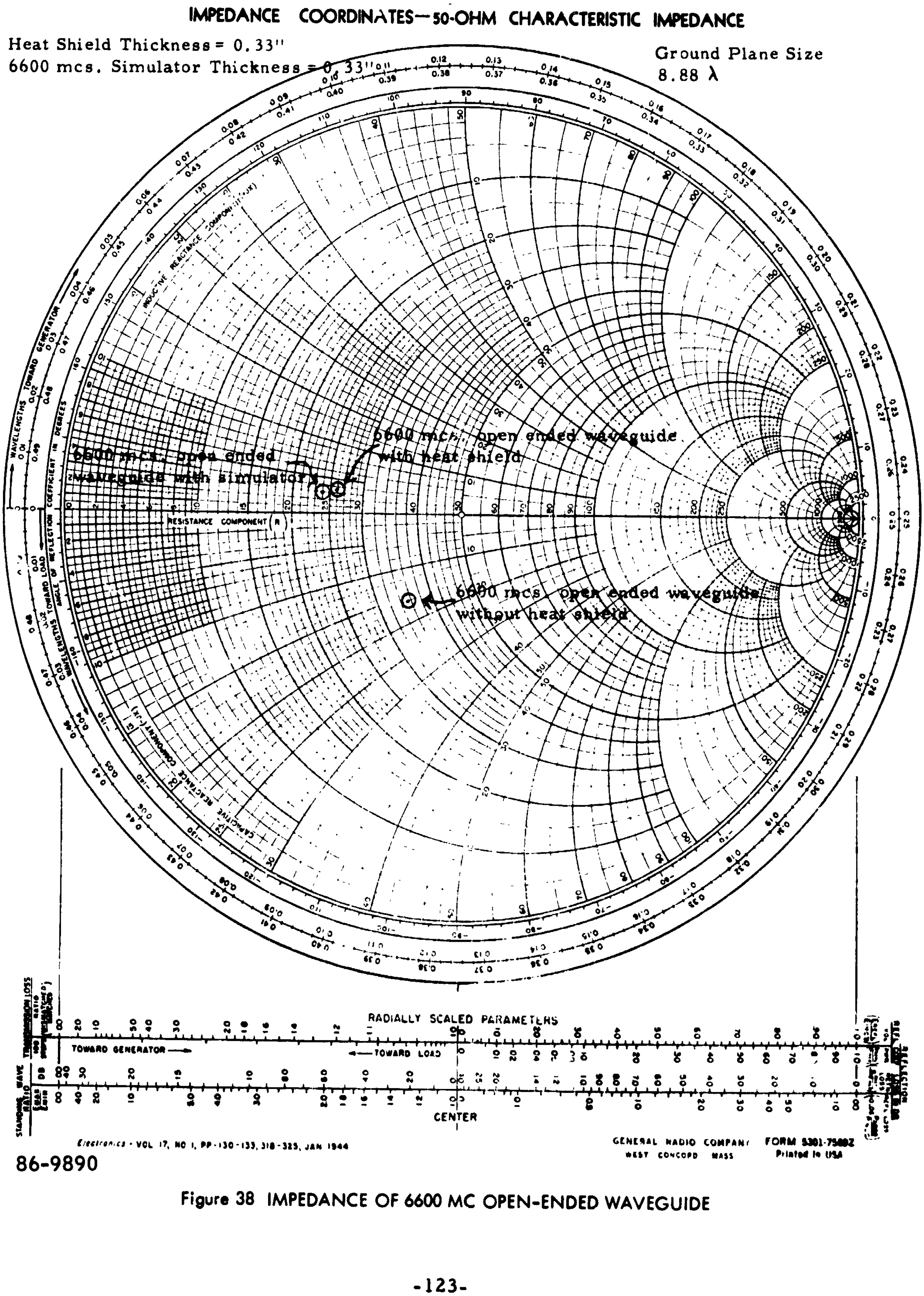

Figure 38 IMPEDANCE OF 6600 MC OPEN-ENDED WAVEGUIDE

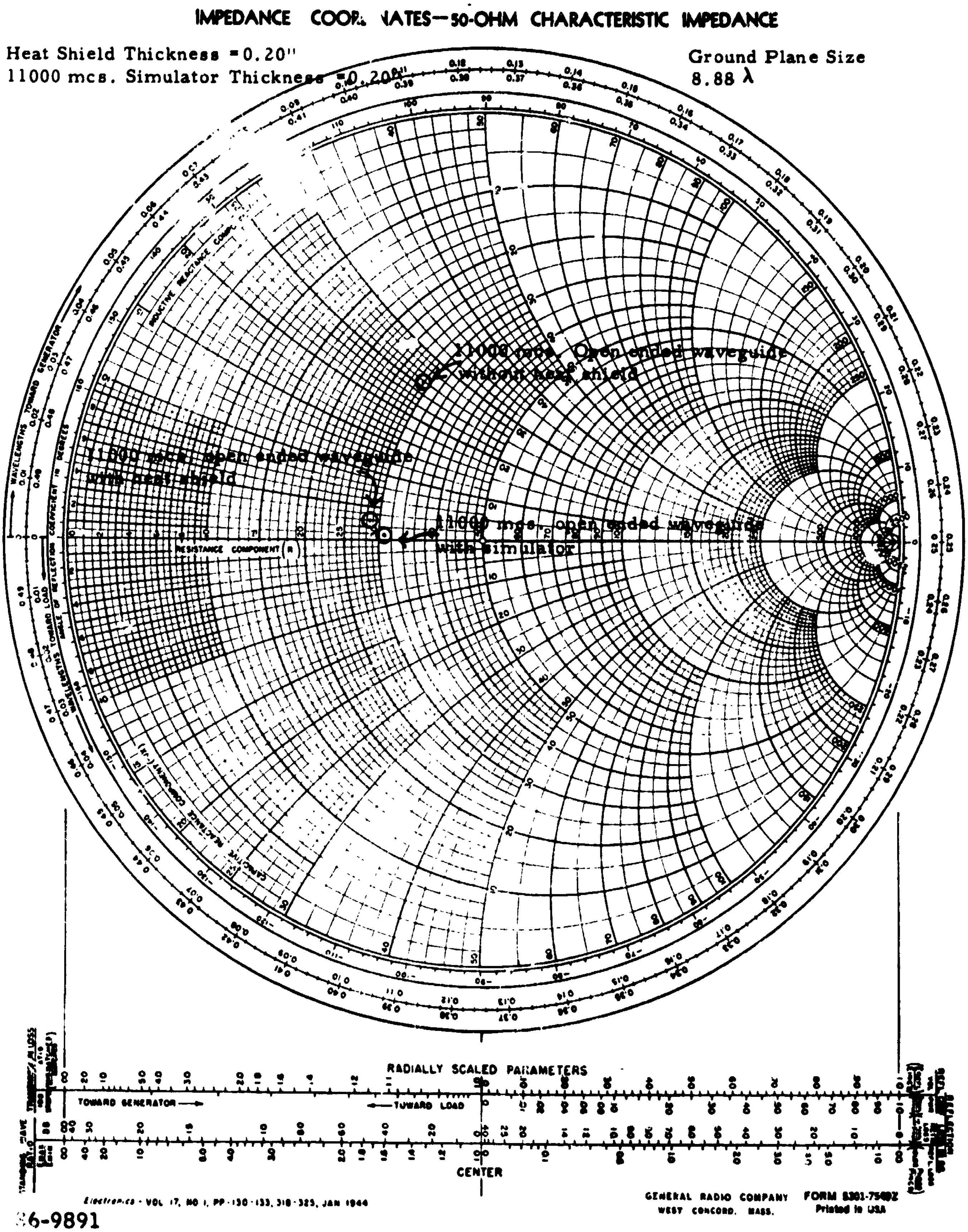

36-9891

Figure 39 IMPEDANCE OF 11000 MC OPEN-ENDED WAVEGUIDE

The experimental results of the char tests are referenced in Table II by experiment numbers 11 through 20. The char tests were the most difficult part of the verification tests. It was originally thought that the heat shield could be charred its full depth and simulated with a single simulator. Heat shields charred their full depth measured approximately 36db attenuation in the E plane. The pattern shape was destroyed and energy seemed to be escaping through cracks in the heat shield. The ablator used for these tests was not bonded to metal sheets prior to charring. This allowed the ablator to be charred on the front and back face. The samples were seriously warped by the heat so they cracked when bonded to ground planes. This indicated that for future charring the heat shield would have to be bonded to the ground planes prior to charring. If the heat shield were to be charred its full depth, the thickness would have to be reduced to minimize the attentuation and pattern degradation to the point where meaningful measurements could be taken.

It was decided to char a 0.25-inch-thick heat-shield its full depth for the verification tests. The heat shield was bonded to the metal plates with high-temperature HT 424 tape.

Charred samples varied considerably in terms of resistivity as a function of heat-shield depth. The idea of charring the heat shield its full depth was abandoned. It was decided to use a surface char.

Since the largest oven did not have the capacity for a 4-foot x 4-foot piece of heat shield, the heat shield was charred in nine sections and reassembled after charring.

A standard Structures Lab furnace made up of a reflector and water jacket with 96 General Electric 1600 watt T3Cl quartz lamps was used to heat the heat shield. The ablator panels were mounted on a transite backup shield and placed a distance of three inches from the lamps. Three ignitron power supplies were used to power the quartz lamps, one ignitron per 32 lamps. A voltage of 440 volts was applied for nine seconds to the furnace resulting in a heating rate of approximately 50 Btu/ft^{2}sec. The tests were conducted in an inert nitrogen atmosphere. Following each test, the furnace was disassembled, cleaned, and reassembled. (See Figures 40, 41 and 42.)

The ablator panels were charred to a depth of between one-sixteenth and one-eighth of an inch.

The ablator appeared to have a higher conductivity at its lower portion and this was probably due to nonuniformity of heating. The resistivities varied from 1.3 ohms per square to 46 ohms per square. Repeated efforts were made to obtain uniform resistivity. Resistivities still varied across the panels.

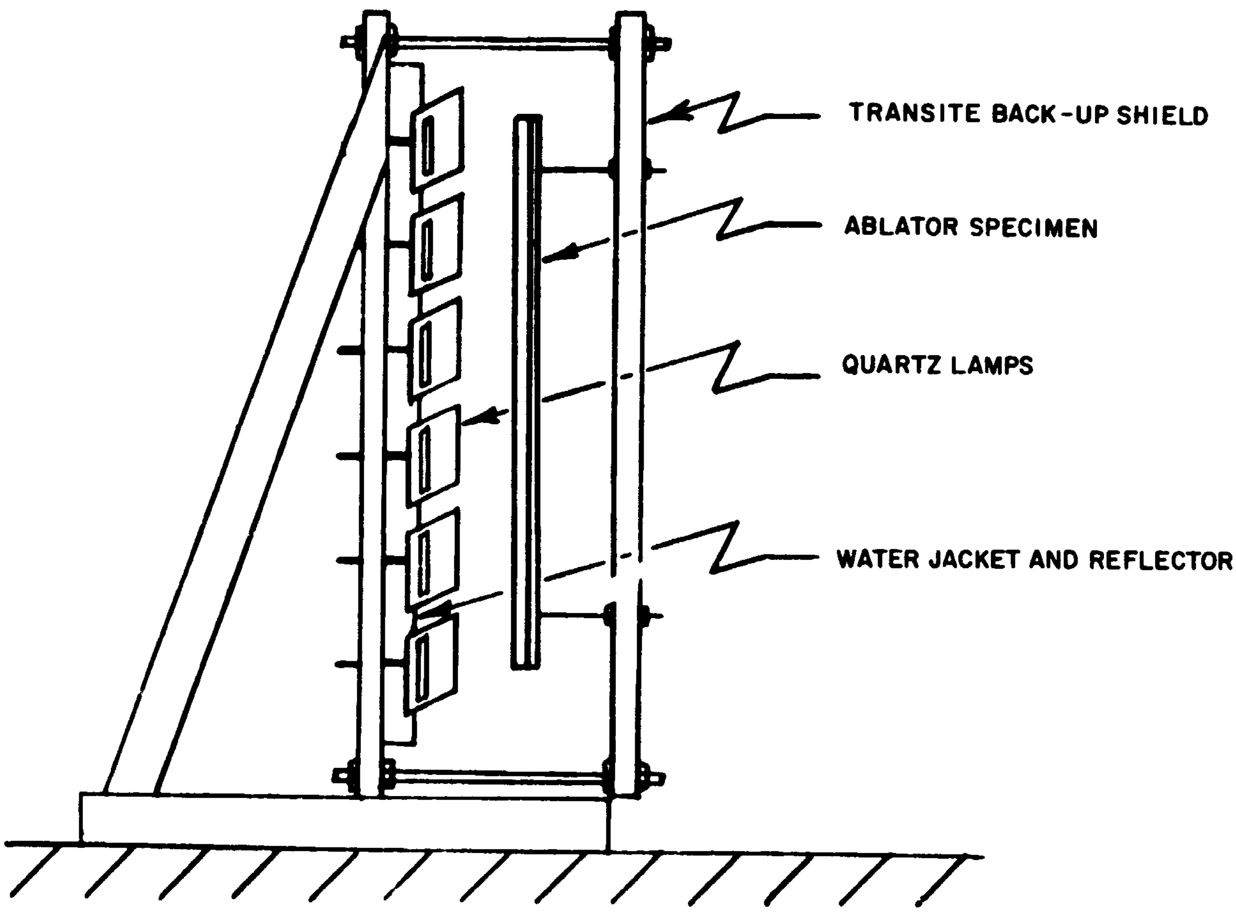

86-9892

Figure 40 OVEN TEST SETUP

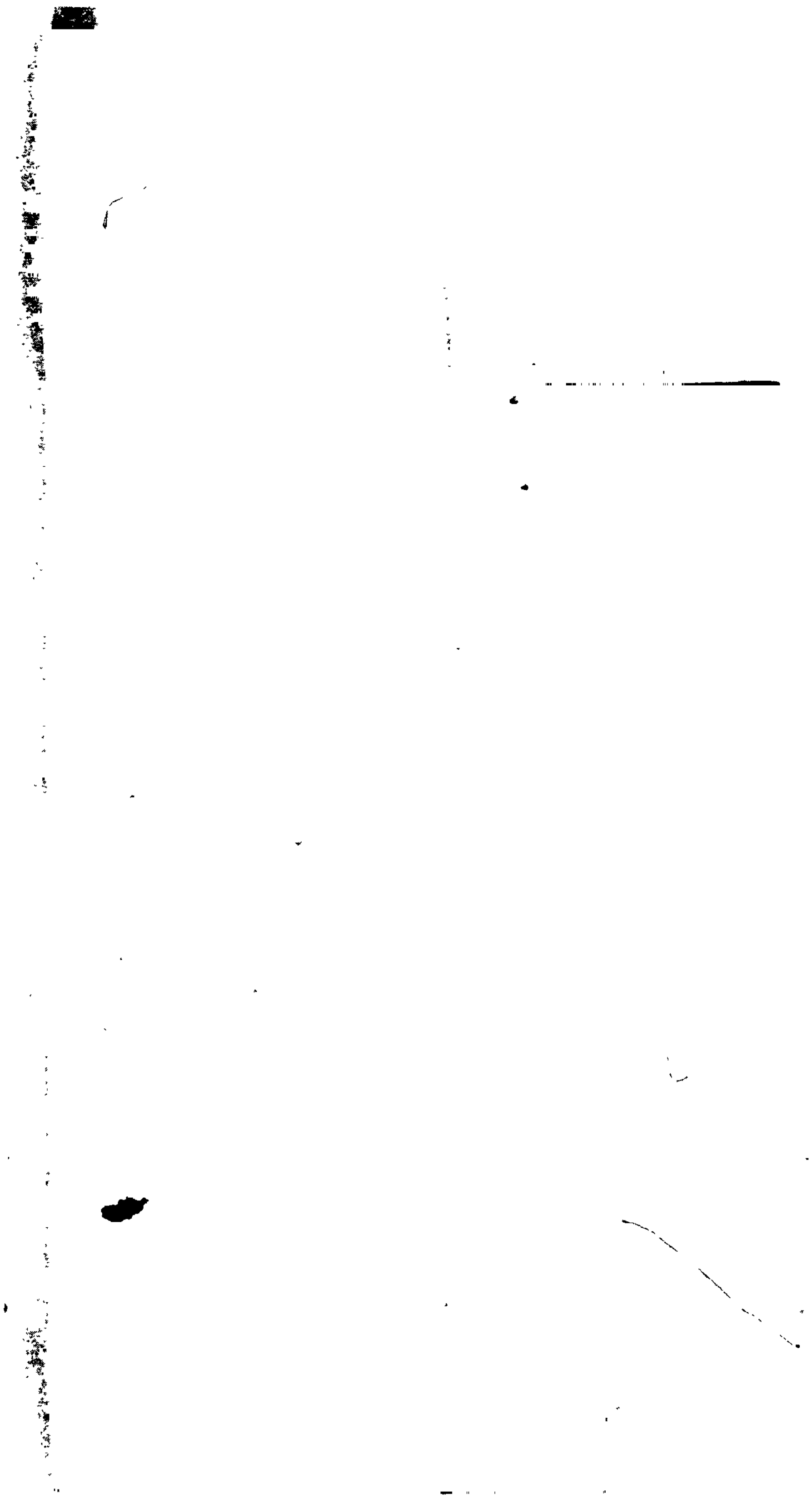

Figure 41 TOP VIEW OF CHARRED AVCOAT 5026-39M

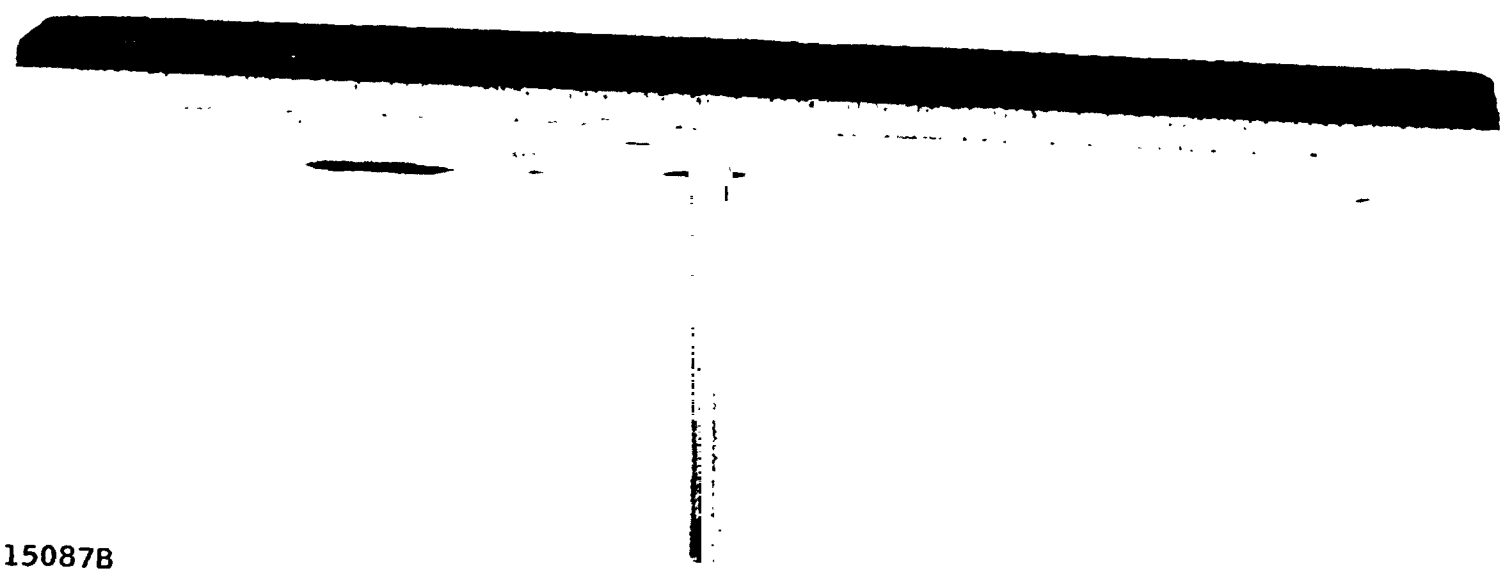

15087B

Figure 42 CROSS-SECTIONAL VIEW OF SURFACE CHAR ON AVCOAT 5026-39M

Table II references the experimental data for the charred Avcoat 5026-39M and its simulators. Note that antenna efficiency was considerably reduced as a result of the char layer over the antenna aperture.

Upon replacing char with a 1/4-inch nylon antenna window, antenna efficiencies of the 300 Mc and 2200 Mc antennas increased to within 6.3 percent and 1.3 percent respectively, of the efficiency measured without heat shield. (See Figure 43.)

The virgin heat shield covered with char was simulated with virgin heat-shield simulator and conductive cloth. The virgin simulator was approximately 7/32-inch thick for full-scale tests. The conductive cloths required to simulate the char were determined experimentally. The number of conductive sheets used for each test, with their equivalent conductivities and resistivities, is given in Table III. The equivalent resistivity and conductivity was obtained by considering the sheets as parallel-circuit elements. This theory was confirmed experimentally. The equivalent conductivities are in no way related to the electromagnetic laws of scaling. Although the errors at 300 Mc, 900 Mc, and 1500 Mc appear large on the patterns, they are actually small if these differences are compared in terms of power to the peak antenna gain without heat shield.

The nonuniformity of the char layer's resistivity affected the antenna patterns at 2200 Mc with a resultant nonuniform E-plane pattern. The charred section over the antenna aperture was replaced with another section. Antenna patterns taken with this char were again nonuniform and in addition, nonrepeatable. One char layer was chosen for the verification tests and simulators were made to simulate its patterns. The simulators developed for the full-scale and scaled cases were designed to give an average pattern since it was impossible to duplicate the nonuniform pattern with the simulators. Again, the variations are not as serious as they appear on the patterns if they are referenced to the peak gain without heat shield.

Impedance measurements were taken in the same manner as previously discussed.

The theoretical radiation patterns were calculated with respect to an infinite ground plane. Since edge effects played a predominate role in the patterns taken at 2200 Mc, the associated theoretical patterns can be compared only in envelope. Although the patterns at 300 Mc did not show any serious edge effects, these patterns can not be compared due to the small ground plane used in the 300 Mc measurements ($l = 1.22\lambda$). The gain at $\phi = 0$ degrees, $\theta = 0$ degrees can be compared.

15087F

Figure 43 300 MC OPEN-ENDED-WAVEGUIDE ANTENNA WITH NYLON ANTENNA WINDOW GROUND PLANE COVERED WITH CHARRED AVCOAT 5026-39M

TABLE III

CHAR SIMULATORS

Frequency	Char Simulator (ohms per square)			Equivalent G (mho per square)	Equivalent R (ohms per square)
	#81 Ω/sq Sheets	#480 Ω/sq Sheets	#660 Ω/sq Sheets		
300 Mc	2		1	0.026	38.2
900 Mc	2			0.025	40.5
1500 Mc	3			0.037	27.0
2200 Mc	1	1	2	0.017	57.3
6600 Mc	1	2	2	0.020	51.1
11000 Mc	1	2	1	0.016	66.7

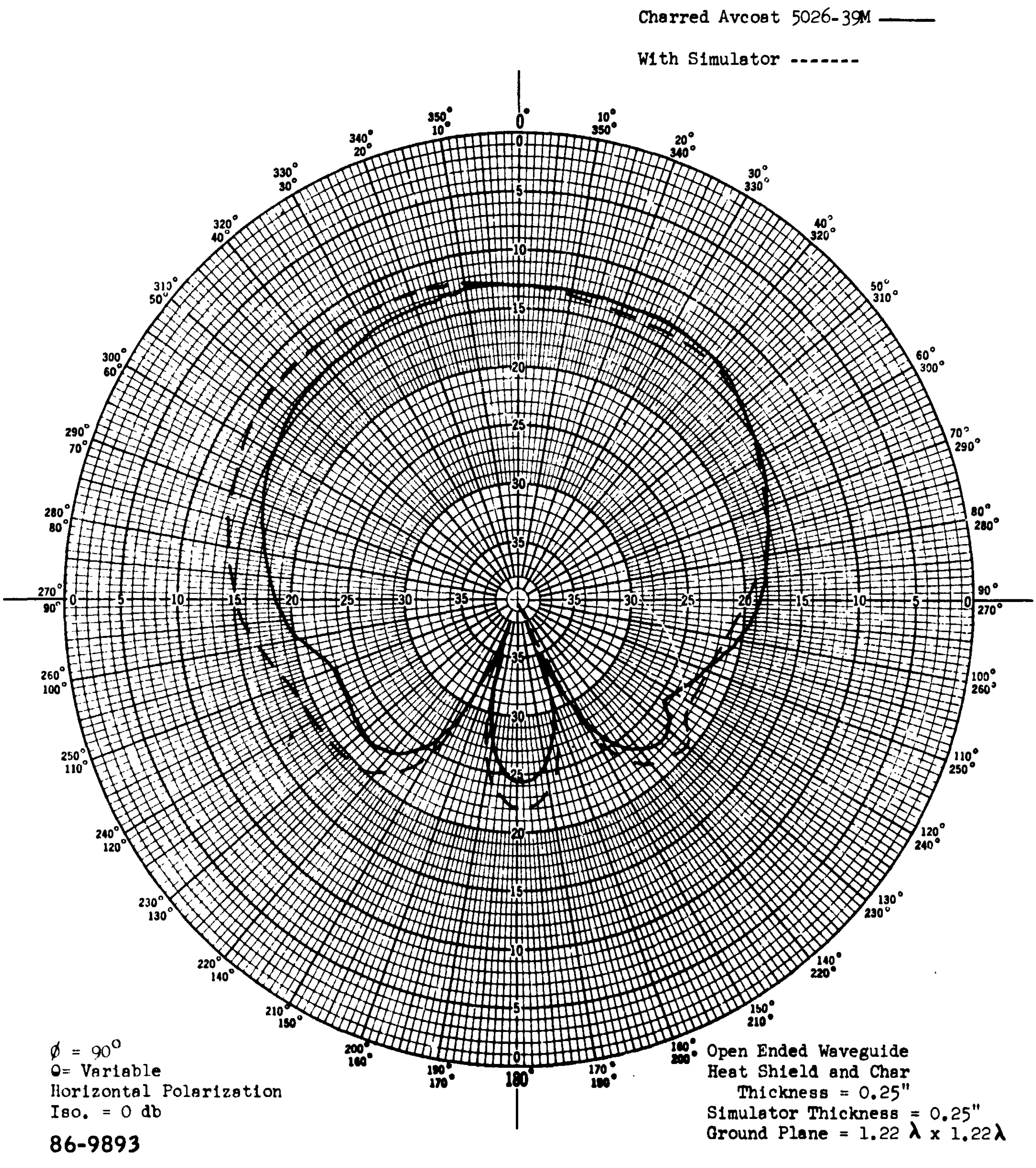

Figure 44 300 MC OPEN-ENDED WAVEGUIDE, COMPARISON BETWEEN CHARRED AVCOAT 5026-39M AND SIMULATOR. E PLANE

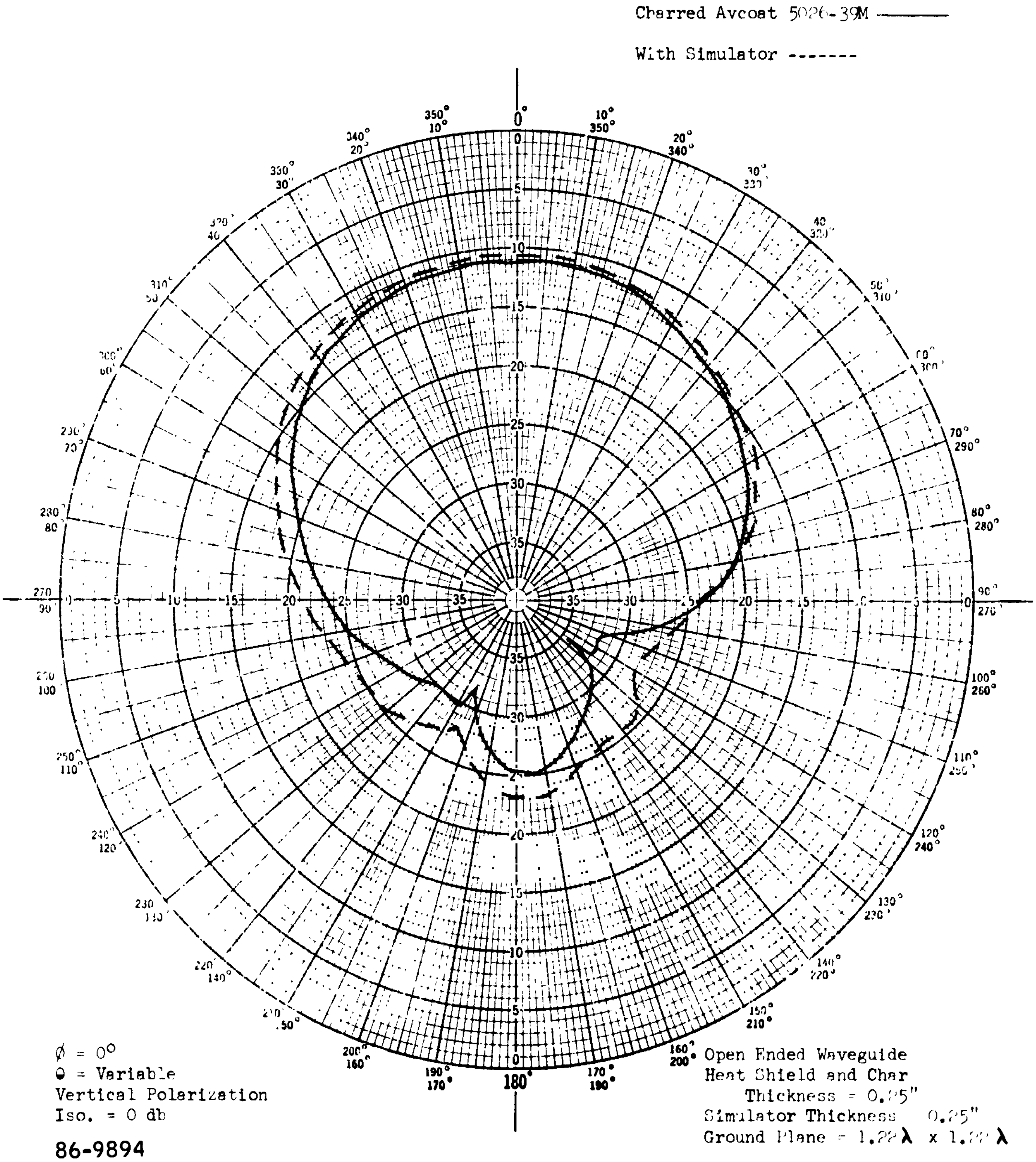

Figure 45 300 MC OPEN-ENDED WAVEGUIDE, COMPARISON BETWEEN CHARRED AVCOAT 5026-39M AND SIMULATOR. H PLANE

f = 300 Mcs
With Charred Avcoat 5026-39M ———

f = 900 Mcs
With 1/3 Scale Simulator ------

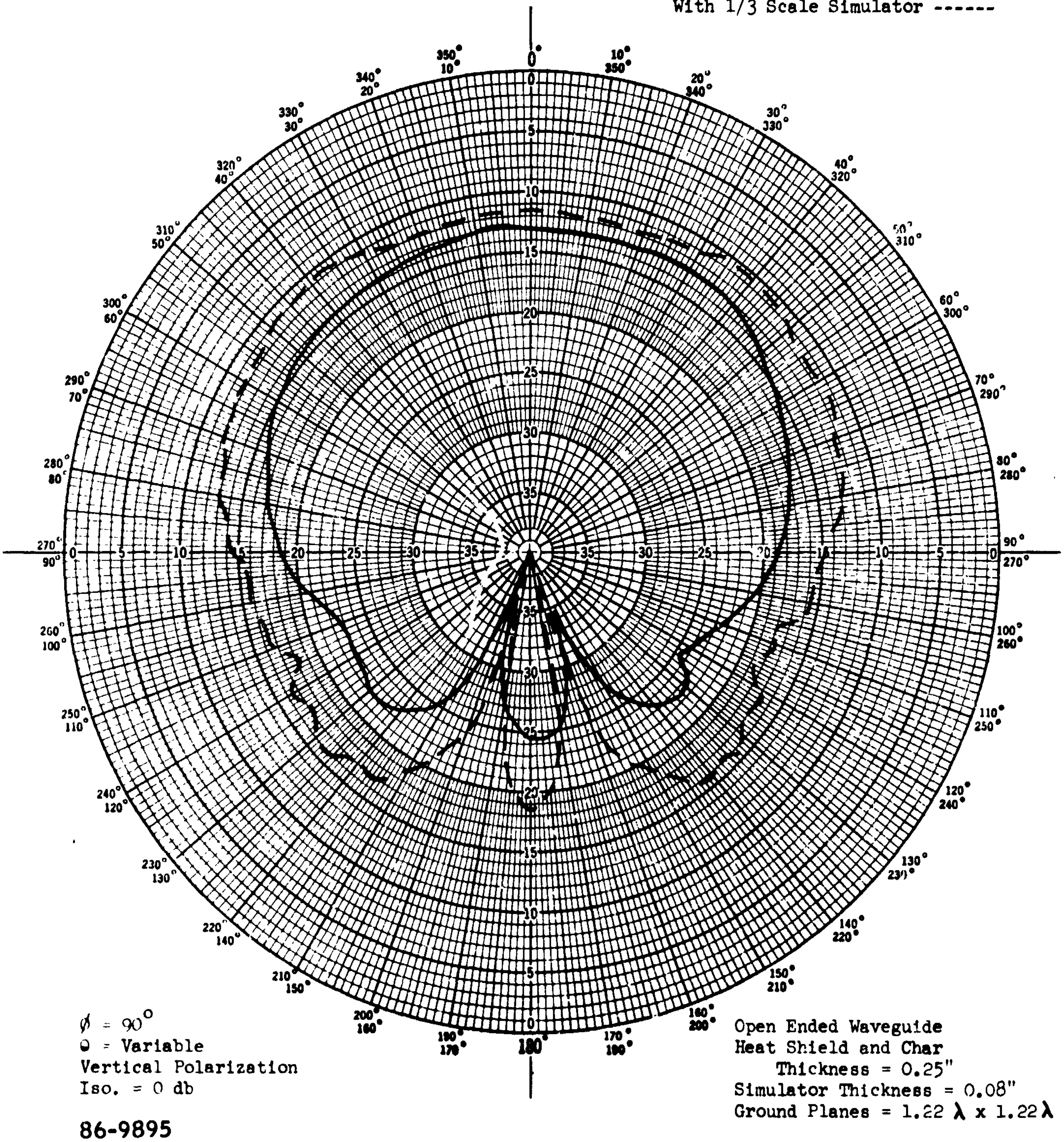

ϕ = 90°
θ = Variable
Vertical Polarization
Iso. = 0 db

86-9895

Open Ended Waveguide
Heat Shield and Char
Thickness = 0.25"
Simulator Thickness = 0.08"
Ground Planes = 1.22 λ x 1.22 λ

Figure 46 300 MC AND 900 MC OPEN-ENDED WAVEGUIDE, COMPARISON BETWEEN CHARRED AVCOAT 5026-39M AND THIRD-SCALE SIMULATOR. E PLANE

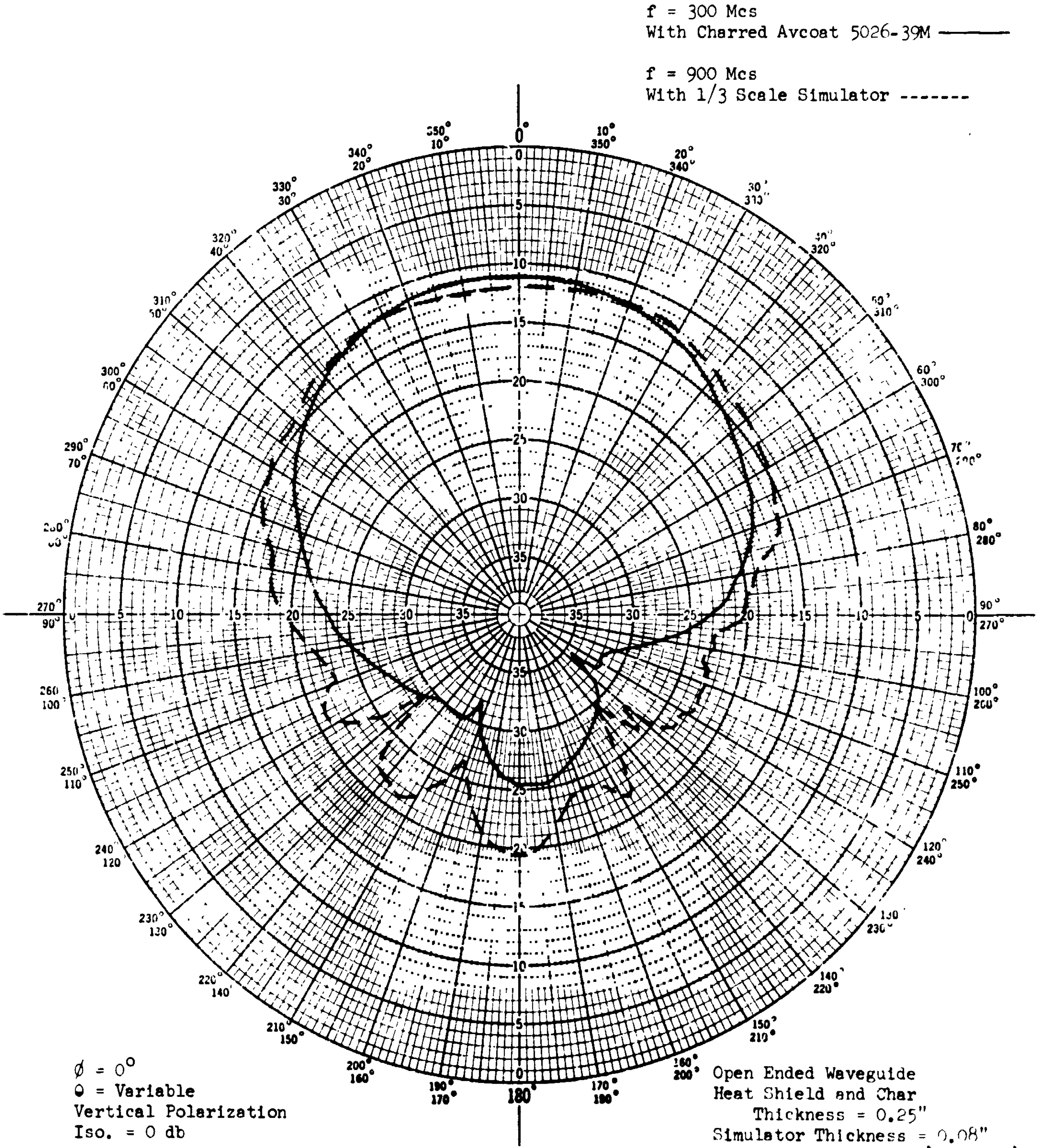

86-9896

Figure 47 300 MC and 900 MC OPEN-ENDED WAVEGUIDE, COMPARISON BETWEEN CHARRED AVCOAT 5026-39M AND THIRD-SCALE SIMULATOR. H PLANE

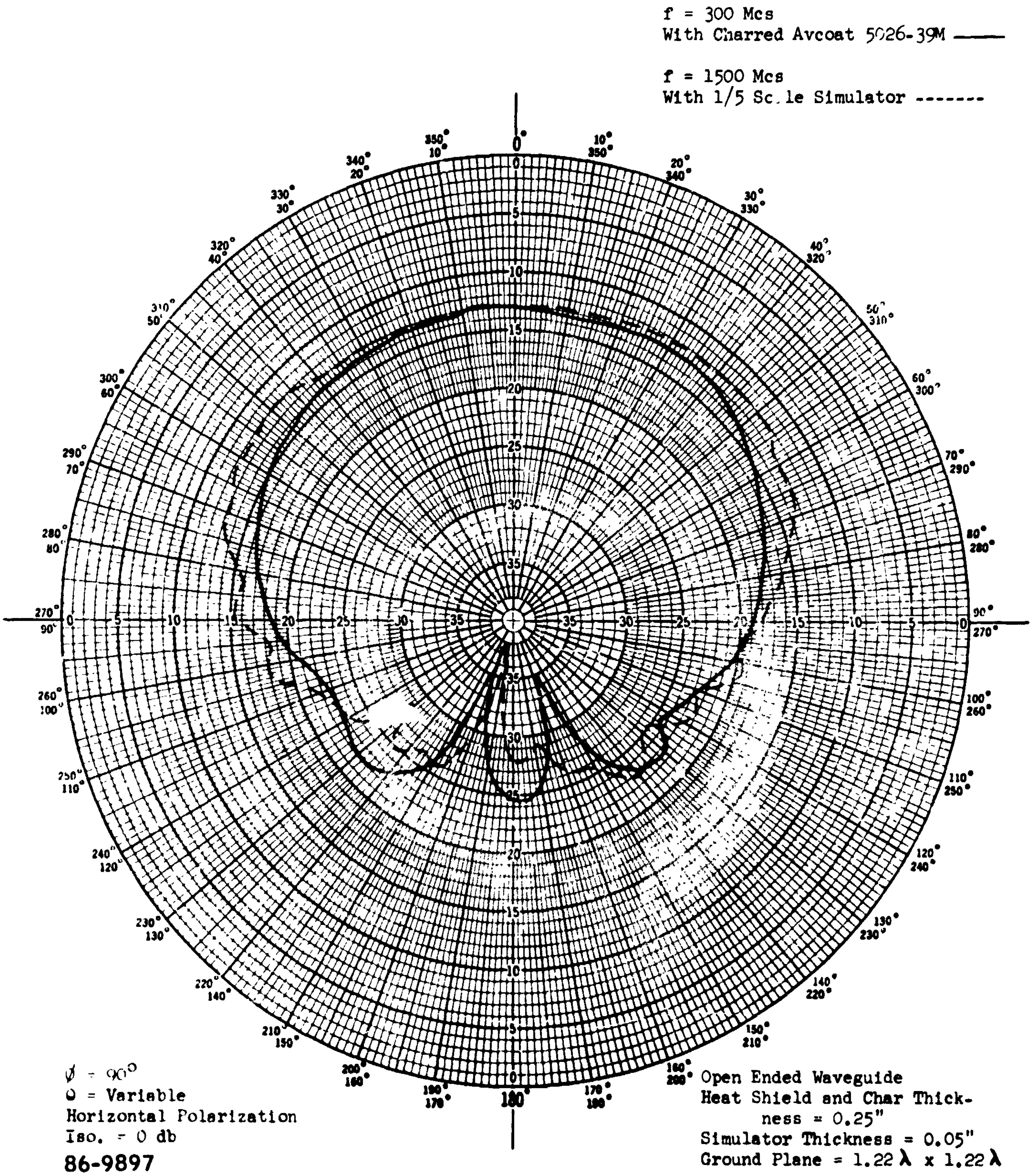

Figure 48 300 MC AND 1500 MC OPEN-ENDED WAVEGUIDE, COMPARISON BETWEEN CHARRED AVCOAT 5026-39M AND FIFTH-SCALE SIMULATOR. E PLANE

f = 300 Mcs
With Charred Avcoat 5026-39M ————

f = 1500 Mcs
With 1/5 Scale Simulator ------

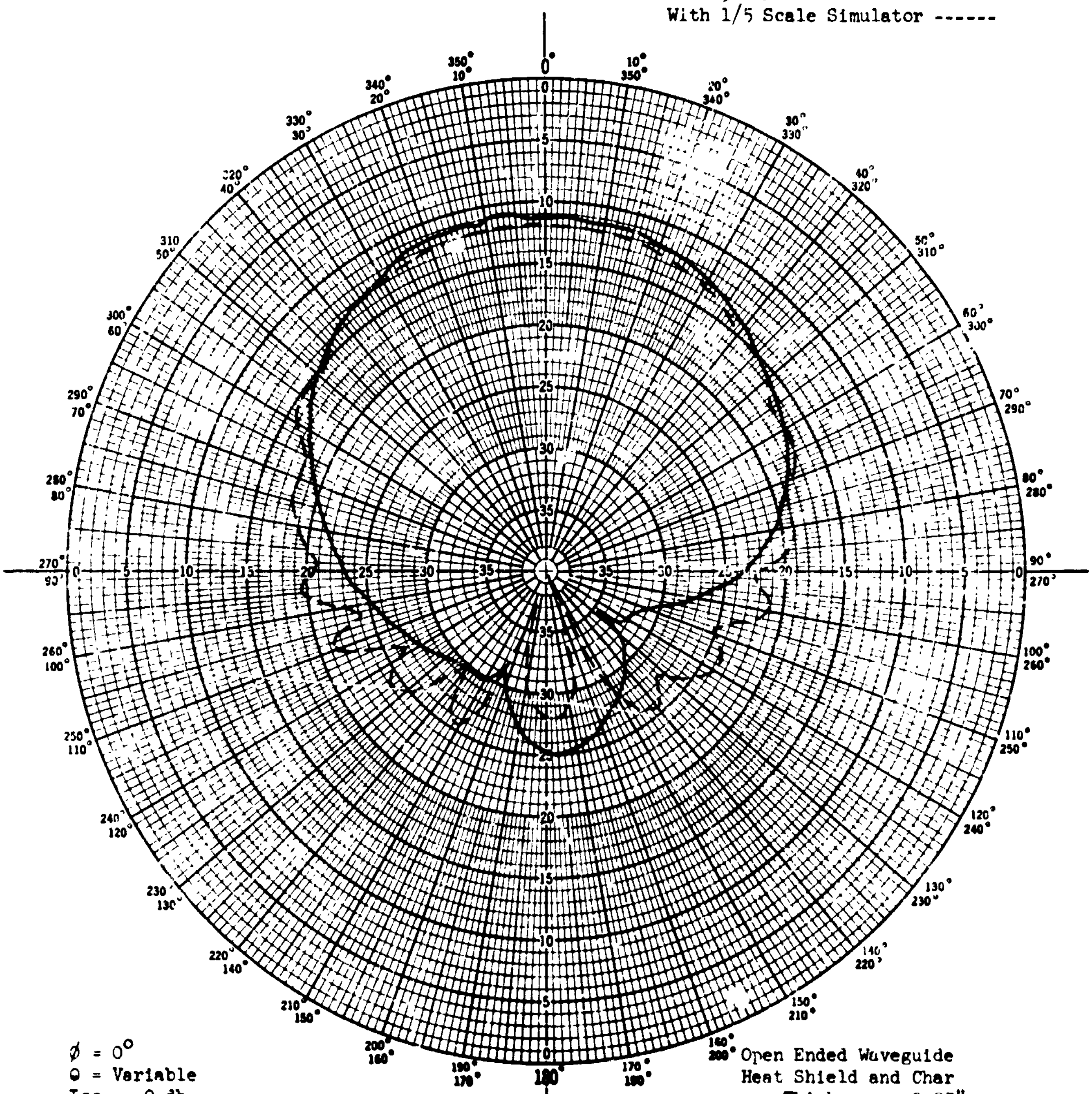

∅ = 0°
Θ = Variable
Iso. = 0 db
Vertical Polarization

86-9898

Open Ended Waveguide
Heat Shield and Char
Thickness = 0.25"
Simulator Thickness = 0.05"
Ground Plane = 1.22 λ x 1.22 λ

Figure 49 300 MC AND 1500 MC OPEN-ENDED WAVEGUIDE, COMPARISON BETWEEN CHARRED AVCOAT 5026-39M AND FIFTH-SCALE SIMULATOR. H PLANE

With Charred Avcoat 5026-39M ____

With Simulator --------

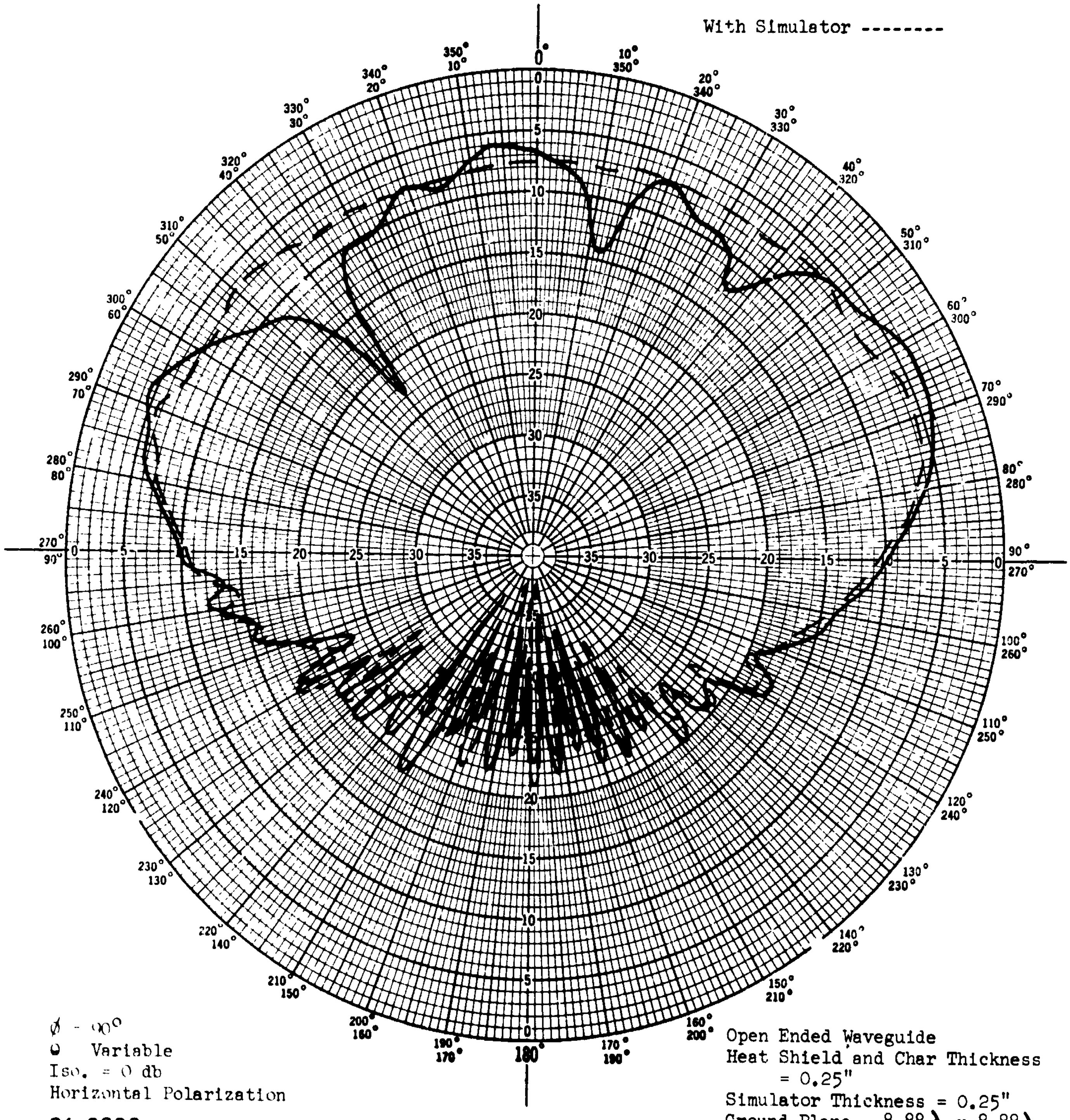

ϕ - 90°
θ Variable
Iso. = 0 db
Horizontal Polarization

86-9899

Open Ended Waveguide
Heat Shield and Char Thickness = 0.25"
Simulator Thickness = 0.25"
Ground Plane = 8.88 λ x 8.88 λ

Figure 50 2200 MC OPEN-ENDED WAVEGUIDE, COMPARISON BETWEEN CHARRED AVCOAT 5026-39M AND SIMULATOR. E PLANE

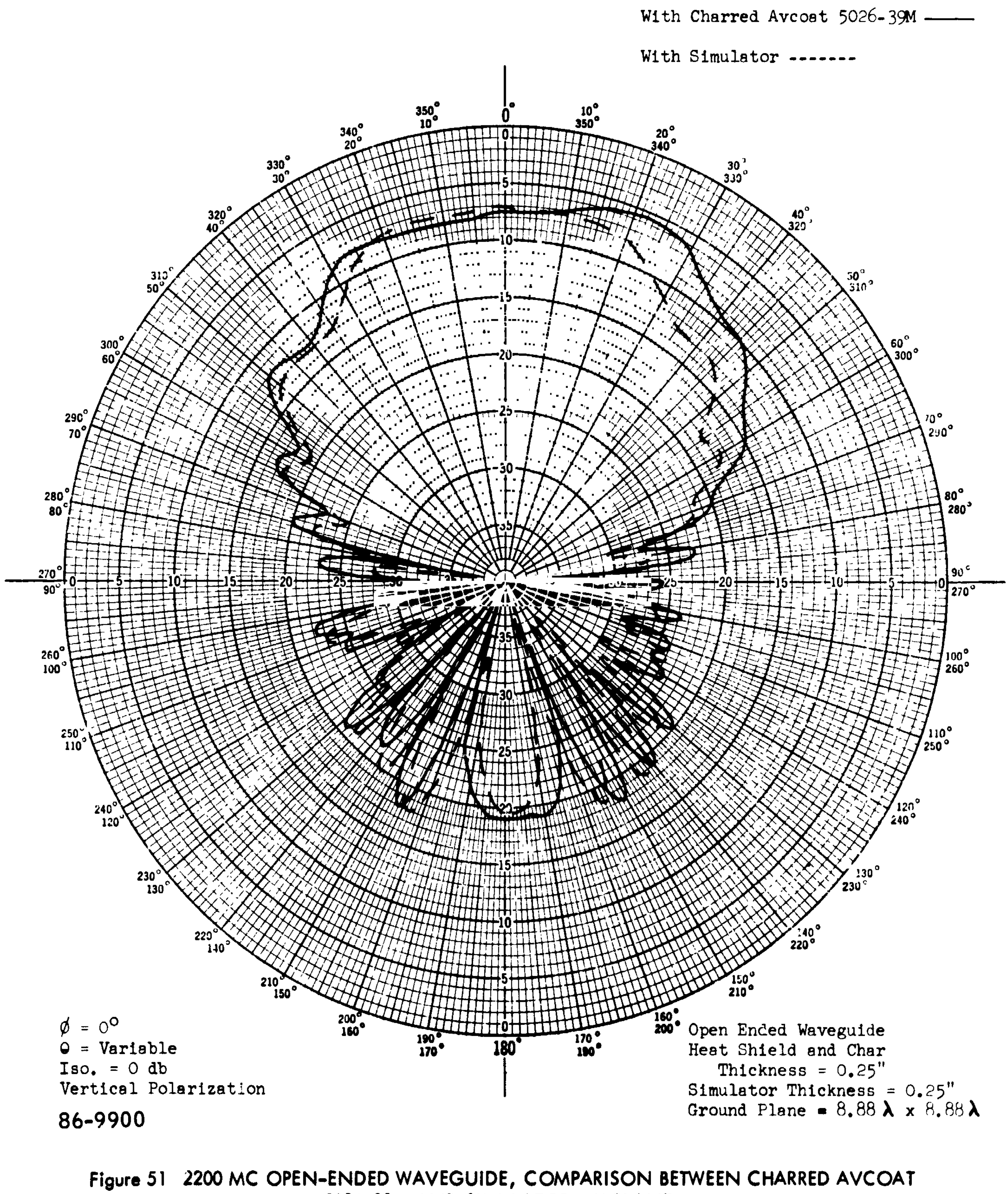

Figure 51 2200 MC OPEN-ENDED WAVEGUIDE, COMPARISON BETWEEN CHARRED AVCOAT 5026-39M AND SIMULATOR. H PLANE

f = 2200 Mcs
With Charred Avcoat 5026-39M ———

f = 6600 Mcs
With 1/3 Scale Simulator -------

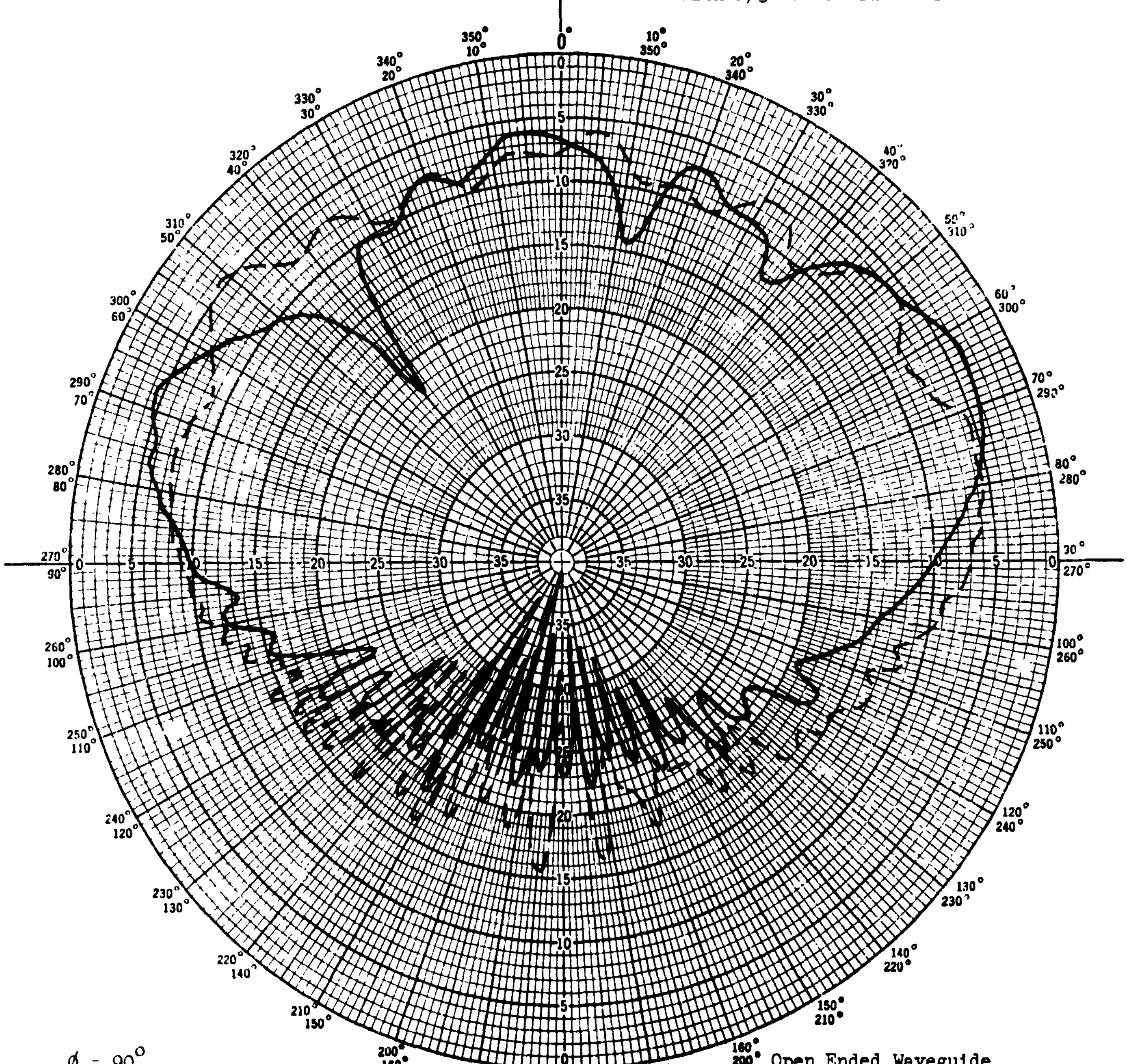

Ø = 90°
Θ = Variable
Horizontal Polarization
Iso. = 0 db

86-9901

Open Ended Waveguide
Charred Heat Shield
Thickness = 0.25"
Simulator Thickness = 0.08"
Ground Planes = 8.88 λ x 8.88λ

Figure 52 2200 MC AND 6600 MC OPEN-ENDED WAVEGUIDE, COMPARISON BETWEEN CHARRED AVCOAT 5026-39M AND THIRD-SCALE SIMULATOR. E PLANE

f = 2200 Mcs
With Charred Avcoat 5026-39M ———

f = 6600 Mcs
With 1/3 Scale Simulator ------

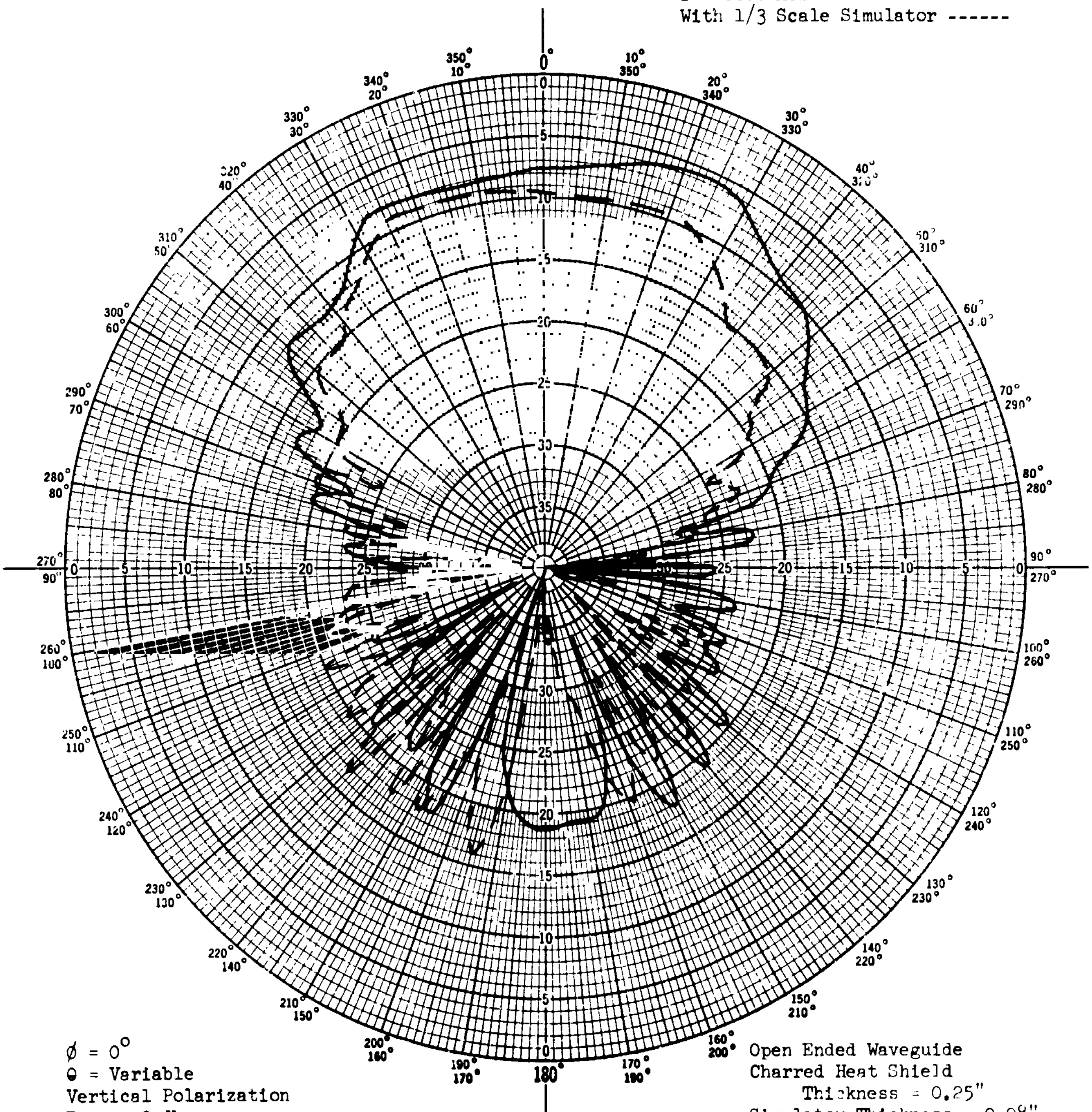

ϕ = 0°
Θ = Variable
Vertical Polarization
Iso. = 0 db

86-9902

Open Ended Waveguide
Charred Heat Shield
Thickness = 0.25"
Simulator Thickness = 0.08"
Ground Planes = 8.88 λ x 8.88 λ

Figure 53 2200 MC AND 6600 MC OPEN-ENDED WAVEGUIDE, COMPARISON BETWEEN CHARRED AVCOAT 5026-39M AND THIRD-SCALE SIMULATOR. H PLANE

f = 2200 Mcs
With Charred Avcoat 5026-39M ———

f = 11000 Mcs
With 1/5 Scale Simulator ------

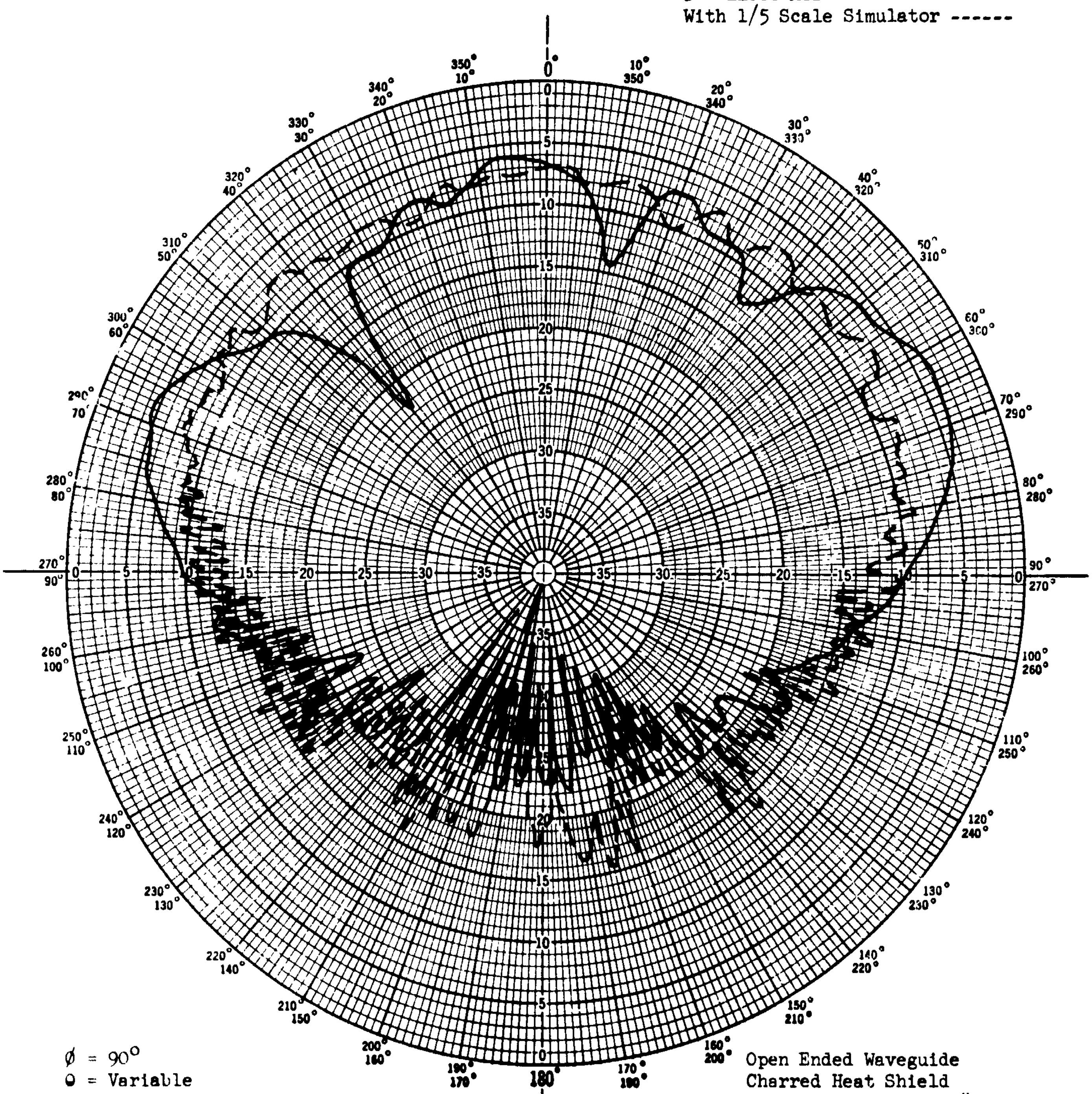

ϕ = 90°
Θ = Variable
Horizontal Polarization
Iso. = 0 db
86-9903

Open Ended Waveguide
Charred Heat Shield
Thickness = 0.25"
Simulator Thickness =.05"
Ground Planes = 8.88 λ x 8.88λ

Figure 54 2200 MC AND 11000 MC OPEN-ENDED WAVEGUIDE, COMPARISON BETWEEN CHARRED AVCOAT 5026-39M AND FIFTH-SCALE SIMULATOR. E PLANE

f = 2200 Mcs
With Charred Avcoat 5026-39M ———

f = 11000 Mcs
With 1/5 Scale Simulator -------

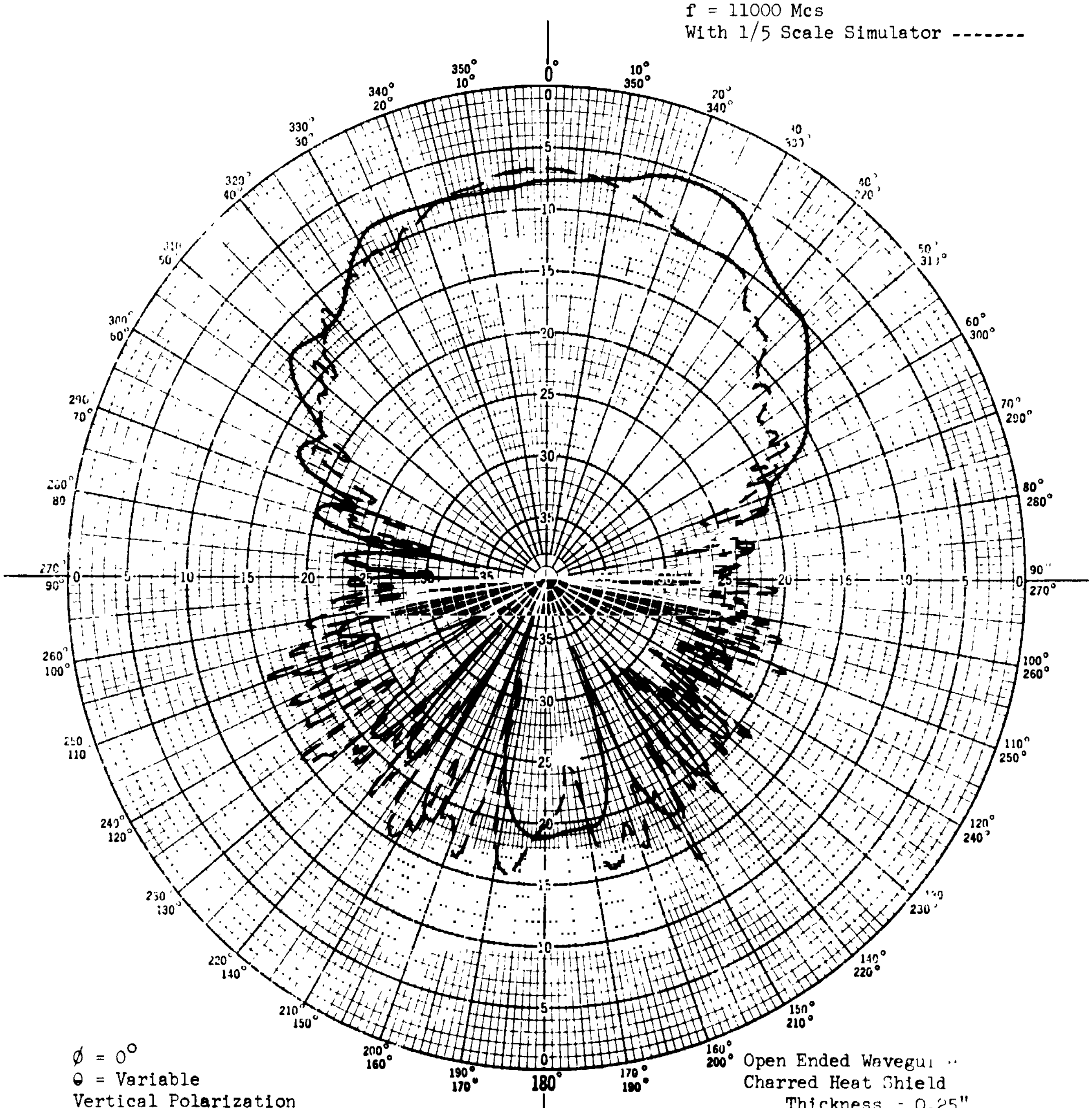

Ø = 0°
Θ = Variable
Vertical Polarization
Iso. = 0 db
86-9904

Open Ended Wavegui..
Charred Heat Shield
Thickness - 0.25"
Simulator Thickness - 0.05"
Ground Plane - 8.88λ x 8.88λ

Figure 55 2200 MC AND 11000 MC OPEN-ENDED WAVEGUIDE, COMPARISON BETWEEN CHARRED AVCOAT 5026-39M AND FIFTH-SCALE SIMULATOR. H PLANE

With Charred Avcoat 5026-39M ———

Charred Avcoat 5026-39M with
Nylon Window -------

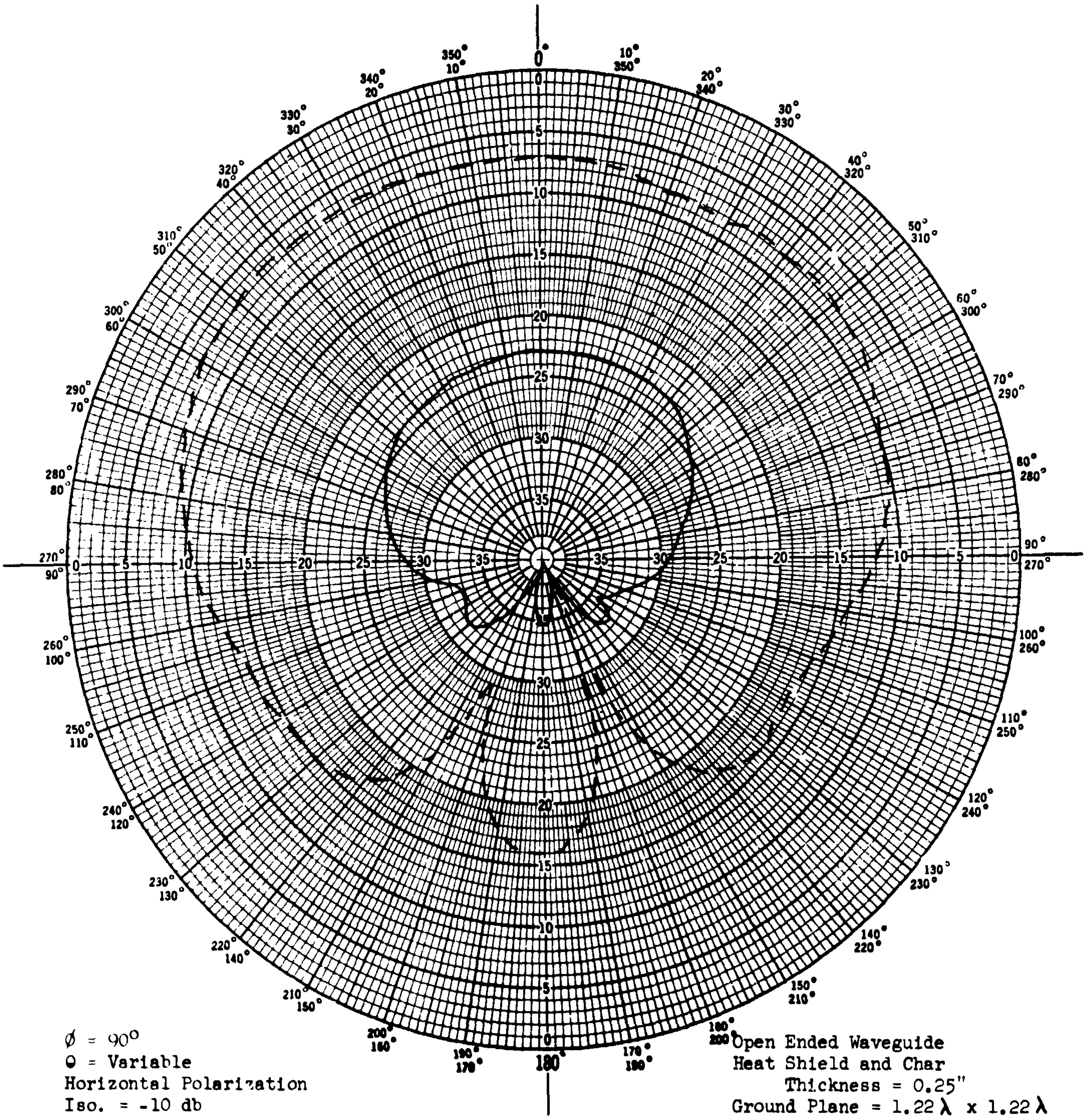

ϕ = 90°
Θ = Variable
Horizontal Polarization
Iso. = -10 db
86-9905

Open Ended Waveguide
Heat Shield and Char
Thickness = 0.25"
Ground Plane = 1.22 λ x 1.22 λ

Figure 56 300 MC OPEN-ENDED WAVEGUIDE, CHARRED 5026-39M AND CHARRED 5026-39M WITH ANTENNA WINDOW. E PLANE

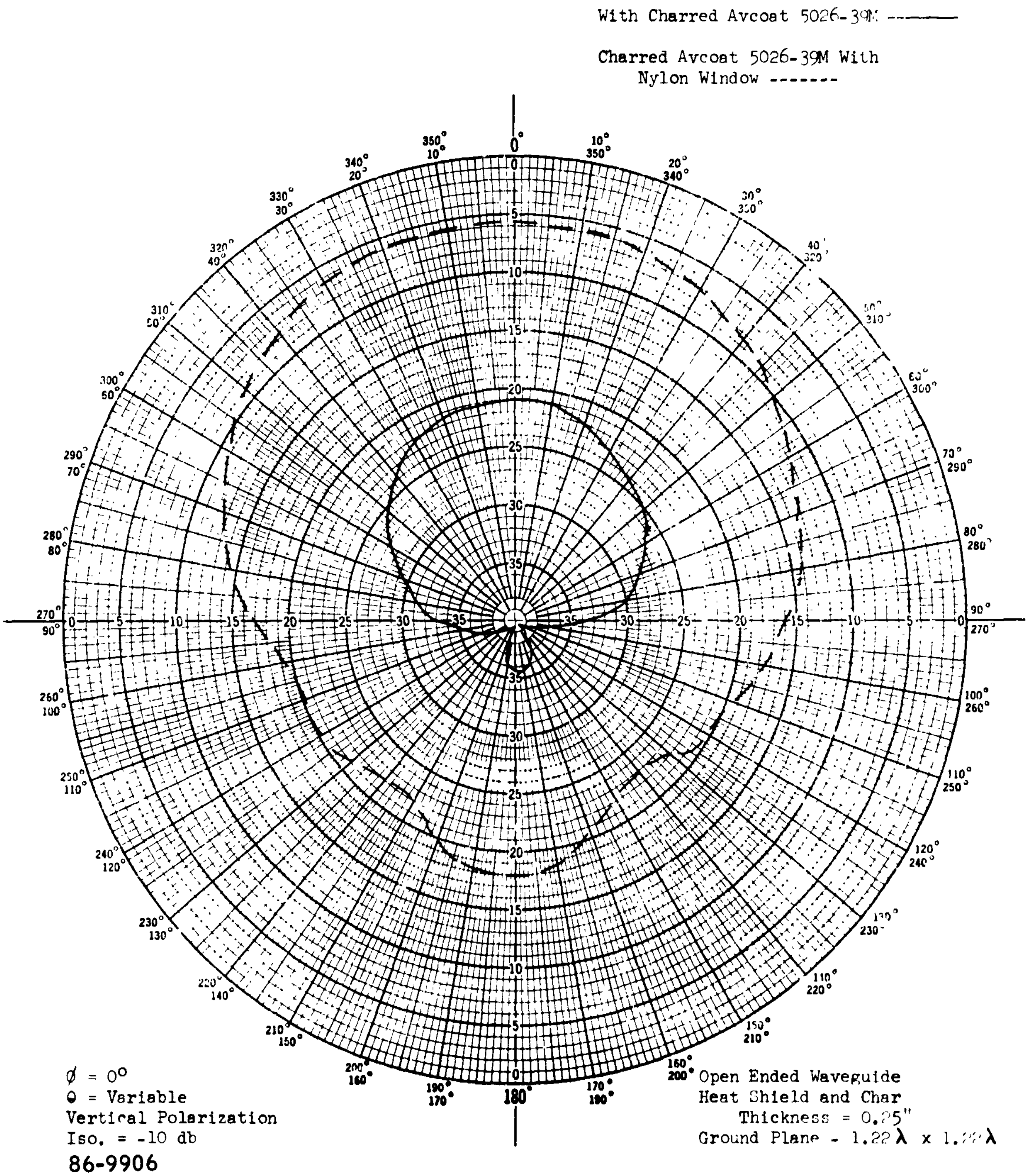

Figure 57 300 MC OPEN-ENDED WAVEGUIDE, CHARRED 5026-39M AND CHARRED 5026-39M WITH ANTENNA WINDOW. H PLANE

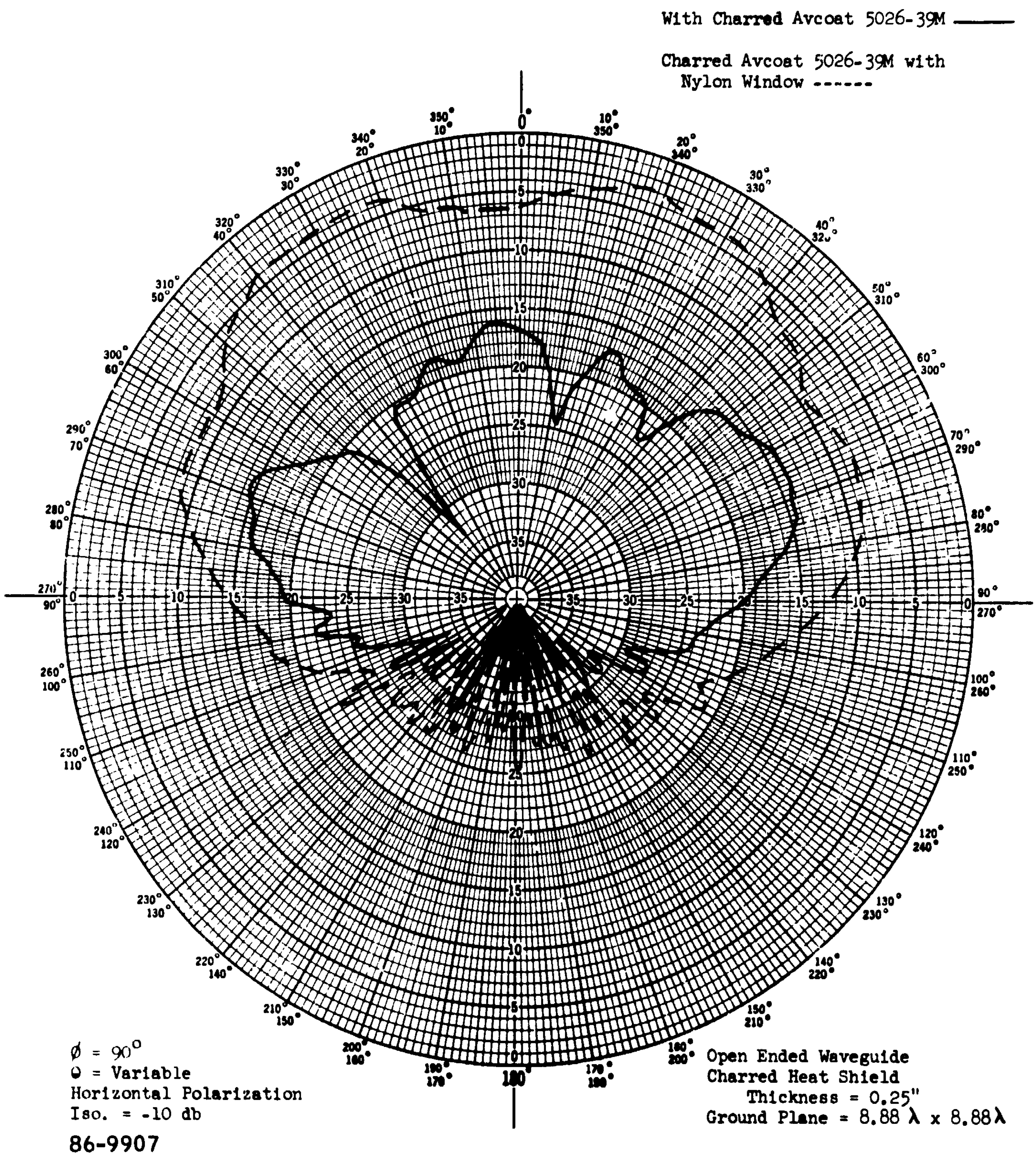

Figure 58 2200 MC OPEN-ENDED WAVEGUIDE, CHARRED 5026-39M AND CHARRED 5026-39M WITH ANTENNA WINDOW. E PLANE

With Charred Avcoat 5026-39M ———

Charred Avcoat 5026-39M With
Nylon Window -------

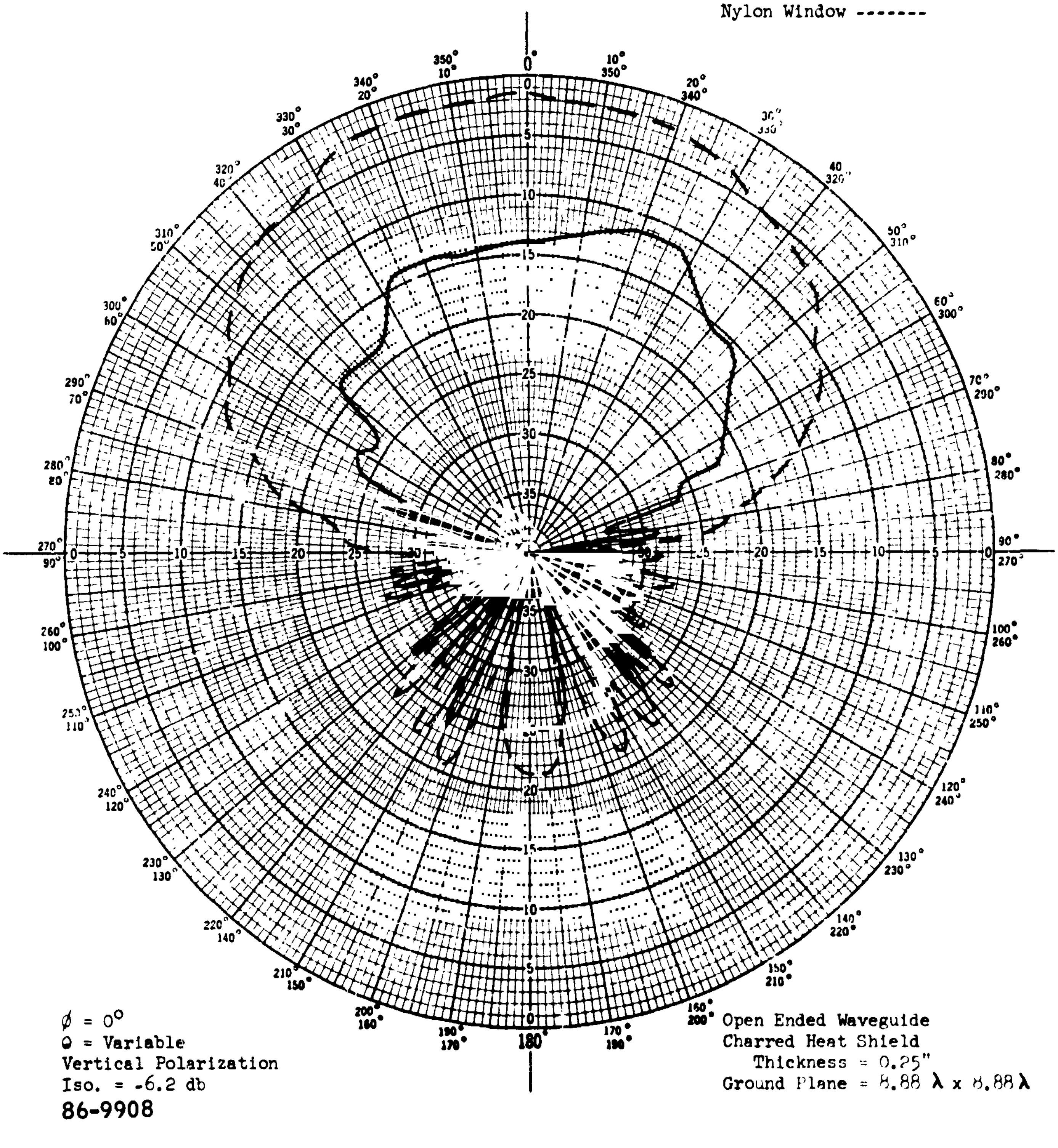

ϕ = 0°
Θ = Variable
Vertical Polarization
Iso. = -6.2 db
86-9908

Open Ended Waveguide
Charred Heat Shield
Thickness = 0.25"
Ground Plane = 8.88 λ x 8.88 λ

Figure 59 2200 MC OPEN-ENDED WAVEGUIDE, CHARRED 5026-39M AND CHARRED 5026-39M WITH ANTENNA WINDOW. H PLANE

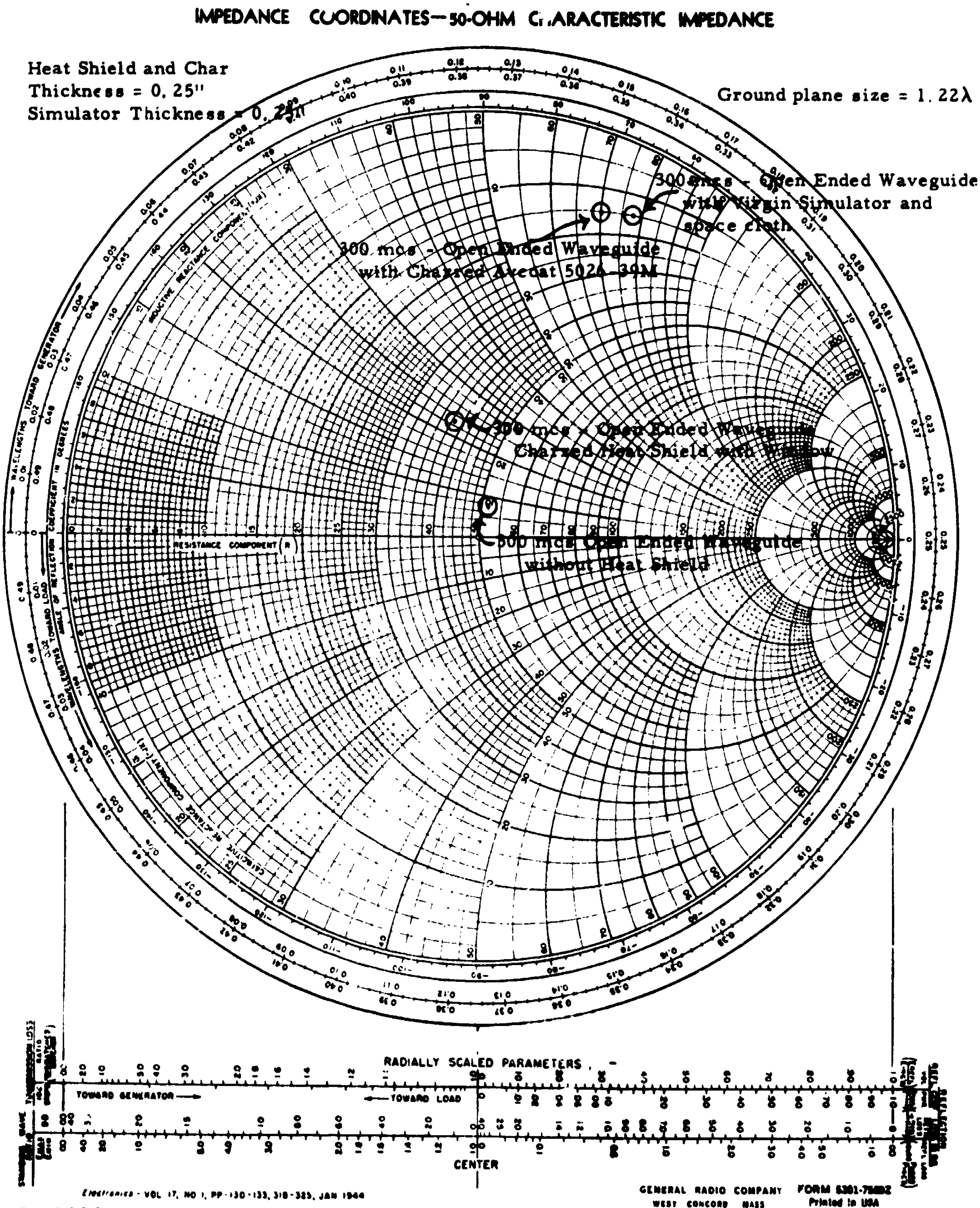

86-9909

Figure 60 IMPEDANCE OF 300 MC OPEN-ENDED WAVEGUIDE WITH CHARRED AVCOAT 5026-39M AND SIMULATOR

IMPEDANCE COORDINATES—50-OHM CHARACTERISTIC IMPEDANCE

Heat Shield and Char Thickness = 0.25"

900 mcs - Simulator Thickness = 0.08"

Ground Plane size - 1.22 λ

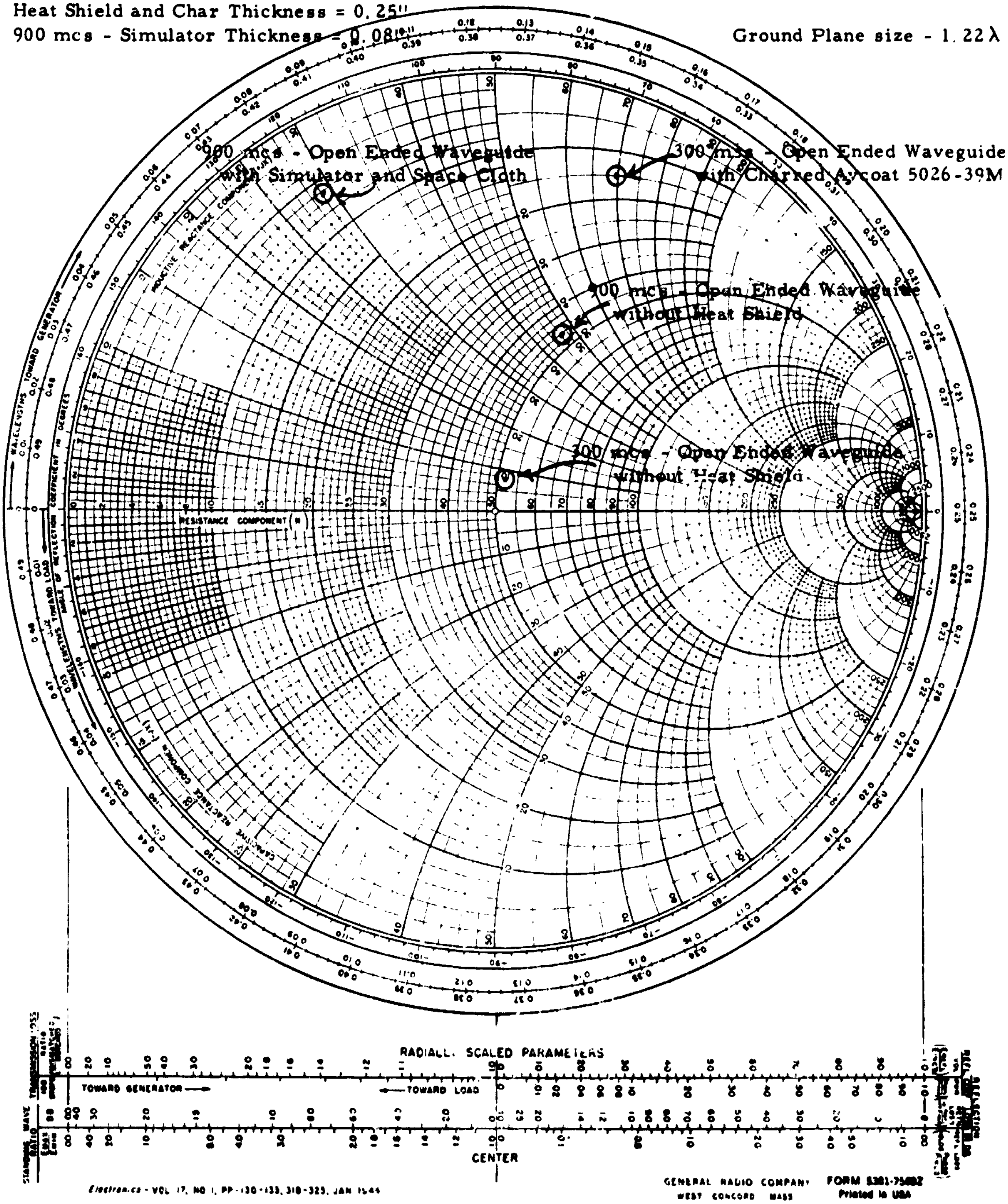

86-9910

Figure 61 IMPEDNACE OF 300 MC AND 900 MC OPEN-ENDED WAVEGUIDE WITH CHARRED AVCOAT 5026-39M AND SIMULATOR

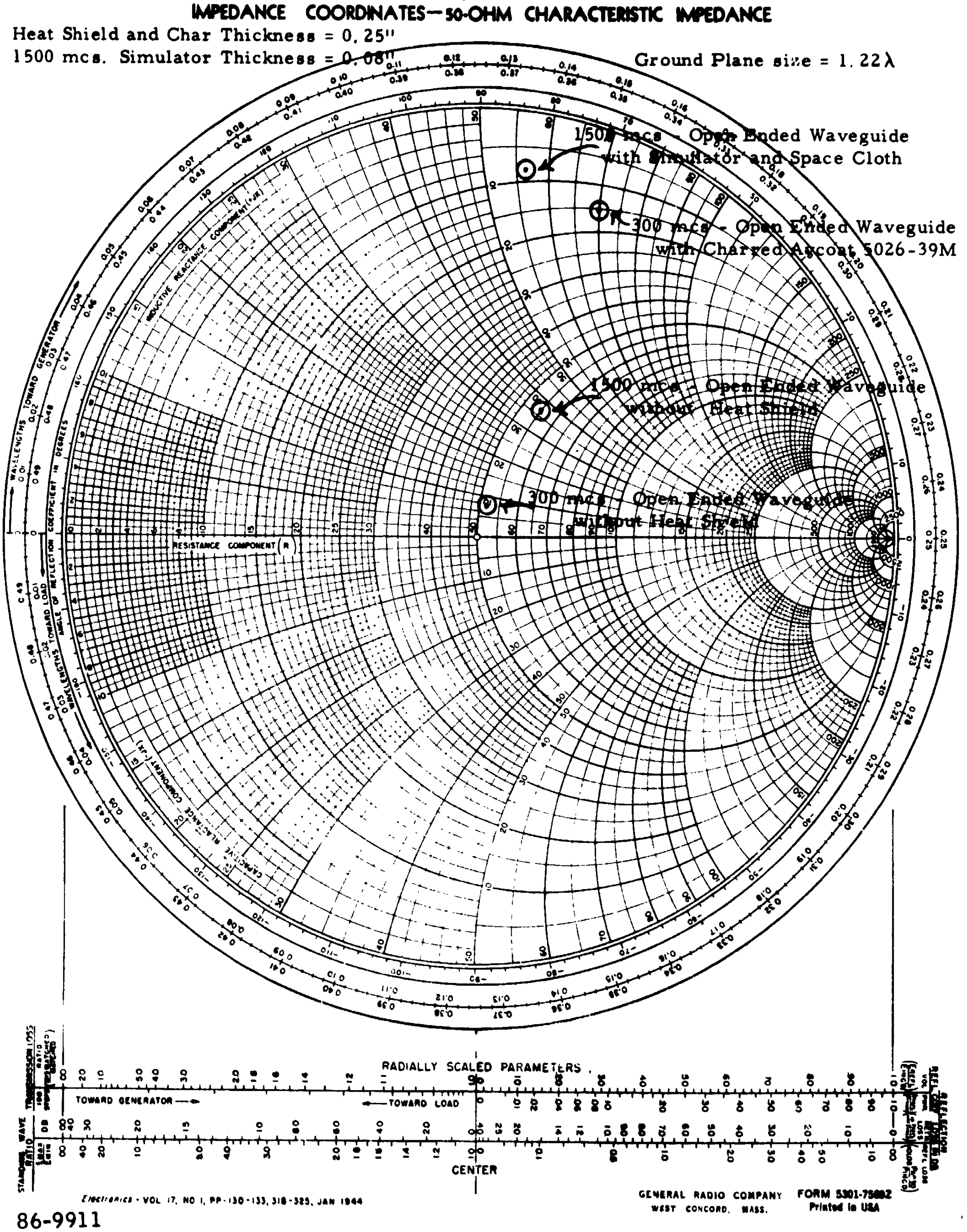

86-9911

Figure 62 IMPEDANCE OF 300 MC AND 1500 MC OPEN-ENDED WAVEGUIDE WITH CHARRED AVCOAT 5026-39M AND SIMULATOR

IMPEDANCE COORDINATES—50-OHM CHARACTERISTIC IMPEDANCE

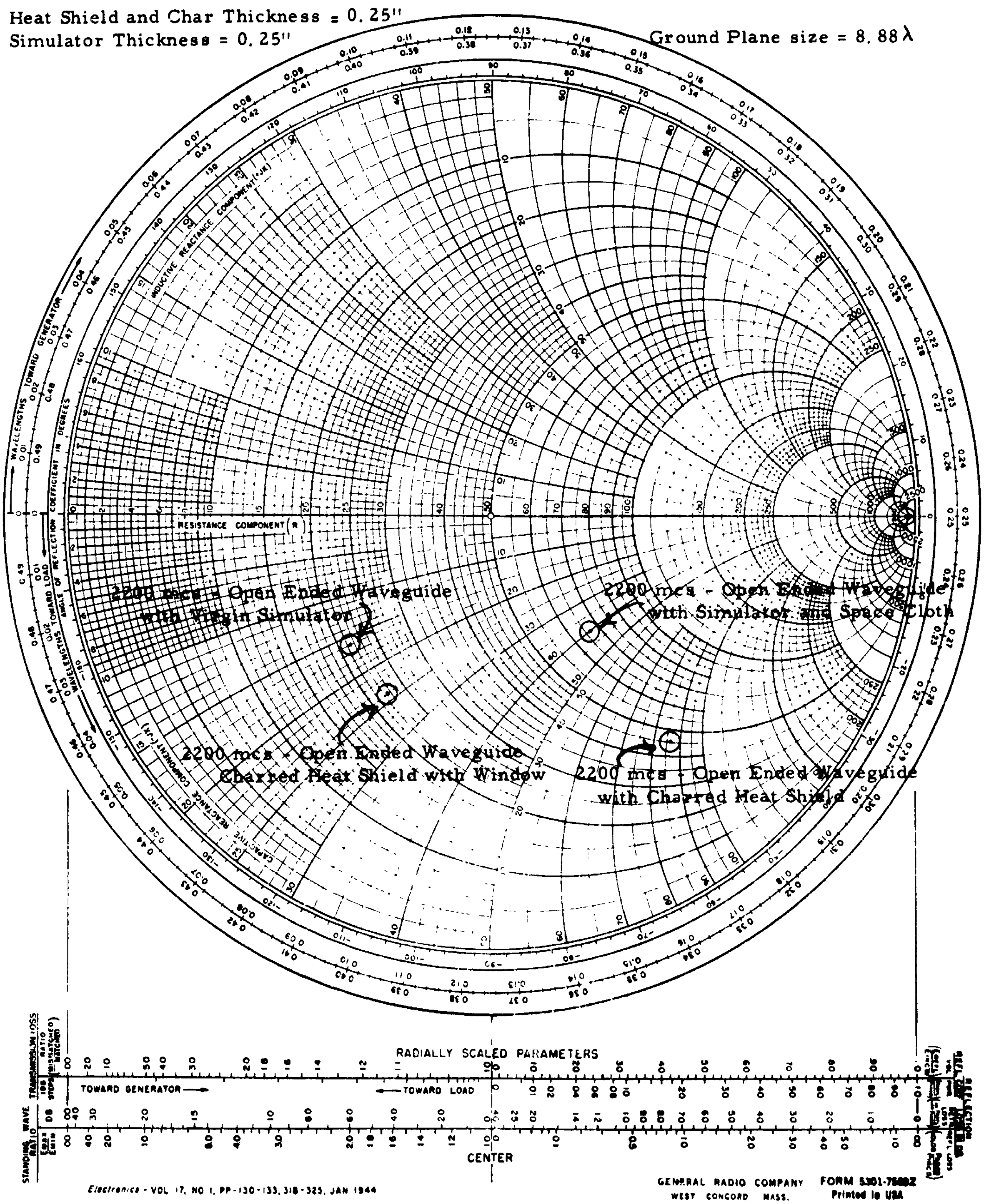

86-9912

Figure 63 IMPEDANCE OF 2200 MC OPEN-ENDED WAVEGUIDE WITH CHARRED AVCOAT 5026-39M AND SIMULATOR

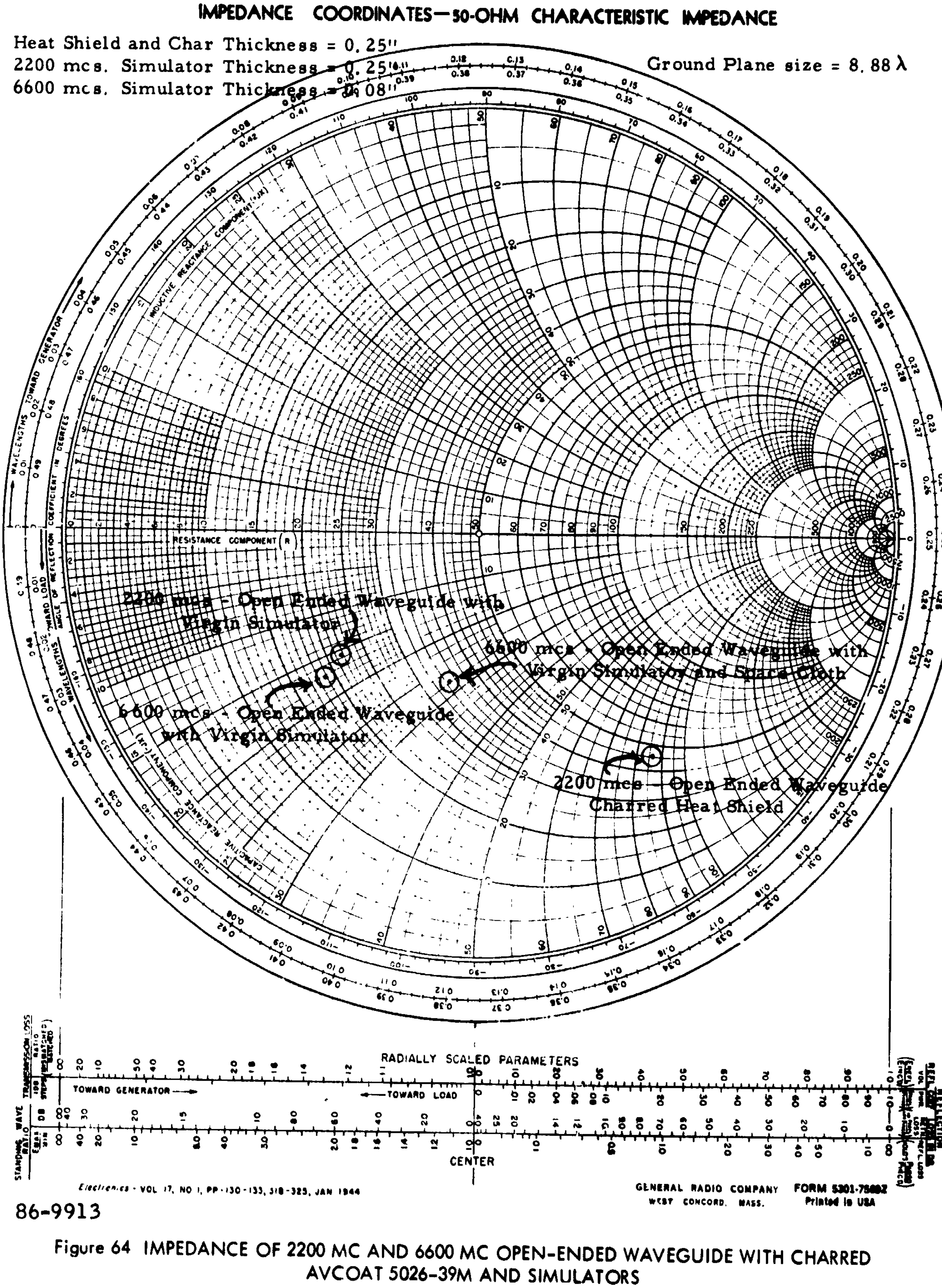

86-9913

Figure 64 IMPEDANCE OF 2200 MC AND 6600 MC OPEN-ENDED WAVEGUIDE WITH CHARRED AVCOAT 5026-39M AND SIMULATORS

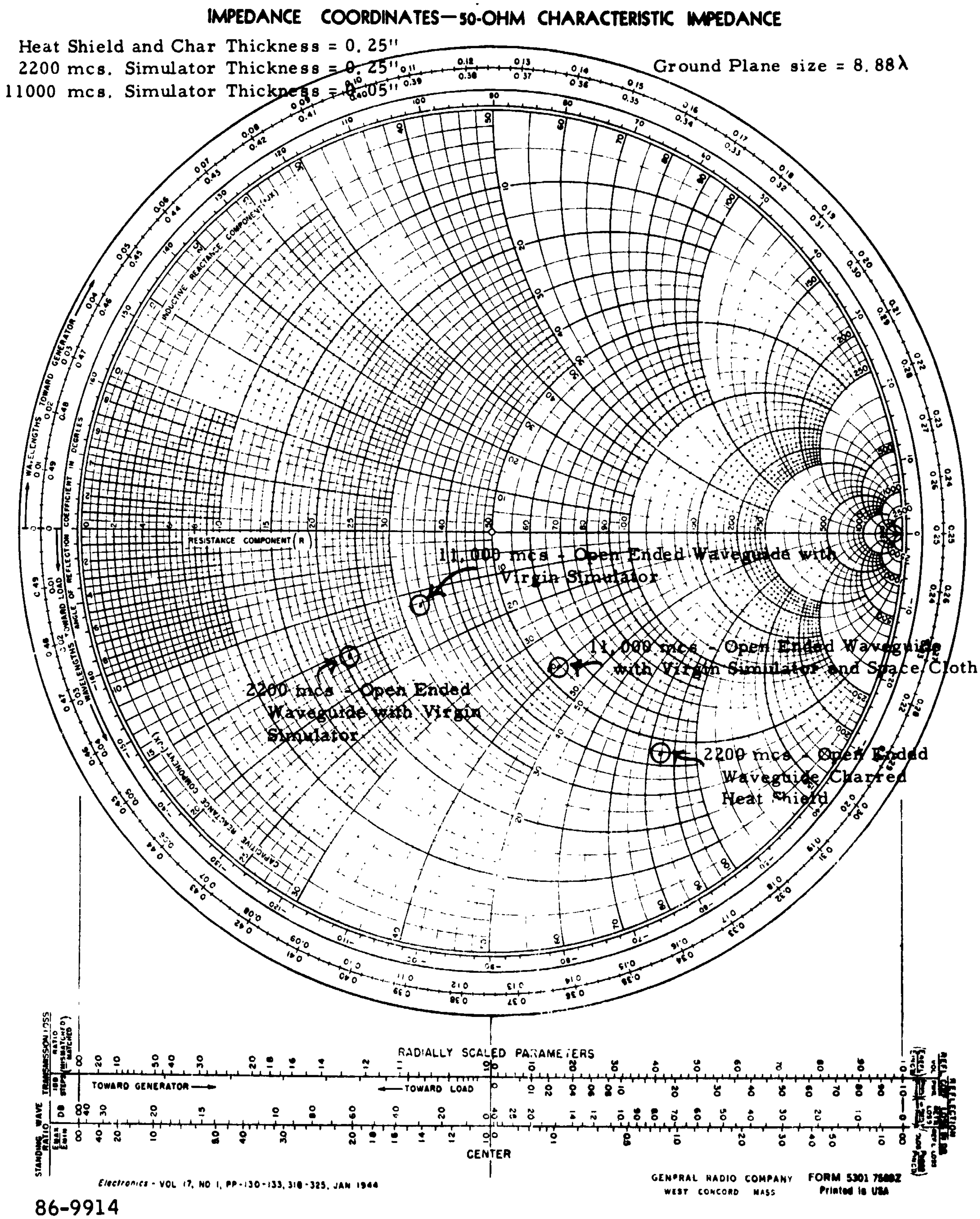

86-9914

Figure 65 IMPEDANCE OF 2200 MC AND 11000 MC OPEN-ENDED WAVEGUIDE WITH CHARRED AVCOAT 5026-39M AND SIMULATORS

Frequency (Mc)	Theoretical Attenuation (db)	Measured Attenuation (db)
300	2.07	1.5
2200	2.30	1.9

The average value for the 2200 Mc antenna was obtained by averaging the ripple in both the E- and H-plane patterns.

Impedance measurements of the antenna aperture were made at 6600 Mc with a 0.33-inch heat-shield cover to check the computer program. The measured aperture impedance was Z = 483 - j 266 without heat shield and with heat shield Z = 222 - j 106.3. The calculated aperture impedance was Z = 478 - j 278 without heat shield, and with heat shield Z = 186 - j 125. The measured and calculated impedances are within 20 percent of one another. This difference is due to approximations in the compuater program for calculation of the Q integrals. Also, there is a measurement error in that the measurements were made on a 8.88 λ ground plane whereas the computer calculations are based on an infinite ground plane.

b. Monopole, Full- and 1/3-Scale-Model Patterns and Impedance

Verification tests made with the monopole antenna are presented in matrix form in Table IV. The matrix references a series of figures which are reprints of measured data. Related patterns have been superimposed to enable the reader to readily compare them.

Only two verification test frequencies were required on the monopole, 2200 Mc and 6600 Mc. The spherical coordinate system used for the monopole-antenna patterns is defined in Figure 66.

Efficiency was calculated for the 2200 Mc monopole antenna with and without virgin heat shield. These efficiency calculations were made in the same manner as described in Subsection D.3.a with one exception, only the horizontal component was considered since the vertical component was negligible. Considerable antenna-pattern distortion was caused by the heat-shield cover. The 2200 Mc simulator performed excellently while the 6600 Mc simulator provided good correlation in respect to pattern shape only.

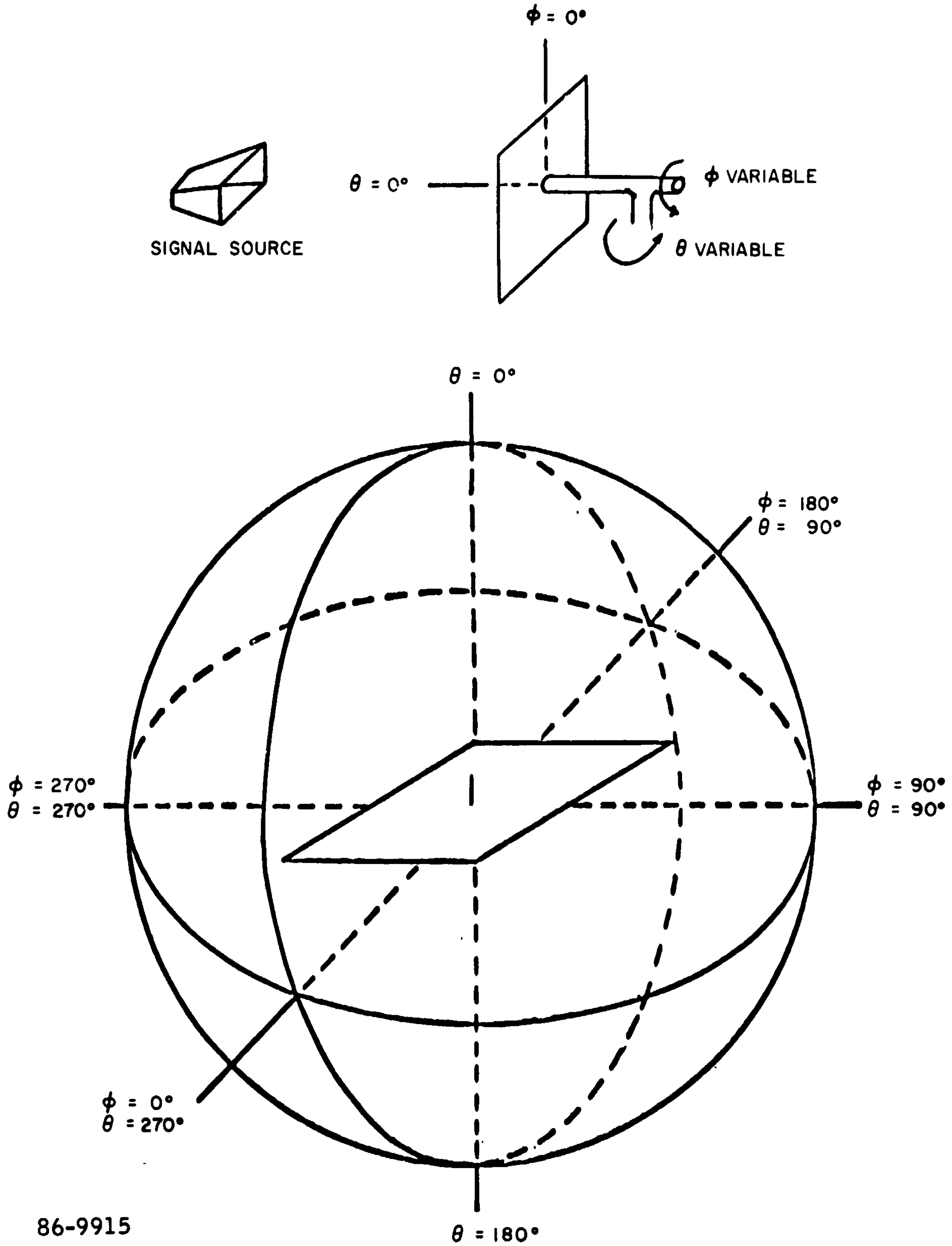

Figure 66 SPHERICAL COORDINATE SYSTEM FOR MONOPOLE

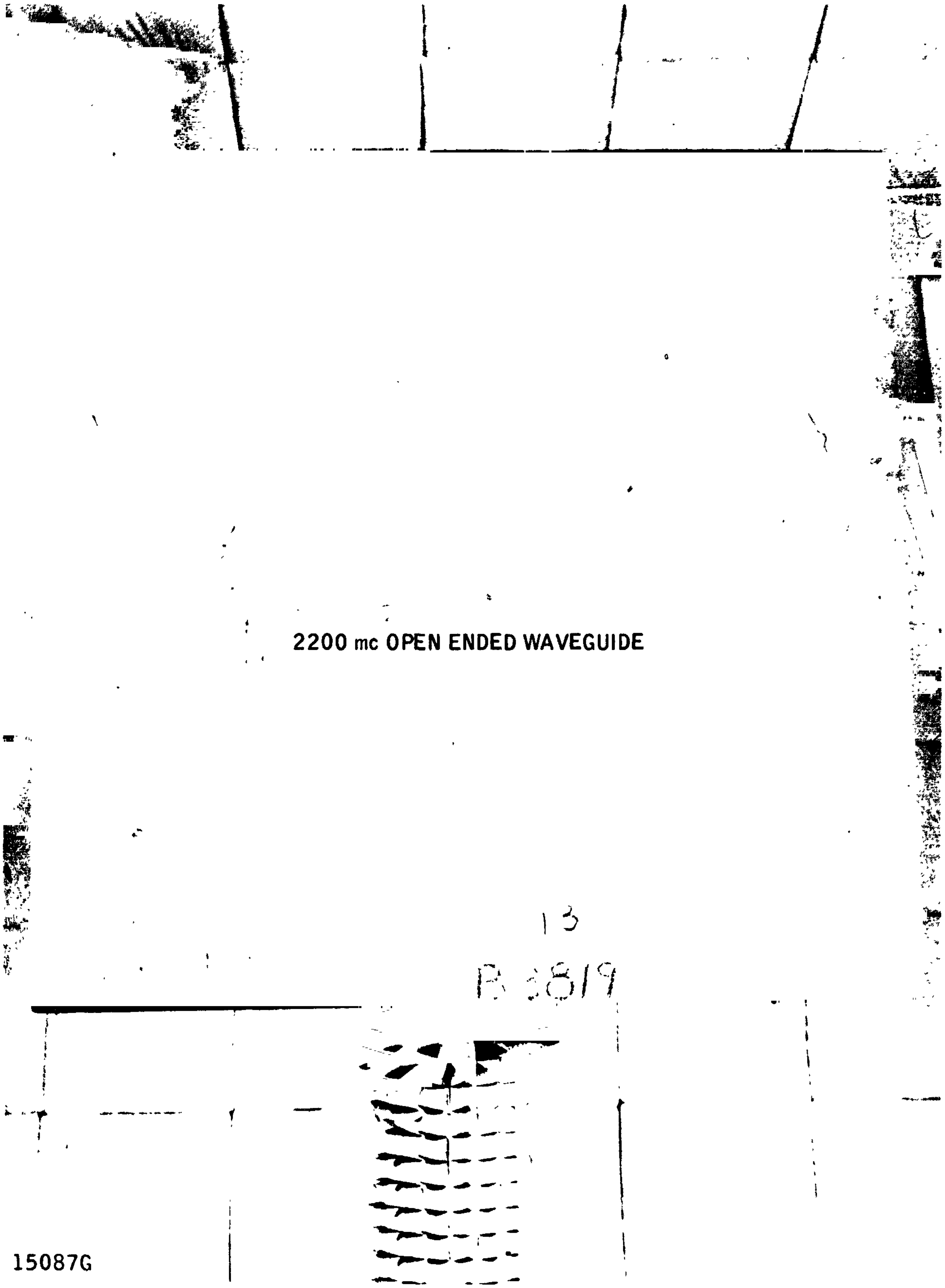

Figure 67 2200 MC MONOPOLE ANTENNA COVERED WITH VIRGIN HEAT-SHIELD SIMULATOR

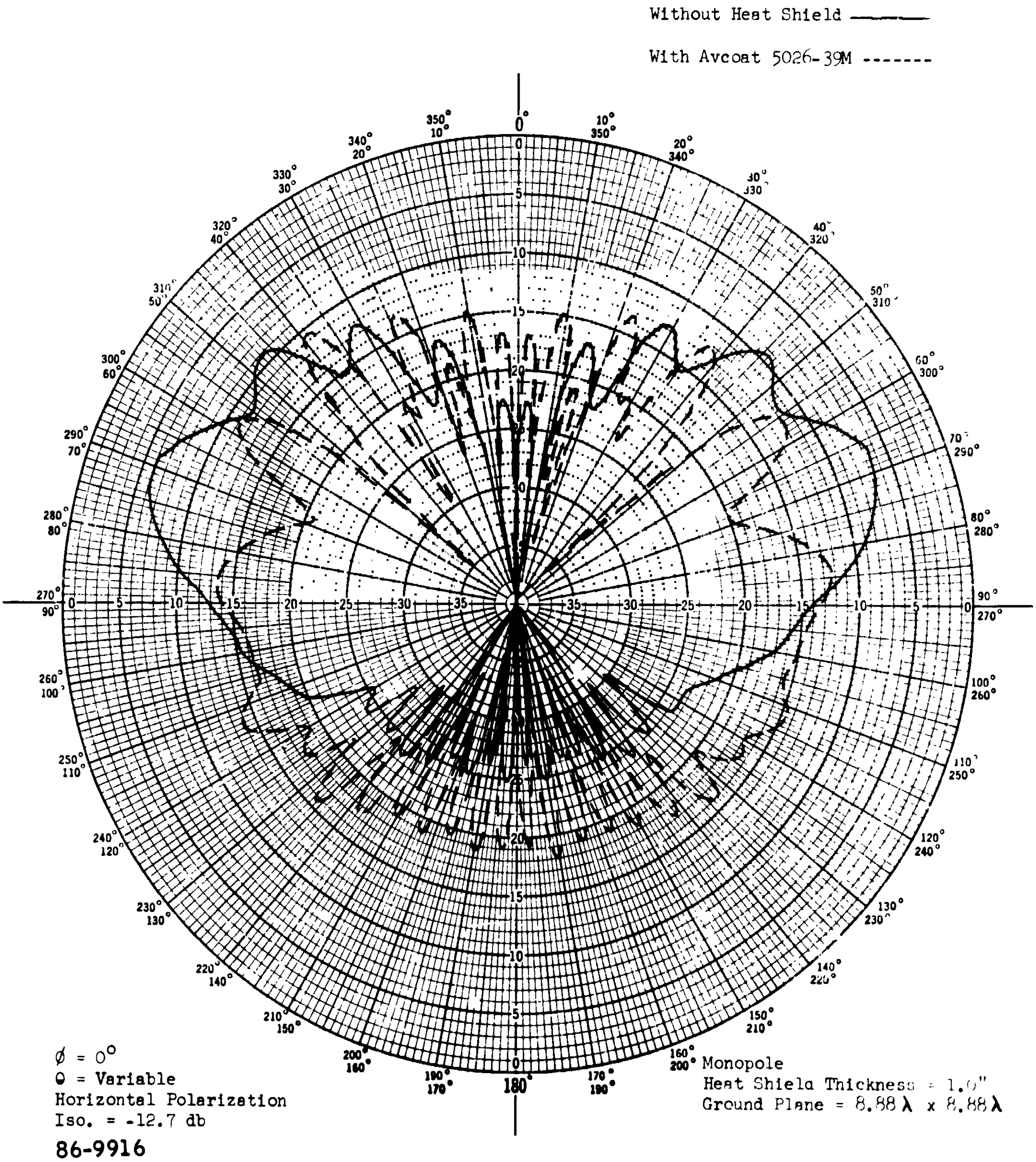

86-9916

Figure 68 2200 MC MONOPOLE, WITH AND WITHOUT AVCOAT 5026-39M

f = 2200 Mcs
With Avcoat 5026-39M ———

f = 6600 Mcs
With Third Scale Simulator ------

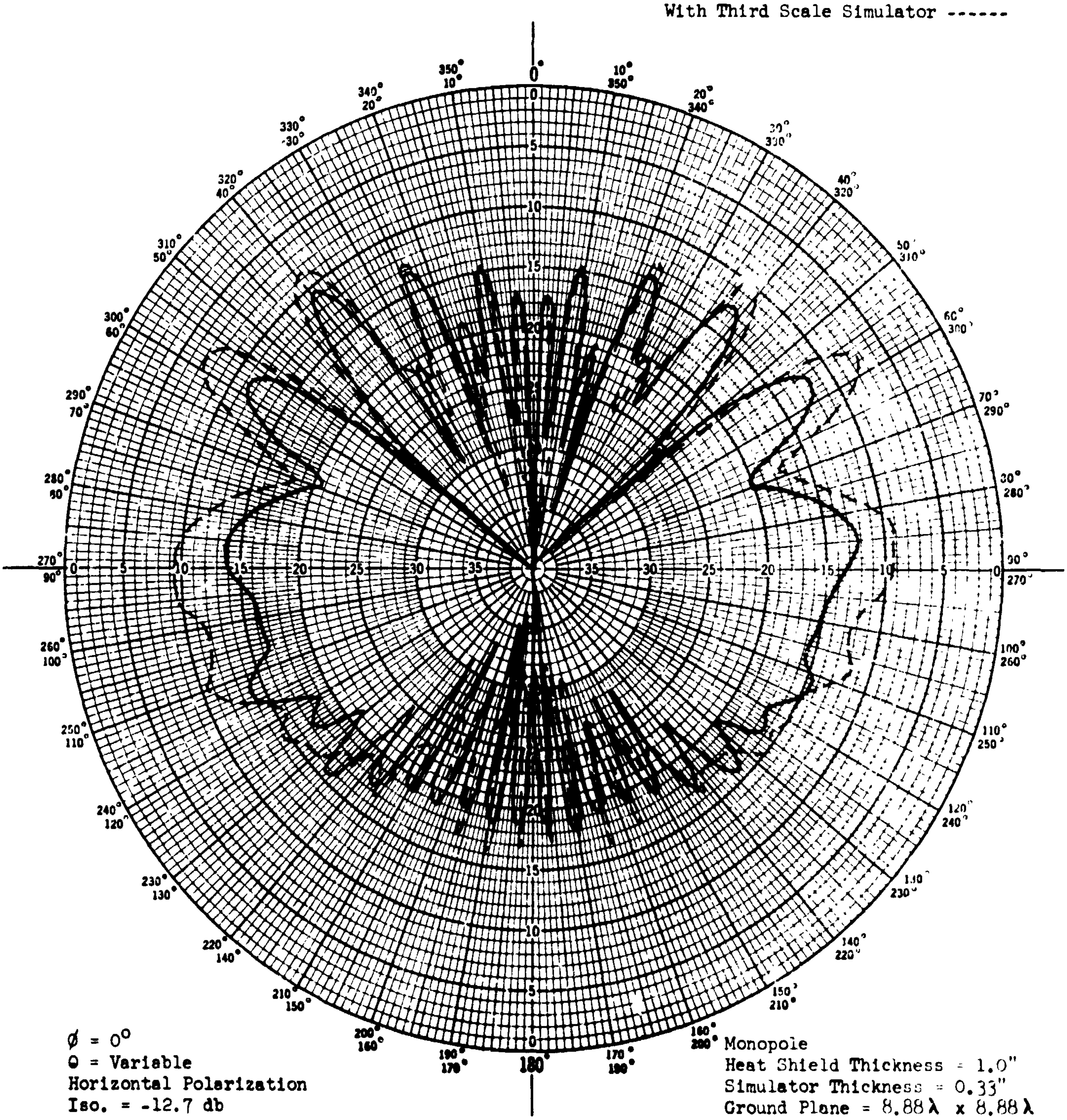

ϕ = 0°
θ = Variable
Horizontal Polarization
Iso. = -12.7 db

Monopole
Heat Shield Thickness = 1.0"
Simulator Thickness = 0.33"
Ground Plane = 8.88 λ x 8.88 λ

86-9918

Figure 70 2200 MC AND 6600 MC MONOPOLE ANTENNAS, COMPARISON BETWEEN AVCOAT 5026-39M AND THIRD-SCALE SIMULATION-POLARIZATION HORIZONTAL

With Avcoat 5026-39M ———

With Simulator -------

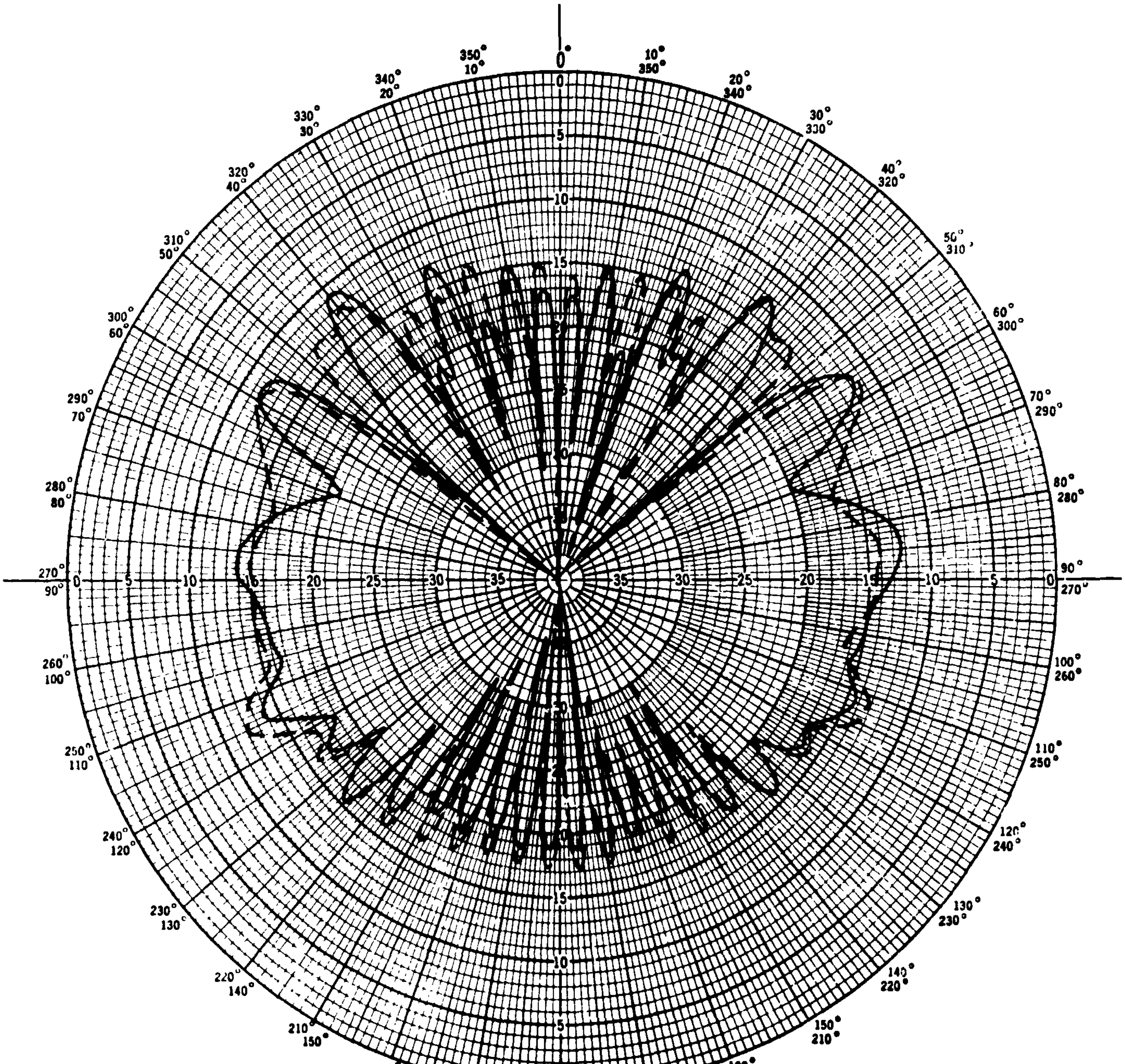

ϕ = 0°
Θ - Variable
Horizontal Polarization
Iso. - -12.7 db

86-9917

Monopole
Heat Shield Thickness = 1.0"
Simulator Thickness = 1.0"
Ground Plane = 8.88λ x 8.88λ

Figure 69 2200 MC MONOPOLE, COMPARISON BETWEEN AVCOAT 5026-39M AND SIMULATOR

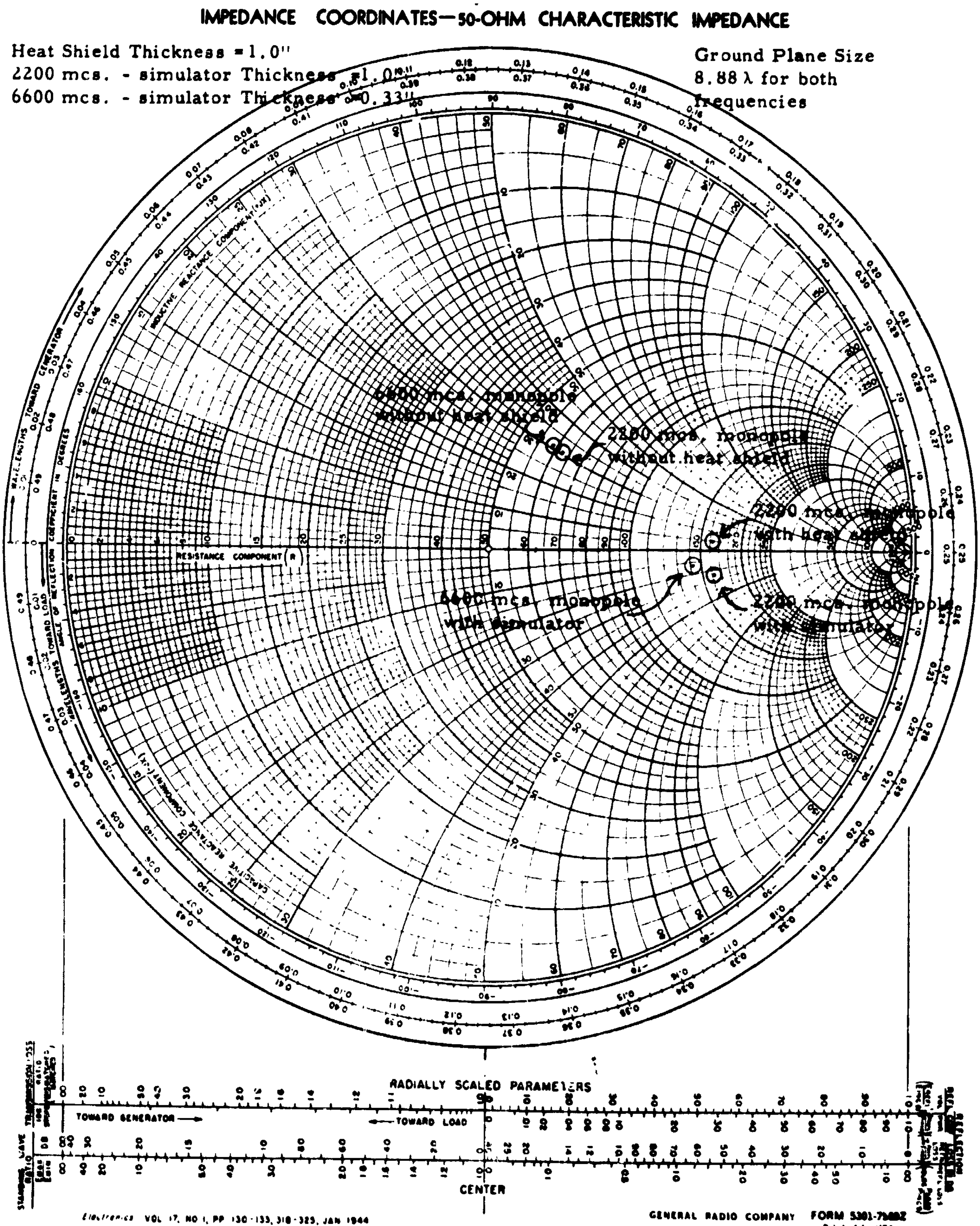

86-9919

Figure 71 IMPEDANCE OF 2200 MC AND 6600 MC MONOPOLE

TABLE IV

VERIFICATION TESTS - MONOPOLE

Experiment	Antenna Cover	Frequency (Mc)	Scale Factor	Efficiency (percent)	Measured 5026-39 Patterns versus Simulator Patterns		Measured 5026-39 Impedance versus Simulator Impedance
					Experiment No.	Figure No.	
1	no cover	2200	1	88.81		68	Figure 71
2	virgin 5026-39	2200	1	64.56	1 with 2	69	Figure 71
3	virgin simulator	2200	1		2 with 3	69	Figure 71
4	virgin simulator	6600	1/3		2 with 4	70	Figure 71

The impedance data showed good correlation. The impedance of the 6600 Mc monopole without simulator was matched to the 2200 Mc monopole without heat shield prior to measuring the 6600 Mc monopole with its simulator.

c. Scimitar and Scimitar-Slot, Full- and 1/3-Scale Model Patterns and Impedance

Verification tests made with the scimitar and scimitar-slot antennas are presented in matrix form in Tables V and VI. The matrix references a series of figures which are reprints of measured data. Related patterns have been superimposed to enable the reader to compare them readily.

The scimitar antenna entails two antennas in one, the scimitar and scimitar slot. The full-scale scimitar was tested at 300 Mc while its associated slot was tested at 2200 Mc. The scaled frequencies were 900 Mc and 6600 Mc.

The spherical coordinate system used for the scimitar and scimitar-slot antenna patterns is defined in Figure 72.

Antenna-efficiency calculations were made using the same method described in Subsection D.3.a. Efficiency calculations were made on both the scimitar and scimitar-slot antennas with and without heat shield.

The simulator patterns showed good correlation with Avcoat 5026-39 patterns except for the vertical-polarization pattern of the scimitar slot. Impedance data compared favorably at the full-scale frequencies but not at the scaled frequencies.

d. Simulation Errors

Table VII is concerned with deviations in scaled and full-scale simulator patterns from the Avcoat 5026-39M patterns at four points in the forward beam. One column gives maximum deviation between simulator and heat shield, excluding null areas. Another column gives deviations at the point of maximum radiation on the pattern to be simulated. The remaining two columns show errors in null areas if any nulls exist in the forward beam. Deviations in null areas are large; however, the percentage error is relative to power. As an example, consider the E-plane pattern of the 6600 Mc open-ended-waveguide antenna with virgin heat shield. At $\theta = 70$ degrees, the deviation is 14.0db. The level of the simulator is -13.8db below the isotropic level while the heat shield is -27.8db below the isotropic level.

TABLE V

VERIFICATION TESTS - SCIMITAR

Experiment No.	Antenna Cover	Frequency (Mc)	Scale Factor	Efficiency (percent)	Measured 5026-39 Patterns versus Simulator Patterns		Measured 5026-39 Impedance versus Simulator Impedance
					Experiment No.	Figure No.	
1	no cover	300	1	87.13		75, 76	Figure 87
2	virgin 5026-39	300	1	69.55	1 with 2	75, 76	Figure 87
3	virgin simulator	300	1		2 with 3	77, 78	Figure 87
4	virgin simulator	900	1/3		2 with 4	79, 80	Figure 87

TABLE VI

VERIFICATION TESTS - SCIMITAR SLOT

Experiment No.	Antenna Cover	Frequency (Mc)	Scale Factor	Efficiency (percent)	Measured 5026-39 Patterns versus Simulator Patterns		Measured 5026-39 Impedance versus Simulator Impedance
					Experiment No.	Figure No.	
1	no cover	2200	1	73.69		81, 82	Figure 88
2	virgin 5026-39	2200	1	65.13	1 with 2	81, 82	Figure 88
3	virgin simulator	2200	1		2 with 3	83, 84	Figure 88
4	virgin simulator	6600	1/3		2 with 4	85, 86	Figure 88

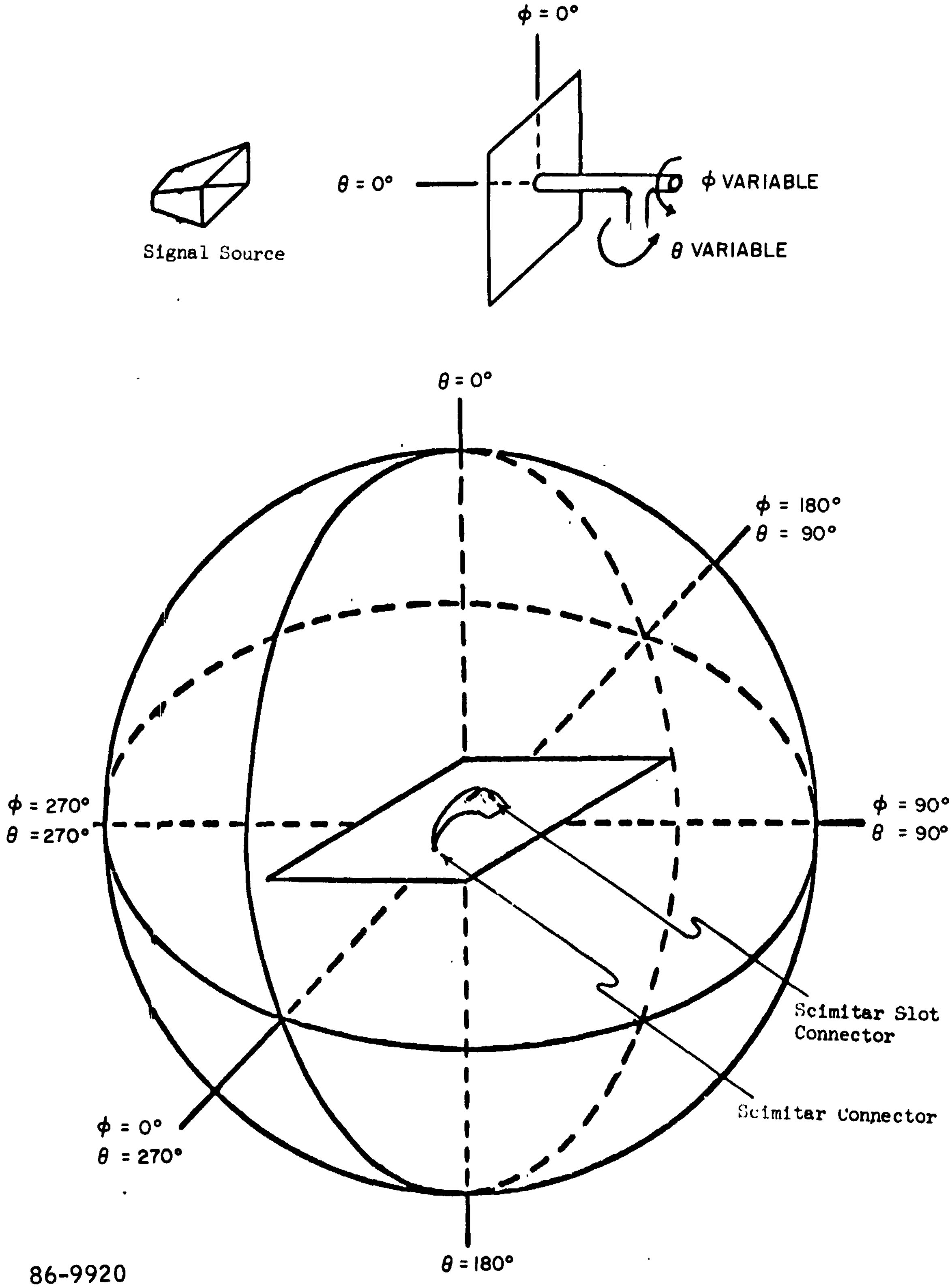

86-9920

Figure 72 SPHERICAL COORDINATE SYSTEM FOR SCIMITAR AND SCIMITAR SLOT

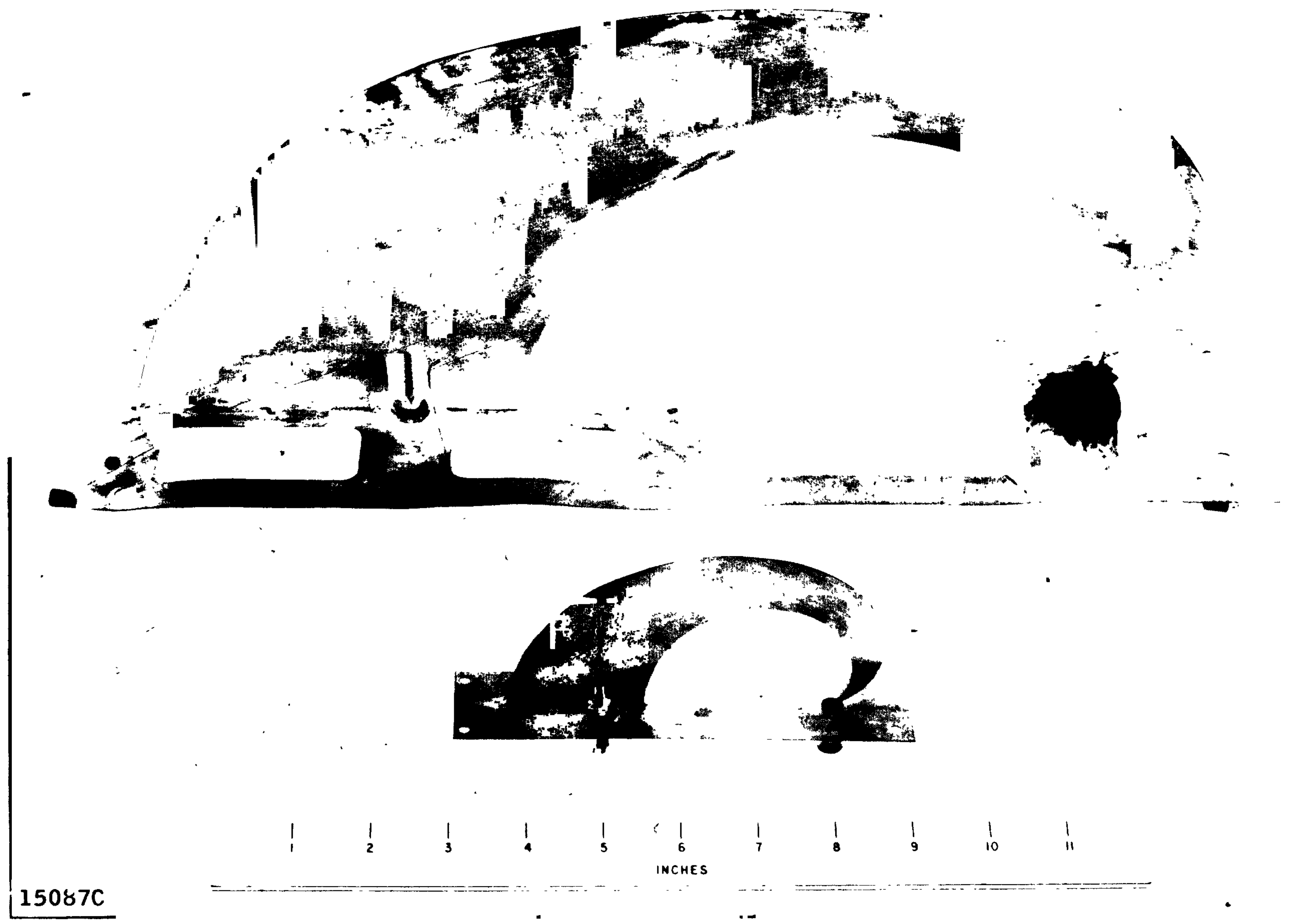

Figure 73 FULL-SCALE AND THIRD-SCALE SCIMITAR AND SCIMITAR-SLOT ANTENNAS

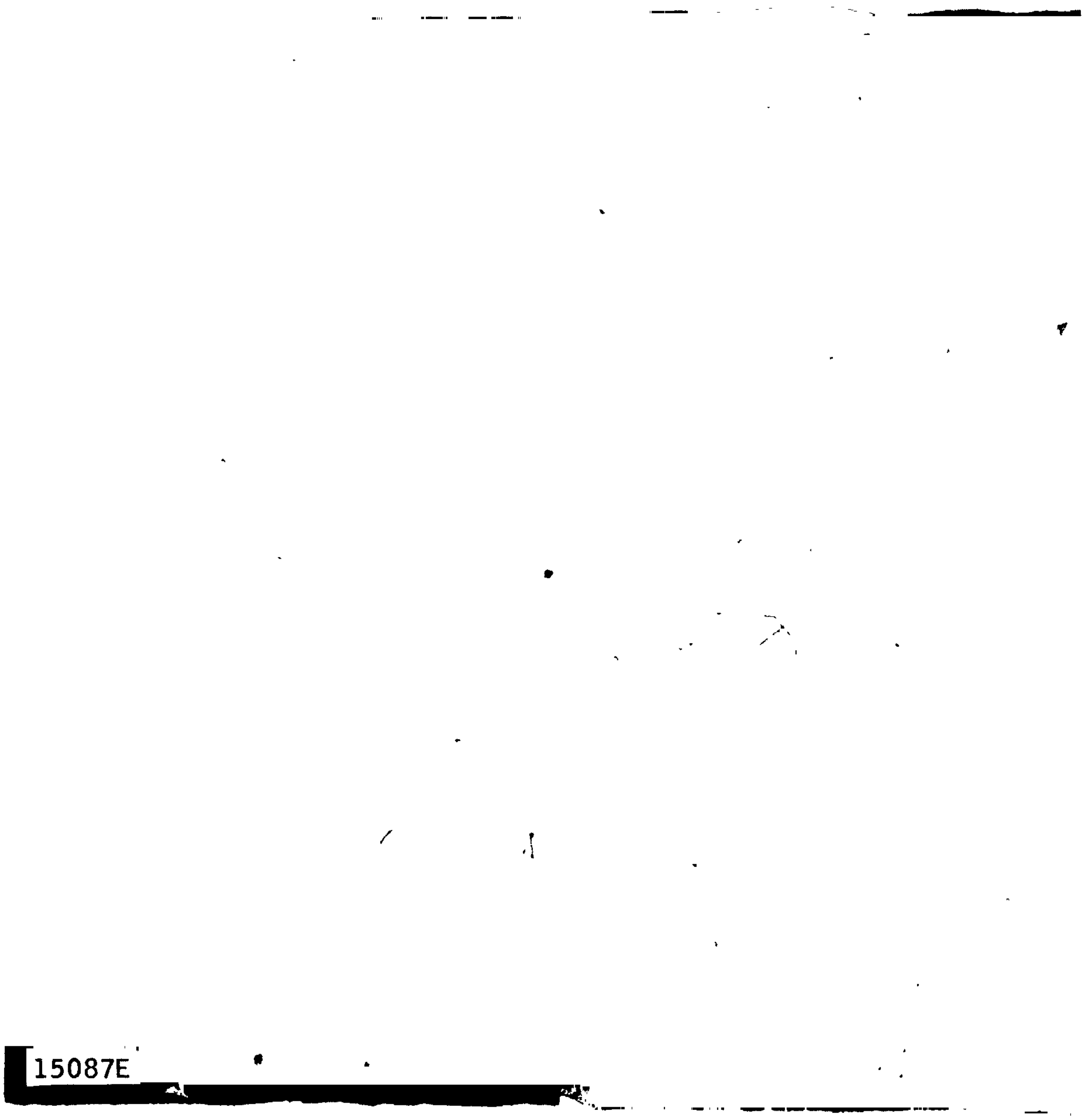

Figure 74 FULL-SCALE SCIMITAR ANTENNA COVERED WITH VIRGIN HEAT-SHIELD SIMULATOR

With Avcoat 5026-39M ———

Without Heat Shield -------

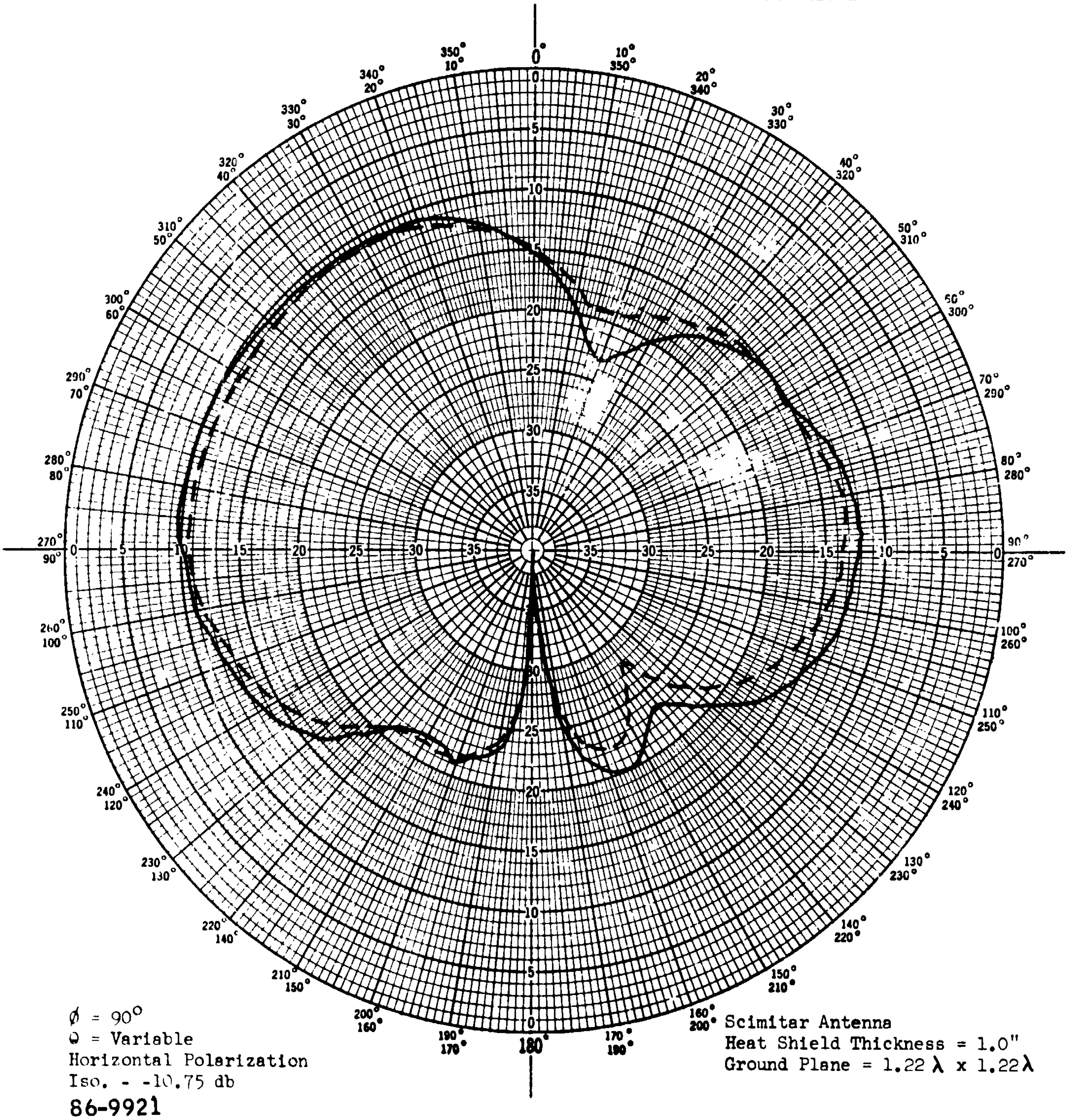

ø = 90°
θ = Variable
Horizontal Polarization
Iso. - -10.75 db

86-9921

Scimitar Antenna
Heat Shield Thickness = 1.0"
Ground Plane = 1.22 λ x 1.22 λ

Figure 75 300 MC SCIMITAR ANTENNA, WITH AND WITHOUT AVCOAT 5025-39M-POLARIZATION HORIZONTAL

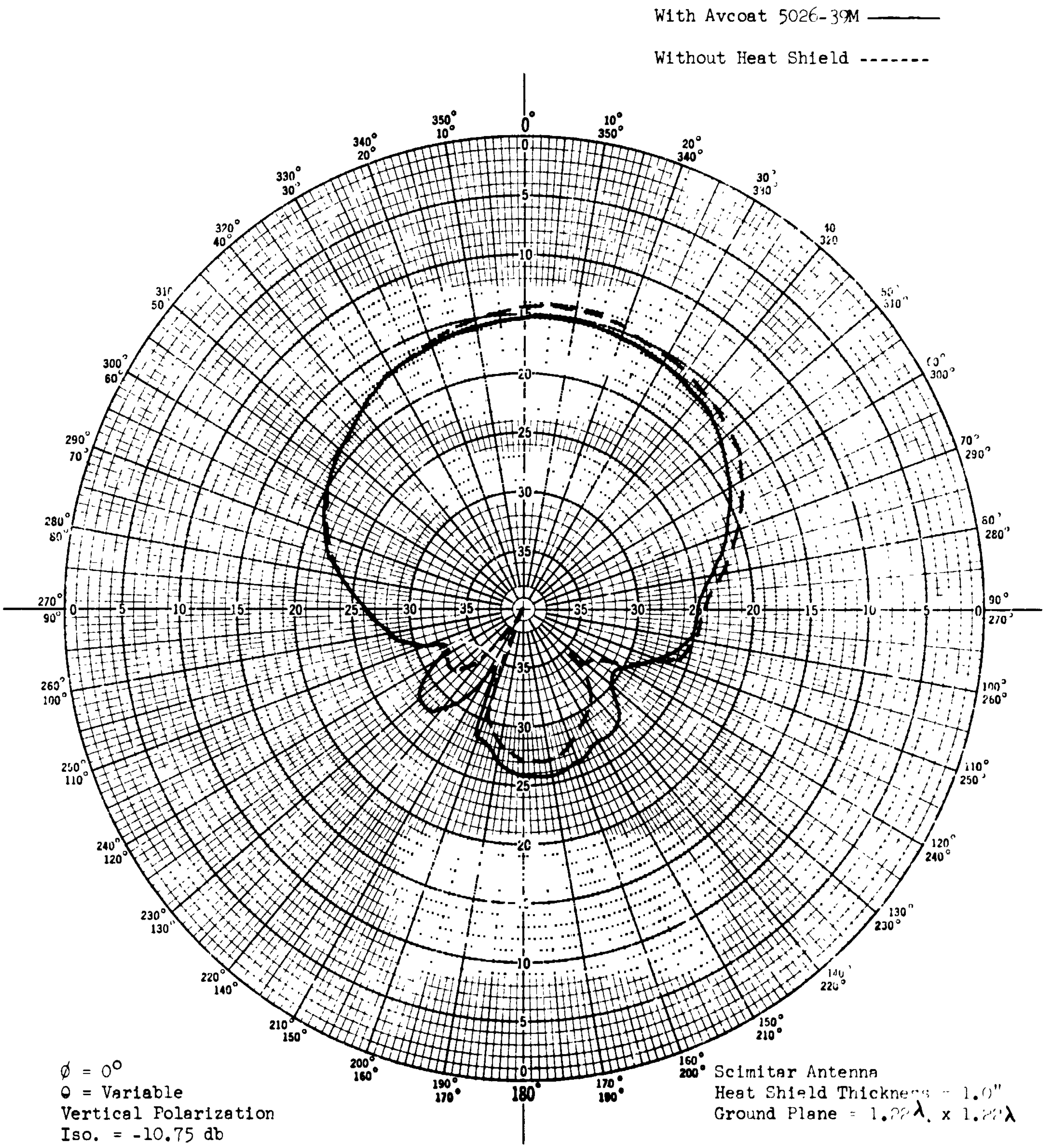

86-9922

Figure 76 300 MC SCIMITAR ANTENNA, WITH AND WITHOUT AVCOAT 5026-39M-POLARIZATION VERTICAL

With Avcoat 5026-39M ————

With Simulator -------

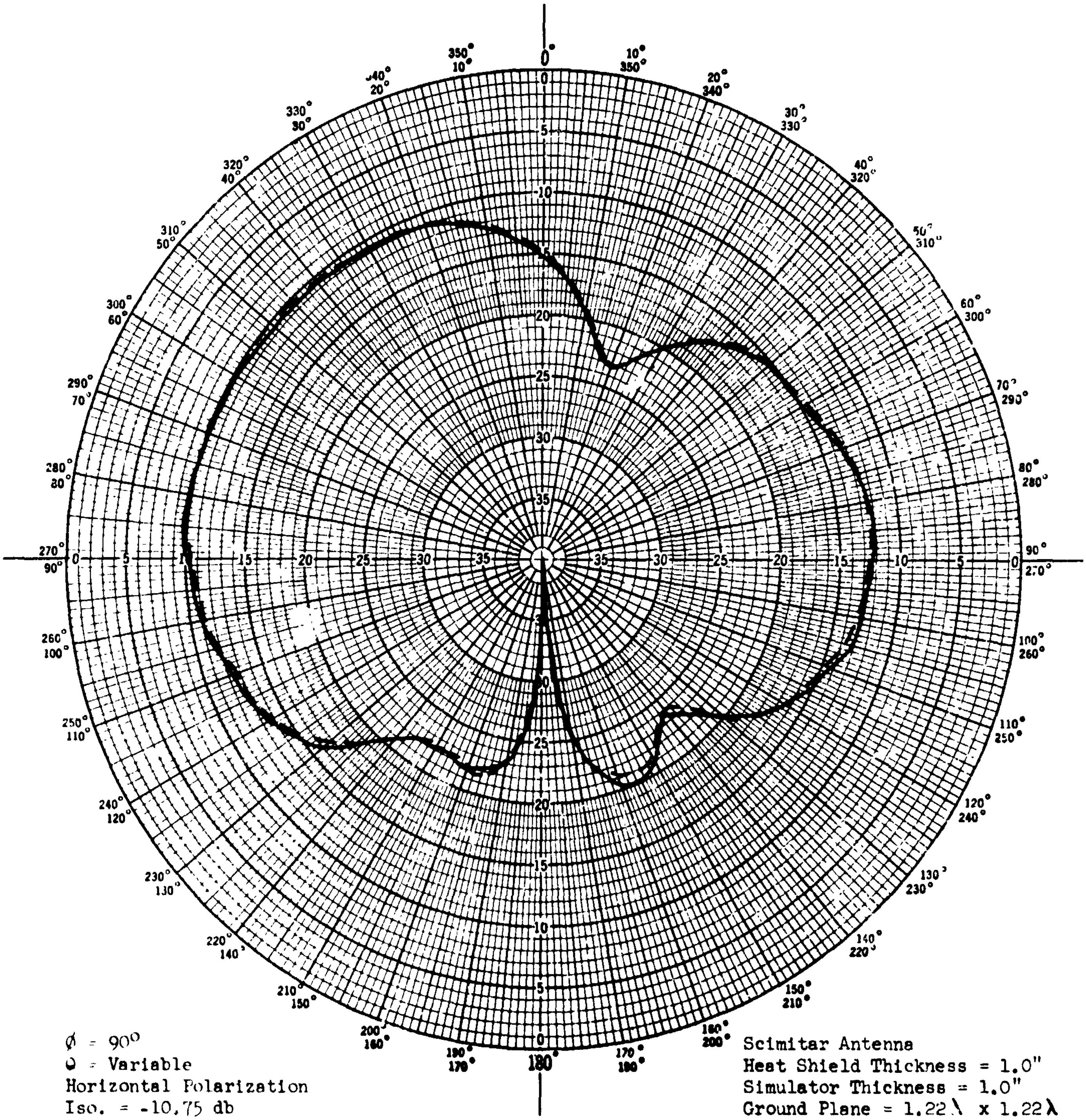

ϕ = 90°
θ = Variable
Horizontal Polarization
Iso. = -10.75 db

Scimitar Antenna
Heat Shield Thickness = 1.0"
Simulator Thickness = 1.0"
Ground Plane = 1.22λ x 1.22λ

86-9923

Figure 77 300 MC SCIMITAR ANTENNA, COMPARISON BETWEEN AVCOAT 5026-39M AND SIMULATOR-POLARIZATION HORIZONTAL

With Avcoat 5026-39M ————

With Simulator --------

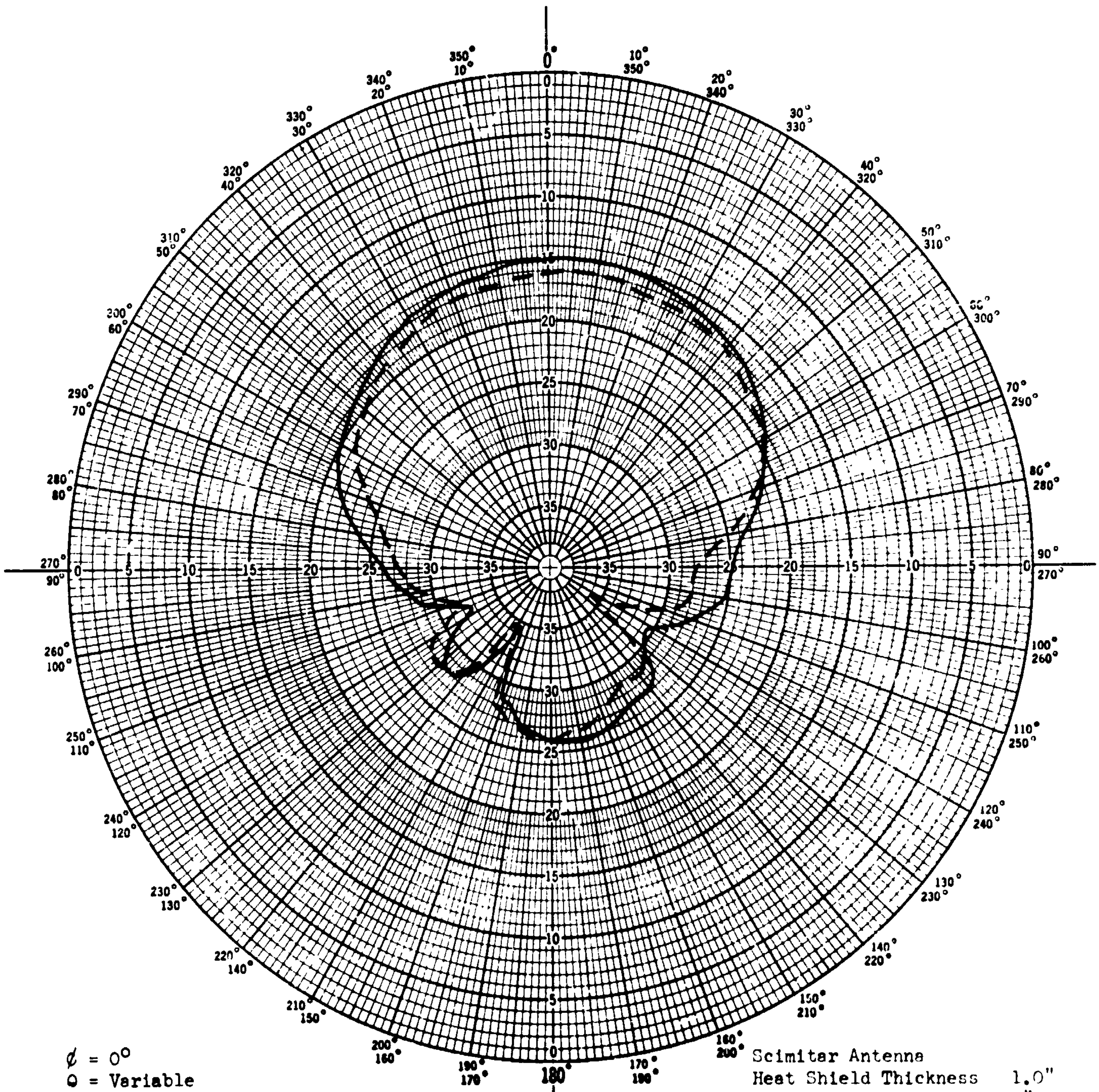

ϕ = 0°
θ = Variable
Vertical Polarization
Iso. = -10.75 db

Scimitar Antenna
Heat Shield Thickness 1.0"
Simulator Thickness - 1.0"
Ground Plane = 1.22λ x 1.22λ

86-9924

Figure 78 300 MC SCIMITAR ANTENNA, COMPARISON BETWEEN AVCOAT 5026-39M AND SIMULATOR-POLARIZATION VERTICAL

f = 300 Mcs
With Avcoat 5026-39M ———

f = 900 Mcs
With 1/3 Scale Simulator ------

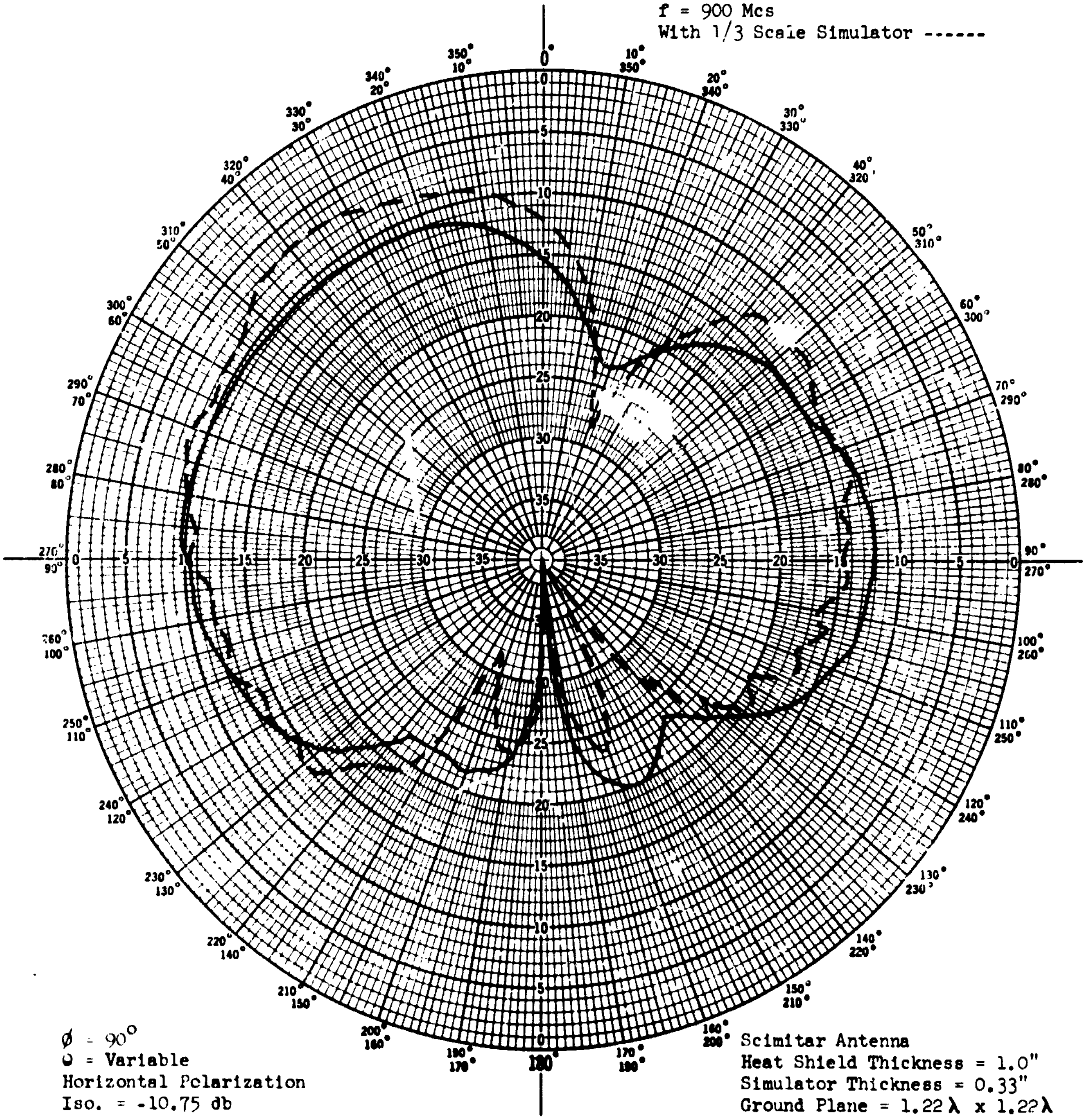

ϕ = 90°
θ = Variable
Horizontal Polarization
Iso. = -10.75 db

Scimitar Antenna
Heat Shield Thickness = 1.0"
Simulator Thickness = 0.33"
Ground Plane = 1.22 λ x 1.22 λ

86-9925

Figure 79 300 MC AND 900 MC SCIMITAR ANTENNAS, COMPARISON BETWEEN AVOCAT 5026-39M AND THIRD-SCALE SIMULATION-POLARIZATION HORIZONTAL

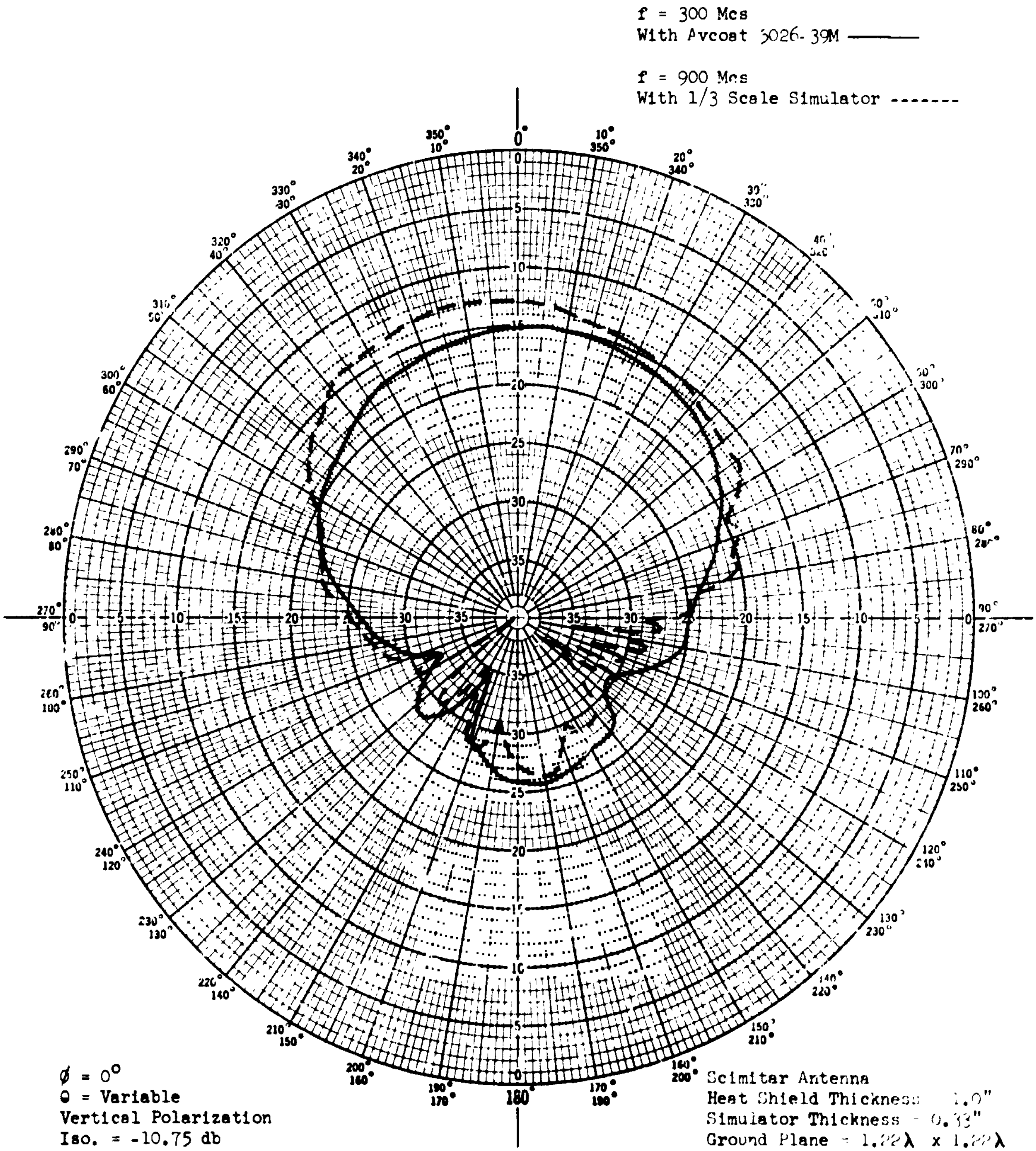

86-9926

Figure 80 300 MC AND 900 MC SCIMITAR ANTENNAS, COMPARISON BETWEEN AVCOAT 5026-39M AND THIRD-SCALE SIMULATION-POLARIZATION VERTICAL

With Avcoat 5026-39M ———

Without Heat Shield ---------

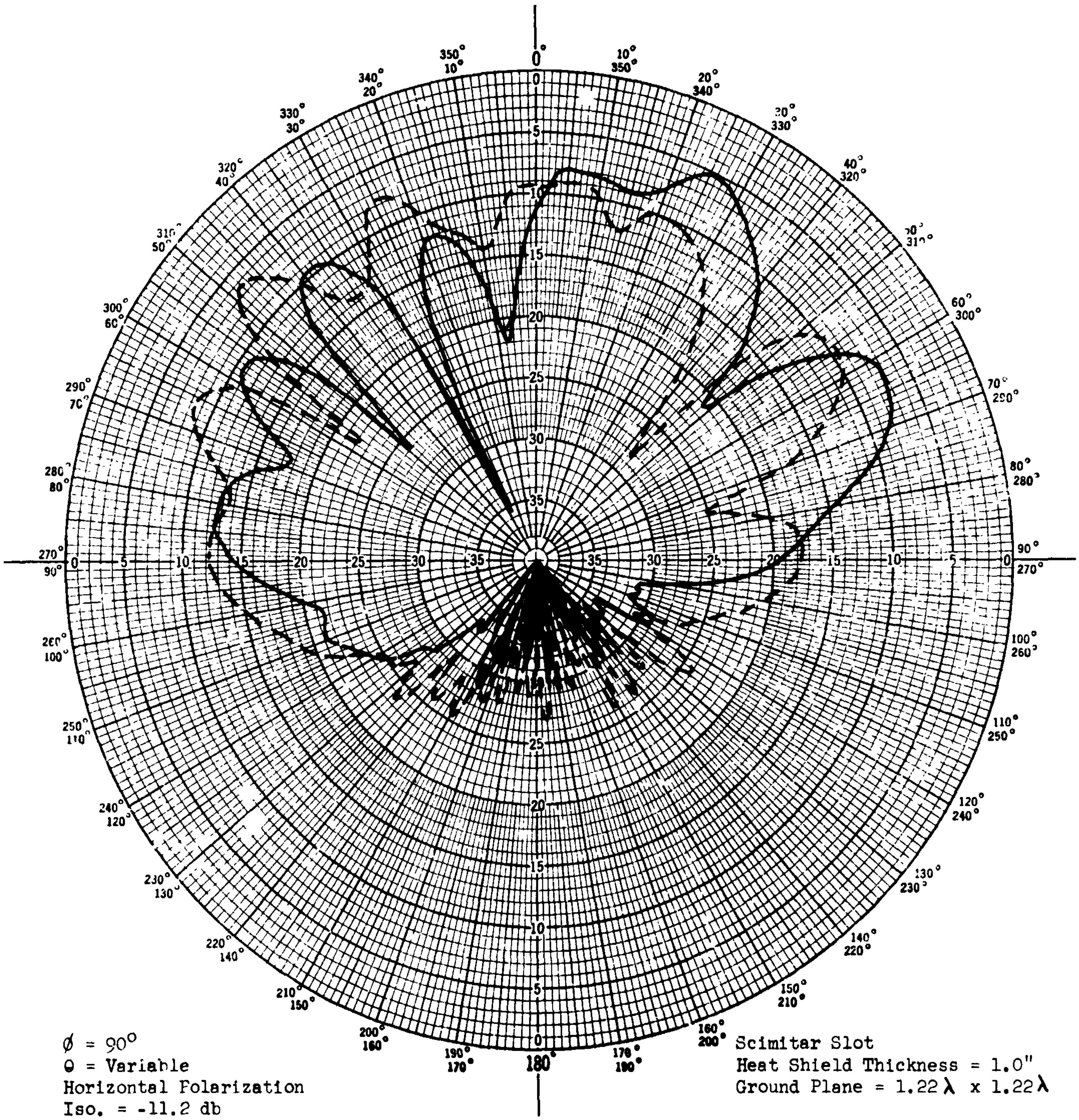

ϕ = 90°
Θ = Variable
Horizontal Polarization
Iso. = -11.2 db

Scimitar Slot
Heat Shield Thickness = 1.0"
Ground Plane = 1.22 λ x 1.22 λ

86-9927

Figure 81 2200 MC SCIMITAR-SLOT ANTENNA, WITH AND WITHOUT AVCOAT 5026-39M- POLARIZATION HORIZONTAL

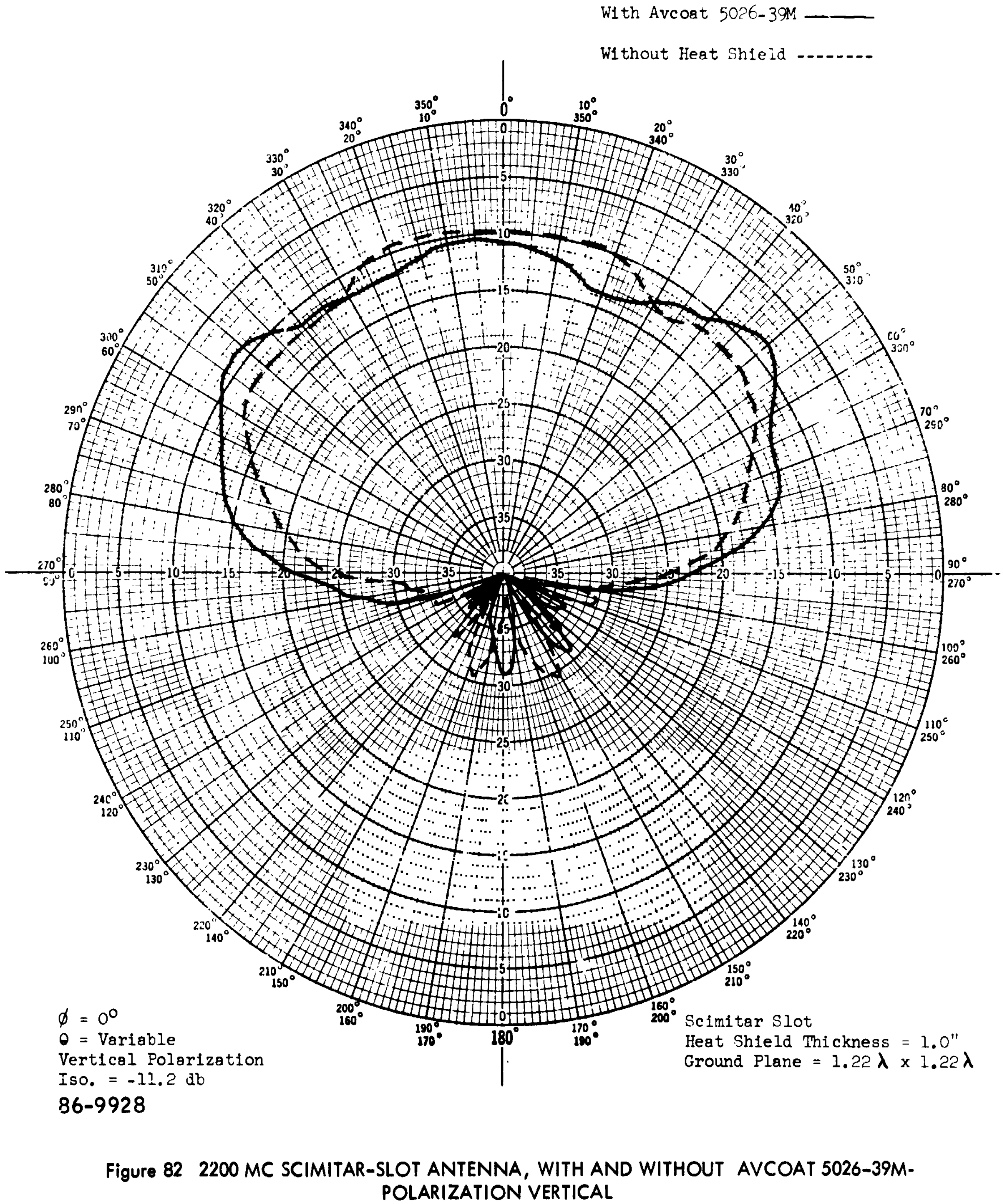

Figure 82 2200 MC SCIMITAR-SLOT ANTENNA, WITH AND WITHOUT AVCOAT 5026-39M-POLARIZATION VERTICAL

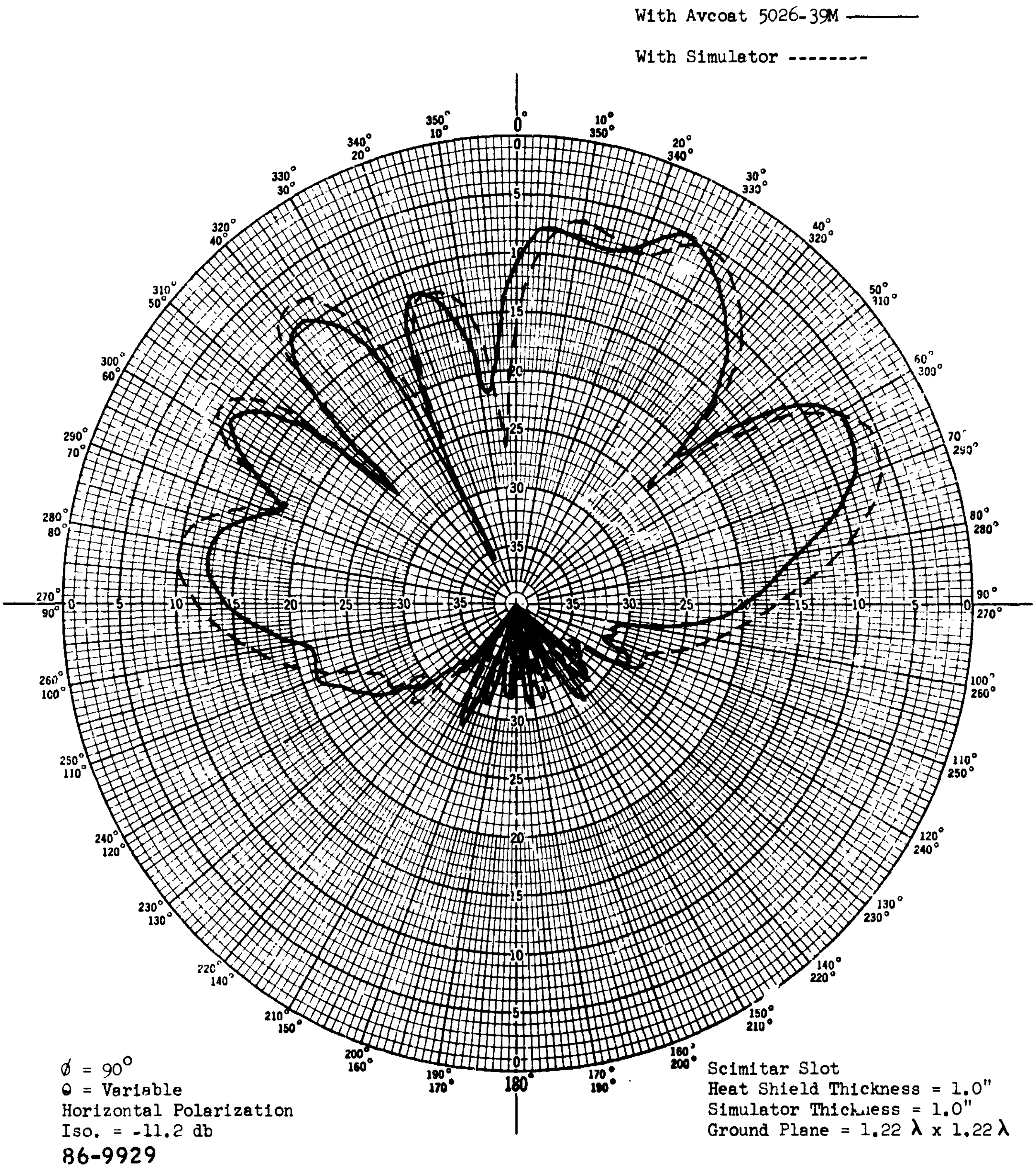

Figure 83 2200 MC SCIMITAR-SLOT ANTENNA, COMPARISON BETWEEN AVCOAT 5026-39M AND SIMULATOR-POLARIZATION HORIZONTAL

With Avcoat 5026-39M ———

With Simulator -------

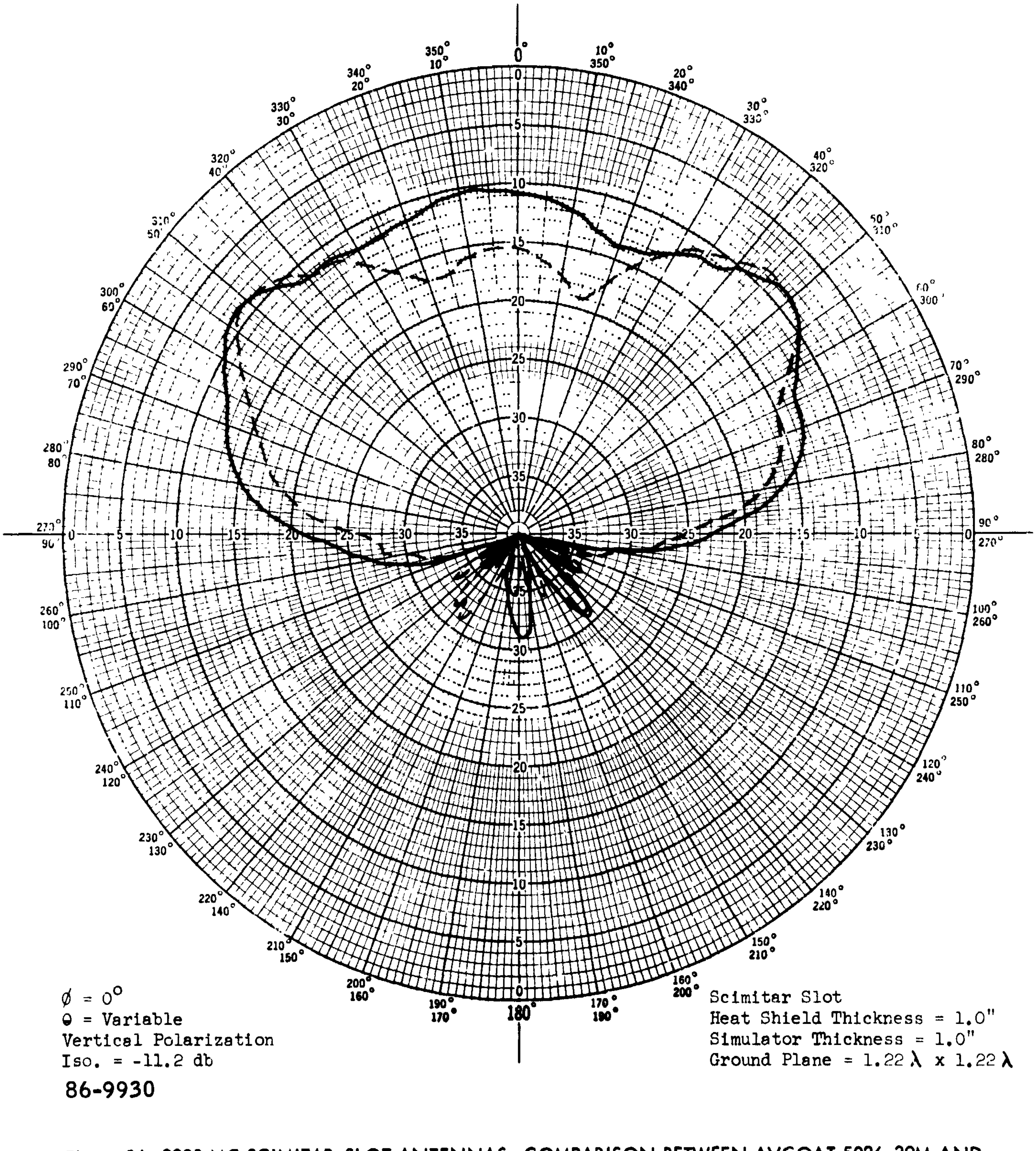

ϕ = 0°
Θ = Variable
Vertical Polarization
Iso. = -11.2 db

Scimitar Slot
Heat Shield Thickness = 1.0"
Simulator Thickness = 1.0"
Ground Plane = 1.22 λ x 1.22 λ

86-9930

Figure 84 2200 MC SCIMITAR-SLOT ANTENNAS, COMPARISON BETWEEN AVCOAT 5026-39M AND SIMULATOR-POLARIZATION VERTICAL

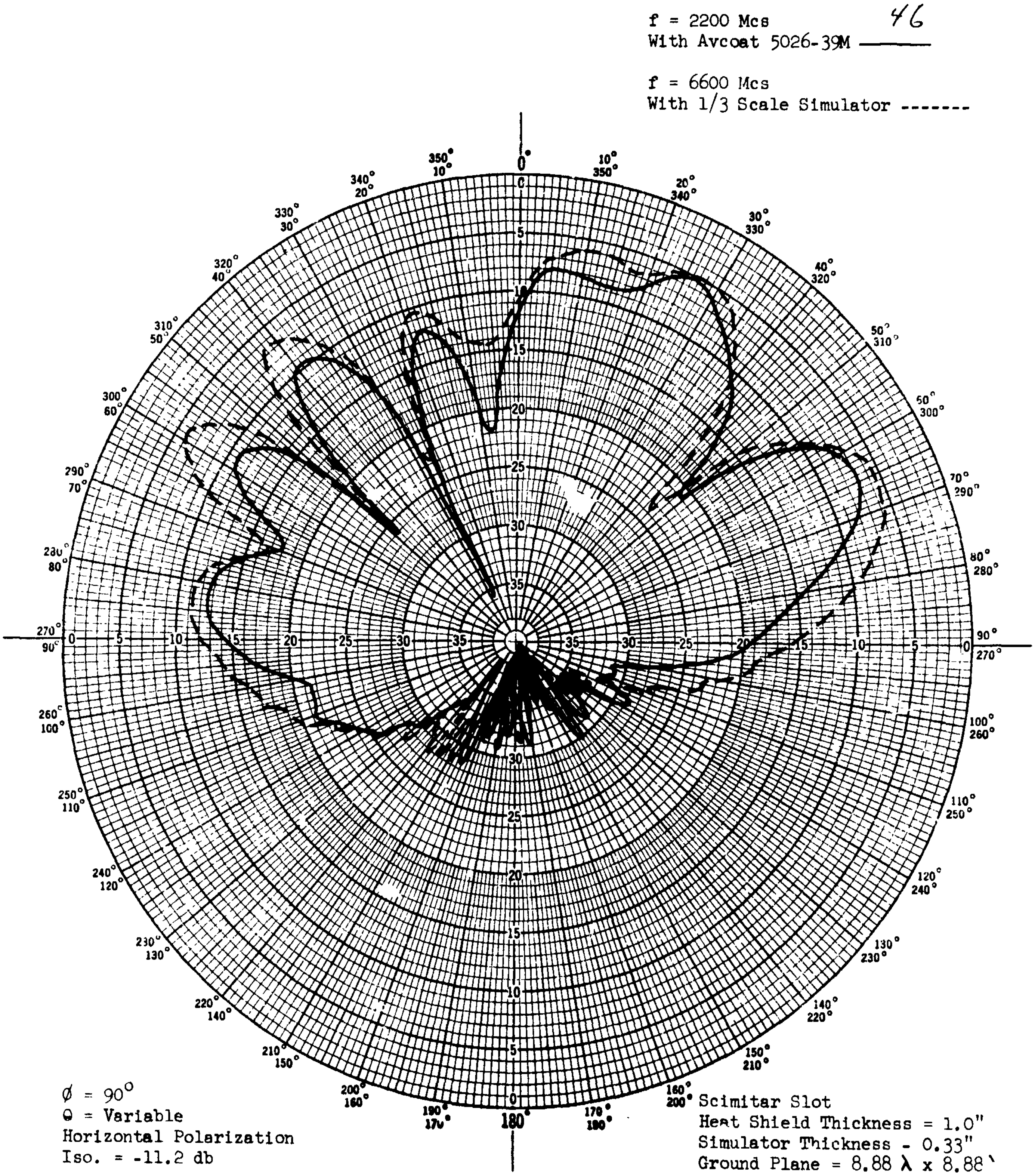

86-9931

Figure 85 2200 MC AND 6600 MC SCIMITAR-SLOT ANTENNAS, COMPARISON BETWEEN AVCOAT 5026-39M AND THIRD-SCALE SIMULATION-POLARIZATION HORIZONTAL

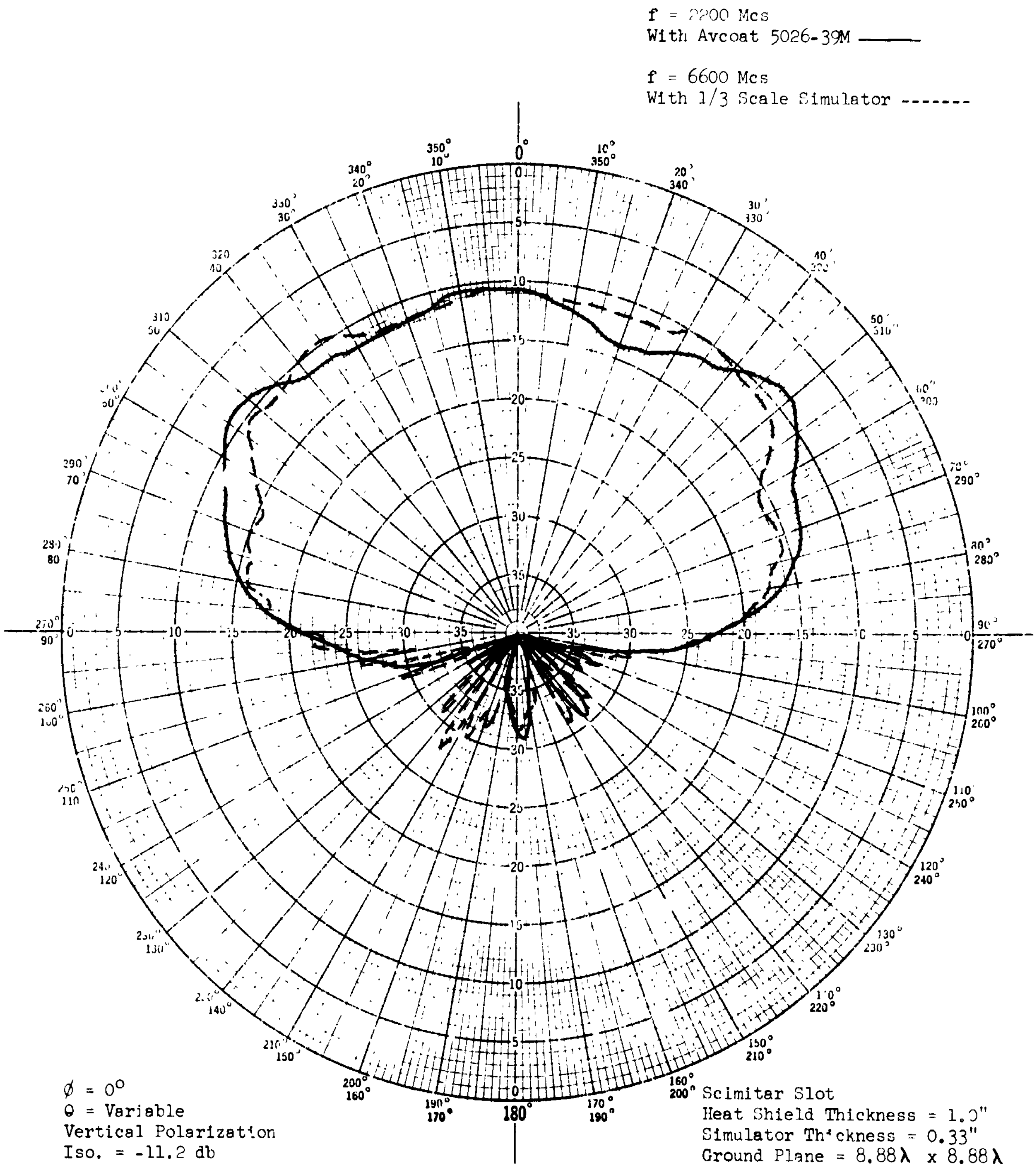

86-9932

Figure 86 2200 MC AND 6600 MC SCIMITAR-SLOT ANTENNAS, COMPARISON BETWEEN AVCOAT 5026-39M AND THIRD-SCALE SIMULATION-POLARIZATION VERTICAL

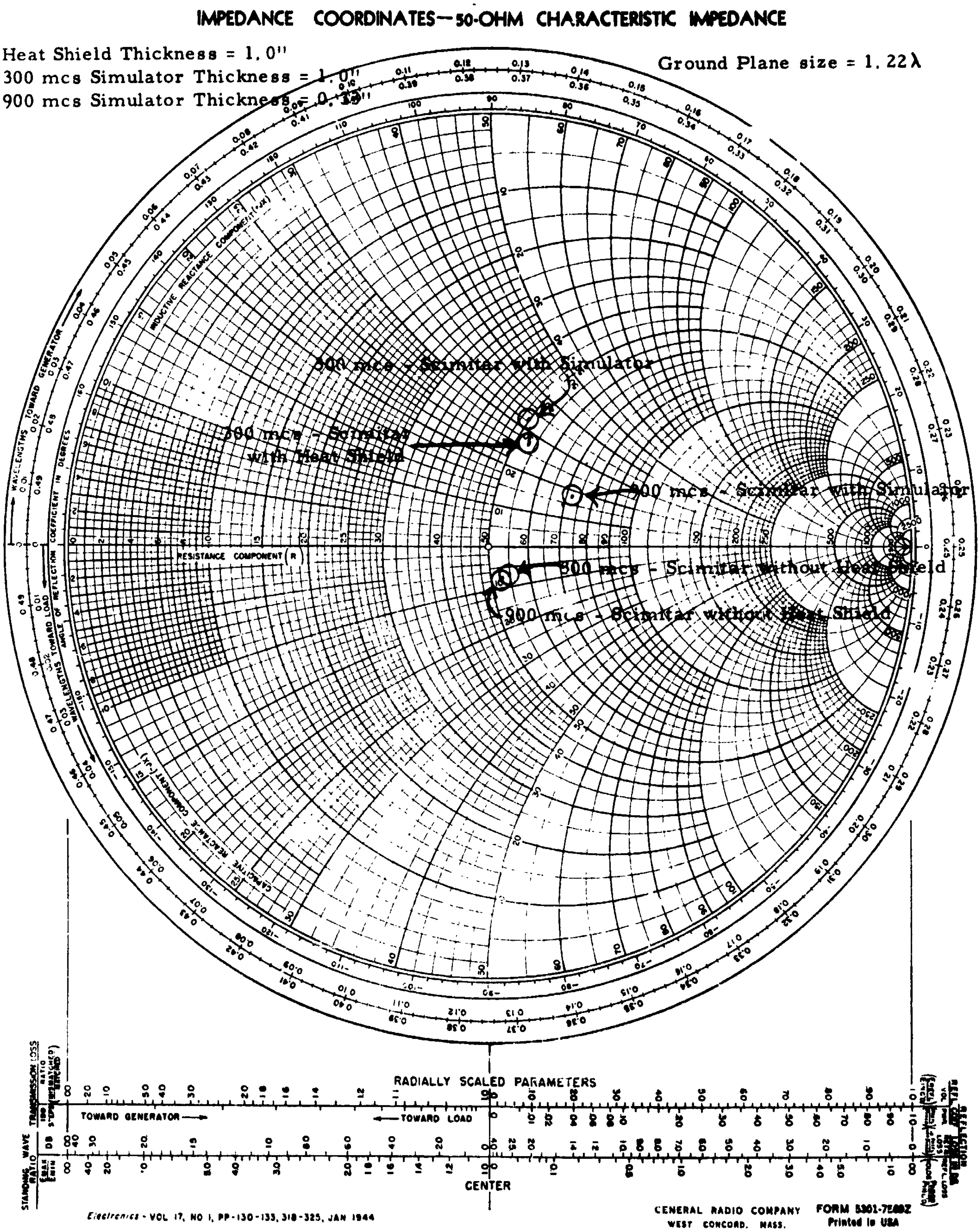

86-9933

Figure 87 300 MC AND 900 MC SCIMITAR

IMPEDANCE COORDINATES—50-OHM CHARACTERISTIC IMPEDANCE

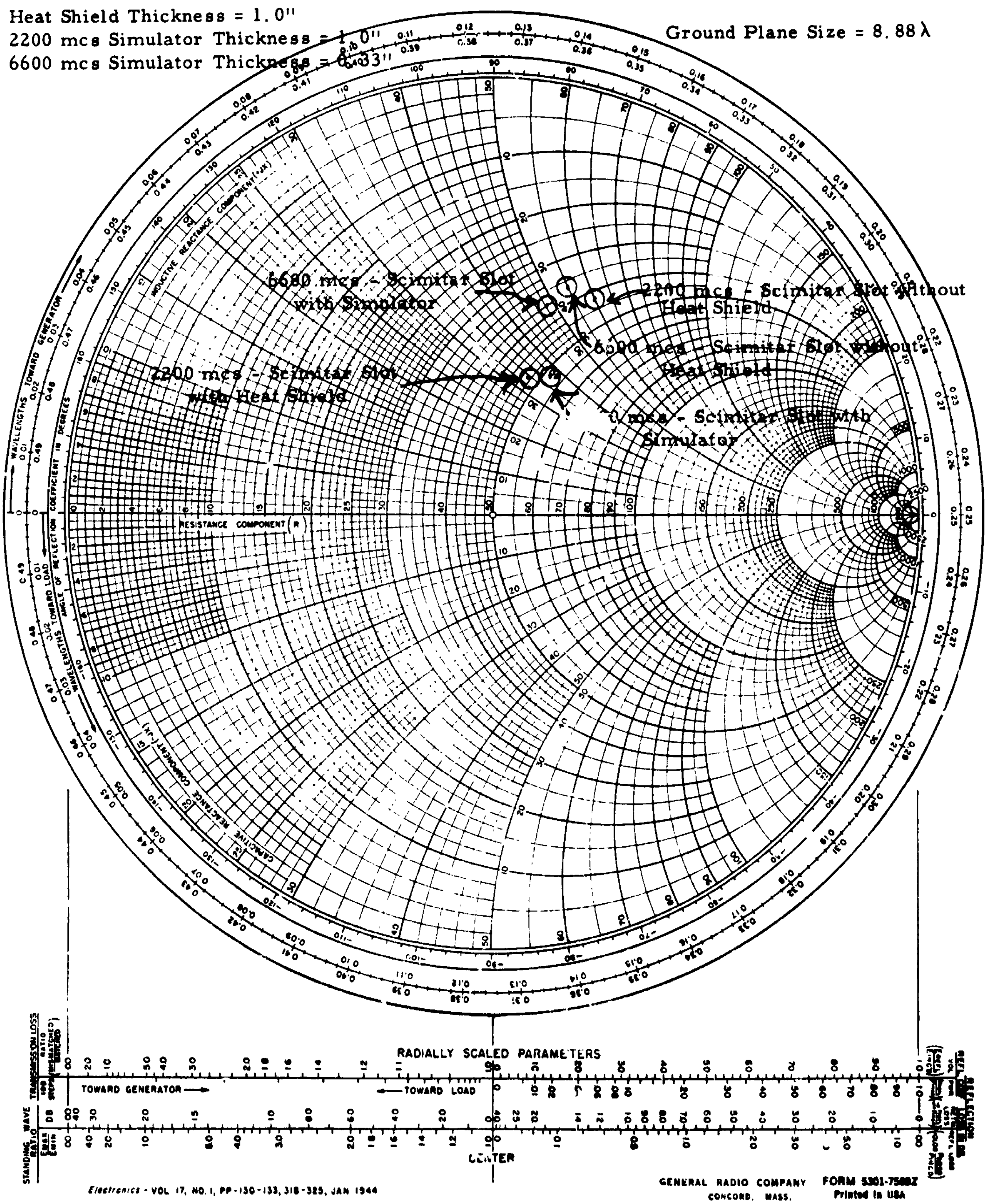

86-9934 Figure 88 2200 MC AND 6600 MC SCIMITAR SLOT

The pattern peak is +5.5db above isotropic. The percentage error with reference to maximum power radiated is

$$\text{Percentage Error} = \frac{0.04169 - 0.00166}{1.884} \times 100 \text{ percent} \quad 2.13 \text{ percent}$$

In other null areas, the percentage error may be considered small although the decibel deviation is large. For sharp nulls, high deviations are partially attributable to small angular-measurement errors.

The chart shows a trend of increasing deviations as the scale factor is reduced.

TABLE VII

DECIBEL DEVIATION BETWEEN AVCOAT 5026-39M AND SIMULATOR IN MAIN BEAM (θ = 270 to 90 Degrees)

Antenna and Heat-Shield State	Frequency (Mc)	Polarization or Plane of Radiation (db)	Maximum Deviation Excluding Nulls (db)	Deviation at Pattern Peak (db)	Null Deviations (db)	Null Deviations (db)
Open-ended waveguide, virgin H/S	300	E	θ = 315° 0.4	θ = 315° 0.4		
Open-ended waveguide, virgin H/S	300	H	θ = 55° 0.3	θ = 0° 0.1		
Open-ended waveguide, virgin H/S	900	E	θ = 285° 1.0	θ = 315° 0.2		
Open-ended waveguide, virgin H/S	900	H	θ = 300° 2.1	θ = 0° 0.0		
Open-ended waveguide, virgin H/S	1500	E	θ = 270° 2.6	θ = 315° 1.0		
Open-ended waveguide, virgin H/S	1500	H	θ = 270° 2.3	θ = 0° 0.0		
Open-ended waveguide, virgin H/S	2200	E	θ = 60° 1.7	θ = 0° 0.4	θ = 70° 8.8	θ = 288° 5.0
Open-ended waveguide, virgin H/S	2200	H	θ = 300° 0.7	θ = 0° 0.5	θ = 48° 1.7	θ = 310° 1.6
Open-ended waveguide, virgin H/S	6600	E	θ = 54° 1.4	θ = 0° 0.5	θ = 70° 14.0	θ = 288° 11.2
Open-ended waveguide, virgin H/S	6600	H	θ = 300° 2.0	θ = 0° 1.0	θ = 48° 0.1	θ = 310° 0.9
Open-ended waveguide, virgin H/S	11000	E	θ = 60° 4.0	θ = 0° 1.0	θ = 70° 6.4	θ = 288° 15.3
Open-ended waveguide, virgin H/S	11000	H	θ = 323° 1.8	θ = 0° 1.5	θ = 48° 0.2	θ = 340° 2.3
Monopole, virgin H/S	2200	Horizontal	θ = 80° 2.3	θ = 320° 1.5	θ = 49° 3.0	θ = 291° 6.5
Monopole, virgin H/S	6600	Horizontal	θ = 57° 4.5	θ = 320° 1.9	θ = 48° 4.0	θ = 326° 9.4
Scimitar, virgin H/S	300	Horizontal	θ = 310° 0.4	θ = 275 0.2	θ = 20° 0.1	
Scimitar, virgin H/S	300	Vertical	θ = 290° 2.6	θ = 10° 1.1		
Scimitar, virgin H/S	900	Horizontal	θ = 325° 3.8	θ = 275° 1.1	θ = 20° 5.0	

TABLE VII (Concl'd)

Antenna and Heat-Shield State	Frequency (Mc)	Polarization or Plane of Radiation	Maximum Deviation Excluding Nulls (db)	Deviation at Pattern Peak (db)	Null Deviations (db)	Null Deviations (db)
Scimitar, virgin H/S	900	Vertical	$\theta = 320°$ 3.4	$\theta = 10°$ 1.4		
Scimitar slot, virgin H/S	2200	Horizontal	$\theta = 278°$ 2.5	$\theta = 25°$ 1.0	$\theta = 49°$ 3.6	$\theta = 333°$ 14.5
Scimitar slot, virgin H/S	2200	Vertical	$\theta = 15°$ 5.9	$\theta = 50°$ 0.0		
Scimitar slot, virgin H/S	6600	Horizontal	$\theta = 300°$ 5.0	$\theta = 25°$ 0.3	$\theta = 353°$ 7.[illegible]	$\theta = 333°$ 12.2
Scimitar slot, virgin H/S	6600	Vertical	$\theta = 60°$ 3.3	$\theta = 50°$ 2.2		
Open-ended waveguide, charred H/S	300	E	$\theta = 270°$ 3.2	$\theta = 353°$ 0.0		
Open-ended waveguide, charred H/S	300	H	$\theta = 270°$ 2.0	$\theta = 5°$ 0.4		
Open-ended waveguide, charred H/S	900	E	$\theta = 280°$ 4.2	$\theta = 353°$ 1.1		
Open-ended waveguide, charred H/S	900	H	$\theta = 280°$ 3.4	$\theta = 5°$ 0.8		
Open-ended waveguide, charred H/S	1500	E	$\theta = 290°$ 2.9	$\theta = 353°$ 0.1		
Open-ended waveguide, charred H/S	1500	H	$\theta = 280°$ 2.4	$\theta = 5°$ 0.9		
Open-ended waveguide, charred H/S	2200	E	$\theta = 353°$ 1.8	$\theta = 65°$ 1.8	$\theta = 320°$ 15.5	$\theta = 12°$ 6.6
Open-ended waveguide, charred H/S	2200	H	$\theta = 30°$ 4.8	$\theta = 22°$ 2.9		
Open-ended waveguide, charred H/S	6600	E	$\theta = 62°$ 4.4	$\theta = 65°$ 3.9	$\theta = 320°$ 14.7	$\theta = 12°$ 4.8
Open-ended waveguide, charred H/S	6600	H	$\theta =$ [illegible]0° [illegible].6	$\theta = 22°$ 3.9		
Open-ended waveguide, charred H/S	11000	E	$\theta = 63°$ 6.1	$\theta = 65°$ 5.9	$\theta = 320°$ 14.5	$\theta = 12°$ 6.8
Open-ended waveguide, charred H/S	11000	H	$\theta = 48°$ 5.9	$\theta = 22°$ 3.3		

APPENDIX A

BIBLIOGRAPHY

APPENDIX A

BIBLIOGRAPHY

Avco Corporation, Research and Development Division, Wilmington, Massachusetts, Apollo Heat Shield Design Status Report, -- Structures, Research and Advanced Development Division
Avco RAD-SR-64-137 (C) (June 1, 1964), p. 305, pp. 4-313.

Bennet, R. B., and J. H. Caldenwood
Measurement of VHF Complex Permittivity of Liquids by Means of an Adjustable Coaxial Line
Proc. IEE, 112, No. 2 (February 1965), pp. 416-420.

Blanck, A. R.
Compliant Electrodes for Dielectric Measurements (U)
Feltman Research Labs, Picatinny Arsenal, Dover, N. J. (August 1960)
AD-243-158, DDC Search Control No. 037175

Brydon, G. M., and D. J. Hepplestone
Microwave Measurement of Permittivity and Tan δ - over the Temperature Range 20-700° C
Proc. IEE, 112, No. 2 (February 1965), pp. 421-425.

Chaplin, K. S. and R. R. Krongard
The Measurement of Conductivity and Permittivity of Semiconductor Spheres by an Extension of the Cavity Perturbation Method
IRE Transactions on Microwave Theory and Techniques (November 1961), pp. 545-551.

Croswell, W. F.
Antennas under Ablation Materials (24), Conference on Langley Research Related to Apollo Mission, Langley Research Center
(22-24 June 1965), 239 and 265.

Cuming, W. R., E. K. Buckley, P. E. Rowe, E. J. Luoma, and M. C. Volk,
Graded Dielectric Absorber (U)
Engineering Report No. 3, Emerson and Cuming, Inc., Canton, Massachusetts
(15 January to 15 April 1964).
AD 350-397, DDC Search Control No. 037175

Dakin, T. W., and C. N. Works
Microwave Dielectric Measurements
J. Appl. Phys., 18, No. 9 (September 1947) pp. 789-796.

BLANK PAGE

East, B. B., and W. B. Westphal
Dielectric Parameters and Equivalent Circuits
Laboratory for Insulation Research, Massachusetts Institute of Technology
Technical Report 189

Emerson, C.
Study of Radar Absorber Materials (U)
Emerson and Cuming, Inc., Canton, Massachusetts (March 1962)
AD-275-425, DDC Search Control No. 037175

Flugge, S.
Dielectric Properties of Mixtures
Encyclopedia of Physics XVII
Electric Fields and Waves, Berlin (1958), pp. 706-710.

Fraser, D. B., and A. C. H. Hallett
The Coefficient of Linear Expansion and Gruneisen of Cu, Ag, Au, Fe, Ni, and Al from 4° K to 300° K
Proceedings of the 7th International Conference on Low Temperature Physics, 1961. University of Toronto Press, pp. 689-692.

Frisco, L. J., A. M. Muhlbaum, A. K. Szymkowi, and A. Edward
Dielectrics for Satellites and Space Vehicles - Final Report (U)
Dielectric Lab. Johns Hopkins University, Baltimore, Maryland (1 March 1962 and 31 March 1963) DDC Search Control No. 037175

Gray, B. C.
Programming for Dielectric Constants
Electronic Industries (August 1961), pp. 106, 107, 222

Grosjean, B. G.
Preparation of Artificial Dielectric Materials with Low Loss
North American Aviation, Inc., Columbus Division, PP. 119-129
OSU-WADD Symposium on Electromagnetic Windows (June 1960), AD-250-268

Gum, P. H., and A. B. Schoomer
A Speedy Method of Computing Dielectric Properties
Electronic Industries (September 1963), pp. 90-94

Hansen, E. F.
Standardization Engineering Practices Study - Quarterly Progress Report No. 2 (U) General Electric Company, Syracuse, N. Y., (1 December 1962 - 28 February 1963)
AD-406-958, DDC Search Control No. 037175

Hansen, E. F.
Standardization Engineering Practices Study, High Frequency Characteristics of Ceramic Materials
(30 September 1963)
AD-440-377

Hazard, K.
Scaling Laws
Avco Corporation, RAD Division, in-plant memo
Memorandum AEDM-F530
(15 February 1965)

Hoare, F. E., L. C. Jackson, and N. Kurti
Experimental Cryophysics
Butterworth and Company, London (1961)

Iizuka, K.
An Experimental Study of the Insulated Dipole Antenna Immersed in a Conducting Medium
IEEE Trans. on Antennas and Propagation (September 1963).

Knop, C. M., and G. I. Cohn
Radiation fron an Aperture in a Coated Plane
Radio Science Journal of Research, 68D, No. 4
(April 1964).

Kohane, T.
The Measurement of Microwave Resistivity by Eddy Current Loss in Small Spheres
IRE Trans. on Instrumentation
(September 1960), pp. 184-168

Koozekani
Dielectric Coated Antenna
Brown University
(May 1961) AD-26 1936 8/1.

Kozhelev, Y. D.
Measurements of Permittivity with an Autodyne Generator
Izmeyitel' Naya Tekhnika
No. 11, pp. 52-53 November 1964

Lewin, L.
The Electrical Constants of a Material Loaded with Spherical Particles
94, Part III pp. 65-68

Lynch, A. C.
Measurement of the Dielectric Properties of Low-Loss Materials
Proc. IEE, 112, No. 2 (February 1965), pp. 426-431

McCammon, R. D., and R. N. Work
Dielectric Measurement of Polymer at 4° K, Review of Scientific Instruments, 36, No. 8 (August 1965), pp. 1170-1172.

Mukharev, L. A., C. Perel, A. M. Man, and N. A. Rogova
Determination of the Dielectric Permittivity of Materials at High Temperature in the Three-Centimetre Range of Radio Waves (U)
Royal Aircraft Establishment Farnborough (England)
AD-274-606, DDC Search Control No. 037175

Perkins, C. L., and Z. Alterman
Radiation Resulting from an Impulsive Current in a Vertical Antenna Placed on a Dielectric Ground
J. Appl. Phys., 28, No. 11

Redheffer, R. M., R. L. Wildman, V. O'Groman
The Computation of Dielectric Constants
J. Appl. Phys., 23, No. 5 (May 1957) pp. 505-508.

Reynolds, J. A., and J. M. Hough
Formula for Dielectric Constant of Mixtures
Proc. Physical Society, London
(July - December 1957), pp. 769-775.

Rohde and Schwarz
Die Kurz Information, Material Characteristics Measurement
(1962)

Shaw, T. M., and J. J. Windle
Microwave Techniques for the Measurement of the Dielectric Constant of Fibers and Films of High Polymers
J. Appl. Phys., 21, (October 1950), pp. 956-961.

Squire, F.
Low Temperature Physics,
McGraw-Hill Book Company, Inc., New York

Surber, Jr. W. H., and G. E. Crouch, Jr.
Dielectric Measurement Methods for Solids at Microwave Frequencies
J. Appl. Phys., 19, (December 1948), pp. 1130-1139.

Sutton, R. W., and N. Grechny
Design and Development of a High Temperature Resonant Cavity Dielectrometer
Proc., OSU-WADD Symposium on Electromagnetic Windows
(June 1960), pp. 497-511, AD-250-268

Von Hippel, Editor, The Technology Press of M.I.T., and Wiley, Sons, Inc., New York
Dielectric Materials and Applications
Chapman and Hall, LTD, London (Copyright 1954)

Von Hippel, R.
Dielectrics and Waves
John Wiley and Sons, Inc., New York (1954)

Von Hippel, A. R., et al.
Studies on the Formation and Properties of High Temperature Dielectrics
Technical Report 191
Laboratory for Insulation Research, M.I.T.

Westphal, W. B.
Dielectric Constant and Loss Measurements on High-Temperature Materials (U)
Laboratory for Insulation Research Mass. Inst. of Tech., Cambridge
(October 1963).
AD-423-686, DDC Search Control No. 037175

Westphal, W. B.
Dielectric Constant and Loss Measurements on High Temperature Materials
Technical Report 182
Laboratory for Insulation Research, M.I.T.

Westphal, W. B.
Dielectric Constant and Loss Measurement on High Temperature Materials
Laboratory for Instrumentation Research, MIT, Cambridge, Massachusetts
(October 1963)

Yatsuk, K. P., V. P. Shestopalov, and V. A. Lyashchenko
Limits of Applicability of the Method of a Helical Waveguide for the Measurement of Dielectric Constants in Matter (U)
Aerospace Technology Div., Library of Congress, Washington, D. C.,
(December 1962).
AD-299-798, DDC Search Control No. 037175

APPENDIX B

MID-TEMPERATURE RANGE COMPLEX DIELECTRIC CONSTANT TEST PROCEDURES FOR AVCOAT 5026-39

APPENDIX B

MID-TEMPERATURE RANGE COMPLEX DIELECTRIC CONSTANT TEST PROCEDURES FOR AVCOAT 5026-39

(Prepared by Avco RAD under NASA/MSC Contract NAS 9-4916)

Input impedance measurements with short samples in a co-axial transmission line will be used to obtain the complex dielectric constant of Avcoat 5026-39 in the mid-temperature range. This measurement method was chosen for its high accuracy with moderate lengths of medium and for measurement simplicity. Equipment required for the measurement is a signal generator, a slotted line, and a short circuited sample holder. See the block diagram and equipment list (figure B-1). The procedure for the dielectric measurements consists of measuring the magnitude of the VSWR and the position of the voltage minima, E min., with the output of the slotted line shorted, and repeating the measurement with the dielectric medium placed against the short circuit. From these measurements the propagation constant of the dielectric medium can be obtained from equation (1):

$$\frac{\tanh \gamma d}{\gamma d} = -j \frac{\lambda_1}{2\pi d} \cdot \frac{\dfrac{E_{min}}{E_{max}} - j \tan \dfrac{2\pi x_o}{\lambda_1}}{1 - j \dfrac{E_{min}}{E_{max}} \tan \dfrac{2\pi x_o}{\lambda_1}} \tag{1}$$

where

γ = complex propagation constant of dielectric medium.

d = length of dielectric sample.

λ_1 = wavelength in co-axial line without dielectric medium.

x_o = shift in position of E min. due to the introduction of the dielectric sample in the coaxial line.

$$\frac{E_{min}}{E_{max}} = \frac{1}{VSWR}$$

The complex dielectric constant is related to the propagation constant by the equation:

$$\gamma = j\omega(\epsilon\mu)^{1/2} \tag{2}$$

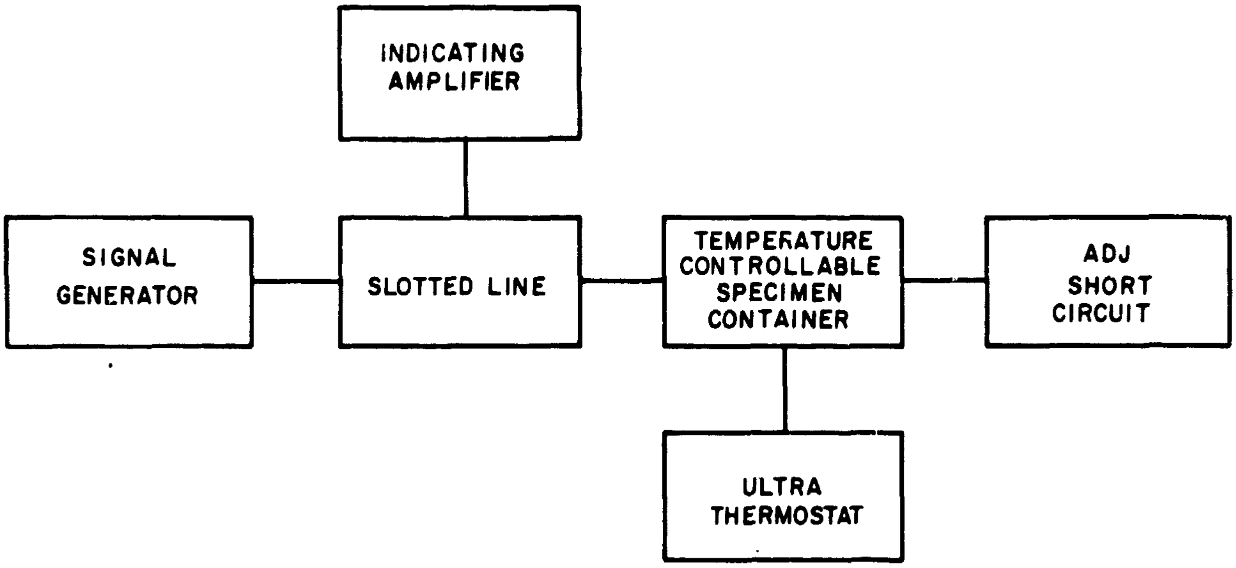

Description	300 to 3000 mc	1650 to 3000 mc	4400 mc .o 8000 mc
Signal Generator	Rohde & Schwarz type SLRD BN 41004 FNR 1400/58	Rohde & Schwarz type NGS BN 95147 Fnr. E32/5/24	Rohde & Schwarz type SMCC BN4143 Fnr. F13849.
Slotted Line	Rohde & Schwarz type LMD BN 39310 Fnr. EF 436/8/26	Rohde & Schwarz type LMC BN 39310 Fnr. 436/8/29	Same as 1650 - 5000 mc
Temperature Control	Rohde & Schwarz 200 mm	Same as 300-3000 mc	Same as 300 - 3000 mc
Specimen Container	BN 39319.		
Adjustable Short	Rohde & Schwarz 50 cm short BN 39592 Fnr. 39592	Rohde & Schwarz 13 cm BN 39591 Fnr. 1439/10	Same as 1650 - 5000 mc
Indicating Amplifier	Rohde & Schwarz type LMC BN 3931 Fnr. KL274/19	Same as 300-3000 mc	Same as 300 - 3000 mc
Ultra Thermostat	Haake type NC Nr 61224	Same as 300-3000 mc	Same as 300 - 3000 mc

85-6940

Figure B-1 BLOCK DIAGRAM OF MIDTEMPERATURE RANGE DIELECTRIC MEASUREMENTS AND EQUIPMENT LIST

These are standard dielectric measurements and the procedure is outlined in detail in references 1, 2, 3, and 4.

The equipment that will be used to make the measurements is the Rohde and Schwarz precision coaxial dielectrometer. The Rohde and Schwarz dielectrometer is specifically designed to take advantage of the accuracy of the input impedance measuring method with short samples. This dielectrometer has a frequency range of 300 to 8000 mc/s and a -50 to +250°C temperature range. See Figure B2.

Because the dielectric constant is not expected to vary appreciably in the mid-temperature range only a limited number of measurements will be performed.

Table B-I is a tabulation of the frequencies, temperatures, and sample types that will be measured.

TABLE B-I

FREQUENCIES, TEMPERATURES, AND SAMPLE TYPES

Frequencies (Mc)	Temperature (Virgin Sample)		Temperature (Charred Sample)
	25°C	180°C	25°C
300	x	x	x
450	x	x	x
1000		x	x
2200	x	x	x
5800	x	x	x

The 5026-39 HCG samples will be machined so that the honeycomb structure is parallel to the coaxial line longitudinal axis. It has already been determined that the dielectric constant does not vary significantly with honeycomb orientation or between 5026-39 HCG and 5026-39 M; therefore only 5026-39 HCG will be measured. The charred samples will be oven heated until the sample is completely visibly charred throughout its volume. A sample in each oven run will be cut open to check for thorough charring.

Sources of Error in Determining the Dielectric Constants

1. Errors resulting from harmonics in the output of the signal generator will have a negligible effect in the measured dielectric constant for the following reasons:

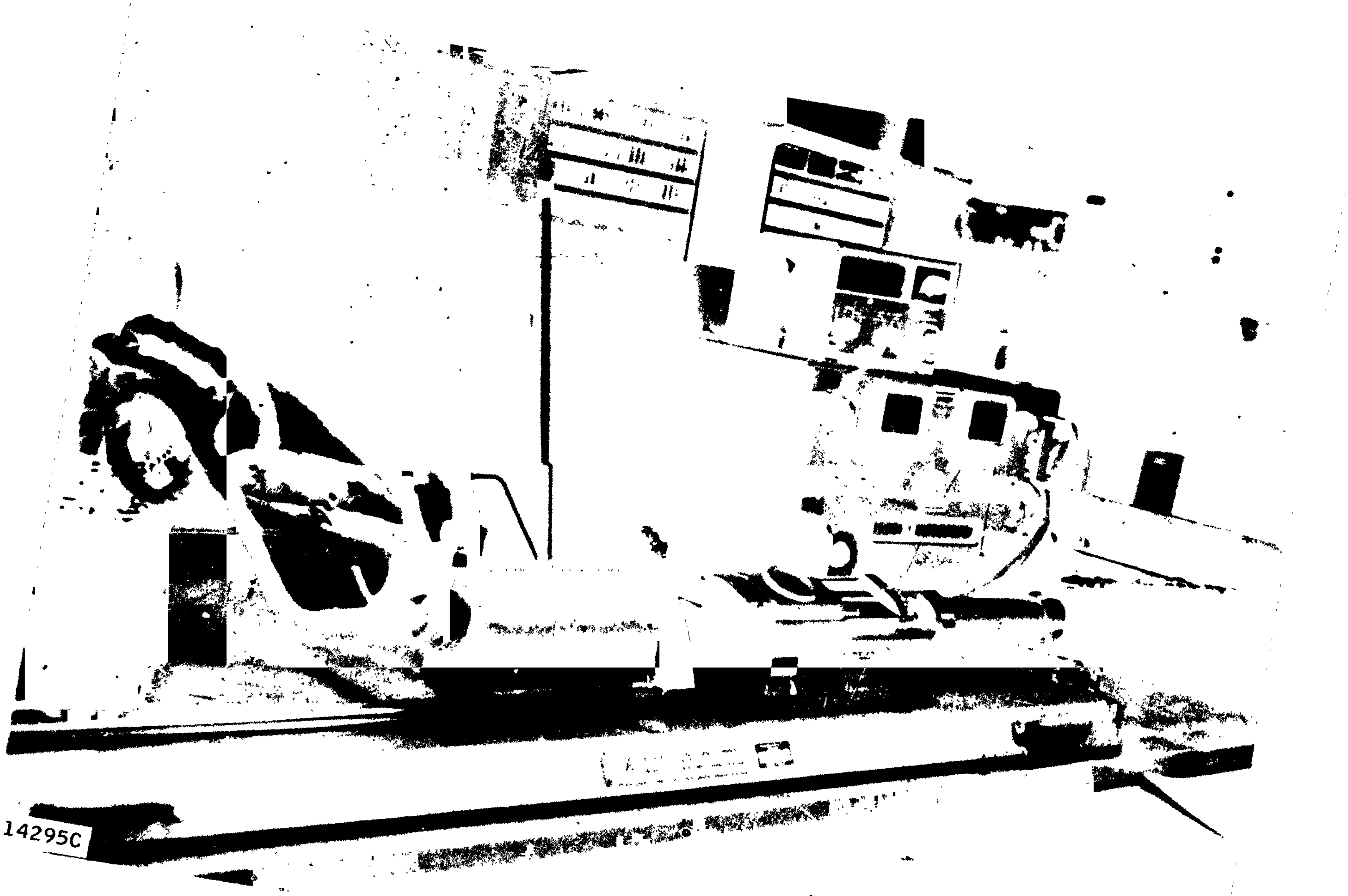

Figure B-2 TEST SETUP FOR 180° C PERMITTIVITY MEASUREMENTS

a. The Rohde and Schwarz signal generators have harmonic suppression filters.

b. The microwave slotted line has harmonic suppression filters.

c. Low pass filters are also used on the signal generator outputs.

2. Errors due to the depth of the pick-up probe in the slotted line are negligible because a high-gain VSWR amplifier is used to amplify the output signal from the probe. The high sensitivity of the amplifier allows the use of very shallow probe depths and therefore the probe produces a negligible perturbation of the electric field in coaxial line. Also by using the one-half minimum method of measuring VSWR, the probe is placed in a low field strength region of the line and this further reduces field perturbations.

3. Possible error due to the slotted line pick-up probe diode detector not being a perfect square law detector will be eliminated by careful calibration of the diode over its operating range.

4. Possible errors due to wall losses in the coaxial line are eliminated by measuring and applying these losses in the calculation of the dielectric constant. The wall losses in the Rohde and Schwarz dielectrometer do, however, set a limit on the minimum measurable sample loss tangent. This minimum value of tan δ is 5×10^{-4}.

5. Errors result from the fact that the dielectric sample does not fit in the coaxial sample holder precisely. By measuring the space distribution along the length and around the periphery of the sample the corrected values of the dielectric constant can be calculated. The error is not very large even if the correction is not applied in the measurements since the sample will be machined to fit into the sample holder with less than 0.001 inch air spacing. The 0.001 spacing would result in an error of 3 percent for ϵ' and 6 percent for tan δ for a dielectric having a $\epsilon' = 2.0$ and a tan δ of 0.02.

No additional error will be introduced due to differential coefficient of thermal expansion between the sample and sample holder over the mid-temperature range. The differential coefficient is approximately 1×10^{-7} so that fit will vary only 1.55×10^{-5} in./in. over the temperature range.

6. Errors due to the inhomogeneity character of the sample were described in the third bi-weekly report of this contract. These errors are a maximum of 2.7 percent of the measured dielectric constant.

7. Although allowances for errors in the specimen dimensions takes care of the main source of error, it is difficult to say exactly how accurate the measured results are. Deviations in frequency during the measurement,

contact errors, and reading errors can influence the measurement of the complex dielectric constant. One method to take all these errors into account is to consider the derivative of expression (1) with respect to γ. Then by obtaining an expression of $\frac{d\gamma}{\gamma}$ relative errors can be analyzed. Another method is to calculate the dielectric constant from the slotted line measurement and then repeat the calculation for the slotted line measurement plus the maximum reading error, frequency deviation, and contact errors.

From either of these two calculations the complex dielectric constant and its accuracy can be obtained. Although the second method would normally be much more difficult, in our case it is easier because the calculation procedure for the complex dielectric constant has already been set up in a computer program. The accuracy in the measurement of dielectric constant for reading errors, contact errors, and frequency deviations is 0.2 percent for ϵ' of 2.0. This error will increase if the dielectric constant increases. If it happens that the dielectric constant does increase in mid-temperature measurements, the computer program will again be used to determine the changes in accuracy.

In conclusion, the overall accuracy of the measurement is 6 percent when all the possible corrections are applied. This error is essentially totally associated with the 2.7 percent error due to the inhomogeneity of the sample and the 3 percent possible error due to the air space between the sample and the coaxial line walls.

REFERENCES

1. Von Hippel, A. R., Dielectric Materials and Applications, The Technology Press of M.I.T. and John Wiley and Sons, Inc., New York.

2. Westphal, W. B., Techniques of Measuring the Permittivity and Permeability of Liquids and Solids in the Frequency Range of 3 c/s to 50 km c/s, Armed Services Tech. Infor. Agency, Alighton Hall Station, Arlington 12, Virginia, Wright Field Microfilm No. R3986F.

3. Sucher, M., and J. Fox, Microwave Measurements, Third Edition, Polytechnic Press of Polytechnic Institute of Brooklyn.

4. Montgomery, C. G., Techniques of Microwave Measurements, M.I.T. Radiation Lab. Series, McGraw-Hill Publishing Company (1947).

APPENDIX C

CYROGENIC TEMPERATURE RANGE COMPLEX DIELECTRIC CONSTANT TEST PROCEDURES FOR AVCOAT 5026-39

BLANK PAGE

APPENDIX C

CRYOGENIC TEMPERATURE RANGE COMPLEX DIELECTRIC CONSTANT TEST PROCEDURES FOR AVCOAT 5026-39

(Prepared by Avco/RAD under NASA/MSC Contract NAS 9-4916)

Test Procedure

Input impedance measurements with short samples on a co-axial transmission line will be used to obtain complex dielectric constants in the cryogenic temperature range. This measurement method was chosen for its high accuracy with moderate lengths of medium and for measurement simplicity. Equipment required for the measurement is a signal generator, a slotted line, a short circuited sample holder and a dewar to cool the sample to cryogenic temperatures. A block diagram and equipment list appears in figure C-1. Figures C-2 and C-3 are sketches of the dewar. The procedure for the dielectric measurements consists of measuring the magnitude of the VSWR and the position of the voltage minima, E min, with the output of the slotted line shorted and repeating the measurement with the dielectric medium placed against the short circuit. From these measurements the propagation constant of the dielectric medium can be obtained from equation:

$$\frac{\tanh \gamma d}{\gamma d} = -j\,\frac{r_1}{2\pi d} \cdot \frac{\dfrac{E_{min}}{E_{max}} - j\tan\dfrac{2\pi x_o}{r_1}}{1 - j\,\dfrac{E_{min}}{E_{max}}\tan\dfrac{2\pi x_o}{r_1}} \qquad (1)$$

where

γ = complex propagation constant of dielectric medium.

d = length of dielectric sample.

r_1 = wavelength in co-axial line without dielectric medium.

x_o = shaft in position of E_{min} due to dielectric sample placed in co-axial line.

$$\frac{E_{min}}{E_{max}} = \frac{1}{VSWR}$$

The complex dielectric constant is related to the propagation constant by the equation:

$$\gamma = j\,\omega\,(\epsilon\mu)^{1/2} \qquad (2)$$

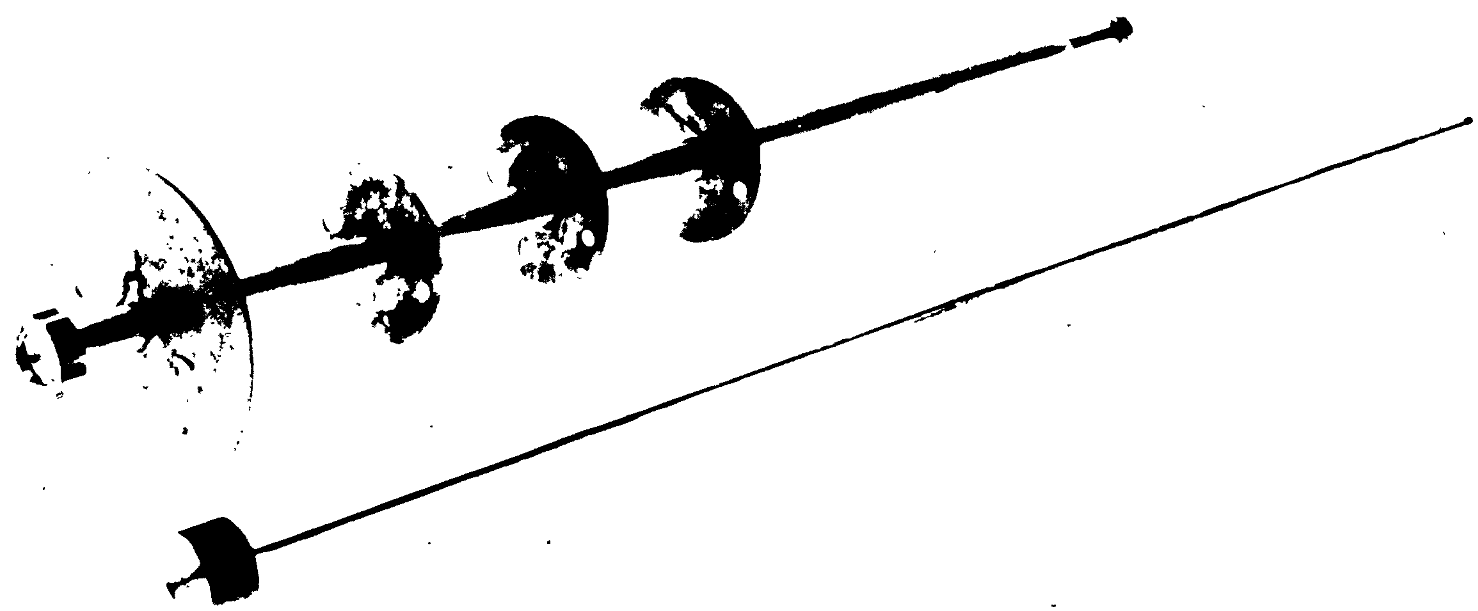

14294

Figure C-1 CRYOGENIC SAMPLE HOLDER

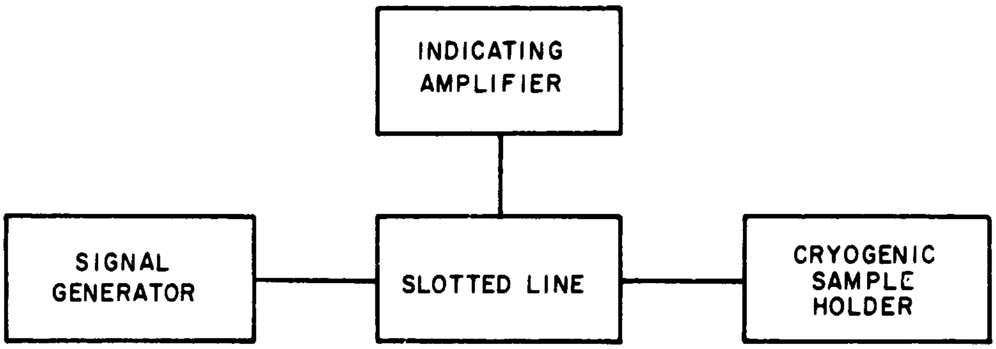

Description	300 - 3000 mc	1650 - 5000 mc	4400 - 8000 mc
Signal Generator	Rohde and Schwarz Type SLR - BN 41004 FNR. 1400/58	Rohde and Schwarz Type NGS BN 95147 FNR. E-362/5/24	Rohde and Schwarz Type SMCC BN 4143 FNR. F13849
Slotted Line	Rohde and Schwarz Type LMD BN 39310 FNR-EF 439/8/26	Rohde and Schwarz Type LMC BN 39310 FNR 436/8/29	Same as 1650 - 5000 mc
Indicating Amplifier	Rohde and Schwarz Type LMC BN 3931 FNR KL 274/19	Same as 300-3000 mc	Same as 300-3000 mc
Cryogenic Sample Holder	AVCO made Zo = 50	Same as 300-3000 mc	Same as 300-3000 mc

85-6941

Figure C-2 BLOCK DIAGRAM OF CRYOGENIC RANGE DIELECTRIC MEASUREMENTS AND EQUIPMENT LIST

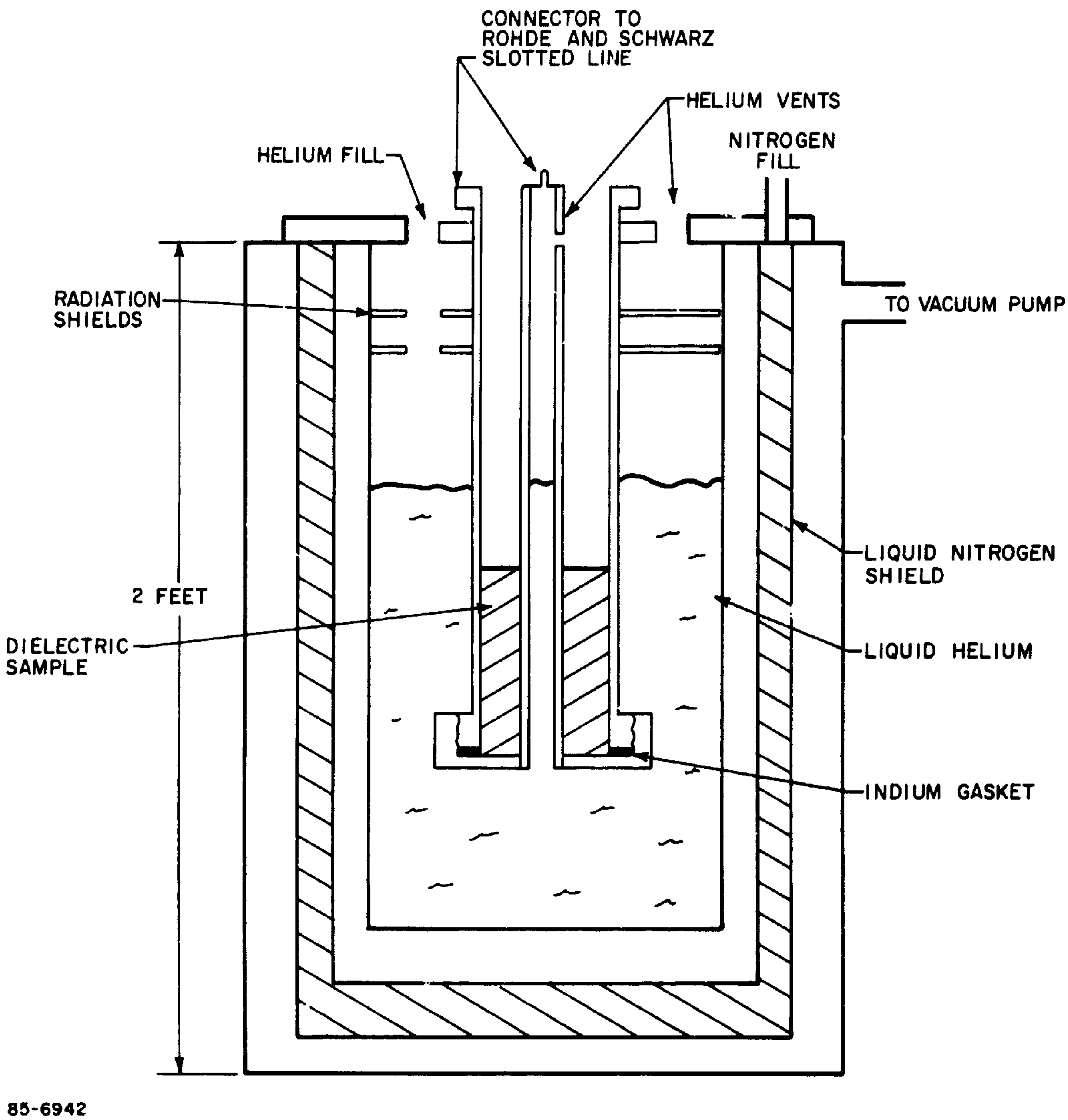

Figure C-3 CRYOGENIC SAMPLE HOLDER

These are standard dielectric measurements and the procedure is outlined in detail in references 1, 2, 3, and 4.

The equipment that will be used to make the measurements is the Rohde and Schwarz precision coaxial dielectrometer (see figure C-1). The Rohde and Schwarz dielectrometer is specifically designed to take advantage of the accuracy of the input impedance measuring method with short samples. This dielectrometer has a frequency range of 300 to 8000 Mc.

Because the dielectric constant is not expected to vary appreciably in the cryogenic temperature range from that of room temperature only a single temperature measurement will be made for each frequency.

Table C-1 is a tabulation of the frequencies and the temperature at which measurements will be made.

Frequencies (Mc)	Temperature (°K)
300	~ 4
450	~ 4
2200	~ 4
5800	~ 4

The 5026-39 HCG samples will be machined so that the honeycomb structure is parallel to the coaxial line longitudinal axes. It has already been determined that the dielectric constant does not vary significantly with honeycomb orientation or between 5026-39 M. Therefore, only 5026-39 HCG will be measured.

Sources of Error in Determining the Dielectric Constants

1. Errors resulting from harmonics in the output of the signal generator will have a negligible effect in the measured dielectric constant for the following reasons:

   a. The Rohde and Schwarz signal generators have harmonic suppression filters.

   b. The microwave slotted line has harmonic suppression filters.

   c. Low pass filters are also used on the signal generator outputs.

2. Errors due to the depth of the pick-up probe in the slotted line are negligible because of a high-gain VSWR amplifier is used to amplify the

output signal from the probe. The high sensitivity of the amplifier allows the use of very shallow probe depths and therefore the probe produces a negligible perturbation of the electric field in coaxial line. Also by using the one-half minimum method of measuring VSWR, the probe is placed in a low field strength region of the line and this further reduces field perturbations.

3. Possible error due to the slotted line pick up probe diode detector not being a perfect square law detector will be eliminated by careful calibration of the diode over its operating range.

4. Possible errors due to wall losses in the coaxial line are eliminated by measuring and applying these losses in the calculation of the dielectric constant. The wall losses in the Rohde and Schwarz dielectrometer do, however, set a limit on the minimum measurable sample loss tangent. This minimum value of $\tan \delta$ is 5×10^{-4}.

5. Errors result from the fact that the dielectric sample does not fit in the coaxial sample holder precisely. This problem is augmented in the cryogenic test because of the differential thermal coefficient of expansion between 5026-39 HCG and the sample holder. A knowledge of the sample to sample holder fit within 0.001 inch at room temperature and a fairly precise knowledge of the differential thermal coefficient of expansion will allow correction of the complex dielectric constant to within 3 percent. The thermal coefficient of expansion curves for 5026-39 HCG are available for temperatures dow 118°K. Since the curves are constant is slope from 300 to 118°K, it will be assumed that the curve does not change slope down to 4°K. Prior to measurement of dielectric constant at 4°K, the diameter of a cylindrical sample will be compared at room temperature and 78°K (liquid nitrogen) to substantiate in part this contention.

6. Error due to the non-homogeneity character of the sample were described in the third bi-weekly report. These errors are 2.7 percent of the measured dielectric constant.

7. Although allowance for errors in the specimen dimensions takes care of the main source of error, it is difficult to say exactly how accurate the measured result is. Deviations in frequency during the measurement, contact errors, and reading errors can influence the measurement of the complex dielectric constant. One method to take all these errors into account is to consider the derivative of expression (1) with respect to γ. Then by obtaining an exppression of $d\gamma/\gamma$ relative errors can be analyzed. Another method is to calculate the dielectric constant from the slotted line measurement and then repeat the calculation for the slotted line measurement plus the maximum reading error, frequency deviation and contact errors.

From either of these two calculations the complex dielectric constant and its accuracy can be obtained. Although the second method would normally be much more difficult, in our case it is easier because the calculation procedure for the complex dielectric constant has already been set up in a computer program. The accuracy in the measurement of dielectric constant for reading errors, contact errors, and frequency deviations is 0.2 percent for ϵ' of 2.0. This error will increase if the dielectric constant increases. If it happens that the dielectric constant does increase in cryogenic temperature measurements, the computer program will again be used to determine the changes in accuracy.

In conclusion, the overall accuracy of the measurements is 6 percent when all the possible corrections are applied. This error is essentially totally associated with the 2.7 percent error due to the inhomogeneity of the sample and the 3 percent possible error due to the air space between the sample and the coaxial line walls.

REFERENCES

1. Von Hippel, A. R., Dielectric Materials and Applications, The Technology Press of M.I.T. and John Wiley and Sons, Inc., New York.

2. Westpha, W. B., Techniques of Measuring the Permittivity and Permeability of Liquids and Solids in the Frequency Range of 3 c/s to 50 km c/s, Armed Services Tech. Infor. Agency, Arlington HallStation, Arlington 12, Virginia, Wright Field Microfilm No. R 3986F.

3. Sucher, M., and J. Fox, Microwave Measurements, Third Edition, Polytechnic Press of Polytechnic Institute of Brooklyn.

4. Montgomery, C. G., Techniques of Microwave Measurements, M.I.T. Radiation Lab, Series, McGraw-Hill Publishing Company (1947).

APPENDIX D

HIGH TEMPERATURE RANGE COMPLEX DIELECTRIC CONSTANT
TEST PROCEDURES FOR AVCOAT 5026-39

APPENDIX D

HIGH TEMPERATURE RANGE COMPLEX DIELECTRIC CONSTANT TEST PROCEDURES FOR AVCOAT 5026-39

(Prepared by Avco/RAD under NASA/MSC Contract NAS 9-4916)

A. INTRODUCTION

Room temperature complex permittivity measurement of materials at microwave frequencies can be readily accomplished by the short-circuited line method. With slight modification, this method can be extended to be melting point of high temperature microwave components. The upper temperature limit for this method is 1500°K, so it is unsuitable for the 2000°K problem at hand.

An alternate technique to be considered is the microwave interferometer or reflectometer. In this method the microwave components can be separated from the hot sample and operated at room temperature. Unfortunately, relatively large sample sheets are required to avoid edge diffraction and it is then difficult to achieve a high uniform temperature throughout the sample. For this reason the method is considered unsuitable.

A resonant cavity dielectrometer will be used to overcome the difficulties inherent in the above dielectrometers in the temperature range of 500°K to 2000°K. In this method a small sample will be introducted into a conventional cavity resulting in a measurable perturbation in the cavity resonant frequency. By progressively varying the sample size (always small compared to one wavelength), an effect on the cavity can be selected to optimize measurement accuracy. A small sample has the obvious advantage of being easily heated. In the method, the sample is heated outside the cavity and rapidly inserted into the cavity to avoid heating the microwave equipment.

Using this technique the complex permittivity of Avcoat 5026-39 will be measured at 2000°K ± 100°K for the following frequencies: 250, 1000 and 3000 Mc.

B. THEORY

Birnbaum and Franeau have developed a perturbation theory[1] which gives the changes in resonant frequency (f) and loaded $Q(Q_L)$ of a cavity due to a small perturbation of the cavity. They considered two cavities, 1 and 2, which differed slightly due to the presence of a dielectric material in cavity 2. If the material has a relative complex dielectric constant of $\epsilon' - j\epsilon''$ and a permeability of 1 then:*

[1]Birnbaum, G., and J. Franeau, Measurement of the Dielectric Constant and Loss of Solids and Liquids by a Cavity Perturbation Method, J. Appl. Phys. (August 1949), pp. 817-818.

*Refer to list of symbols.

$$\frac{f_1 - f_2}{f_2} = \left[\frac{\epsilon' - 1}{2}\right] \frac{\int_{V_2} E_1 E_2 \, dV_2}{\int_{V_1} E_1^2 \, dV_1} \tag{1}$$

$$\frac{1}{Q_2} - \frac{1}{Q_1} = \epsilon'' \frac{\int_{V_2} E_1 E_2 \, dV_2}{\int_{V_1} E_1^2 \, dV_1} \tag{2}$$

where V_2 and V_1 are the volume of the dielectric and the cavity respectively, and E_1 and E_2 are the electric field intensities of cavity 1 and 2.

These equations become useful when the perturbation of the cavity is small enough so that E_1 and E_2 are approximately equal. The relative error due to this approximation is of the order:

$$\frac{f_1 - f_2}{f_2} + \frac{1}{Q_2} \tag{3}$$

The error can be kept small by controlling the sample size.

A TM010 cavity has been selected because it provides a maximum sensitivity for the dielectric measurements. In addition, the field configuration is such that a dielectric sample off the cavity axis does not create a serious error. The field equations for a TM010 cavity in cylindrical coordinates are given by:[2]

$$\bar{E}_r = \bar{E}_\theta = 0 \tag{4}$$

$$\bar{E}_z = \bar{E}_n J_0 (\rho r) \tag{5}$$

where $(\rho r) = \frac{2.405}{a}$ and a is the radius of the cavity.

Figure D-1 is a diagram of a cylindrical dielectric rod in a cavity for the case where $r_0 < a$. Equation (1) and (2) become respectively (6) and (10) when generalized to include the effects of the dielectric rod being slightly off axis. Equation (1) becomes:

[2]Montgomery, C.G., Technique of Microwave Measurements, Radiation Lab Series; McGraw-Hill (1947), p. 299.

$$\frac{f_1 - f_2}{f_2} = \frac{1/2\,(\epsilon' - 1) \int_0^{l} dz \left[\int_{3/2\pi}^{\pi/2} \int_0^{r_o \cos\theta + \sqrt{b^2 - r_o^2 \sin^2\theta}} r J_o^2(\rho r)\, dr\, d\theta + \int_{\pi/2}^{3/2\pi} \int_0^{\sqrt{b^2 - r_o^2 \sin^2\theta} - r_o \cos\theta} r J_o^2(\rho r)\, dr\, d\theta \right]}{\int_0^{l} \int_0^{2\pi} \int_0^{a} r J_o^2(\rho r)\, dr\, d\theta\, dz} \tag{6}$$

The effect of the dielectric rod being off-center in the cavity ($r_o < b$) can be examined by expanding $J_o^2\ (\rho r)$ in an infinite series and integrating the first few terms.

$$J_o(\rho r) = \sum_{n=0}^{\infty} \frac{(-1)^n \left(\frac{\rho r}{2}\right)}{(n!)^2} = 1 - \frac{\rho^2 r^2}{4} + \frac{\rho^4 r^4}{64} - \ldots, \tag{7}$$

$$J_o^2(\rho r) = 1 - \frac{\rho^2 r^2}{2} + \frac{3}{32} \rho^4 r^4 - \ldots \tag{8}$$

Substituting equation (8) into (6) and integrating with respect to r, θ, z yields

$$\frac{f_1 - f_2}{f_2} = 1\ 85\,(\epsilon' - 1) \frac{b^2}{a^2} \left(1 - 1\ 45 \frac{b^2}{a^2} - 2.90 \frac{r_o^2}{a^2}\right) \tag{9}$$

and equation (2) becomes

$$\frac{1}{Q_2} - \frac{1}{Q_1} = 3\ 70\ \epsilon'' \frac{b^2}{a^2} \left(1 - 1.45 \frac{b^2}{a^2} - 2.90 \frac{r_o^2}{a^2}\right) . \tag{10}$$

For this case where $a \geq b \geq r_o$, the correction factor to the volume fraction of dielectric sample is negligible. Typically, $a \approx 20\ b$; therefore, the correction factor would be of the order of 2 percent if the dielectric rod is displaced such that $r_o = b$. The second term in the correction expression results from terminating the series expansion of the Bessell function after only two terms. In the limit, correction terms involving only $(b/a)^n$ should sum to zero.

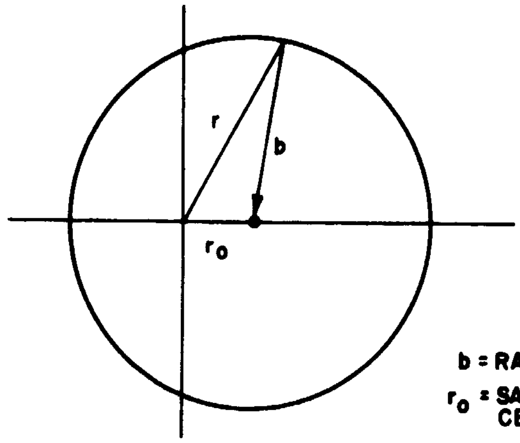

85-6943

Figure D-1 DIELECTRIC ROD DISPLACED (μ_o < b)

The change in Q and resonant frequency can be measured by a number of techniques if the dielectric is stationary in the cavity, However, when the dielectric is dropped through the cavity, time does not permit the usual measurements. Instead, phase shift and transmission loss, which are directly related to the Q and the frequency shift, are measured. From the measured phase shift and transmission loss the following equations may be solved to obtain the complex permittivity.

The transmission loss of a cavity near resonance is given by:[2]

$$T_L = \frac{\rho_o}{\rho_1} = \frac{4\beta_1\beta_2}{(1+\beta_1+\beta_2)^2 + 4\,Q_o^2\left(\frac{\Delta f}{f_o}\right)^2} \qquad (11)$$

When the resonant frequency, f_o , of the cavity is applied, $\Delta f = 0$

The impedance of the cavity is given by

$$Z = R\left[1+\beta_1+\beta_2+2\,j\,Q_o\left(\frac{\Delta f}{f_o}\right)\right] . \qquad (12)$$

from which the phase angle becomes

$$\phi - \tan^{-1}\left[\frac{2\,Q_o\,\frac{\Delta f}{f_o}}{1+\beta_2+\beta_2}\right] \qquad (13)$$

[2] Montgomery, op. cit., pp. 289-291.

Introduction of the dielectric sample into the cavity is equivalent to including an additional resistance and reactance in series with the equivalent circuit of the cavity. This results in an additional coupling term, β_d, in addition to the frequency shift. Equations (11) and (13) are changed to include the coupling

$$T_2 = \frac{4\beta_1\beta_2}{(1+\beta_1+\beta_2+\beta_d)^2 + 4Q_o^2\left(\frac{\Delta f}{f_o}\right)^2} \tag{14}$$

$$\phi_2 = \tan^{-1}\left[\frac{2Q_o\frac{\Delta f}{f_o}}{1+\beta_1+\beta_2+\beta_d}\right] \tag{15}$$

Using equation (10) and neglecting the off axis correction factor, the following expression for Q_2 is obtained.

$$Q_2 = \frac{Q_1}{3.70\,V_f\,Q_1\epsilon'' + 1} \tag{16}$$

where

$$V_f = \frac{a^2}{b^2}$$

The quantities to be measured are:

1. The ratio of transmission loss with the sample in the cavity to the transmission loss of the empty cavity measured at the empty cavity resonant frequency.

2. The phase shift of this signal with and without the sample in the cavity substituting the relations.

$$Q_o = (1+\beta_1+\beta_2)\,Q_1 = (1+\beta_1+\beta_2+\beta_d)\,Q_2 \tag{17}$$

and following this procedure using equations (9) and (10), neglecting the off axis correction factor, equations (14) and (15) become:

$$\frac{T_2}{T_1} = \left\{(3.70\,Q_1V_f\epsilon'' + 1)^2 + [3.70\,Q_1V_f(\epsilon' - 1)]^2\right\}^{-1} \tag{18}$$

$$\phi_2 = \tan^{-1}\frac{3.70\,V_fQ_1(\epsilon' - 1)}{3.70\,V_f\,Q_1\epsilon'' + 1}\ . \tag{19}$$

Solving these equations simultaneously yields ϵ' and ϵ'' in terms of phase shift and attenuation.

$$\epsilon' = 1 + \frac{\left[\frac{T_1}{T_2} \cdot \frac{1}{\left(\frac{1}{\tan^2 \phi_2} + 1\right)}\right]^{1/2}}{3.70\, Q_1 V_f}$$

$$\epsilon'' = \frac{\left[\frac{T_1}{T_2} \cdot \frac{1}{(\tan^2 \phi_2 + 1)}\right]^{1/2} - 1}{3.70\, Q_1 V_f}$$

C. MEASURING SYSTEM

Phase and transmission measurement of the signal passing through the test cavity can be conveniently measured with a bridge circuit (see figures D-2, D-3, and D-4 and tables D-I, D-II, and D-III). The receivers used to monitor the output of the bridge are capable of continuous measurements with 10 μsec time resolution. This resolution is more than adequate to monitor the perturbation resulting from the sample being dropped through the cavity.

The bridge is designed around the vector addition property of the microwave tee or resistor combiner. If the reference and cavity arm input signals to the tee and their vector sum are measured, a vector triangle can be established with three known sides. The enclosed angle which is the phase shift of the cavity can then be calculated using the law of cosines.

Sensitive receivers are used to detect the output of the cavity arm and the sum output. Since the reference arm remains fixed throughout the measurements, it needs only to be set initially. It should be noted that adequate isolation has been incorporated in the bridge to avoid interaction between the bridge arms and the local oscillators of the receivers.

D. MEASUREMENT ERROR

The sum and cavity receiver outputs are displayed in time by means of an oscilloscope. Since the vector bridge and receivers are calibrated by precision attenuators, the only significant measurement error is due to the resolution limitation of the oscilloscope display. This reading error will be maintained at approximately 2 percent by proper selection of the oscilloscope vertical deflection sensitivity. By applying the 2 percent reading error of the receiver outputs to the law of cosines, the phase error can be determined. It should be noted that small inaccuracies in the measurements of the receiver outputs can cause large errors in the phase, if the vector triangle does not approximate an equilateral triangle. Therefore, the amplitude and phase angle of the reference

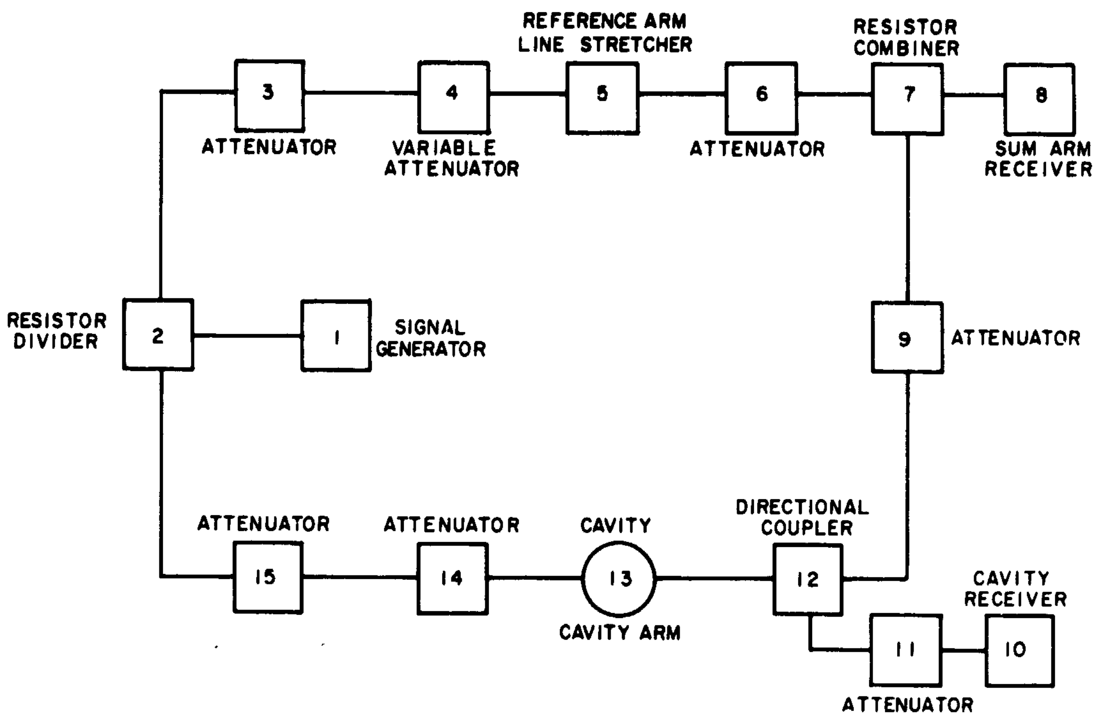

Table D-1 Equipment List for Figure D-2

No.	Description	Manufacturer's Model No.
1.	Signal Generator	Hewlett Packard 608C Serial No. 1497
2.	Resistor Divider	Micro Lab DA 4 MN
3.	Attenuator Step	Hewlett Packard 355C
4.	Attenuator Variable	Weinchel Eng.905 Serial No. 265
5.	Line Stretcher	Micro Lab ST 05N
6.	Attenuator Step	Hewlett Packard 355D
7.	Resistor Combiner	Micro Lab DP 5 MN
8.	Receiver	Nems Clark 1670 F Serial No. 314
9.	Attenuator	Micro Lab AB 10 N
10.	Receiver	Nems Clark 1670 E Serial No. 380
11.	Attenuator	Micro Lab AB 05 N
12.	Directional Coupler	Narda 3000-10 Serial No. 619
13.	Cavity	AVCO made TM 010 fc 250.4 mc Q 1240
14.	Attenuator Step	Hewlett Packard 355 C
15.	Attenuator Step	Hewlett Packard 355 D

85-6944

Figure D-2 HIGH-TEMPERATURE DIELECTRIC MEASURING SYSTEM (f = 250 mc)

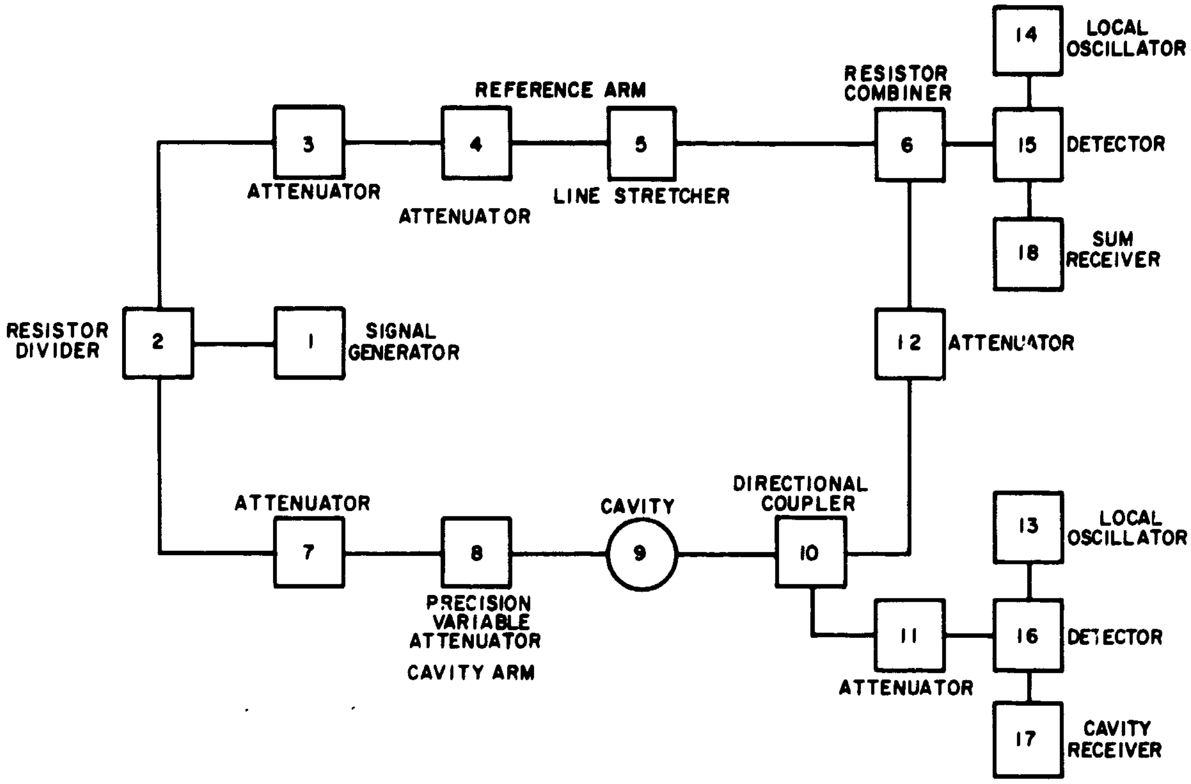

Table D-2 Equipment List for Figure D-3

No.	Description	Manufacturer's Model and Serial No.
1.	Signal Generator	Polarad MSG-1 SN166
2.	Resistor Divider	Micro Lab DA 4 MN
3.	Attenuator	Micro Lab AB 20 N
4.	Attenuator	Micro Lab AB 20 N
5.	Line Stretcher	Micro Lab SR 05 N
6.	Resistor Combiner	Micro Lab DA 5 MN
7.	Attenuator	Micro Lab AB 10 N
8.	Attenuator	Hewlett Packard Model 394A Serial No. 058
9.	Cavity	AVCO made fc 1010 Mc Q 927
10.	Directional Coupler	Narda Model 3002-10 Serial No. 1112
11.	Attenuator	Micro Lab AB 20 N
12.	Attenuator	Micro Lab AB 20 N
13.	Local Oscillator	Hewlett Packard 614A SN 1108
14.	Local Oscillator	Hewlett Packard 612A SN 637
15.	Detector	Hewlett Packard 440 A
16.	Detector	Hewlett Packard 440 A
17.	Receiver Amplifier	LEL Mod 301 D50 Serial No. 7050
18.	Receiver Amplifier	LEL Mod 301 D50 Serial No. 7053

85-6945

Figure D-3 HIGH-TEMPERATURE DIELECTRIC MEASURING SYSTEM (f = 1000 mc)

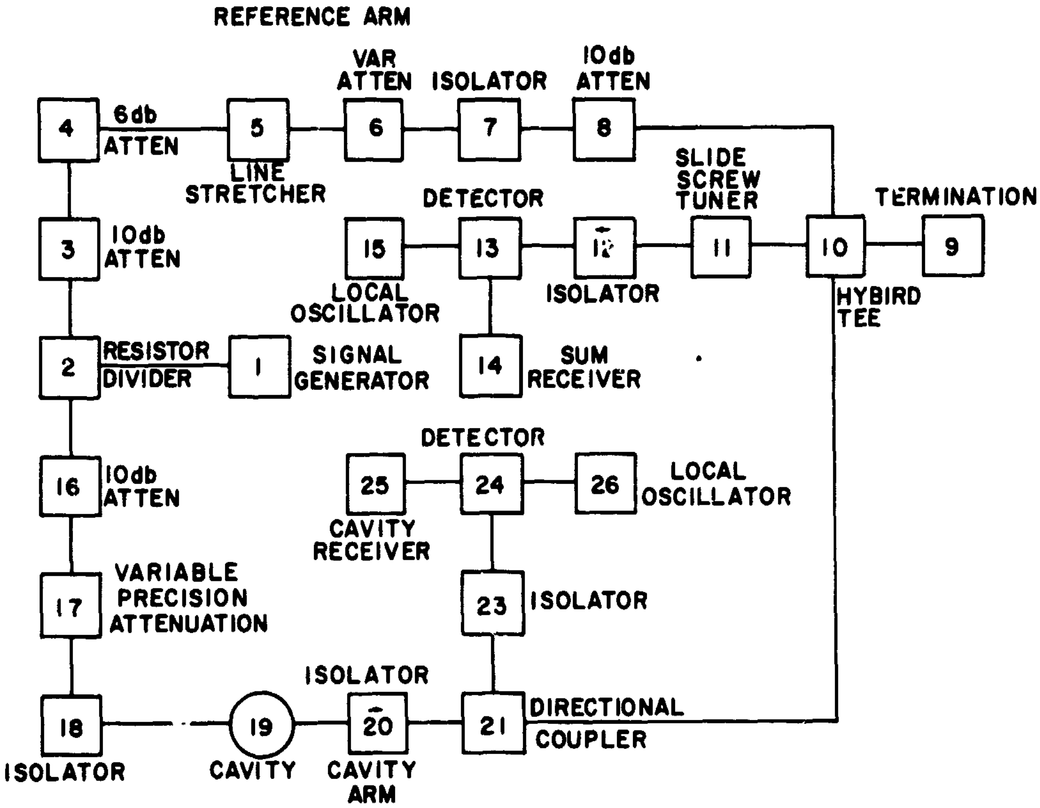

Table D-3 Equipment List for Figure D-4

No.	Description	Manufacturer's Model No. and Serial No.
1.	Signal Generator (Sta-Lo)	Lab for Elec. Mod 814-S-1 Serial No. 409
2.	Resistor Divider	Micro Lab - Mod. DA 4MN
3.	Attenuator	Narda 757-10 Serial No. 700
4.	Attenuator	Narda 757-6 Serial No. 483
5.	Line Stretcher	Micro Lab SR-05N
6.	Attenuator	Demorhay Bonardi L430 Serial No. 2671
7.	Isolator	Microwave Assoc. Mod 170 Serial No. 16
8.	Attenuator	Narda 757-10 Serial No. 701
9.	Termination	FXR - Mod S501B Serial No. 274
10.	Hybrid Tee	FXR - Mod 5622A Serial No. 042
11.	Slide Screw Tuner	FXR - Mod 5211A Serial No. 317
12.	Isolator	Microwave Assoc. Mod 170 Serial No. 12
13.	Detector	Hewlett-Packard Mod 440A
14.	Receiver - IF Amplifier	LEL Mod 301 D50 Serial No. 7051
15.	Local Oscillator	Hewlett Packard 616A Serial No. 1995
16.	Attenuator	Micro Lab Mod. AB 10 N
17.	Precision Attenuator	Demorhay Bonardi L410 Serial No. 2670
18.	Isolator	Microwave Assoc. Mod 170 Serial No. 15
19.	Cavity	AVCO made fc 3000 mc Q 1300
20.	Isolator	Microwave Assoc. Mod 170 Serial No. 15
21.	Directional Coupler	Narda Mod 3003-10 Serial No. 600
22.	Attenuator	Narda 757-6 Serial No. 482
23.	Isolator	Microwave Assoc. Mod 170 Serial No. 4
24.	Detector	Hewlett Packard Mod 440A
25.	Receiver - IF Amplifier	LEL Mod 301 D 50 Serial No. 7052
26.	Local Oscillator	TS 403 B/U Serial No. 279
	Coaxial to Waveguide Adapters	FXR Mod S311A

85-6946

Figure D-4 HIGH-TEMPERATURE DIELECTRIC MEASURING SYSTEM (f = 3000 mc)

voltage will be adjusted so that the phase shift caused by the sample passing through the cavity will create an equilaterial triangle.

If the 2 percent reading error is applied to the differentiated law of cosines for an equilateral triangle, the following results evolve:

$$d\phi = \frac{\bar{S}\, d\bar{S} + \bar{C}\, d\bar{C} + \bar{R} \cos\phi\, d\bar{C}}{\bar{R}\, \bar{C} \sin\phi} \tag{20}$$

where

$\bar{S}$ = sum

$\bar{C}$ = cavity vector

$\bar{R}$ = reference vector

$$d\phi = \frac{0.02 + 0.02 + 0.01}{0.88} \tag{21}$$

$$d\phi = 0.0575 \text{ radians} \approx 3 \text{ degrees.} \tag{22}$$

Since the reference arm amplitude is accurately measured under static conditions and does not change under dynamic conditions, its error has been neglected.

Applying the errors of 2 percent in measuring transmission loss through the cavity and the 3 degree error in phase shift to formulas 9 and 10, the measuring accuracies of ϵ' and ϵ'' may be obtained. When the loss tangent ϵ''/ϵ' is less than 1, the errors in ϵ' and ϵ'' are approximately 5 percent. As the loss tangent increases from 1 to 20, the accuracy of ϵ' degenerates rapidly and for loss tangents above 20, ϵ' can no longer be obtained from equations (9) and (10). However, the accuracy of ϵ'' remains approximately 5 percent throughout the measuring range of the equipment.

It can be shown that for loss tangents greater than 10, the real part of the complex dielectric constant need not be known to calculate attenuation through a dielectric.

The equation that describes attenuation through a dielectric for tan δ from 0.05 to 50 is:

$$8.686\,\alpha = \frac{17.37}{\lambda}\, \pi \sqrt{\frac{\epsilon'\mu}{\mu_0} \; \frac{\sqrt{1+\tan^2\delta} - 1}{2}} \tag{23}$$

Substituting $\frac{\epsilon''}{\epsilon'}$ for $\tan\delta$ and setting $\mu_o = 1$

$$8.686\,\alpha = \frac{17.37}{\lambda}\,\pi\sqrt{\frac{\epsilon'\;\sqrt{1+(\epsilon''/\epsilon')^2} - 1}{2}}$$

for $\frac{\epsilon''}{\epsilon'} \geq 10$

$$8.686\,\alpha = \frac{17.37}{\lambda}\,\pi\sqrt{\frac{\epsilon'}{}\left(\frac{\epsilon''/\epsilon' - 1}{2}\right)}$$

$$8.686\,\alpha = \frac{17.37}{\lambda}\,\pi\sqrt{\frac{\epsilon'' - \epsilon'}{2}}$$

knowing that $\epsilon'' \geq 10\epsilon'$ the second term in the numerator may be neglected. This assumption introduces a maximum error of 10 percent which diminishes as $\tan\delta$ increases. Equation (23) becomes:

$$8.686\,\alpha = \frac{17.37}{\lambda}\,\pi\sqrt{\frac{\epsilon''}{2}}$$

It can be seen that for high loss tangents the attenuation through a dielectric is a function of ϵ''. Therefore, to calculate or to simulate the attenuation through a material with $\tan\delta \geq 10$, only the imaginary part of the complex dielectric constant (ϵ'') needs to be known.

E. LIMITATIONS OF MEASURING RANGE

As previously stated, cavity perturbation depends not only on the electrical properties of the material, but also on the fractional volume of the cavity occupied by the sample. Therefore, as the dielectric constant of the sample increases, the volume of the sample will be decreased in order that the cavity perturbation remain in the measuring range of the test equipment. This reduction in sample size has a practical limit of approximately a 1/4 inch diameter rod. Below this thermal cooling of the sample would become a problem as it is dropped from the oven through the cavity. This lower limit in sample size also limits the upper measurable range of the sample's loss tangent because the skin depth becomes less than the sample radius for high loss tangents, therefore perturbation theory no longer applies. This upper limit of the loss tangent is 10^4 and 10^2 for the 300 Mc and 3 kMc cavities, respectively, when the dielectric constant (ϵ') is approximately 2.

F. CALIBRATION OF CAVITY DIELECTROMETER

The cavity dielectrometer accuracy will be checked by measuring the known properties of several dielectric rods. The room temperature dielectric constants of these rods will be approximately that of the Apollo heat shield at elevated temperatures. The dielectric properties of the rods will be measured in the Rohde and Schwarz dielectrometer prior to the measurements. By this procedure, a correction factor will be applied to the discrepancies in the cavity perturbation method.

G. SAMPLE TEMPERATURE CONTROL

A cylindrical oven containing four 18 inch 6-kw GE quartz heater lamps will be mounted above the cavity. The oven and cavity will be purged with nitrogen during the heating and measuring process to prevent decomposition of the sample.

The internal temperature of the sample will not be measured directly with each test due to complications that arise in removing the thermocouple from the center of the sample before it is dropped through the cavity. The internal temperature will be measured indirectly by relating the internal sample temperature to a thermocouple located outside the sample. This will be done by placing a thermocouple outside the sample in addition to one inside the sample and measuring the rise times of both thermocouples until they reach an equilibrium at 2000 °K. Using these two curves, the thermocouple outside the sample will be used to monitor the internal temperature of the sample.

MEASUREMENT PROCEDURE

1. Calibrate receiver.

2. Null bridge by adjusting variable attenuator and phase shifter in the reference arm of the bridge. This will make the reference and cavity arms of the bridge equal in amplitude and in phase.

3. Insert 60 degrees phase shift in reference arm of the bridge. The equilateral triangle is now set. (The cavity, reference and sum outputs of the bridge are all equal when the equilateral triangle is set.)

4. Insert sample into cavity.

5. Record amplitude changes in cavity and sum outputs of bridge (see figure D-5).

6. Apply cavity and sum outputs in step 5 to law of cosines and obtain phase angle between reference and cavity arms of bridge.

DATA SHEET

SAMPLE I.D. NUMBER	TEMP OF SAMPLE	OVEN CYCLING TIME	CENTER FREQUENCY OF CAVITY EMPTY	Q OF EMPTY CAVITY	SAMPLE VOLUME	CAVITY VOLUME	ATTENUATION DUE TO SAMPLE PERTURBATION		ϕ ANGLE BETWEEN REFERENCE ARM AND CAVITY ARM	
							SUM ARM	CAVITY ARM	CAVITY EMPTY	CAVITY WITH SAMPLE

85-6947

Figure D-5 DATA SHEET

7. Apply the attenuation in the cavity arm of the bridge and the change in phase between cavity and reference arms of the bridge when the dielectric sample is inserted into the cavity to equations (9) and (10). This will yield the dielectric constants of the sample that was inserted into the cavity.

LIST OF SYMBOLS (All Units mks)

a	cavity radius
b	radius of sample
$\bar{C}$	cavity vector
E	electric field
E_1	electric field intensity of cavity 1*
E_2	electric field intensity of cavity 2*
f	frequency
f_1	resonant frequency of cavity 1
f_2	resonant frequency of cavity 2
Δf	$f_1 - f_2$
j	$\sqrt{-1}$
l	length of cavity
P_o	power out of cavity
P_1	power into cavity
Q_o	unloaded cavity
Q_1	loaded Q of cavity 1
Q_2	loaded Q of cavity 2
r_o	distance between cavity and dielectric sample center lines
$\bar{R}$	reference vector
$\bar{S}$	sum vector
T_1	transmission loss of cavity 1
T_2	transmission loss of cavity 2

*Cavity 1 is without dielectric sample.
*Cavity 2 is with dielectric sample.

LIST OF SYMBOLS (All Units mks) (Concl'd)

V_1	volume of cavity
V_2	volume of sample
V_f	fraction of sample volume to cavity volume
Z	impedance
z	cavity axis
β_1	input cavity coupling coefficient
β_2	output cavity coupling coefficient
β_d	dielectric coupling coefficient
ϵ	absolute complex permittivity
ϵ_o	free-space permittivity
ϵ'	real part of relative complex permittivity
ϵ''	imaginary part of relative complex permittivity
μ_o	free-space permeability
ϕ_1	phase shift of cavity without sample
ϕ_2	phase shift of cavity with sample

Unclassified
Security Classification

DOCUMENT CONTROL DATA - R&D

(Security classification of title, body of abstract and indexing annotation must be entered when the overall report is classified)

1 ORIGINATING ACTIVITY (Corporate author) Avco Corporation Space Systems Division Lowell, Massachusetts	2a REPORT SECURITY CLASSIFICATION Unclassified 2b GROUP

3 REPORT TITLE

A Study of Ablation Material Effects on Antenna Performance

4 DESCRIPTIVE NOTES (Type of report and inclusive dates)

Final Report 7 July 1965 to 12 October 1966

5 AUTHOR(S) (Last name, first name, initial)

Fante, Ronald L.
McLaughlin, John R. Trousdale, John E.

6 REPORT DATE	7a. TOTAL NO OF PAGES	7b NO OF REFS
12 October 1966	244	44

8a CONTRACT OR GRANT NO. NAS 9-4916 b. PROJECT NO. c d	9a. ORIGINATOR'S REPORT NUMBER(S) AVSSD-0277-66-RR 9b. OTHER REPORT NO(S) (Any other numbers that may be assigned this report)

10 AVAILABILITY/LIMITATION NOTICES

Qualified Requesters may obtain copies of this report from DDC.

11 SUPPLEMENTARY NOTES	12. SPONSORING MILITARY ACTIVITY
	NASA/MSC Houston, Texas

13 ABSTRACT N67-14923

Artificial dielectrics were developed to electrically simulate the Apollo command module heat shield, Avcoat 5026-39. The simulators were developed for hot and cold conditions of the heat shield so that its effect on antenna performance could be measured at room temperature. For scaled measurements, third-scale and fifth-scale simulators were fabricated. Complex permittivity of Avcoat 5026-39 was measured from 4° K to 2000° K to characterize its electrical properties for simulator development. Simulator performance was checked by comparing radiation patterns of antennas covered with full-, 1/3-, and 1/5-scale simulators to those covered with Avcoat 5026-39. A computer program to calculate the radiation patterns and impedance of an open-ended-waveguide antenna covered with a dielectric on a flat ground plane is given.

Author

DD FORM 1 JAN 64 1473

Unclassified
Security Classification

Unclassified
Security Classification

14 KEY WORDS	LINK A ROLE	LINK A WT	LINK B ROLE	LINK B WT	LINK C ROLE	LINK C WT
Antenna Simulators Dielectric Measurements Antenna Radiation Pattern Computation Apollo Heat Shield						

INSTRUCTIONS

1. ORIGINATING ACTIVITY: Enter the name and address of the contractor, subcontractor, grantee, Department of Defense activity or other organization *(corporate author)* issuing the report.

2a. REPORT SECURITY CLASSIFICATION: Enter the overall security classification of the report. Indicate whether "Restricted Data" is included. Marking is to be in accordance with appropriate security regulations.

2b. GROUP: Automatic downgrading is specified in DoD Directive 5200.10 and Armed Forces Industrial Manual. Enter the group number. Also, when applicable, show that optional markings have been used for Group 3 and Group 4 as authorized.

3. REPORT TITLE: Enter the complete report title in all capital letters. Titles in all cases should be unclassified. If a meaningful title cannot be selected without classification, show title classification in all capitals in parenthesis immediately following the title.

4. DESCRIPTIVE NOTES: If appropriate, enter the type of report, e.g., interim, progress, summary, annual, or final. Give the inclusive dates when a specific reporting period is covered.

5. AUTHOR(S): Enter the name(s) of author(s) as shown on or in the report. Enter last name, first name, middle initial. If military, show rank and branch of service. The name of the principal author is an absolute minimum requirement.

6. REPORT DATE: Enter the date of the report as day, month, year, or month, year. If more than one date appears on the report, use date of publication.

7a. TOTAL NUMBER OF PAGES: The total page count should follow normal pagination procedures, i.e., enter the number of pages containing information.

7b. NUMBER OF REFERENCES: Enter the total number of references cited in the report.

8a. CONTRACT OR GRANT NUMBER: If appropriate, enter the applicable number of the contract or grant under which the report was written.

8b, 8c, & 8d. PROJECT NUMBER: Enter the appropriate military department identification, such as project number, subproject number, system numbers, task number, etc.

9a. ORIGINATOR'S REPORT NUMBER(S): Enter the official report number by which the document will be identified and controlled by the originating activity. This number must be unique to this report.

9b. OTHER REPORT NUMBER(S): If the report has been assigned any other report numbers *(either by the originator or by the sponsor)*, also enter this number(s).

10. AVAILABILITY LIMITATION NOTICES: Enter any limitations on further dissemination of the report, other than those imposed by security classification, using standard statements such as:

(1) "Qualified requesters may obtain copies of this report from DDC."

(2) "Foreign announcement and dissemination of this report by DDC is not authorized."

(3) "U. S. Government agencies may obtain copies of this report directly from DDC. Other qualified DDC users shall request through ______________."

(4) "U. S. military agencies may obtain copies of this report directly from DDC. Other qualified users shall request through ______________."

(5) "All distribution of this report is controlled. Qualified DDC users shall request through ______________."

If the report has been furnished to the Office of Technical Services, Department of Commerce, for sale to the public, indicate this fact and enter the price, if known.

11. SUPPLEMENTARY NOTES: Use for additional explanatory notes.

12. SPONSORING MILITARY ACTIVITY: Enter the name of the departmental project office or laboratory sponsoring *(paying for)* the research and development. Include address.

13. ABSTRACT: Enter an abstract giving a brief and factual summary of the document indicative of the report, even though it may also appear elsewhere in the body of the technical report. If additional space is required, a continuation sheet shall be attached.

It is highly desirable that the abstract of classified reports be unclassified. Each paragraph of the abstract shall end with an indication of the military security classification of the information in the paragraph, represented as *(TS)*, *(S)*, *(C)*, or *(U)*.

There is no limitation on the length of the abstract. However, the suggested length is from 150 to 225 words.

14. KEY WORDS: Key words are technically meaningful terms or short phrases that characterize a report and may be used as index entries for cataloging the report. Key words must be selected so that no security classification is required. Identifiers, such as equipment model designation, trade name, military project code name, geographic location, may be used as key words but will be followed by an indication of technical context. The assignment of links, rules, and weights is optional.

Unclassified
Security Classification